MINERALOGY AND PETROLOGY OF THE TOWNLANDS IRON-RICH ULTRAMAFIC PEGMATITE

by

DAVID PHILLIPS, B.Sc. (Hons)

THESIS PRESENTED FOR THE DEGREE OF
MASTER OF SCIENCE

Department of Geology
Rhodes University
Grahamstown

September 1984

DECLARATION

This thesis represents the original work of the author except where specific acknowledgement is made to the work of others.

SIGNED: _____

D PHILLIPS
Department of Geology
Rhodes University
Grahamstown

September 1984

ABSTRACT

The Townlands iron-rich ultramafic pegmatite is a relatively large pipe-like body situated in the western corner of Rustenburg Section, Rustenburg Platinum Mines. It is characterised by a strong negative magnetic signature and transgresses the noritic layered sequence of the upper critical zone of the Bushveld Complex. The layered rocks are downwarped in the vicinity of the pipe and are in sharp contact with the pegmatitic material.

The pegmatite varies in composition between dunite and wehrlite, with the marginal zones being more wehrlitic in composition. Olivine (Fo_{30} - Fo_{52}) and clinopyroxene ($Wo_{45}En_{30}Fs_{25}$ - $Wo_{45}En_{37}Fs_{18}$) are the dominant constituents and accessory phases include ilmenite, Ti-magnetite, apatite, amphiboles, chlorite-group minerals, biotite, ilvaite and a host of unusual ore minerals. The Fe-Ti oxides exhibit exsolution textures typically found in slowly cooled igneous rocks and temperatures of formation are considered to be in excess of 800°C. The UG2 chromitite leader layers intersected by borehole TLP.1 are enriched in Fe and Ti and exhibit compositions intermediate between chromite and Ti-magnetite. The ore mineral assemblage includes a primary sulphide assemblage consisting of troilite, chalcopyrite, cubanite and pentlandite, and an array of unusual phases formed by late-stage secondary processes. The unusual sulphides mooihoekite and haycockite, that occur in certain parts of the pegmatite, are considered to have formed by partial replacement of the primary assemblage and a possible paragenetic sequence is discussed.

Mineral compositions and whole rock geochemical data are consistent with an origin for the pegmatite by crystallization from a fractionated melt. It is suggested that intercumulus fluids, trapped during the crystallization of the noritic layered sequence, accumulated in an area of structural weakness, in response to an increasing overburden pressure and/or tectonic activity. Evidence is also presented that indicates that the Townlands pegmatite may consist of at least two separate, but adjoining pegmatite bodies.

CONTENTS

1. INTRODUCTION

The occurrence of discordant bodies of ultramafic pegmatite in the layered mafic sequence of the Bushveld Igneous Complex has been described by various authors. The expansion of mine workings on the Merensky reef in recent years combined with the use of geophysical techniques have revealed the presence of large numbers of these bodies. The pegmatites vary widely in size and nature and include the well-known Mooihoek, Onverwacht and Driekop pipes of the eastern Bushveld Complex, which contain platiniferous cores of hortonolite dunite. Efforts to locate additional platinum-bearing pegmatites have been largely futile, and in general, the pegmatites have a detrimental effect on mining. Despite their widespread occurrence and diverse nature, very few ultramafic pegmatite bodies have been examined in detail. As a result, the Townlands ultramafic pegmatite, or Townlands pipe, as it has become known in mining circles, was selected by J.C.I. (Johannesburg Consolidated Investment Company) for investigation. Viljoen et. al. (1983) presented a report stressing the structural aspects and ore mineralogy of the Townlands pipe, while the present study, which emphasizes mineralogical and petrological aspects, was conceived in order to complement the work of Viljoen et. al. (1983).

The Townlands pipe is situated in the far western corner of Rustenburg Section of RPM (Rustenburg Platinum Mines) in the western part of the Bushveld Complex (Fig. 1). It consists of a large body of iron-rich ultramafic pegmatite that transgresses the layered sequence of the upper critical zone. Pegmatitic material is exposed on surface some 100m above the sub-outcrop of the Merensky Reef and the surface expression of the pipe takes the form of a gentle rise, which is marked by a change in soil colour from the black of typical Bushveld turf to a deep reddish brown. The pegmatite is poorly exposed, and although surface rubble is fairly abundant, much of it has been disturbed by agricultural activities. On surface, the pipe is roughly oval in shape with estimated dimensions of 250 x 350m.

Ultramafic pegmatites, similar to the Townlands pipe and containing varying proportions of olivine and clinopyroxene, occur throughout the upper critical and lower main zones of the Bushveld Complex. Their abundance, as indicated by the investigations of Viljoen & Scoon (in press), suggests a close relationship between the pegmatites and the

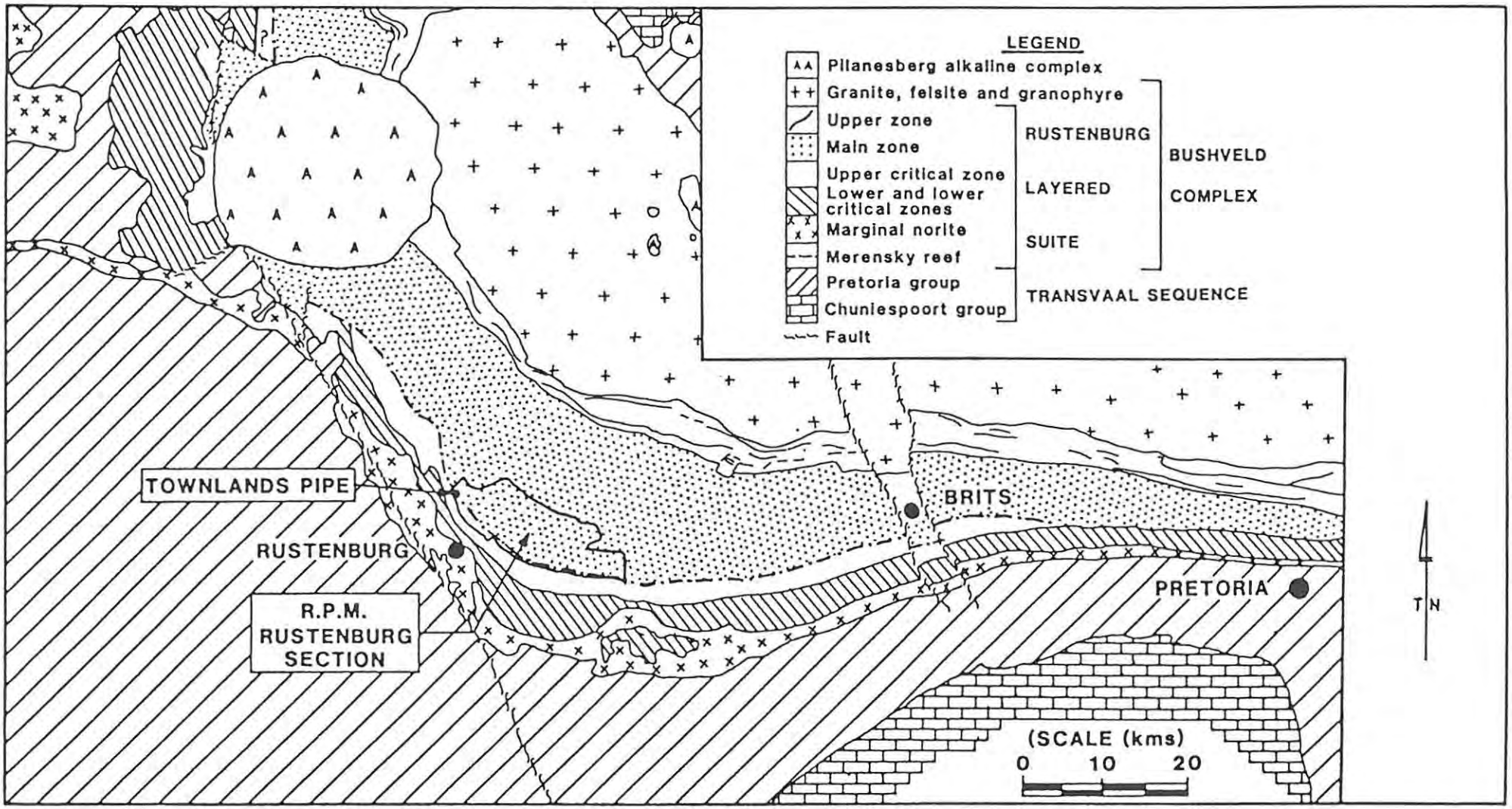

Figure 1. Locality map. (Modified after an unpublished map compiled by the geology department, Rustenburg Platinum Mines Ltd., Rustenburg Section.).

crystallisation history of the Bushveld Complex. Some debate exists with regard to the genesis of these ultramafic bodies and various models have been proposed for their origin. These include genesis by metasomatic replacement of the existing layered rocks (inter alia Cameron & Desborough, 1964), magmatic replacement of the layered rocks (inter alia Wagner, 1929; Viljoen & Scoon, in press) and forceful intrusion (inter alia Willemse, 1969a).

1.1 Sampling Procedure

The Townlands pipe is intersected by underground mine workings along its eastern periphery, while 6 level haulage cuts across the northeastern margin of the pipe. A total of 5 surface boreholes were drilled into the central portion of the pegmatite by J.C.I. (Fig.2). The deepest borehole, TLP.1, was drilled to a depth of 270m, and intersected the UG2 chromitite layer. Borehole TLP.2 reached a depth of about 80m, while TLP.3, TLP.4 and TLP.5 represent shallower boreholes, 30-40m in extent. TLP.1 and TLP.2 were drilled into the cores of geophysical anomalies, as determined by the J.C.I. geophysical surveys (Viljoen, et. al., 1983) (Fig. 2).

Access to the underground exposures of the Townlands pegmatite was unfortunately limited to 6 level haulage, due largely to inadequate ventilation in other areas adjacent to the pipe. Samples of pegmatitic material and adjacent 'spotted' anorthosite (norite) were collected from the exposures along 6 level haulage, with particular attention being given to the contact areas between the two rock types. The core from the 5 boreholes was carefully logged and extensively sampled, according to variations in grain-size and modal proportions of the constituent minerals. The upper 20-25m of each borehole exhibits intense alteration, due to surface weathering and all samples were collected from below this level. Sampling of the UG2 chromitite layer in borehole TLP.1 was not permitted, but sections from the overlying chromitite leaders in this borehole were kindly made available for this study. Detailed borehole logs and a list of all sample localities are presented in appendix 1.

Thin sections of all samples were prepared and examined under the microscope in transmitted light. On the basis of these studies, a comprehensive suite of samples was selected for the preparation of polished thin sections for use in electron microprobe analyses. An

additional suite of samples was collected, at approximately 10m intervals, from boreholes TLP.1 and TLP.2, and the underground material, for detailed geochemical studies. Sulphide-bearing samples were examined under the binocular microscope and representative material was selected for the preparation of a suite of polished sections for reflected light studies.

1.2 Aims of the Present Study

Very little published geochemical data are currently available for iron-rich ultramafic pegmatites, such as the Townlands pipe. Consequently, the geochemical study was undertaken in order to investigate possible chemical changes within the pipe, as well as differences between the pegmatite and surrounding layered rocks. A major objective of the present study was the documentation of the mineralogy of the pegmatite body. In view of this, the silicate and oxide phases were examined and are discussed in some detail. Viljoen et. al. (1983) investigated aspects of the ore mineralogy of the pipe, and the ore minerals are re-examined in this study, with particular emphasis on textural relationships that were not covered in the earlier report. Finally, it was hoped that this work would complement that of Viljoen et. al. (1983) and assist in evaluating the genesis of the Townlands and similar ultramafic pegmatites.

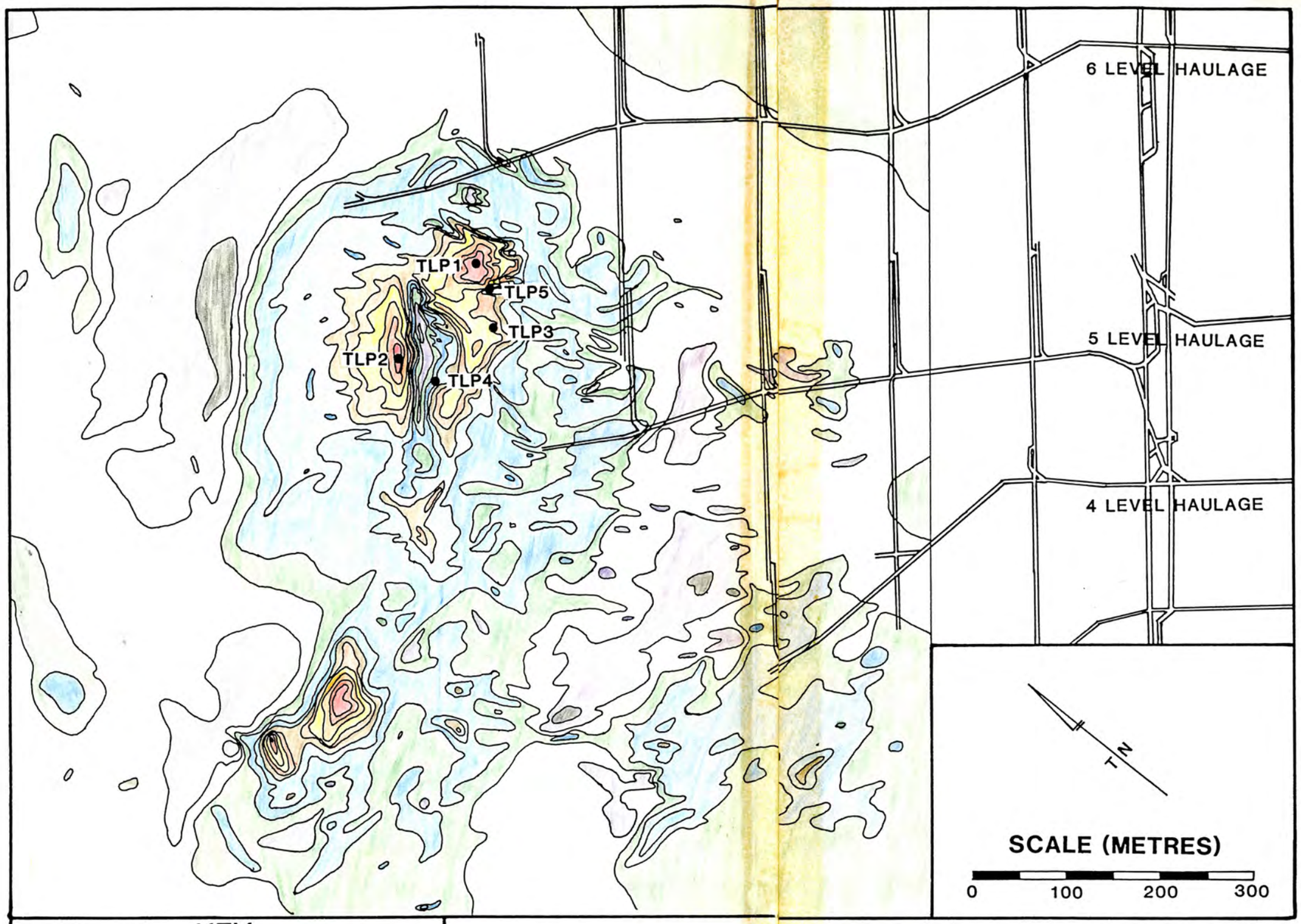

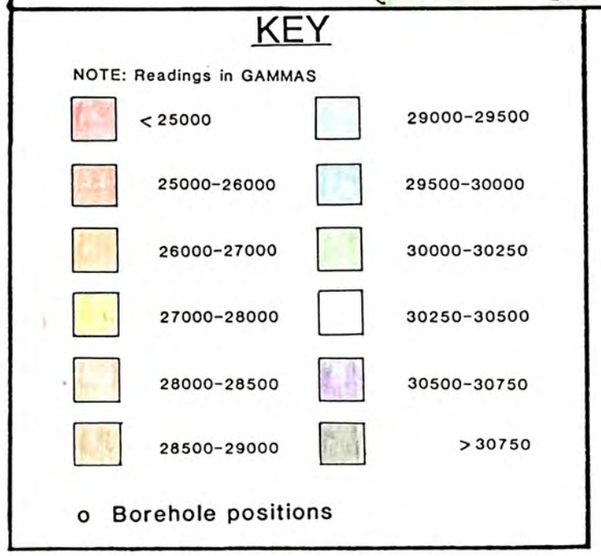

Figure 2. The magnetic signature of the Townlands pipe, as indicated by the magnetometer survey, superimposed on a plan of the underground workings (Reproduced with the permission of Rustenburg Platinum Mines Ltd., Rustenburg Section).

2. PREVIOUS WORK

There has been little concensus with regard to the terminology for ultramafic pegmatites amongst previous authors. Wagner (1929) used the terms 'hortonolite dunite' and 'wehrlite', Cameron & Desborough (1964) described magnetite-bearing pegmatites, while Willemse (1969b) preferred the name 'ultramafic pegmatoid'. In a comprehensive review on pegmatites, Jahns (1955) suggested that the term 'pegmatite' be applied to 'holocrystalline rocks that are at least in part very coarse grained, whose major constituents include minerals typically found in ordinary igneous rocks, and in which extreme textural variations, especially in grain size, are characteristic'. On the basis of this definition, Irvine (1982) concluded that the word 'pegmatoid', which means 'like pegmatite', is superfluous. Consequently, 'ultramafic pegmatite' was the description preferred by Viljoen & Scoon (in press) and is adopted in the present study.

The Townlands ultramafic pegmatite is one of a large suite of mafic and ultramafic bodies that transgress the layered sequence of the Bushveld Complex. The pegmatites display considerable variation in both mineralogy and morphology. They occur as small irregular pods, veins and sills, and as large plug-like or pipe-like masses. Investigations have resulted in the recognition of several distinct groupings, some of which may be genetically related (Viljoen & Scoon, in press). Wagner (1929), Söhnge (1963), Willemse (1969a), Tankard et. al. (1982) and Viljoen & Scoon (in press) have all discussed and attempted to classify many of these bodies.

The earliest comprehensive classification was that of Willemse (1969a), who recognised the following categories:

a) Bronzitite pegmatoids, which form pipe-like features in the lower zone of the Bushveld Complex. They contain bronzite, phlogopite and nickeliferous sulphides.

b) Hortonolite dunites and dunites, from the upper parts of the lower zone and basal parts of the critical zone. Both platiniferous and non-platiniferous bodies are included.

c) Diallagite (clinopyroxene) pegmatoids, from the critical zone and sometimes from the main and upper zones. They form irregular masses, anastomosing veins and pipes transgressive to the layering.

d) Magnetite pegmatoids, from the main and upper zones, resulting from an increased magnetite content in diallagite pegmatoids.

e) Vermiculite pegmatoids, occurring as pipe-like bodies in the upper zone of the Bushveld Complex.

Tankard et. al. (1982) included a further category to incorporate the ultramafic pipe-like bodies reported by Ferguson & McCarthy (1970). These bodies contain rounded inclusions of feldspathic amphibolite plus lesser amounts of amphibolite, chromitite and mottled anorthosite.

An alternative classification scheme was proposed by Viljoen & Scoon (in press) with the following sub-divisions:

a) Forsterite - chrysolite dunite bodies, which are small, non-platiniferous pipe-like bodies, occurring in the lower and critical zones of the Bushveld Complex.

b) Platiniferous ultramafic pipes, from the critical zone of the eastern Bushveld Complex. They are composed of a small platiniferous core of hortonolite or hyalosiderite dunite surrounded by forsterite-chrysolite dunite and a thin outer shell of wehrlite or clinopyroxenite.

c) Iron-rich ultramafic pegmatites, consisting of Fe-rich olivine, clinopyroxene and minor titanomagnetite, ilmenite and sulphides. They occur in the upper critical and main zones of the Bushveld Complex. The Townlands pipe is included in this category.

d) Ti-magnetite bodies and pipes, of which there are 2 types:
   i) Chromium-rich magnetite lenses adjacent to or replacing cumulate chromitites of the critical zone.
   ii) Larger monomineralic cores within ultramafic pegmatites in the main zone and discrete pipes within the upper zone.

e) This group includes the Vlakfontein nickel (bronzitite) pipes, anorthositic pegmatites, pyroxenitic pegmatites and vermiculite-bearing pegmatites, all of which may, or may not, be related.

Much information on ultramafic pegmatites has become available since the discussion by Willemse (1969a). For this reason, the above classification of Viljoen & Scoon (in press), is preferred for the current study. The literature relevant to each category is discussed for completeness.

According to Viljoen & Scoon (in press), forsterite-chrysolite bodies are uncommon, but include the pipe-like bodies described by Schwellnus et. al. (1962) and some of the dunite pipes reported by Coertze (1960, 1974). Viljoen & Scoon (in press) also suggest that the "mafic" pipes reported by Gain (1980), from the eastern Bushveld Complex, may in part be composed of chrysolite dunite.

The platiniferous ultramafic pipes were described in some detail by Wagner (1925, 1929) and include the Mooihoek, Onverwacht and Driekop pipes, all of which have been mined in the past. As a result of their economic significance, these ultramafic pipes have attracted more attention than any of the other ultramafic bodies in the Bushveld Complex. Descriptions of one or more of these pipes have been given by Bateman (1951), Lombaard (1956), Cameron & Desborough (1964), Schiffries (1982) and Scoon (1983). Aspects of the silicate mineralogy have been documented by Wagner (1929), Lombaard (1956), Heckroodt (1959), Cameron & Desborough (1964), Schiffries (1982) and Scoon (1983). The spinels have received attention from Wagner (1929), Lombaard (1956), Cameron & Desborough 1964), Stumpfl & Rucklidge (1982), Reynolds & Scoon (1983) and Scoon (1983). Tarkian & Stumpfl (1975) and Cabri et. al. (1977a,b,c) have described the platinum group minerals, while Peyerl (1982) investigated the platinum group mineralogy of the UG2 chromitite layer adjacent to the Driekop pipe. Cabri & Hall (1972) discovered the two unusual sulphides mooihoekite and haycockite, in samples from the Mooihoek pipe.

Lenses and veins of Ti-magnetite (group d(i)) are rare, but all are related to chromitite layers (Viljoen & Scoon, in press). Similar lenses from the northwestern Bushveld Complex are described by Wasserstein (1936). These are all associated with chromitite horizons and

Wasserstein (1936) noted a transition from chromitite to magnetite at one locality. Cameron & Glover (1973) examined the spinel compositions of magnetite/chromitite layers from ultramafic pegmatites of the eastern Bushveld Complex. The second group of large pipe-like bodies of magnetite and ultramafic pegmatite-magnetite (group d(ii)) are much more widespread within the main and upper zones of the Bushveld Complex. These bodies are distinguished from Fe-rich ultramafic pegmatites on the basis that they form discrete segregations of pure titanomagnetite plus ilmenite, as opposed to the disseminated oxides of Fe-rich ultramafic pegmatites (Viljoen & Scoon, in press). Von Gruenewaldt (1973) recognised over 100 small magnetite plugs in the eastern Bushveld Complex, while other occurrences have been reported by Wasserstein (1936), Coertze & Schumann (1962), and Coertze (1966). Composite magnetite-ultramafic pegmatites have been investigated by Coertze (1960, 1966, 1974), Coertze & Schumann (1962), Schwellnus et. al. (1962) and Cameron & Desborough (1964).

The nickeliferous Vlakfontein pipes have been described by Schwellnus (1935), Söhnge (1963), Liebenberg (1970), Vermaak (1976) and Von Gruenewaldt (1979). Two vermiculite-bearing pegmatites were noted by Von Gruenewaldt (1973) in the upper zone of the eastern Bushveld Complex. Viljoen & Scoon (in press) reported the presence of a variety of anorthositic and pyroxenitic pegmatite bodies from the critical zone of the western Bushveld Complex, while small anorthositic pegmatites also occur in the eastern Bushveld Complex (Von Gruenewaldt, 1973).

The Fe-rich ultramafic pegmatites, which include the Townlands pipe, and magnetite-ultramafic pegmatites make up the majority of the pegmatitic bodies present within the Bushveld Complex. Wagner (1925,1929) recognised more than 60 separate occurrences of "hortonolite dunite" in the Lydenburg (eastern Bushveld Complex) and Rustenburg (western Bushveld Complex) districts. Apart from the platinum-bearing pipes, the majority occur as sheets, lenses and irregular masses in Fe-rich ultramafic (diallagite) pegmatites (Wagner, 1925,1929). De Bruyn (1944) described the presence of mineralised hortonolite dunite, hortonolite wehrlite and peridotite rocks from an ultramafic pegmatite on the farm Middellaagte in the Rustenburg district. The body is emplaced into the critical zone, below the Merensky reef (De Bruyn, 1944). Von Backström (1960) noted the presence of magnetite-bearing 'dunite' pipes in the vicinity of the Merensky and Bastard cyclic units in the Rustenburg area. Coertze (1960,

1970, 1974) reported ultramafic pegmatites in the western Bushveld Complex, particularly along the Rustenburg fault zone, south of Pilansberg. Cameron & Desborough (1964) examined similar ultramafic bodies from the Steelpoort valley area in the eastern Bushveld Complex. Jones (1974) investigated several ultramafic pegmatites from the critical and main zones of the Bushveld Complex, on the Bafokeng Leasehold, 10km northwest of Rustenburg. These pegmatites occur as large composite pipe-like features as well as smaller, irregular bodies. They transgress the layering and consist largely of varying amounts of clinopyroxene, olivine (Fo_{34-63}) and oxides. Viljoen & Scoon (in press) identified numerous other ultramafic pegmatites from magnetic surveys of the lower parts of the main zone, south of Pilansberg. The Fe-rich pegmatites are confined largely to the upper critical and lower main zones of the Bushveld Complex, where norites and anorthosites are abundant. Very few occur in the lower and lower critical zones (Viljoen & Scoon, in press). They also noted that many of the ultramafic bodies are concentrated in clusters and are usually associated with structural disturbances.

The only investigation directly relevant to the present study is that by Viljoen et. al. (1983) on the Townlands pipe itself. Magnetometer, geochemical and gravity surveys were performed over the outcrop of the Townlands pipe to ascertain the structural features of the pipe. The results of the surveys were summarised by Viljoen et. al. (1983) and are discussed in more detail in the chapter dealing with the morphology of the Townlands pipe. Viljoen et. al. (1983) also examined the mineralogy of the pegmatite, with particular emphasis on the identification of the ore minerals present. Frequent references to the work by Viljoen et. al. (1983) are made in the following chapters.

The majority of the above-mentioned studies have been largely of a descriptive nature and only limited quantitative data are available on whole rock geochemistry (major and trace elements), mineralogy and textural relationships. These aspects are given priority in this thesis, which, it is hoped, will lead to a greater understanding not only of the Townlands and other ultramafic pegmatites, but also of the crystallisation history of the Bushveld Complex, as a whole.

3. MORPHOLOGY

The available data indicate that the Townlands pipe is a large, discordant Fe-rich ultramafic pegmatite with an irregular marginal contact. The irregularity of the outline is illustrated by the alternating 'patches' of ultramafic pegmatite and 'spotted' anorthosite (norite) exposed along 6 level haulage, at the periphery of the main pegmatite body. The overall structure of the Townlands pegmatite is interpreted by Viljoen et. al. (1983), on the basis of magnetometer, geochemical and gravity surveys. A detailed discussion of their findings is given in this chapter, as an understanding of the gross structure of the body is essential for the evaluation of any genetic models.

According to Viljoen et. al. (1983), ground and air-borne magnetometer surveys revealed the presence of a "main" magnetic anomaly as well as a smaller anomaly to the southwest (Fig.2). The "main" anomaly occurs between 5 and 6 level haulages of the mine and appears to be cut by a dyke-like feature that strikes in a northeasterly direction (Viljoen et. al., 1983). There is, however, no information available as to the exact nature of this dyke-like body. Viljoen et. al. (1983) suggest, on the basis of computer modelling, that the "main" anomaly is oval-shaped with dimensions of 200 x 75m and is surrounded by a low amplitude anomaly with a diameter of about 450m. Viljoen et. al. (1983) have interpreted the magnetic anomalies as resulting from the presence of at least two causative bodies, each consisting of a central core that contains more magnetite than their peripheries.

The soil geochemical survey yielded evidence of copper and nickel anomalies, that correspond closely with the position of the 'main' magnetic anomaly. The gravity survey also yielded results that were in agreement with the magnetometer surveys. Modelling of the gravity data, however, suggests that the Townlands pipe extends to a limited depth of approximately 500m below surface (Viljoen et. al., 1983).

The contact relationships between the ultramafic pegmatite and adjacent layered rocks may be sharp, which appears to be the usual case, or gradational over a distance that seldom exceeds one or two metres. The nature of the contact zones that were studied is discussed in more detail in the following chapter. The surrounding layered sequence is dominated by 'spotted' anorthosite and anorthositic layers, with pyroxenitic

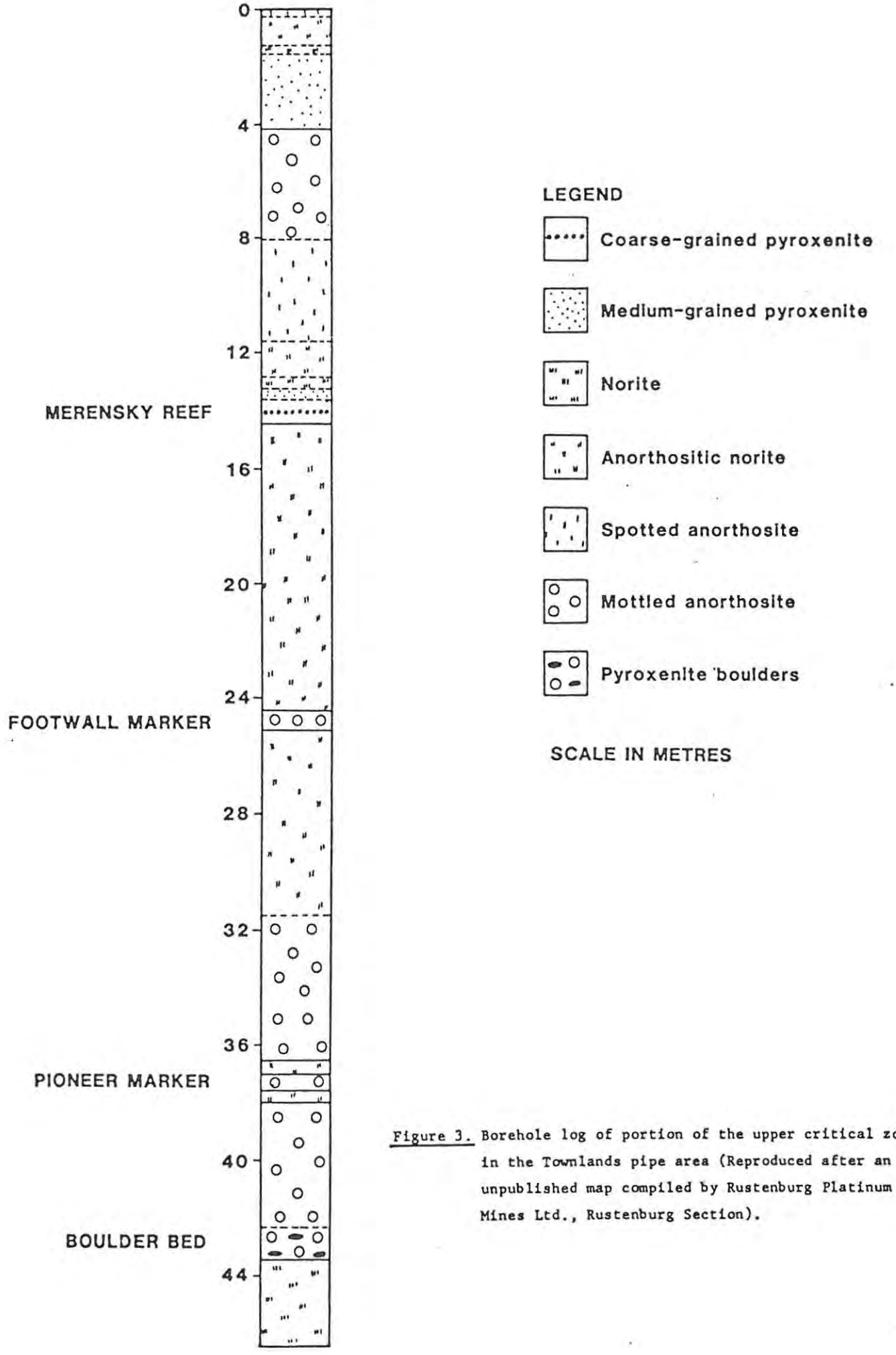

Figure 3. Borehole log of portion of the upper critical zone in the Townlands pipe area (Reproduced after an unpublished map compiled by Rustenburg Platinum Mines Ltd., Rustenburg Section).

horizons being less common (Fig.3). Pegmatitic material is first encountered along 6 level haulage immediately below the level of the 'boulder bed'. It was not possible to discern the structural effects of the Townlands pegmatite on the layered rocks along 6 level haulage, as the exposed section is almost a strike section. However, an example of structural disturbance of the layered sequence was pointed out to the author by J.C.I. geologists. In this case, the 'footwall marker', which consists of an anorthosite layer containing a thin (±10cm) band of norite ('central' norite), is exposed in a crosscut adjacent to the Townlands pipe on 6 level. The anorthosite dips at 9° to the northeast, or away from the body of the pegmatite, which corresponds to the usual dip of the layered sequence in the Rustenburg area. As the pipe is approached, however, the anorthosite horizon bend in towards the pipe, assuming an apparent dip of ±20° towards the southwest, and eventually pinches out (Fig.4). Similar downwarping of the Merensky reef and UG2 chromitite layer, over a distance of several tens of metres from the pipe, was noted by Viljoen et. al. (1983).

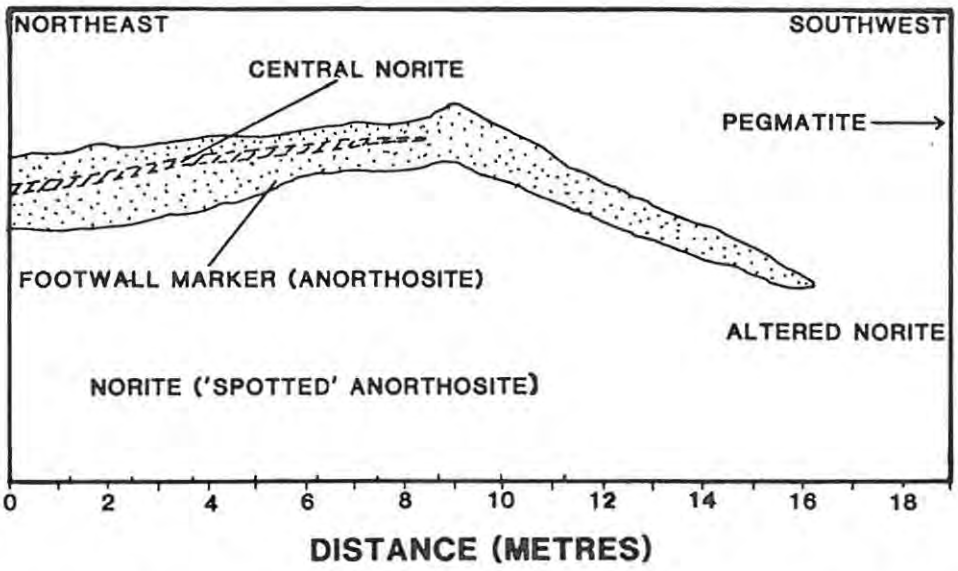

Figure 4. Sketch section indicating the downwarping of the footwall marker anorthosite adjacent to the Townlands pipe. (Regional dip: 9° towards the NE).

Reports of structural disturbances of the layered sequence surrounding other ultramafic pegmatites are rare. Mossom (1977) reported an increase in the dip of the UG1, UG2 and UG3 chromitites adjacent to the Driekop pipe in the eastern Bushveld Complex (Fig.5). This feature has been discussed by Schiffries (1982) and re-examined by Scoon (1983). Gain (1980) studied the upper group chromitite layers from an area south of the Driekop pipe and noted that all the chromitites are downwarped in

the vicinity of 'mafic' pegmatite pipes. A borehole drilled into one of these pipes failed to intersect any of the chromitite horizons at depth (Gain, 1980).

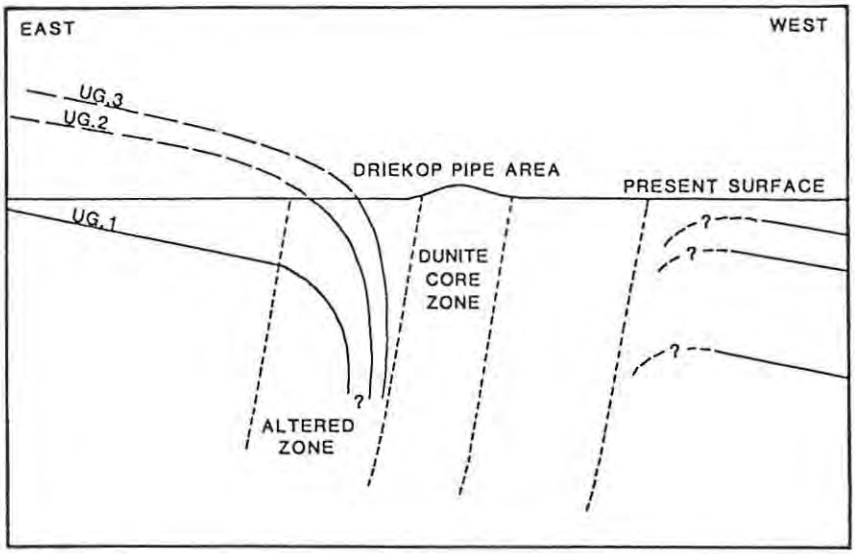

Figure 5. East-west section across the Driekop pipe showing the steepening of dip of the chromitite layers adjacent to the pipe (from Mossom, 1977).

A 4m thick zone of apparently unaffected layered rock was intersected at the bottom of borehole TLP.1. This zone contains the UG2 chromitite and its leader layers plus orthopyroxenite horizons. No other recognisable layer is known to have been preserved within the Townlands pegmatite, although Viljoen et. al. (1983) report a significant increase of platinum group elements in pegmatitic material at the expected position of the Merensky reef in borehole TLP.1. According to Viljoen et. al. (1983), the UG2 chromitite horizon within the Townlands pipe is 20m above its expected level, which they attribute to "doming" of the stratigraphy within the pegmatite body. An alternative suggestion is that this "unreplaced" zone may represent part of a large xenolithic body, incorporated into the pegmatite during its emplacement. Large xenoliths and slabs of chromitite, dipping at various angles, have been reported from the Onverwacht pipe by Wagner (1929) who interpreted the pipe as being of intrusive origin. It must, however, be noted that authors such as Cameron & Desborough (1964) suggest that the chromitite slabs may be remnants of partially replaced layered sequences.

Viljoen et. al. (1983) commented on the existence of a series of northeasterly trending faults on the northern side of the Townlands pipe. Unfortunately, however, no data are currently available on the

effects of this faulting on the Townlands pipe itself. It should be noted, however, that Viljoen & Scoon (in press) identified numerous Fe-rich ultramafic pegmatites in the upper critical and lower main zones, using information gained via magnetometer surveys of large parts of the Bushveld Complex, and concluded that many of the pegmatites are associated with structural disturbances in the form of faults and dykes. The pegmatites are less common in undisturbed areas, but where present, are generally small and associated with anorthositic layers (Viljoen & Scoon, in press). There are three possible explanations for the presence of the northeasterly trending faults reported by Viljoen et. al. (1983). Either the faults developed prior to the formation of the Townlands pipe, in which case they may have acted as a zone of weakness for the accumulation of pegmatitic material, or they developed as a direct result of the formation of the pipe, or they formed at some later date and are unrelated to the genesis of the pegmatite.

In conclusion, the Townlands pipe appears to be a large, transgressive Fe-rich ultramafic pegmatite with an overall plug-like or pipe-like shape. It is confined to the upper portion of the critical zone of the Bushveld Complex and has caused some disruption of the surrounding layered sequence. If the chromitite layers, preserved in borehole TLP.1, are displaced from their original position and represent part of a larger xenolith, this would provide support for an intrusive origin, at least for the central portions, of the pipe. However, their pr e ce in a single borehole core does not provide unequivocal evidence for the layers being part of a xenolith, and consideration of other aspects of this study are essential for the construction of any genetic model for the Townlands pipe.

4. PETROGRAPHY

4.1 Introduction

The petrographic characteristics of the Townlands ultramafic pegmatite are discussed in terms of a central and a marginal zone. The central zone is considered to include boreholes TLP.2, TLP.3, TLP.4, the upper portion of TLP.1 and possibly TLP.5. The marginal zone is represented by the exposures of pegmatitic material from 6 level haulage and a section in contact with the layered zone at the base of TLP.1. Both zones are composed largely of olivine and clinopyroxene, but there are significant differences with regard to modal proportions and textural relationships. It must, however, be emphasized that the above sub-division is not definitive, as an interpretation of any horizontal or vertical zonation is not possible on the basis of only 5 vertical boreholes and one underground intersection. A description of the contact relationships between the pegmatite and layered rocks as well as a discussion of the alteration of the various phases present are also included in this chapter.

4.2 The Central Zone

The ultramafic rocks of the Townlands pegmatite appear dark brown to black in freshly fractured hand specimens and the distinction between olivine and clinopyroxene is not readily discernable. In core samples or clean-cut surfaces, however, the olivine appears grey-green in colour, in contrast to the clinopyroxene which appears grey. Estimation of modal proportions and grain-size variations is therefore readily achieved by an examination of core samples or sawn slabs.

All the pegmatite samples fit the definition for 'pegmatites' as proposed by Jahns (1955), in that they display extreme variations in grain-size. The central zone samples exhibit a range in grain-size of $<$ 0.5mm-30mm, in which 2 categories can be distinguished (Fig.9(a)):

i) Clusters of interstitial polygonal grains with diameters of 0.5mm or less may be present, surrounded by
ii) larger grains averaging 6-8mm in diameter.

In general, the clinopyroxene grains tend to be slightly larger than their co-existing olivine crystals. The grain-size of the minor

co tituents, with the exception of some hornblende crystals, seldom exceeds 1-2mm. Hornblende tends to exhibit a very variable grain-size, with individual crystals occasionally attaining 20-25mm in length.

Modal proportions are difficult to estimate in thin section because of the coarseness and extreme variation in grain-size. Visual inspection of the borehole core, however, revealed variations in mineral proportions within, and between individial boreholes. The visually estimated average proportions of the major phases present in samples from the various localities are summarised in Table 1. Boreholes TLP.1, TLP.2, TLP.4 and TLP.5 are all dominated by olivine, while TLP.3 contains more or less equal proportions of olivine and clinopyroxene. Accessory phases seldom exceed 3-5% by volume, although they may be locally more abundant. On the basis of mineralogy and gross modal proportions, the pegmatite samples from the upper part of TLP.1 may be classified as dunites, while the remaining borehole samples fall into the category of wehrlites.

LOCALITY	RATIO OF OLIVINE: CLINO-PYROXENE	Fe-Ti OXIDES	SULPHIDES	AV. GRAIN SIZE (mm)	ROCK-TYPE
Central Zone					
TLP.1	90 : 10	1%	1 - 2%	8	DUNITE
TLP.2	80 : 20	1 - 3%	1%	8	WEHRLITE
TLP.3	40 : 60	1%	1%	7	OLIVINE CLINO-PYROXENITE
TLP.4	80 : 20	1%	1%	8	WEHRLITE
TLP.5	60 : 40	±1%	1%	6	WEHRLITE
Marginal Zone					
6 Level Haulage	50 : 50	2 - 4%	1%	5	WEHRLITE
TLP.1 'Marginal' Zone	50 : 50	1%	1%	6	WEHRLITE

Table 1. Estimated modal proportions of the Townlands pipe samples.

Olivine occurs in most sections as large, anhedral grains that are traversed by numerous cracks and fractures, but interstitial aggregates of small polygonal grains may also be present. The overall shape of the olivine grains varies from sub-rounded to elongate, with grain boundaries being very irregular. A characteristic feature of the pegmatite olivine crystals is the presence of small, skeletal opaque oxides, oriented parallel to the (101) planes in the olivine structure (Putnis, 1979).

These dendritic inclusions take the form of thin lamellae or rhombic platelets that are concentrated in the cores of many olivine crystals (Fig.9(b)). Their small size and skeletal nature precludes quantitative microprobe analysis. Putnis (1979), on the basis of electron-microscope observations, concluded that the inclusions are a result of oxidation of small parts of the olivine, which subsequently break down to form dendritic intergrowths of magnetite and pyroxene.

Clinopyroxene, in the presence of abundant olivine, forms aggregates of large anhedral grains, usually with irregular grain boundaries. Smaller grains, which are sometimes fairly altered, may occur in the interstices between olivine grains. A significant textural feature of the clinopyroxene crystals is the presence of small, often embayed, olivine inclusions, which are often optically continuous with larger, adjacent olivine grains (Fig.9(c)). Similar textures were noted by Jackson (1961) in ultramafic rocks of the Stillwater complex. Jackson (1961) concluded that the textures resulted by reaction-replacement between cumulus olivine and intercumulus magma to form augite. The textures exhibited by the pegmatite samples suggest that this process, involving olivine/liquid reaction to form late-stage clinopyroxene, may well have been operative during formation of the pegmatitic rocks.

Opaque oxides and sulphides are the most abundant of the minor constituents present in the Townlands pegmatite. The opaque oxides are more common in borehole TLP.2 than in the remaining boreholes, while TLP.1 contains the greatest abundance of sulphide minerals. The opaque oxides include ilmenite and titaniferous magnetite, which together with the sulphides, are discussed in detail in the chapters dealing with mineralogy. Hydrous minerals may be relatively abundant locally, with borehole TLP.2 containing greater amounts than the other boreholes. The amphiboles present include large anhedral hornblende grains, laths and needles of tremolite and actinolite. Small 'books' of dark red-brown biotite were noted in some samples, while chlorite-group minerals are also sometimes present (Fig.9(d)). Occasional, partially altered, irregular plagioclase grains occur in some sections, but plagioclase is invariably a rare constituent. Clusters of small, polygonal apatite crystals were observed in samples from borehole TLP.1 and are most common towards the base of the study section. The unusual Fe-Ca-Mn silicate, ilvaite, was encountered in a number of samples and because of its relative rareity is discussed more fully in the chapter dealing with silicate mineralogy (Fig.9(e)).

4.3 The Marginal Zone and Contact Relationships

The ultramafic pegmatite in contact with the layered sequence intersected at the base of borehole TLP.1, may not be truly marginal, but it has a similar mineralogy and texture to that of the underground exposures and the two areas are, therefore, discussed together. The sequence begins immediately below the UG2 chromitite horizon and extends to the upper chromitite leader layer (Fig.6). No other layers are recognisable either above or below this zone. The material between the chromitite layers consists largely of orthopyroxenite and is composed of subhedral cumulus bronzite crystals together with lesser amounts of intercumulus clinopyroxene and occassional plagioclase. These lithologies are identical to the usual layered sequence of alternating chromitite and bronzitite horizons present in the adjacent layered suite of the Bushveld Complex.

Pegmatitic material, in the form of scattered interstitial olivine and minor clinopyroxene grains, is first encountered above the lowermost chromitite leader, at 261.1m (Fig. 6). The pegmatite constituents become more abundant with increasing height, until the uppermost leader layers are bordered on both sides by wehrlite. With increasing distance from the layered section, olivine becomes more abundant and, at $\pm$15m above the uppermost chromitite leader, the wehrlite gives way to dunite. This zone of wehrlite above the layered sequence is referred to as the TLP.1 'marginal' zone in the succeeding chapters. It is interesting to note, however, that in the case of the lowermost chromitite leaders, olivine and clinopyroxene are most common in the area immediately adjacent to the chromitite. This suggests that the chromitite/orthopyroxenite contact may have been sufficiently permeable to facilitate the introduction of pegmatitic material. The orthopyroxene grains in the vicinity of the lowermost chromitite leader layers have corroded grain boundaries and are often rimmed by serpentinized olivine. The orthopyroxene crystals that have not undergone alteration have well-defined polygonal grain boundaries, a situation that is unusual in the layered suite adjacent to the Townlands pegmatite (I.M. Reynolds, pers. comm.). The orthopyroxene crystals appear, therefore, to have been annealed and this may be indicative of high temperatures prevailing during the formation of the pegmatite body.

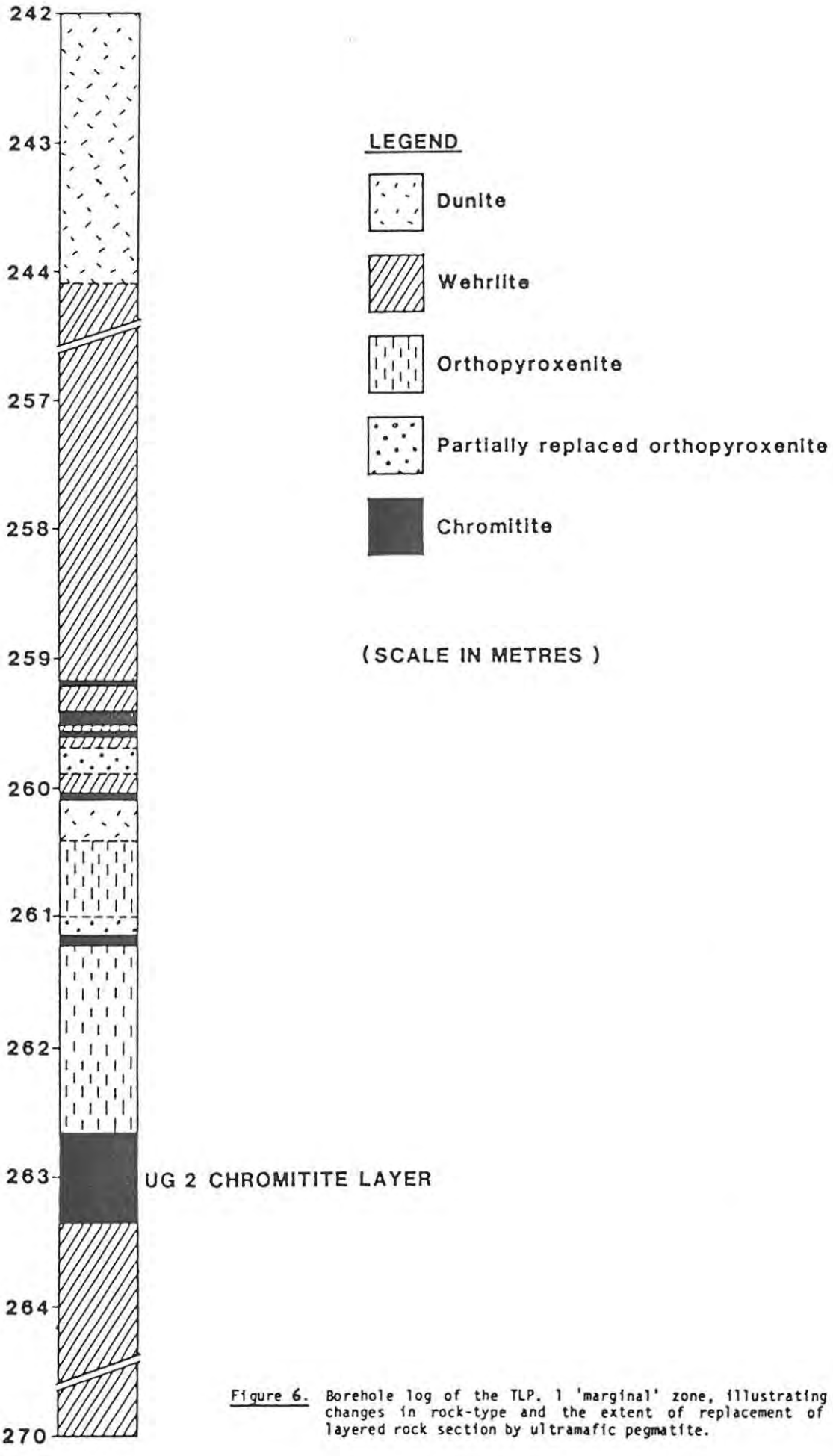

Figure 6. Borehole log of the TLP. 1 'marginal' zone, illustrating the changes in rock-type and the extent of replacement of the layered rock section by ultramafic pegmatite.

The only true marginal zone examined is that exposed along 6 level haulage, where ultramafic pegmatite is in contact with 'spotted' anorthosite. The 'spotted' anorthosite consists of plagioclase and orthopyroxene, together with minor amounts of intercumulus clinopyroxene. The irregularity of the pipe outline permitted examination of several different contact zones and as a result, two types of contact relationships were distinguished in the underground section. The majority of the contacts are 'sharp', with a contact zone of only 2-3cm in width (Fig.10(a),(b)). In a few areas adjacent to the main body of the pegmatite, small 'pods' of ultramafic material were found to have more gradational contact zones of 20cm or more. A schematic representation of a 'sharp' contact zone is presented in Fig.7. As the

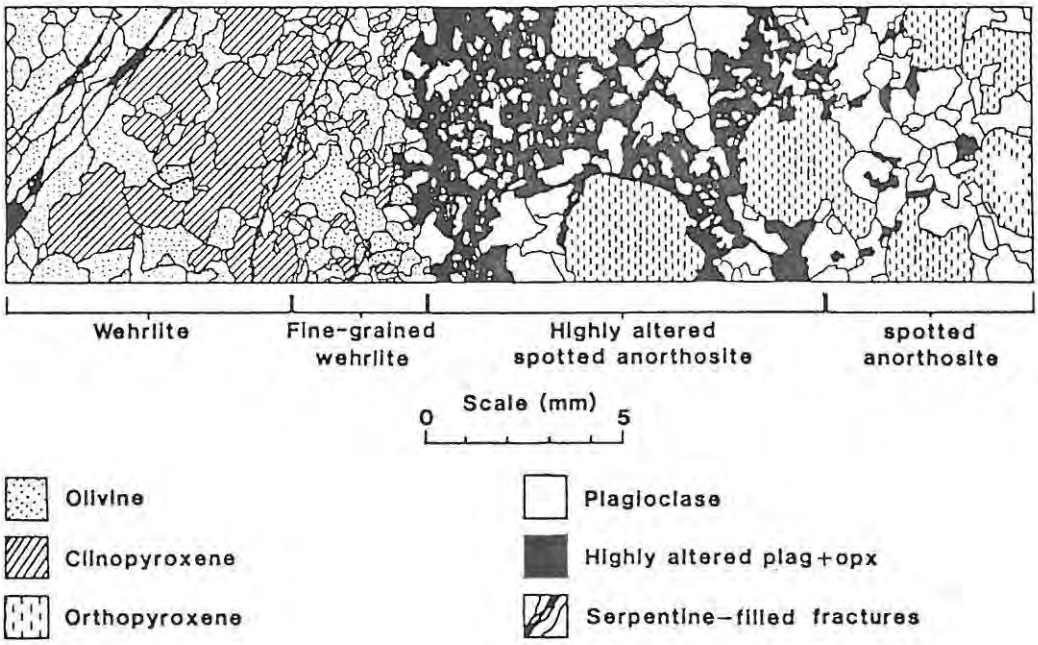

Figure 7. Schematic representation of a 'sharp' contact between ultramafic pegmatite and 'spotted' anorthosite from the exposure along 6 level haulage.

ultramafic material is approached, the 'spotted' anorthosite becomes altered to a fine-grained, dark brown alteration product that contains fragmented and embayed remnants of plagioclase crystals. In other instances, the degree of alteration is much less and coarse-grained plagioclase crystals are developed at the contact. This alteration zone gives way to fine-grained wehrlite, which exhibits an increase in grain-size and in the abundance of clinopyroxene, away from the contact zone. In one sample of 'spotted' anorthosite, collected at ±15cm from a 'sharp' contact zone, several small olivine grains were observed. The relationship between these olivine crystals and the variation in mineral

chemistry across the 'sharp' contact zones are examined in chapter 5. The 'pods' of ultramafic pegmatite, which have somewhat gradational contacts, are separated from the 'spotted' anorthosite by a very coarse-grained zone consisting largely of plagioclase and olivine (Fig.8). The ultramafic pegmatite itself contains olivine and clinopyroxene, but the contact areas are largely devoid of clinopyroxene grains.

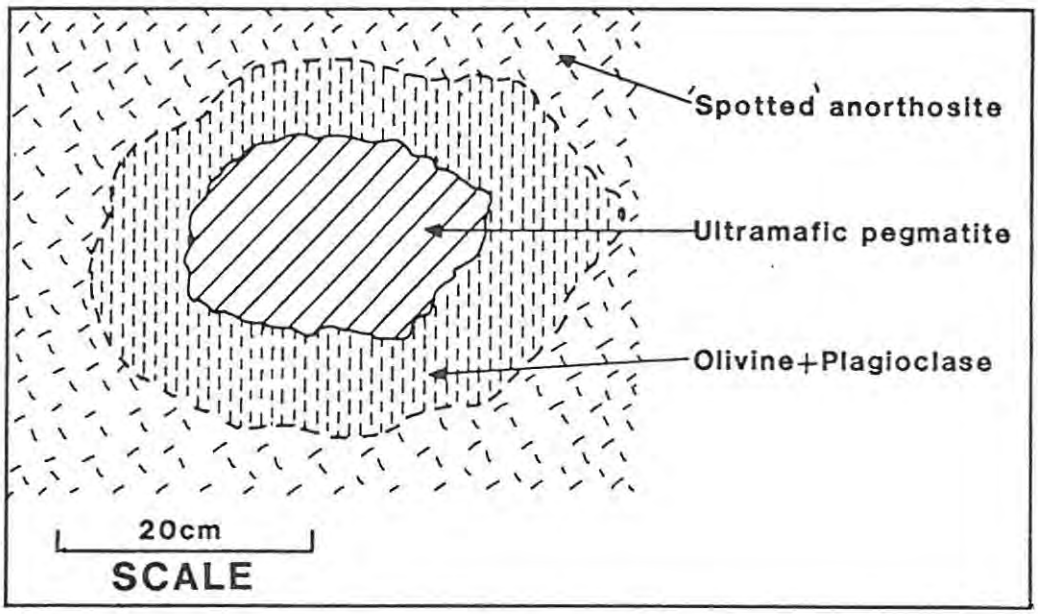

Figure 8. Field sketch showing a pod of ultramafic pegmatite adjacent to the main body of the pegmatite, hosted by 'spotted' anorthosite.

The marginal zone rocks in general, exhibit a smaller grain-size range and contain a higher proportion of clinopyroxene in comparison with the central zone samples. Their grain-size is usually less than 8mm, while olivine and clinopyroxene are present in more or less equal amounts. A characteristic feature of the marginal zone clinopyroxene grains is the development of multiple twinning parallel to (100), which appears to be of a polysynthetic nature (Fig.9(f)). The number of twinned grains decreases with increasing distance from the pipe margins and are uncommon in samples of the central zone. The rocks of TLP.5 also contain multiply twinned clinopyroxene grains, which suggests that the borehole may be sited towards the margin of the pipe. The aggregates of small polygonal olivine and clinopyroxene grains described from the central zone samples are also present in the marginal zone rocks. The 'reaction-replacment' textures observed in the central zone pegmatite, in which clinopyroxene appears to be replacing olivine, are also present in the wehrlite from borehole TLP.1, but are not as well defined in the underground sample suite.

The ultramafic rocks from 6 level haulage contain accessory amphiboles, opaque oxides, apatite, biotite and chlorite in much greater quantitites than samples from other localities. The amphiboles include hornblende, tremolite and actinolite, while the opaque oxides inlcude ilmenite, Ti-magnetite and minor chromite. Additional phases noted include plagioclase, clinozoisite, ilvaite and sulphide minerals. The plagioclase grains are mostly embayed and somewhat saussuritized.

4.4 Alteration

The Townlands pegmatite is characterised by the presence of numerous serpentine-filled fractures and veinlets, that vary from hair-line cracks to veinlets that may exceed 5mm in width. The larger veinlets often exhibit a zoned pattern (Fig.10(c)), in which the centre of the veinlets consist of discontinuous stubby stringers of secondary magnetite, surrounded by serpentine which varies in colour from colourless to dark green or yellow-green. The serpentine itself is made up of a fine mesh-like intergrowth of interlocking needles and fibres, although in a few veinlets, a botryoidal texture was observed, suggesting chemical deposition of the serpentine. The margins of the thicker veinlets are sometimes marked by the presence of secondary magnetite, iddingsite and tremolite, while the thinner veinlets and fractures frequently form sub-parallel, anastomosing patterns. The veinlets and fractures are most abundant in the TLP.1 samples, especially towards the bottom of the borehole, but are nevertheless common throughout the pegmatite body.

The veinlets and fractures cut across the mineral grains of the pegmatite and the textural evidence indicates that they were introduced subsequent to the formation of the pegmatite. The thicker veinlets and fractures appear to define two sets, having near-vertical preferred orientations. It is possible, therefore, that these sets of veinlets and fractures may represent cooling joints, which provided the necessary permeability for the movement of fluids or volatiles that caused the partial serpentinization of the pegmatite olivine grains. The serpentinization of olivine is usually accompanied by small volume changes and this may account for the presence of the finer fractures and cracks.

The mineral phases adjacent to the serpentine-filled veinlets and fractures have undergone varying degrees of alteration. The serpentinization of olivine is the most noteable feature of the

alteration and is most severe in the vicinity of the TLP.1 layered sequence, where sepentine-filled veinlets are relatively common (Figs.10(d),(e)). The alteration of clinopyroxene is variable and usually less intense than in the case of olivine. The cores of the clinopyroxene grains are replaced by a mixture of hornblende and actinolite, needles of which nucleate along cleavage planes, while tremolite in the form of radiating sheafs and needles may rim grain margins. Similar aggregates of tremolite plus chlorite are sometimes found surrounding opaque oxides in the vicinity of 'alteration' veinlets. The occassional plagioclase grains are usually somewhat saussuritized and may contain chlorite, tremolite and clinozoisite bodies near the grain margins (Fig.10(f)). The effect of the alteration is generally localised and is confined to the immediate vicinity of fractures and veinlets.

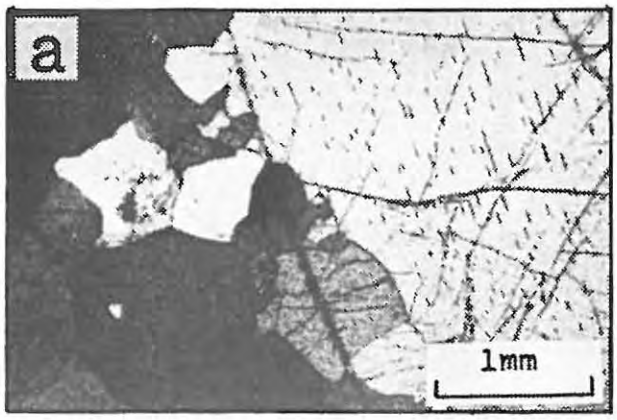
a
1mm

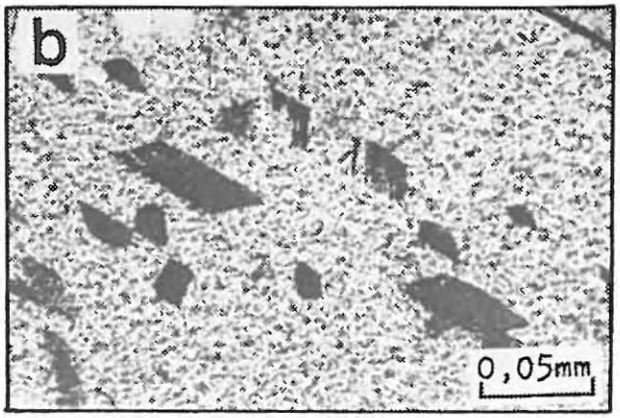
b
0,05mm

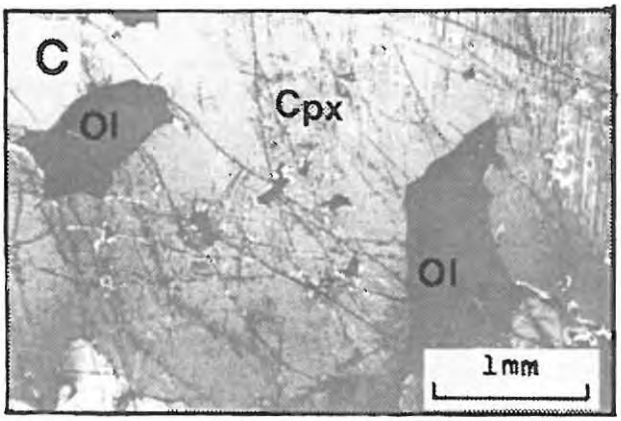
c
Ol
Cpx
Ol
1mm

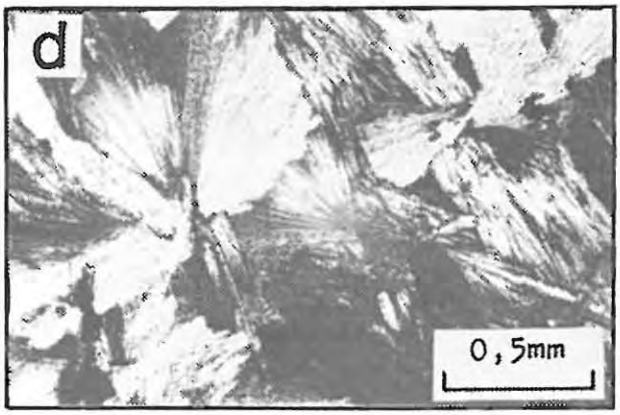
d
0,5mm

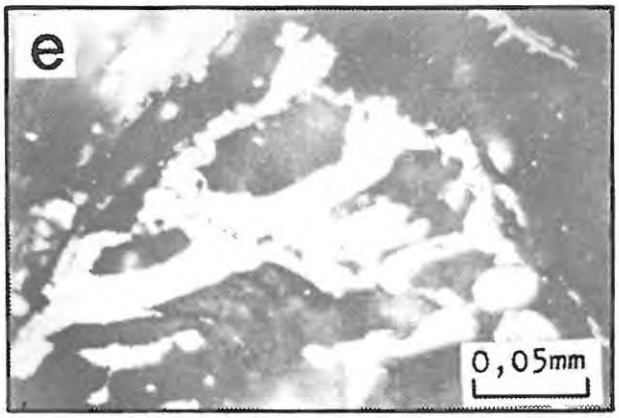
e
0,05mm

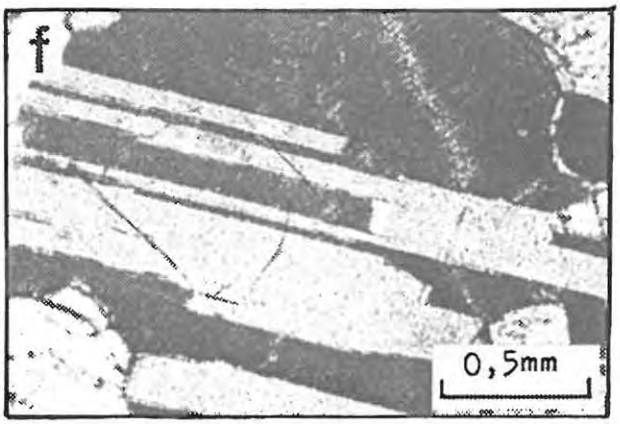
f
0,5mm

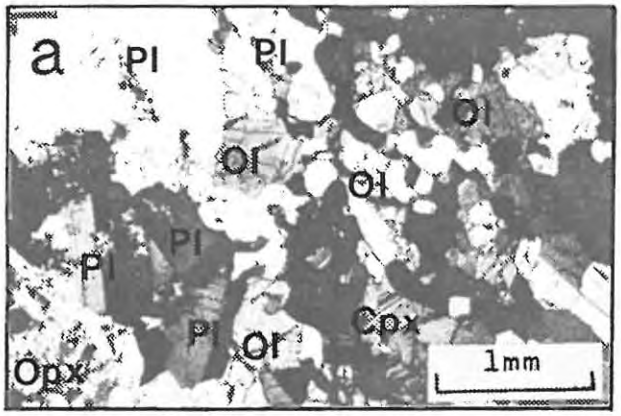
a
Pl
Pl
Ol
Or
Ol
Pl
Pl
Pl
Or
Cpx
Opx
1mm

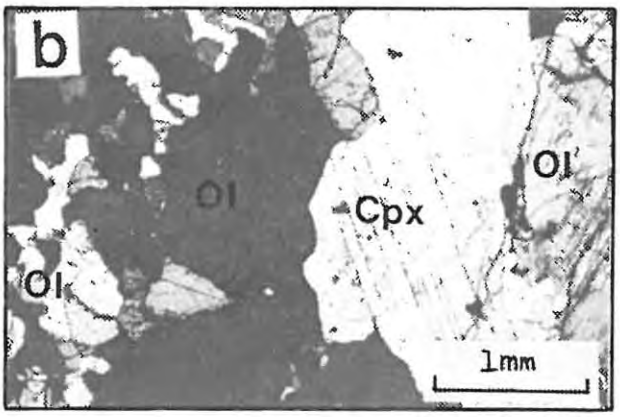
b
Ol
Ol
Cpx
Ol
1mm

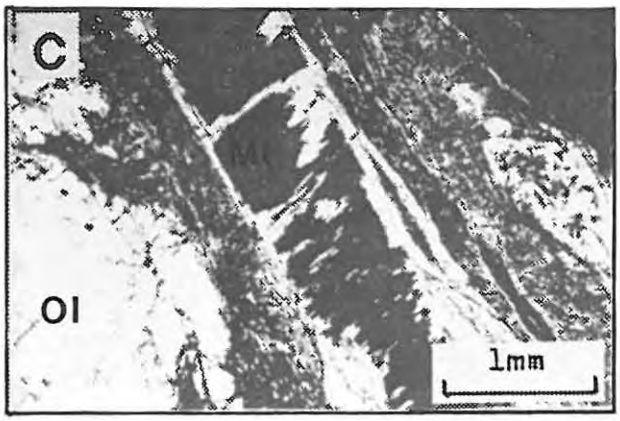
c
Ol
1mm

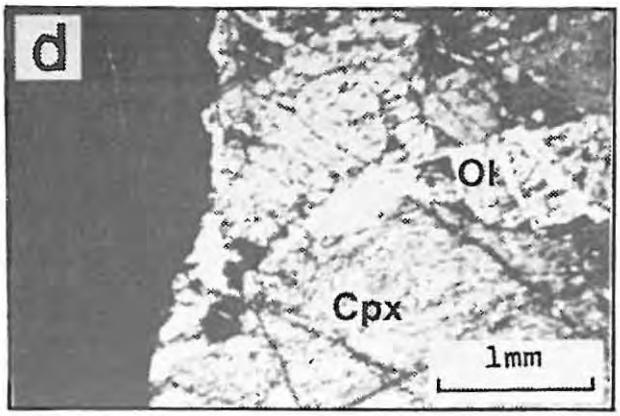
d
Ol
Cpx
1mm

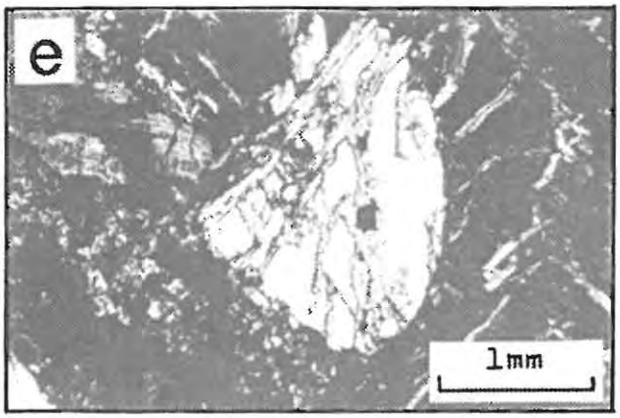
e
1mm

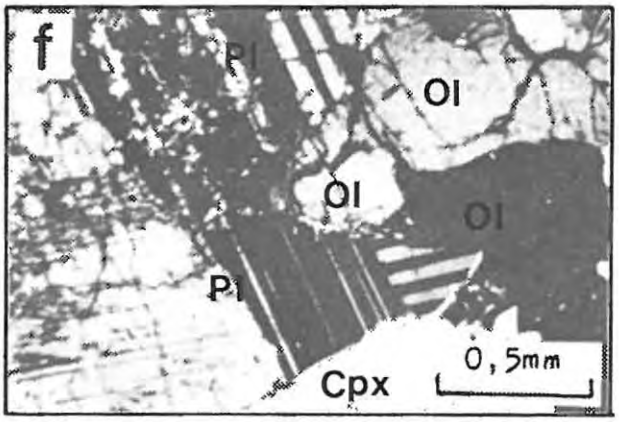
f
Pl
Ol
Ol
Ol
Pl
Cpx
0,5mm

5. SILICATE MINERALOGY

5.1 Introduction

Olivine and clinopyroxene are by far the most abundant constituents of the Townlands ultramafic pegmatite and representative electron microprobe data is presented for the two mineral phases from all sample localites. For comparative purposes, microprobe analyses were performed on several olivine, clinopyroxene and orthopyroxene grains from the associated layered rocks exposed along 6 level haulage and intersected by borehole TLP.1. Microprobe data are also presented for ilvaite. Microprobe analyses of olivine and pyroxene grains, together with a description of analytical procedures and operating conditions are given in appendix 2. The relevant sample locations are indicated in appendix 1.

The compositional and textural features of the major silicate phases (olivine + clinopyroxene) constituting the Townlands pegmatite closely resemble those of mafic igneous rocks that have crystallised from fractionated magmatic liquids. The compositional variations are also clearly illustrated by standard techniques that are generally applied to the treatment of silicate mineral data from fractionated mafic igneous rock suites. The use of such procedures is therefore followed in this chapter and the validity of this approach is discussed in section 5.5.

5.2 Olivine

Members of the olivine group are characteristic components of many mafic and ultramafic rocks. They have orthorhombic symmetry and may be represented by the chemical formula $(Mg,Fe)_2SiO_4$. The structure of the olivines, which is based on silicon-oxygen tetrahedra bonded together by divalent cations in octahedral coordination, is discussed in detail by Deer et. al. (1982). A complete solid solution series exists between the two end-members Mg_2SiO_4 (forsterite) and Fe_2SiO_4 (fayalite). The common trivalent ions Fe^{3+} and Al^{3+} are rare components of the olivine structure, but there is limited substitution of Mg and Fe by the divalent cations of Ca, Mn, Cr and Ni (Deer et. al., 1982). The occurrence of small exsolved dendritic platelets and lamellae of magnetite in many grains, however, suggests that small amounts of Fe^{3+} may have been incorporated into the olivine during crystallization.

The most noteable features of the Townlands pipe olivine crystals are their high Fe content and the existence of several distinct compositional groupings, spanning the range Fo_{31}-Fo_{67}. The olivine grains all exhibit higher Fe contents than their co-existing clinopyroxene grains, but the linear trend between their respective MMF (Mg/Mg+Fe) ratios (Fig.11), indicates the existence of an equilibrium relationship between the two phases. The grouping of the olivine compositions is best illustrated in Fig.13. The pegmatite samples from borehole TLP.2 and and 6 level haulage display a remarkable consistency in olivine composition, with an average corresponding to Fo_{32}. The olivine crystals of the TLP.1 dunite zone have intermediate compositions and range between Fo_{51} at the top and Fo_{47} near the base of the zone. The remaining borehole samples, although more variable in composition, generally plot in the vicinity of the TLP.1 dunite olivine grains.

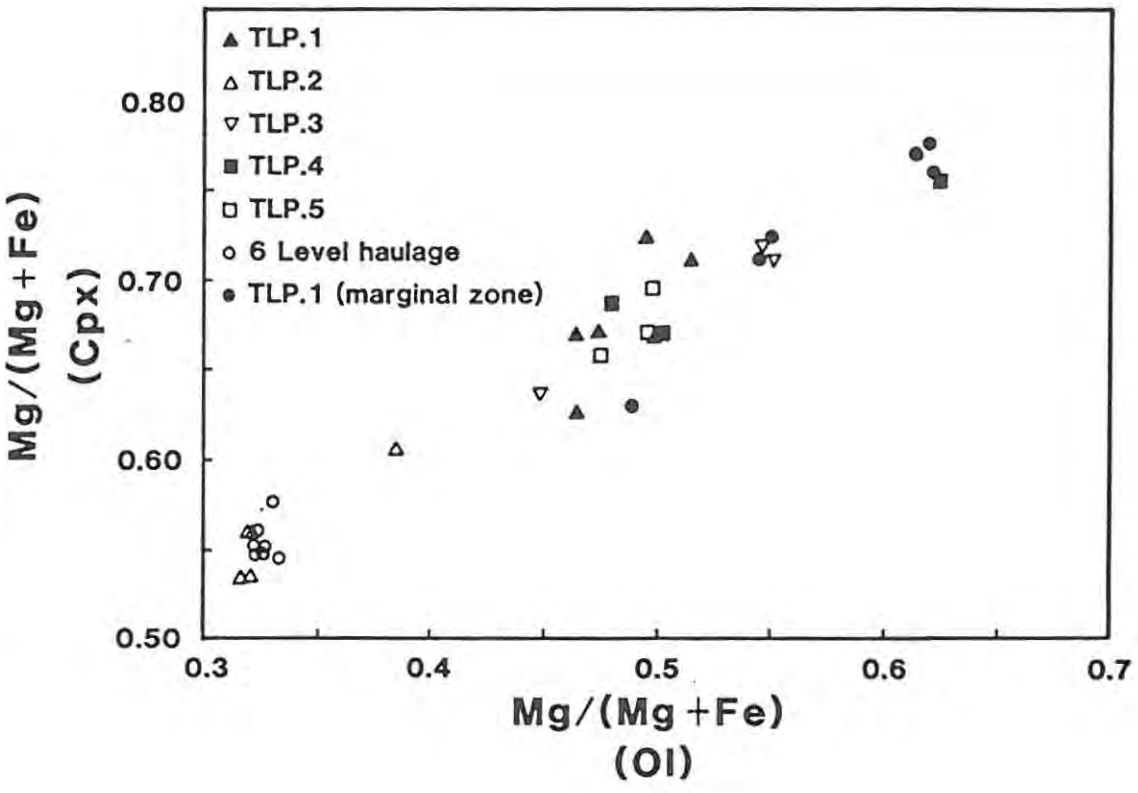

Figure 11. Diagram illustrating the linear trend between the MMF (Mg/(Mg + Fe)) ratio of olivine and that of coexisting clinopyroxene.

Two small anhedral olivine grains, hosted by 'spotted' anorthosite adjacent to pegmatitic material from 6 level haulage, were found to be chemically similar to olivine crystals from the upper critical zone that were examined by De Klerk (1982) (Fig.12). These olivine grains (Fo_{79}) may, therefore, exhibit true cumulus compositions and have not been

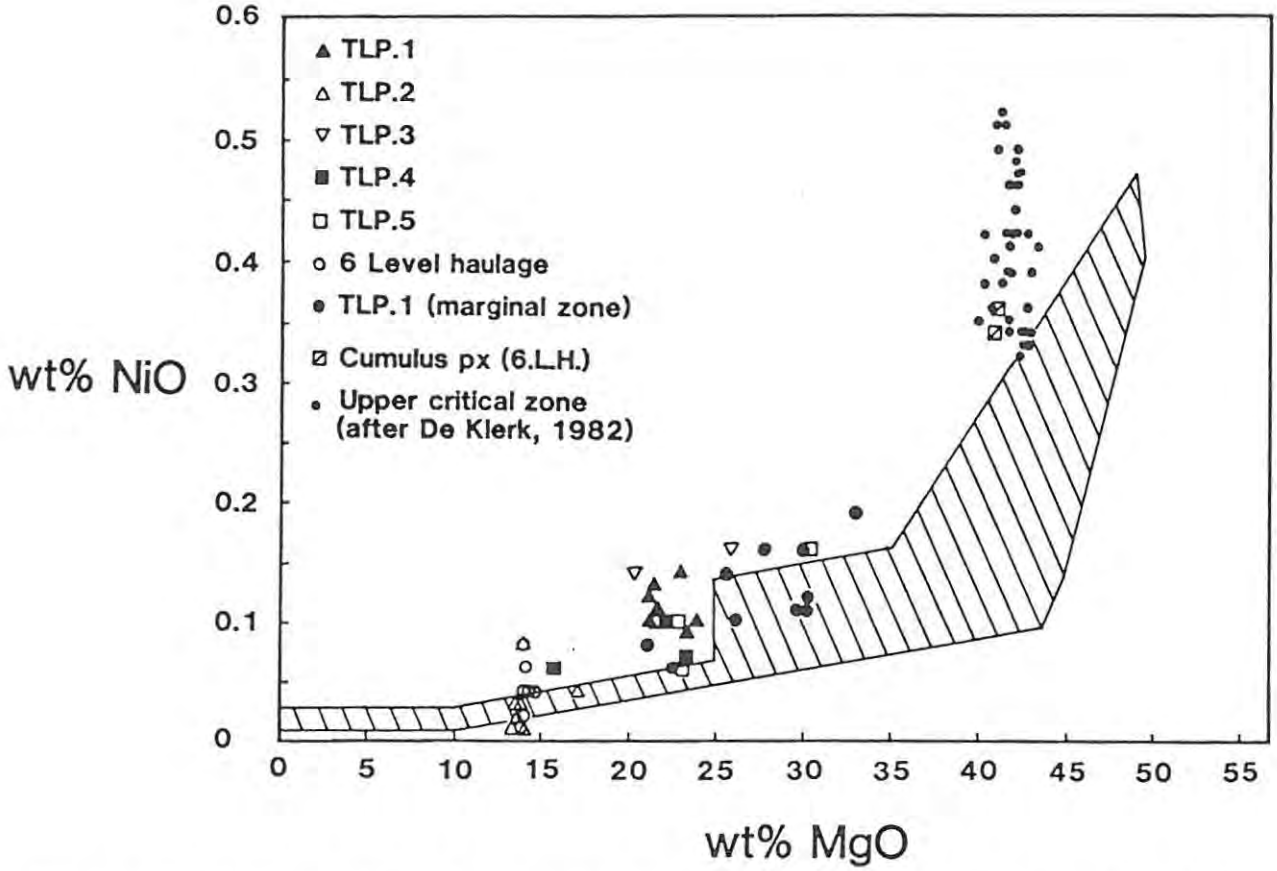

Figure 12. Plot of wt% NiO versus wt% MgO for olivine. The shaded area comprises data from a variety of basalts, diabases and layered intrusions (from Fleet et. al., 1977), defining a diffuse hyperbolic trend.

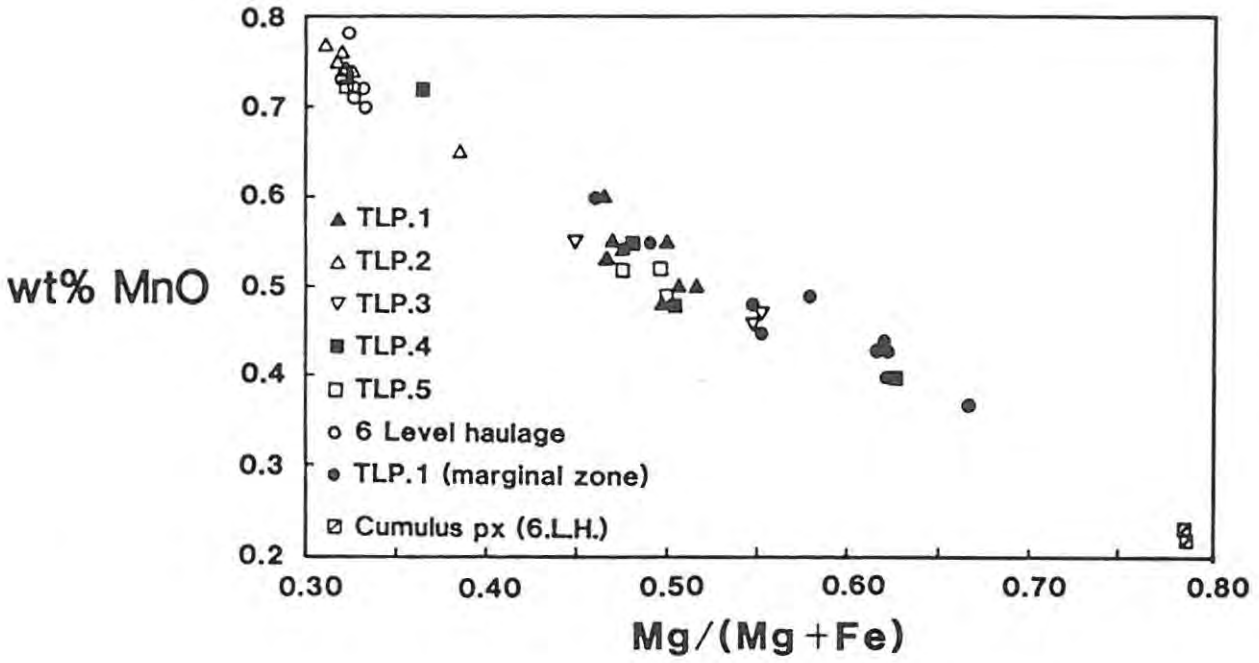

Figure 13. Plot of wt% MnO versus the MMF ratio for olivine, illustrating the linear relationship between the Mn and Fe contents.

modified during the development of the adjacent pegmatite. Olivine crystals from the TLP.1 'marginal' zone wehrlite exhibit a wide range in composition (Fo_{49} - Fo_{67}). The most Mg-rich olivine grains occur in the vicinity of the TLP.1 layered sequence, and become increasingly Fe-rich as the TLP.1 dunite zone is approached. The olivine compositions appear to define a mixing line between olivine of cumulus composition (Fo_{79}) and that of the TLP.1 dunite (Fo_{47}) (Fig.13). The existence of this intermediate compositional trend in the olivine crystals from the TLP.1 'marginal' zone, suggests that some form of reaction has occurred between the TLP.1 layered sequence and the main pegmatite body. This may have occurred either as a result of metasomatic replacement by pegmatitic fluids, or by magmatic replacement, or by the assimilation of layered material by an intrusive pegmatite melt.

The peripheral exposure of ultramafic pegmatite along 6 level haulage is characterised by a consistency in olivine composition (Fo_{32}). Microscopic examination of textural relationships indicate that the contact zones between the pegmatite and 'spotted' anorthosite are surprisingly sharp (Fig.10(a),(b)), and this is also illustrated by the olivine compositional data. The olivine and pyroxene compositions in three separate contact zones were investigated. The results revealed a constant olivine composition to within about 1cm of the contact itself. It is only over this narrow zone that the olivine was seen to change composition from Fo_{32} to Fo_{47} (Fig.14). The variations in pyroxene compositions are discussed in section 5.3.

The olivine crystals in a small pod of ultramafic pegmatite adjacent to the main body were also analysed. The pod exhibits a coarsely pegmatitic gradational contact between the pegmatite and 'spotted' anorthosite (Section 4.3). The pegmatite core of the pod is very serpentinized, but analyses of olivine grains in the vicinity of the contact zone yielded compositions ranging from Fo_{46}, near the core of ultramafic pegmatite, to Fo_{50}, adjacent to the surrounding 'spotted' anorthosite.

Of all the minor elements that substitute for Mg and Fe in olivine, Ni has received most attention in the literature. The preferential fractionation of Ni relative to Mg into olivine has been noted by a number of authors, inter alia Wager & Mitchell (1951), Simkin & Smith (1970) and Fleet et. al. (1977). This behaviour of Ni in olivine is, however, contrary to the Goldschmidt and Ringwood rules for the

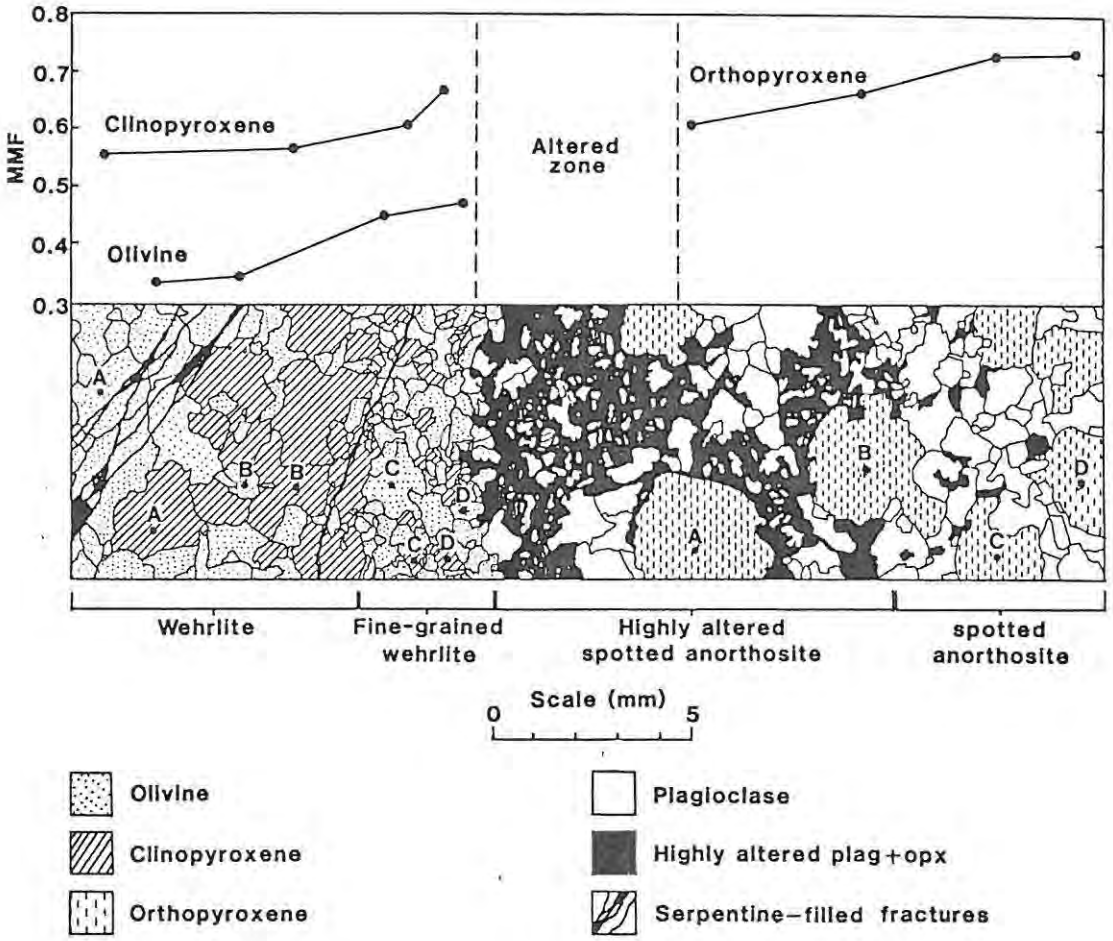

Figure 14. Schematic representation of a 'sharp' contact zone from the exposure along 6 level haulage, illustrating the changes in mineral composition across the contact zone. Microprobe analytical positions are indicated by the dots (Sample TU60).

partitioning of minor elements (Burns, 1970). In terms of these rules, Mg possesses the more suitable ionic radius and electronegativity for incorporation into the olivine structure. Burns & Fyfe (1966) and Burns (1970) suggested that the partitioning of Ni into olivine may be explained in terms of crystal field theory. The Ni^{2+} ion exhibits a high octahedral site preference energy and if the co-existing magma contains abundant tetrahedral sites, Ni will partition preferentially into early-formed Mg-rich olivines. Burns & Fyfe (1966) postulated that melts rich in silica and alkalis will contain a large array of tetrahedrally coordinated sites, which was more or less confirmed by the experimental investigations of Irvine & Kushiro (1979). Gunn (1971) demonstrated that the octahedral site preferences of olivine crystals in the Kilauea Iki were in the order Ni > Mg > Co > Fe > Mn > Zn.

The partitioning of Ni may be described in terms of partition or distribution coefficients and there has been extensive experimental investigation into this subject by workers such as Mysen (1978), Hart & Davis (1978), Leeman & Lindström (1978) and Takahashi (1978). These studies yielded controversial results and although the distribution coefficient of Ni for olivine is probably high, it appears to be variously dependent on temperature, bulk composition, pressure and Ni-content of the magma. A high distribution coefficient of Ni for olivine would cause a rapid depletion in the Ni content of a melt co-existing with early-formed Mg-rich olivine. Consequently, Fe-rich olivine, crystallizing at a later stage would be expected to have low Ni contents. Fleet et. al. (1977) compiled a diagram of NiO versus MgO for olivine from a wide range of basalts, diabases and layered intrusions, which revealed a diffuse exponential variation of NiO with MgO content (Fig.12). Included in Fig.12 are the analyses of pegmatite olivines from the various sample localites, cumulus olivine from the upper critical zone as determined by De Klerk (1982), and the two olivine analyses from the 'spotted' anorthosite samples of 6 level haulage. Olivine grains from the pegmatite exhibit low NiO and MgO contents, and generally appear to conform to the hyperbolic trend shown in Fig.12, although Fleet et. al. (1977) present limited data for intermediate Fe-rich olivine compositions.

Other important minor elements that substitute for Mg and Fe in olivine include Mn, Ca, and Cr. According to Deer et. al. (1982), Mn and Ca are more common in Fe-rich olivine, while Cr and Ni favour Mg-rich olivine. The Cr_2O_3 content of olivine is usually < 0.05 wt percent and seldom exceeds 0.01wt percent (Deer et al., 1982). As a result, Cr_2O_3 was not determined for the Townlands pipe olivine crystals. The majority of the pegmatite olivine crystals contain between 0.04 and 0.15 wt percent CaO, and inspection of the data showed that no correlation exists between CaO content and that of the major elements. Simkin & Smith (1970) presented microprobe data for a wide range of olivine compositions and noted that most plutonic rocks contain < 0.14wt percent CaO, but as in the present study, display little relationship to major element trends. The MnO content of the pegmatite olivine varies between 0.22 and 0.78wt percent. In Fig.13 the MnO content is plotted against the MMF ratio of the analysed olivine grains, revealing a strong positive correlation with Fe content. Simkin & Smith (1970) reported a similar trend which they

attributed to crystal-chemical controls, with variables such as pressure, temperature and bulk composition exerting a lesser affect.

5.3 Pyroxene

Pyroxenes are one of the most important of the mineral groups found in mafic and ultramafic rocks. The Ca-poor orthopyroxenes of the (Mg, Fe) SiO_3 series have orthorhombic symmetry, while the rest of the group are monoclinic. Most pyroxenes can be considered as part of the 4 component system $CaMgSi_2O_6$ (diopside), $CaFeSi_2O_6$ (hedenbergite), $Mg_2Si_2O_6$ (clinoenstatite) and $Fe_2Si_2O_6$ (clinoferrosilite), within which complete solid solution exists between diopside, hedenbergite and augite (Deer et. al. 1978). The structure pertaining to the various members of the pyroxene group is discussed at length by Deer et. al. (1978). It consists essentially of SiO_4 tetrahedra linked by 2 out of 4 corners to form continuous chains bonded together by cations occupying two slightly different sites, M1 and M2. The coordination of the M1 site is octahedral, while that of the M2 site may be 6-fold or 8-fold, depending on the ion present.

The chemical formula for the pyroxene group, as proposed by Berman (1937) and modified by Hess (1949), may be represented by:

$$(W)_{1-p}\ (X, Y)_{1+p}\ Z_2\ O_6$$

where W = Ca, Na; X = Mg, Fe^{2+}, Mn, Ni, Li; Y = Al, Fe^{3+}, Cr, Ti and Z = Si, Al.

The value of p varies between 0 and 1 in the Ca-rich pyroxenes and approximates 1 in the Ca-poor pyroxenes. There are a large variety of substitution possibilities for the pyroxene structure, but the replacement combinations are limited by the sum of the ionic charges of the W, X, Y and Z groups, which must equal 12 (Deer et. al., 1978).

The fractionation trends exhibited by large mafic and ultramafic intrusive bodies can be expressed in terms of pyroxene composition, as has been done by many workers, inter alia Brown (1957), Atkins (1969) and Eales & Booth (1974). Consequently, the major and minor element distributions of the Townlands pipe pyroxene crystals were investigated to determine whether any variations might be consistent with their having

crystallized from a melt. Pegmatite clinopyroxene compositions from all sample localities, together with cumulate clino- and orthopyroxene compositions are plotted on a Ca-Mg-Fe ternary diagram (Fig.12). Also represented is the differentiation trend established for clinopyroxene crystals from the Bushveld Complex by Atkins (1969).

Fig.15 reveals a similar grouping of the clinopyroxene data to that established for olivine. The samples from TLP.2 and 6 level haulage again represent the most Fe-rich compositions ($Wo_{45}\ En_{30}\ Fs_{25}$), while the clinopyroxene grains from the TLP.1 dunite zone exhibit compositions averaging $Wo_{45}\ En_{37}\ Fs_{18}$. The clinopyroxene crystals of the other 3 boreholes (TLP.3, TLP.4 and TLP.5) exhibit a wide compositional range, but generally plot in the vicinity of the TLP.1 samples. The analysed cumulus clinopyroxene grains plot close to the Bushveld Complex differentiation trend of Atkins (1969), which displays a gradual decrease in Ca content with increasing fractionation towards more Fe-rich compositions. In contrast, the pegmatite clinopyroxene grains show a marked deviation from this trend, towards more Ca-rich compositions. The persistence of high Ca levels, despite a significant increase in Fe-content of the TLP.2 and 6 level haulage samples, is difficult to reconcile, but a possible explanation may be related to the general absence of plagioclase as a co-existing Ca-bearing phase. The significance of the low plagioclase content of the Townlands pegmatite is discussed in more detail in chapter 8.

The compositions of clinopyroxene grains from the TLP.1 'marginal' zone, in sympathy with the variations in olivine composition, lie along a mixing line between the cumulus compositions and those of the TLP.1 dunite. This mixing trend is also illustrated in the clinopyroxene variation diagrams presented in this section (Figs.16-20), and reinforces the idea of reaction between the TLP.1 layered sequence and adjacent pegmatitic material, described in section 5.2. A number of orthopyroxene analyses from the TLP.1 layered sequence are also plotted in Fig.15. The samples in the vicinity of the UG2 horizon have an average composition of $Wo_2En_{77}Fs_{21}$, which approaches that of the orthopyroxene grains in unaltered 'spotted' anorthosite from 6 level haulage. As the pegmatite is approached, the orthopyroxene grains become progressively more Fe-rich, until a maximum of $Wo_2En_{65}Fs_{33}$ is attained.

Figure 15. Ca-Mg-Fe plots of clinopyroxene from the ultramafic pegmatite and adjacent layered sequence, and orthopyroxene from the layered rocks exposed in 6 level haulage and borehole TLP.1.

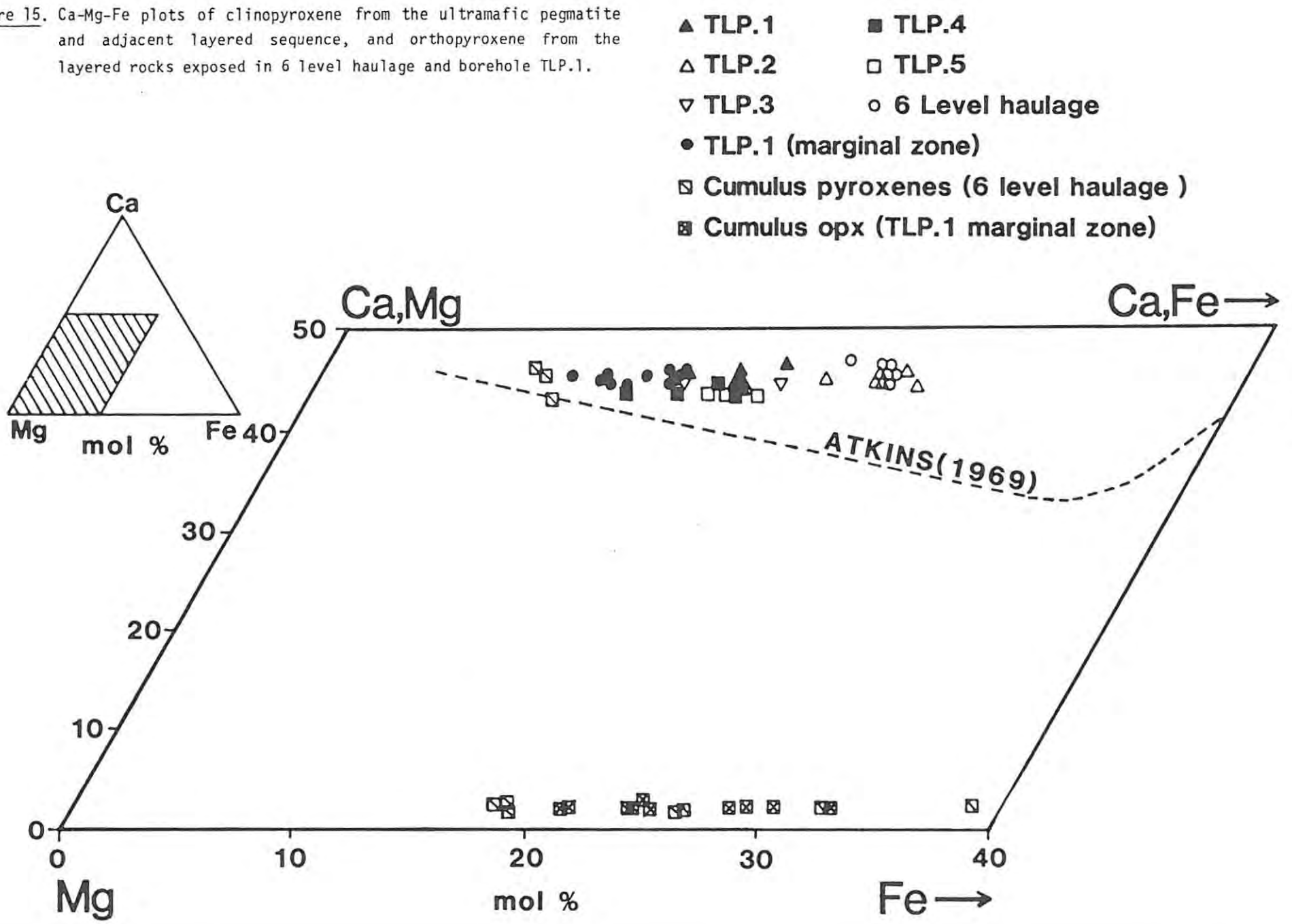

The 'sharp' contact zones from 6 level haulage that were analysed for changes in olivine chemistry, were also analysed in terms of pyroxene chemistry, and similar results were obtained (Fig. 14). The clinopyroxene grains of the ultramafic pegmatite maintain a fairly uniform composition to within about 1cm of the contact. Thereafter, they become progressively more Mg-rich across the $\pm$1cm zone as the adjacent 'spotted' anorthosite is approached. Their composition varies from $Wo_{44}En_{31}Fs_{25}$ to $Wo_{44}En_{38}Fs_{18}$ at the contact. Several orthopyroxene crystals from the 'spotted' anorthosite side of the contact were also analysed (Fig.15) and display a predictable sharp increase in Fe-content where they are in contact with pegmatitic material. The orthopyroxene composition changes progressively from $Wo_3En_{59}Fs_{38}$ at the contact to $Wo_3En_{79}Fs_{18}$, which is typical of the orthopyroxene compositions in the adjacent layered suite of the Bushveld Compex (R.N. Scoon, pers. comm.). The variations in composition occur across a zone, 1-2cm in width, at the contact.

The most important minor elements that substitute for Ca, Mg, Fe and Si in the pyroxene structure are Na, Al and the transition elements Mn, Cr, Ti and Ni (Deer et. al., 1978). The relative partitioning of the minor elements into the pyroxene structure depends on their respective ionic radii, electronegativities, crystal field stabilisation energies (CFSE) and charge balance (Campbell & Borley, 1974). The CFSE is most important in the case of the transition elements and for divalent cations in octahedral coordination it increases in the order $Mn \rightarrow Fe \rightarrow Co \rightarrow Ni$, while for the trivalent ions $Cr > V > Ti > Fe > Al$ (Burns, 1970).

Most of the aluminium (Al^{3+}) present in the pyroxene lattice substitutes for Si^{4+} occupying tetrahedral sites, which creates a charge imbalance that may be eliminated by the simultaneous entry of Cr^{3+}, Ti^{4+}, Fe^{3+} or Al^{3+} into octahedral sites (Campbell & Borley, 1974). The pyroxene analyses listed in appendix 2 are recalculated on the basis of 6 oxygens and deficiencies in the Z group are made up by the addition of Al. The pegmatite clinopyroxene crystals have relatively low Al contents, which range from 1.0 to 2.1wt percent Al_2O_3. In Fig.16, weight percent SiO_2 is plotted against Mg/(Mg+Fe) (MMF ratio) and indicates that those samples with low SiO_2 values exhibit correspondingly high Al_2O_3 levels (Fig.17), and vice versa. This trend is in agreement with the observations of Schweitzer et. al. (1979), who noted that a decrease in the SiO_2 content of

pyroxenes is compensated by an increase in tetrahedrally coordinated Al, thereby creating a charge imbalance.

Chromium in the form of Cr^{3+} has a very high CFSE, and Duke (1976) calculated distribution coefficients for Cr^{3+} in clinopyroxene ranging from 8 to 36. Chromium therefore partitions strongly into early-formed clinopyroxene and, according to Deer et. al. (1978) occurs in only trace amounts in clinopyroxene containing more than 15% of the $FeSiO_3$ component. Chromium favours the trivalent state and in substituting for Mg^{2+} or Fe^{2+}, requires contemporaneous replacement of Si^{4+} by Al^{3+} or the entry of Na^{+} into a W site (Campbell, 1977). The pegmatite clinopyroxene grains, with the exception of those from the

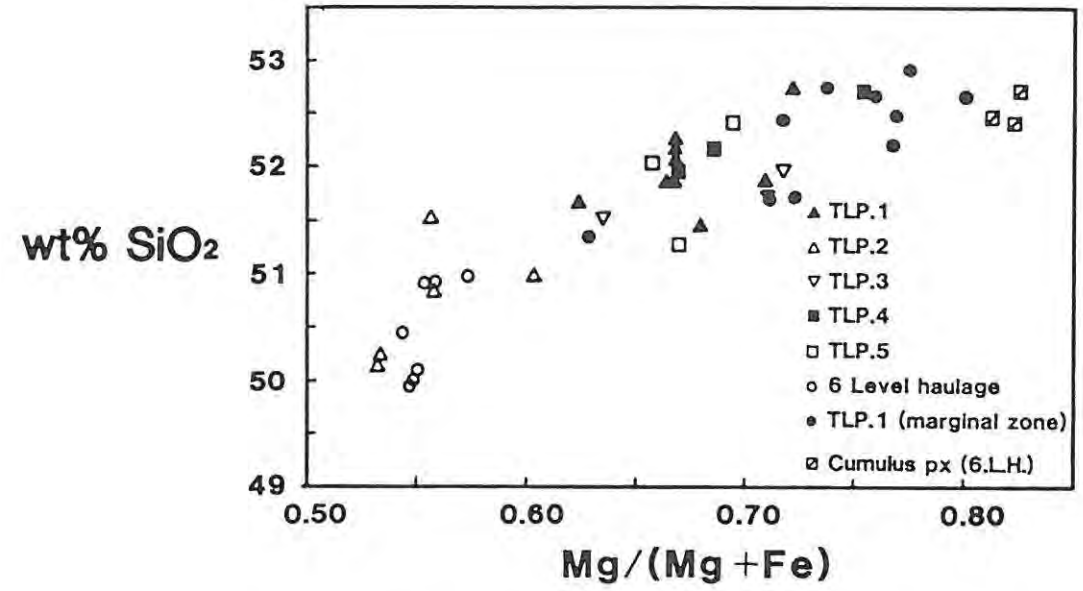

Figure 16. Plot of wt% SiO_2 versus the MMF ratio for pyroxene grains.

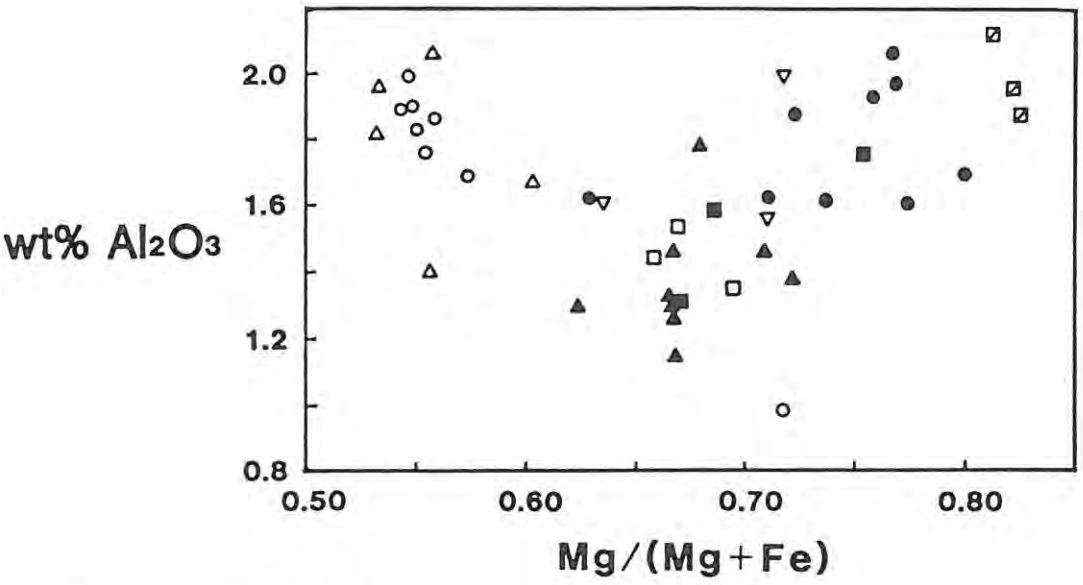

Figure 17. Plot of wt% Al_2O_3 versus the MMF ratio for pyroxene grains.

TLP.1 'marginal' wehrlite, have Cr_2O_3 contents not exceeding 0.2wt percent (Fig.18). In contrast, the analysed cumulus grains contain 0.7-0.8wt percent Cr_2O_3, which suggests that if the pegmatite pyroxene crystals crystallised from a fractionated liquid most of the Cr must have been depleted during prior crystallisation.

The low Cr content of the pegmatite pyroxene crystals cannot, therefore, account for the charge imbalance created by the substitution of Si^{4+} by Al^{3+}. Microprobe analyses do not distinguish between Fe^{2+} and Fe^{3+} present in the clinopyroxene structure. The abundance of Fe^{3+}, although rarely exceeding 3 wt percent Fe_2O_3 (Atkins, 1969; Deer et. al., 1978), will undoubtedly compensate for a fair proportion of the charge imbalance. The remaining charge imbalance, therefore, requires the presence of Ti^{4+} or Al^{3+} in octahedral sites.

Titanium favours the 4+ valence state in octahedral coordination, but has zero CFSE (Burns, 1970). Consequently, in the early stages of pyroxene crystallisation, Ti^{4+} must compete with Cr^{3+} for octahedral sites and only becomes important once most of the Cr has been removed from the melt (Campbell & Borley, 1974). The clinopyroxene grains of TLP.2 and 6 level haulage exhibit the highest Al_2O_3 contents (Fig.17) and consequently the highest concentration of TiO_2 of all the pegmatite samples (Fig.19). The cumulus clinopyroxene grains, in general, exhibit the lowest TiO_2 and Al_2O_3, while those of the other sample localities contain intermediate levels. The substitution of Ti^{4+} into 6-fold sites is, therefore, important in maintaining charge balance for the pegmatite clinopyroxenes.

The inclusion of Mn^{2+} and Ni^{2+} in the pyroxene lattice requires no charge balance equilibration. Ni^{2+} has a high CFSE and partitions strongly into early-formed olivine and pyroxene, becoming depleted in the melt with increasing fractionation (Campbell & Borley,1974). This behaviour is reflected in the very low NiO contents of the pegmatite pyroxene grains, which do not exceed 0.04wt percent NiO. Divalent manganese (Mn^{2+}) has zero CFSE (Burns, 1970) and only becomes important in Fe-rich pyroxene. In addition, Mn^{2+} has a similar ionic radius to Fe^{2+}, but is larger than Mg^{2+} (Campbell & Borley, 1974), which probably accounts for the positive correlation between MnO and FeO displayed in Fig.17.

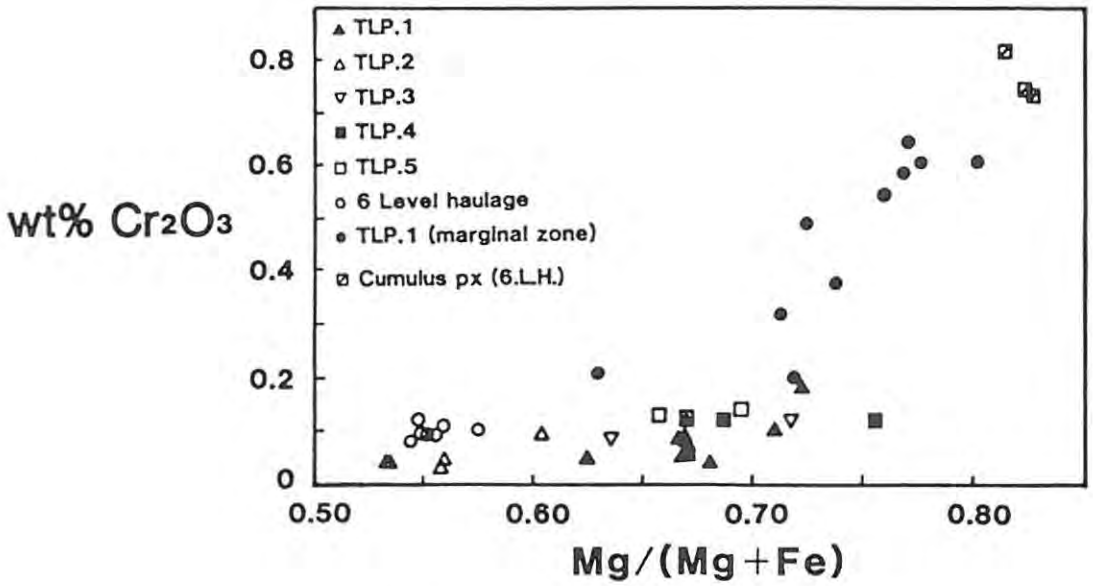

Figure 18. Plot of wt% Cr_2O_3 versus the MMF ratio for pyroxene.

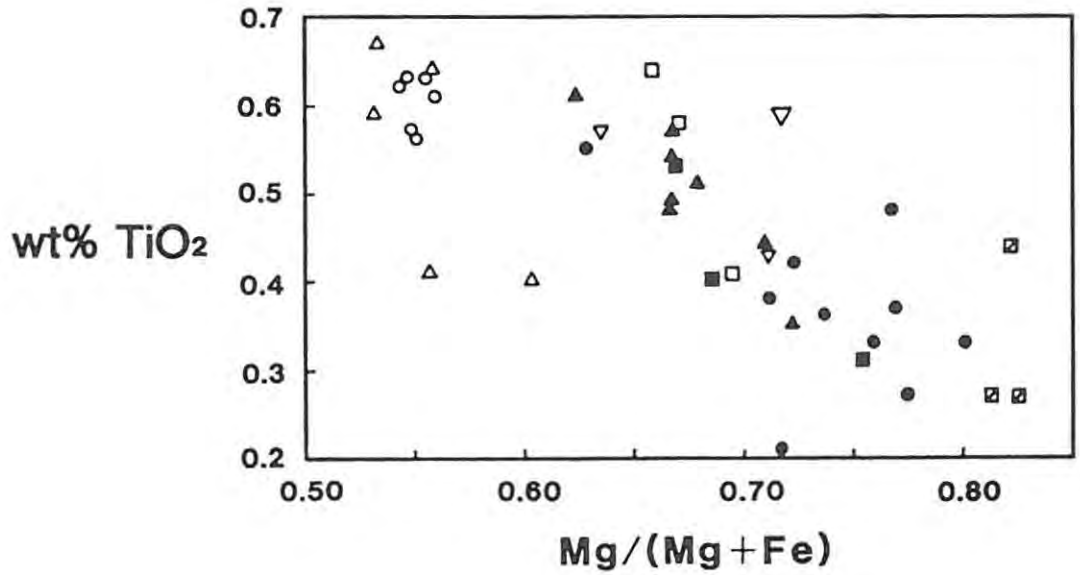

Figure 19. Plot of wt% TiO_2 versus the MMF ratio for pyroxene.

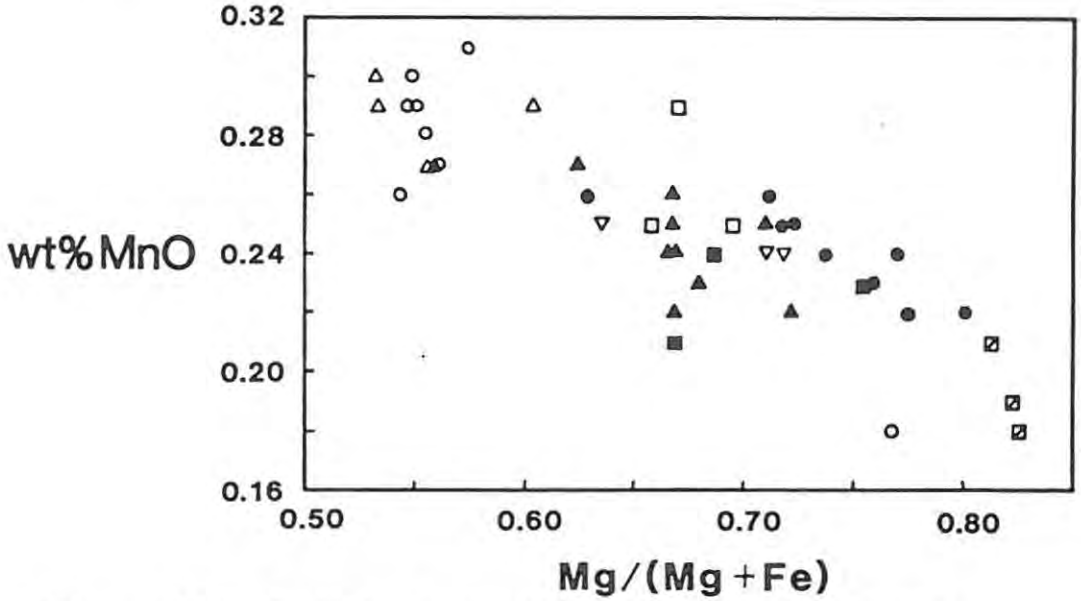

Figures 20. Plot of wt% MnO verus the MMF ratio for pyroxene.

The Na_2O content of most augite grains varies between 0.3 and 0.7wt percent (Deer et. al., 1978), but according to Brown (1957) decreases during fractionation. The Na_2O content of the pegmatite clinopyroxene grains ranges between 0.03 and 0.30 wt percent Na_2O, and exhibits no direct relationship to major element trends. The low Na_2O levels would, therefore, have had little effect on any charge imbalance.

5.4 Ilvaite

Ilvaite is a relatively uncommon hydrated calcic-ferrous-ferric silicate, usually occurring as a late stage mineral in Ca-Fe-Si skarn deposits (Burt, 1971). The ideal chemical formula, as proposed by Leonard et. al. (1962), is $Ca(Fe^{2+},Mn,Mg)_2(Fe^{3+},Al)(SiO_4)_2OH$. The structure is made up of isolated Si_2O_7 groups linked by infinite chains of edge-shared $(Fe^{2+}, Fe^{3+})O_5OH$ octahedra, to a 3-dimensional framework (Beran, 1980). Ilvaite exhibits a wide compositional range in which Mn is the most variable element. Leonard et. al. (1962) noted that Mn ranges between 0.3 and 11.9wt percent MnO, while alumina may vary between <0.02 and 6.74wt percent. Plimer & Ashley (1978) described an ilvaite containing 13.5wt percent MnO, in which the Mn substitutes for Fe^{2+} in the ilvaite lattice.

Although most typically found in skarn deposits, ilvaite has also been reported in mafic igneous intrusions. Desborough & Amos (1961) concluded that the ilvaite present in olivine diabase, olivine gabbro and gabbro from Missourri is a late magmatic mineral, unrelated to deuteric or hydrothermal solutions. Naslund et. al. (1983) examined the occurrence of ilvaite from the upper part of the Skaergaard intrusion of East Greenland and suggested that the mineral is an alteration product of fayalitic olivine. Ilvaite has also been reported from the upper zone of the Bushveld Complex by Willemse (1969b) and Reynolds (in press). Reynolds (in press) noted that the ilvaite is also present as an alteration product of fayalitic olivine, its mode of occurrence being similar to those in the Skaergaard intrusion. The Skaergaard ilvaite grains are usually associated with serpentine and a similar relationship was observed for the ilvaite grains of the Townlands pegmatite. The mineral is opaque in thin section, but exhibits a low reflectivity and strong anisotropy from grey-blue to orange/red. It occurs as small, anhedral grains and aggregates associated with serpentine. It can, therefore, be found adjacent to serpentinised olivine, along

serpentine-filled cracks and veinlets, and in the vicinity of sulphide bodies rimmed by serpentine and secondary magnetite. Representative microprobe analyses of ilvaite grains from 2 samples are presented in table 2. The pegmatite ilvaite crystals contain significantly more Mg than those of the Skaergaard intrusion, which may be a result of the higher Mg content of the pegmatite olivine grains compared to the Fe-rich fayalitic olivine grains of Skaergaard.

	TLP.5/5	TLP.1/32	Theoretical
SiO_2	29.77	30.67	29.40
TiO_2	0.02	0.02	-
FeO	34.02	33.25	35.15
Fe_2O_3	18.90	18.48	19.53
MnO	1.10	0.75	-
MgO	1.31	3.41	-
CaO	13.04	12.64	13.72
H_2O	2.11	2.17	2.20
TOTAL	100.27	101.45	100.00
Cations per 9 oxygens			
Si	2.12	2.13	2.00
Ti	0.00	0.00	-
Fe^{2+}	2.03	1.93	2.00
Fe^{3+}	1.01	0.96	1.00
Mn	0.07	0.04	-
Mg	0.14	0.35	-
Ca	1.00	0.94	1.00
H	1.00	1.00	1.00
	7.37	7.35	

Al_2O_3 0.05%
Fe^{2+}/Fe^{3+} assumed to be 2/1; H_2O calculated on the basis of $1H^+$ per 9 oxygens (After Naslund et. al., 1983).

Table 2. Electron microprobe analyses of ilvaite.

Burt (1971) postulated that ilvaite crystallises under conditions of high fH_2O, low fCO_2 and moderate temperatures. Naslund et. al. (1983) concluded that the formation of the Skaergaard ilvaites was facilitated, by the removal of MgO and FeO from olivine grains and the addition of CaO, H_2O and O_2, by circulating hydrothermal fluids. Burt (1971) also attributed the rareity of ilvaite to the fact that retrograde reactions usually occur in the presence of Mg and Al, both of which are largely incompatible in the ilvaite structure. It appears likely, therefore, that late-stage hydrothermal fluids caused the partial

serpentinisation of the Fe-rich Townlands pipe olivine grains, thereby creating the necessary environment for the formation of ilvaite, whether by direct crystallisation or by alteration of olivine.

5.5 Discussion

The dominant silicate minerals of the Townlands pegmatite are homogeneous, well-annealed phases indicative of a high temperature origin. Furthermore, they have compositions that are analogous to those of mafic igneous rocks that have crystallised from a fractionated magmatic liquid. Consequently, the discussion of the mineral compositions in terms of a fractionating melt appears to be justified and illustrates that the olivine and clinopyroxene, which have high iron contents and characteristic minor element variations, could be interpreted as having been derived from a melt that has undergone considerable fractionation.

The existence of distinct compositional groupings within the pegmatite may be significant in terms of the morphology of the pipe. The similarity in mineral composition between the TLP.2 and 6 level haulage samples, as well as between those of TLP.1, TLP.3, TLP.4 and TLP.5 may indicate that the Townlands pipe consists of two or more adjoining pegmatite bodies of differing composition. This suggestion is, however, tentative and additional sampling of other areas is required to resolve the situation. The silicate mineralogical evidence also indicates that the contact between the main pegmatite body and the surrounding layered suite is generally very sharp. In addition, the 'spotted' anorthosite exposed in 6 level haulage is unaffected by pegmatitic material, except in the area immediately adjacent to the contact. These features are difficult to reconcile in terms of a metasomatic replacement origin, as has been suggested for other such bodies by Cameron & Desborough (1964) and Schiffries (1982). On the basis of the available data the only part of the Townlands pegmatite that might be interpreted as being of replacement origin is the TLP.1 'marginal' zone, which appears to have formed by reaction between the layered sequence and pegmatitic material. A model for the genesis of the pipe will not, however, be considered at this stage, and the discussion is resumed in chapter 9, after consideration of other aspects of the pegmatite.

6. OXIDE MINERALOGY

6.1 Introduction

The oxide minerals of the Townlands pegmatite, although present only as accessories, are nonetheless important as petrogenetic indicators. A distinction is made between the oxides within the main body of the pegmatite and those associated with the chromitite leader layers in contact with the TLP.1 'marginal' zone. Ilmenite was found to be the dominant oxide phase within the pegmatite, with Ti-magnetite being common only in samples from borehole TLP.2 and 6 level haulage. Representative microprobe analyses of Cr-spinels, Ti-magnetite and ilmenite, together with the appropriate analytical conditions are presented in appendix 2. The locations of the various samples analysed is indicated in appendix 1.

6.2 The Spinel Group

The spinel group of oxide minerals is extremely variable in terms of composition, due largely to a highly flexible structure, which is able to accommodate at least 30 different elements with valence states from +1 to +6 (Lindsley, 1976). The spinels have cubic symmetry and a face-centred unit-cell containing 32 oxygen ions. The structure, as discussed by Deer et. al. (1962) and Lindsley (1976), consists essentially of alternating layers of cations and oxygen anions, where cation layers have cations in both octahedral (B) and tetrahedral (A) coordination. The spinels may be represented by the general formula $R^{2+}_{8}\ R^{3+}_{16}\ O_{32}$, but occur in two structural types, namely 'normal' and 'inverse', with the following ion distributions:

Normal : $8R^{2+}$ in A, $16R^{3+}$ in B
Inverse : $8R^{3+}$ in A, $8R^{2+} + 8R^{3+}$ in B (Deer et. al., 1962).

Most spinels encountered in natural systems are, however, intermediate between the two structural types (Lindsley, 1976). The spinel group may be subdivided on the basis of the dominant R^{2+} and R^{3+} ions present, as depicted by the Steven's prism (Fig.21), within which 3 basic groups forming the spinel (Al), magnetite (Fe^{3+}) and chromite (Cr) series, may be recognised (Deer et. al., 1962). Members of the spinel group not included in these series are maghemite (γ-Fe_2O_3) and ulvöspinel (Fe_2TiO_4). In natural spinels there is more or less complete solid

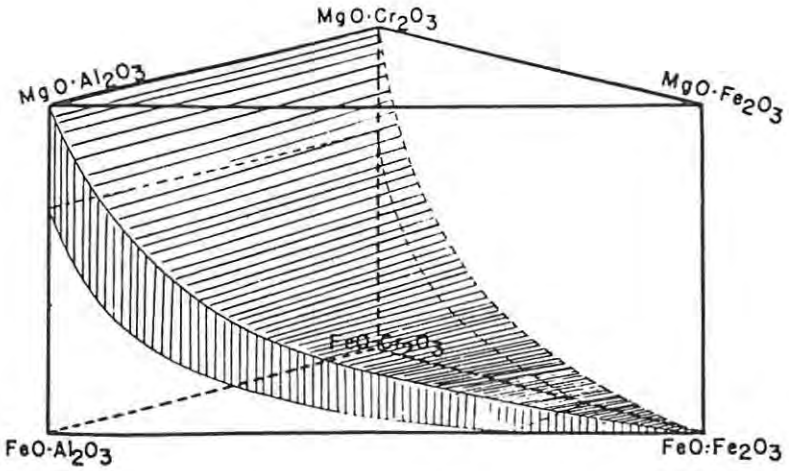

Figure 21. Steven's prism indicating the common spinel end-members and solid solution field (from Stevens, 1944).

solution within each series, but less miscibility exists between the series at low temperatures (Deer et. al., 1962).

The spinel grains within the main body of the Townlands pegmatite represent intermediate compositions within the ulvöspinel (Fe_2TiO_4) - magnetite (Fe_3O_4) solid solution series (Fig.22). As already mentioned, they are most abundant in samples from borehole TLP.2 and 6 level haulage, and very few grains were detected in samples from the remaining four boreholes. In general, the Ti-magnetite grains are anhedral with a maximum diameter of $\pm$4mm, and are usually associated with aggregates of ilmenite grains. The discrete Ti-magnetite crystals that were observed are small and interstitial to silicate minerals, while occassional grains associated with sulphide bodies were also noted. The Ti-magnetite crystals examined, exhibit a range of microstructures commonly observed in Ti-magnetite grains that have crystallized from a slowly cooled magmatic liquid. Consequently, the processes responsible for the formation of igneous spinel microstructures are discussed below.

At low temperatures ($<600°C$), the magnetite-ulvöspinel solvus is intersected and the solid solution becomes unstable (Haggerty, 1976). During slow cooling, under low oxygen fugacities (fO_2), exsolution lamellae of ulvöspinel develop parallel to the (100) crystallographic planes of magnetite (Haggerty, 1976). Many Ti-magnetite grains, however, contain lamellae of rhombohedral ilmenite, which is virtually insoluble in cubic magnetite (Buddington & Lindsley, 1964). This phenomenon was

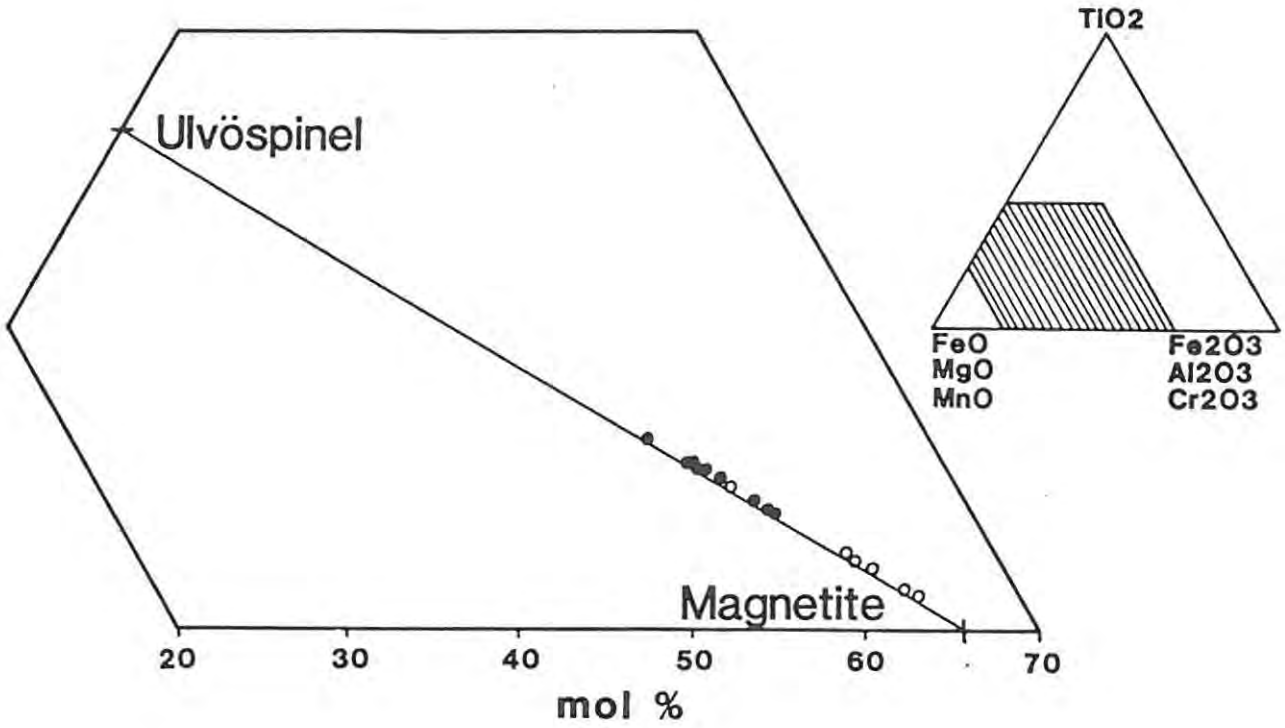

Figure 22. Diagram illustrating the extent of solid solution between the magnetite and ulvöspinel components of the TLP.2 and 6 level haulage samples. Open circles represent TLP.2 samples and the dots represent 6 level haulage samples.

explained by Buddington & Lindsley (1964), as being due to a contemporaneous 'oxidation-exsolution' mechanism, whereby the ulvöspinel component of the solid solution is oxidised to yield ilmenite plus magnetite, during subsolidus cooling. The ilmenite is then expelled from the magnetite structure parallel to the (111) crystallographic planes (Buddington & Lindsley, 1964; Haggerty, 1976). The nature of the microstructures produced by these mechanisms depends on fO_2, initial composition and cooling rate (Reynolds, 1978). Reynolds (1978), therefore, proposed a series of cooling stages to account for the more common microstructures observed in Ti-magnetite grains from slowly cooled igneous rocks, and these stages are summarised as follows:

A. The crystallization of a magnetite-ulvöspinel solid solution at temperatures in excess of 800°C.

B. Oxidation of the solid-solution at the highest subsolidus temperatures, above the magnetite-ulvöspinel solvus, will cause exsolution of ilmenite by 'oxidation-exsolution'. Ionic mobilities will be high and ilmenite granules may nucleate at grain boundaries and grow inwards into the magnetite host, parallel to (111).

C. This stage overlaps stage B and spans a wide temperature range, from the start of cooling to the magnetite-ulvöspinel solvus at ±600°C. There are a number of possibilities:

i) Low fO_2: The magnetite-ulvöspinel solid solution remains stable.

ii) Intermediate fO_2: Some oxidation of ulvöspinel occurs and ilmenite is exsolved, as sparse granules and lamellae at high temperatures, and trellis networks at lower temperatures.

iii) High fO_2: Complete oxidation of the solid solution occurs, producing abundant lamellar ilmenite.

D. This stage occupies the temperature range from immediately below the magnetite-ulvöspinel solvus to ±500°C. The possibilities are as follows:

i) Low fO_2: Exsolution of ulvöspinel along (100) in the host phase, producing the well-known cloth textures.

ii) Intermediate fO_2: Some ulvöspinel exsolves along (100), but is oxidised to ilmenite, which migrates to the (111) planes of the host magnetite.

iii) High fO_2: Both the exsolved ulvöspinel and that in solid solution is oxidised to ilmenite and exsolves as trellis networks parallel to (111).

E. In the temperature range 500°C - 400°C, there are again several possibilities:

i) Low fO_2: Ulvöspinel continues to exsolve along (100).

ii) Intermediate fO_2: Pre-existing ulvöspinel lamellae are oxidised to ilmenite, which migrates towards the octahedral planes, forming tiny irregular ilmenite grains.

iii) High fO_2: Ulvöspinel in solid solution is oxidised to ilmenite, which may form internal granules.

F. In the lowermost subsolidus temperature range, at low fO_2, the exsolution bodies will coarsen, while at high fO_2, the ulvöspinel in solid solution is oxidised to ilmenite and exsolved as internal granules.

G. Low temperature oxidation of exsolved ulvöspinel can occur at any stage during the subsequent history of the Ti-magnetite.

In addition to the above-mentioned microstructures, any Al contained in the Ti-magnetite structure will also exsolve as pleonaste bodies along the margins of ilmenite grains or as tiny lamellae oriented parallel to (100) in the host magnetite (Haggerty, 1976; Reynolds, 1978). Consequently, the range of microstructures displayed by Ti-magnetite can be extremely varied and will reflect any changes in fO_2 that may have occurred during the subsolidus cooling history of the Ti-magnetite (Reynolds, 1978).

The most common microstructures exhibited by the Ti-magnetite grains of the Townlands pegmatite are fine-scale trellis networks of ilmenite lamellae, developed parallel to (111) in the host magnetite (Fig. 28(a) - (c)). External granules and larger lamellae of ilmenite, although relatively rare, were noted from a few Ti-magnetite grains (Fig. 28(d)). The trellis networks vary in size and, in general, are coarser and more abundant in Ti-magnetite grains from borehole TLP.2 than in those from 6 level haulage. The larger ilmenite lamellae are thin and tapered, but seldom exceed 0.4mm in length. Ulvöspinel, exsolved parallel to (100) in magnetite and displaying typical cloth textures, was observed in a few Ti-magnetite grains from 6 level haulage samples. The ulvöspinel has a patchy occurrence and is associated with tiny pleonaste bodies. Pleonaste lamellae were noted in several Ti-magnetite grains, where they invariably occur either as tiny discrete lamellae oriented parallel to (100) (Fig. 28(c)), or as minute granules along the margins of larger ilmenite lamellae contained in host magnetite.

The sparse development of coarse ilmenite lamellae and external granules (Stage B) suggests that oxygen fugacities were relatively low during subsolidus cooling of the pegmatite Ti-magnetite grains. The presence of occasional ilmenite lamellae and granules and the abundance of fine trellis networks of ilmenite are indicative of intermediate fO_2 and stage C. At lower temperatures, on intersection of the magnetite-ulvöspinel solvus, the fO_2 may have decreased slightly to enable the exsolution of minor ulvöspinel. The preservation of the ulvöspinel cloth textures indicates that the fO_2 must have remained low throughout the subsequent cooling history of the Ti-magnetite grains. Whatever the mechanisms involved in their formation, it is clear that the pegmatite Ti-magnetite grains contain microstructures analogous to those formed in Ti-magnetite that has crystallized from a melt at high temperatures and has subsequently undergone slow cooling under low to intermediate fO_2 conditions.

As a result of the fine-scale nature of the ilmenite trellis networks in the majority of the pegmatite Ti-magnetite grains, the microprobe analyses presented in appendix 2 for Ti-magnetite represent bulk analyses of Ti-magnetite and exsolved ilmenite. Recalculation of the Ti-magnetite and ilmenite data is based on the methods proposed by Stormer (1983). The Ti-magnetite analyses indicated that there are significant variations in Cr and Ti contents between the Ti-magnetite grains of borehole (TLP.2 and those of 6 level haulage. The 6 level haulage Ti-magnetite grains are enriched in both Cr (4.0 - 6.7wt% Cr_2O_3) and Ti (8.38 - 15.85wt% TiO_2) with respect to those of TLP.2 ($<$0.1wt% Cr_2O_3; 2.51 - 10.14wt% TiO_2). The difference in Ti content is illustrated in Fig.22 and may reflect variations in the original compositions of the magnetite - ulvöspinel solid solutions for the two sample localities.

From studies on the $FeO-Fe_2O_3-TiO_2$ experimental system, Buddington & Lindsley (1964) concluded that the compositions of co-existing pairs of Ti-magnetite and ilmenite grains are determined by the temperature and fO_2 existing at the time of their crystallisation. They produced a temperature/fO_2 determinative diagram relevant to such co-existing pairs, which has since been revised by Spencer & Lindsley (1981). This geothermometry technique will only yield liquidus temperatures when applied to co-existing oxide pairs in rapidly cooled igneous rocks. It has, however, been applied to more slowly cooled rocks by numerous workers, inter alia Haggerty, 1976; Bowles, 1977, and is believed to yield temperatures at which large-scale subsolidus re-equilibration effectively ceased. Several co-exsiting pairs of coarse ilmenite and Ti-magnetite grains were selected from the TLP.2 and 6 level haulage pegmatite samples for microprobe analysis. The analyses (appendix 2) were performed in the vicinity of the grain boundaries between the co-existing mineral grains, but it must be noted that the Ti-magnetite analyses represent bulk compositions of Ti-magnetite and fine-grained exsolved ilmenite. The compositions of the co-existing pairs are plotted on the Spencer-Lindsley diagram (Fig.23), and are all located in the vicinity of the QFM (Quartz-Fayalite-Magnetite) buffer line, which is the usual case for basic igenous rocks (Haggerty, 1976). The compositions that plot off the QFM buffer line may indicate that those co-existing pairs are not in complete equilibrium with one another. The compositions span a temperature range of 580-800°C with corresponding log fO_2 values of between -17 and -21. The temperatures almost certainly represent minimum temperatures of subsolidus re-equilibration, indicating that the actual temperature of formation of the oxides may be somewhat higher.

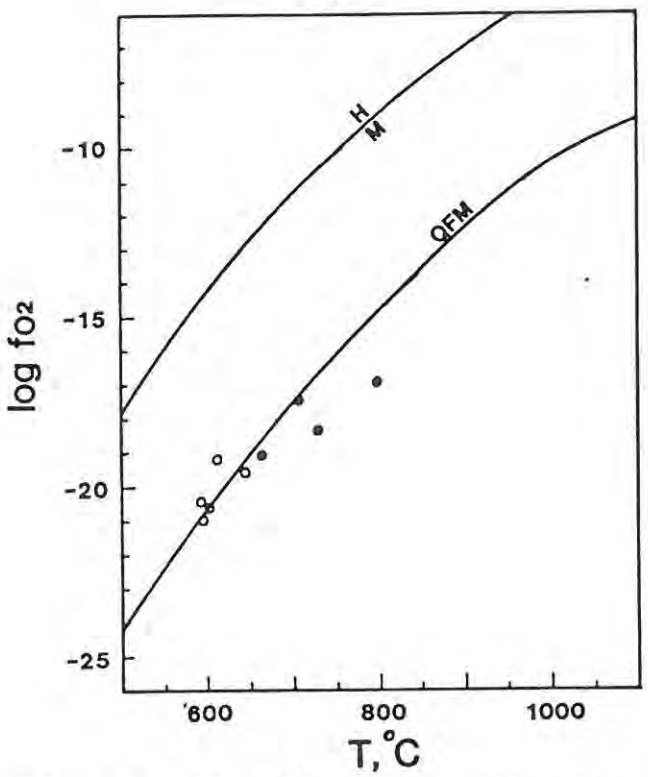

Figure 23. Plots of co-existing Ti-magnetite/ilmenite pairs from TLP.2 and 6 level haulage samples on the Spencer & Lindsley (1981) geothermometer. H/M represents the hematite/magnetite buffer curve and QFM is the quartz-fayalite-magnetite buffer curve.

The chromitite leader layers in contact with pegmatitic material of the TLP.1 'marginal' zone, display a marked departure in chemistry and textural relationships from normal chromitites of the adjacent layered suite. The most notable difference is the presence of ilmenite, in various textural forms, which decreases in abundance with increasing distance from chromitite/pegmatite contacts. The chromitite leader layers investigated, all exhibit granular or foam-like textures with well- developed triple junctions between the chromite grains, and contain only small amounts of interstitial silicate material. This situation is in marked contrast to that observed in the UG2 chromitite layers of the adjacent layered suite of the Bushveld Complex (I.M. Reynolds, pers. comm.). In the latter case, the chromitite layers contain far more interstitial silicate material than those associated with the Townlands pegmatite, and the individual chromite grains exhibit euhedral to subhedral outlines. Disseminated chromite grains in the orthopyroxenite layers between the chromitite layers of the layered suite display typical euhedral morphologies, while those associated with the pegmatite occur as anhedral grains or polygonal aggregates (Fig. 28(f)). Many of these disseminated grains associated with the pegmatite are also rimmed or cut by thin veinlets of Ti-poor secondary magnetite, which was probably produced during serpentinization of the host olivine (Fig. 28(f)). The

chromitite horizons associated with the Townlands pegmatite appear, therefore, to have acquired additional oxide-forming material and to have been subsequently well annealed.

The development of ultramafic pegmatite along the margins of the chromitite leader layers has produced systematic variations in chromite composition, with increasing distance from the contact area. As the margin of the layer is approached, the chromite crystals become increasingly rich in Fe and Ti and exhibit decreases in the amounts of Cr, Al, and Mg. Representative microprobe analyses from two separate contact zones are presented to illustrate these chemical changes. Fig.24

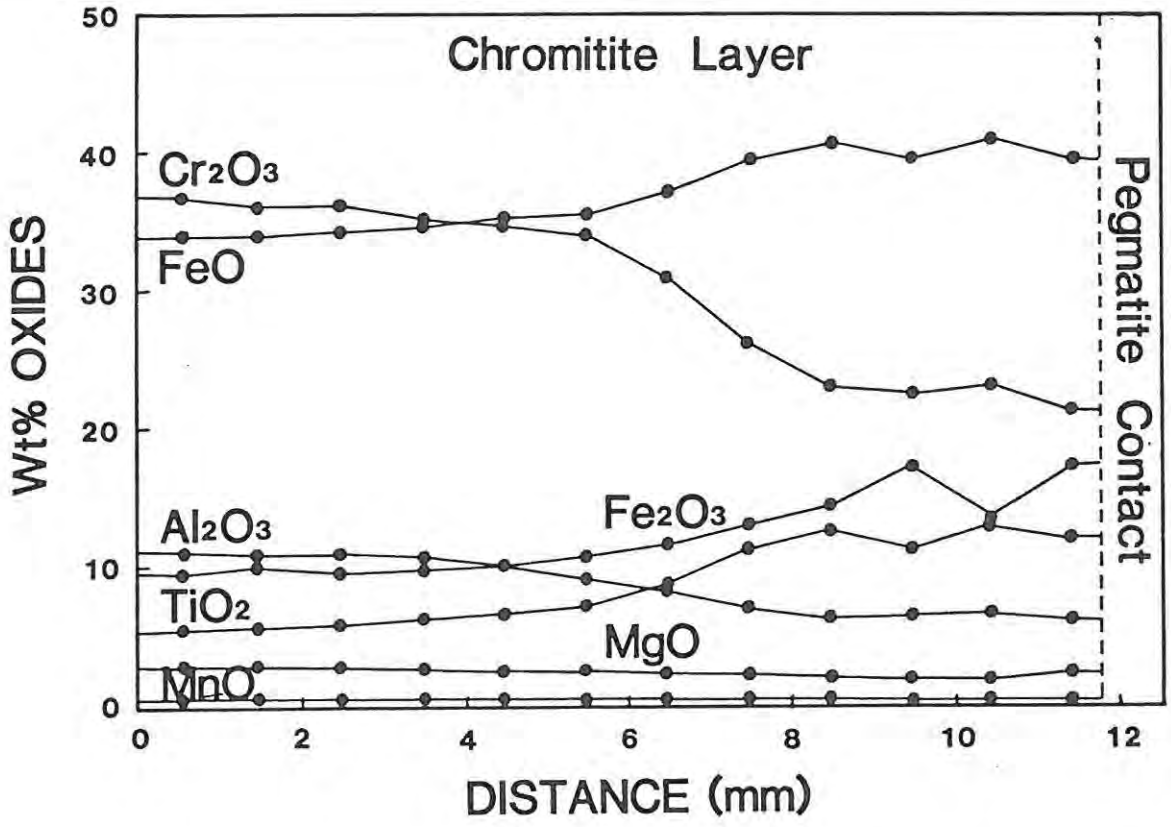

Figure 24. Microprobe traverse from the chromite/pegmatite contact of sample T1/19, illustrating the regular changes in spinel composition, away from the contact.

shows the chemical variations within the upper part of the lowermost chromitite leader (sample T1/19), while Fig.25 displays the changes within the basal part of one of the topmost leaders (sample T1/33). In both cases, there is a continuous progression in spinel composition from Ti-poor aluminium chromite to spinels intermediate between chromite and Ti-magnetite (Fig.26). Similar relationships were documented by Cameron & Glover (1973) for chromitite layers that were altered by ultramafic pegmatites, previously described by Cameron & Desborough (1964). The

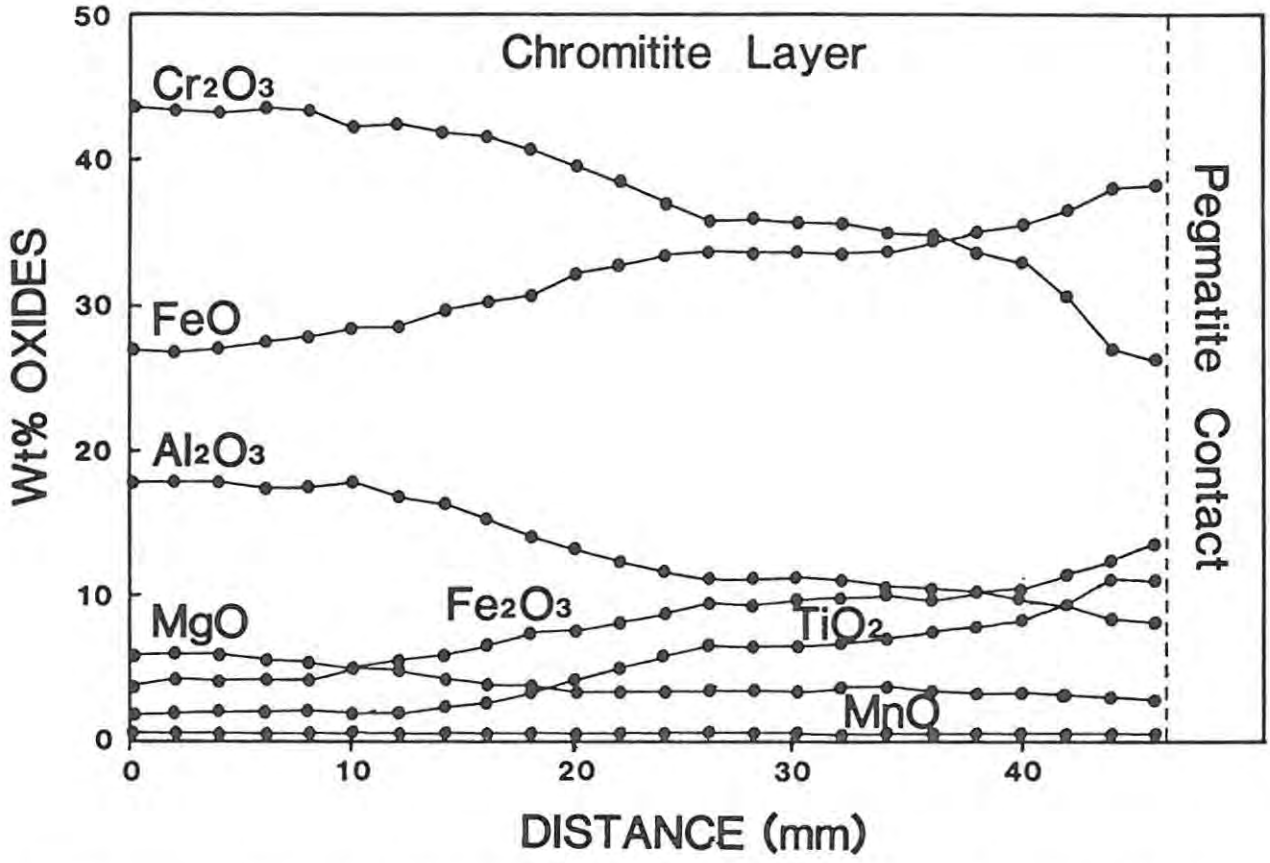

Figure 25. Microprobe traverse from the chromite/pegmatite contact of sample T1/33, illustrating the regular changes in spinel composition, away from the contact.

chromitites layers examined by Cameron & Glover (1973), however, display a continuous range in composition from Ti-poor chromites to Ti-magnetite. They also noted the presence of a layer of Ti-magnetite (0.5 - 20cm in thickness) along either the upper or the lower surface of the chromitite layers. The compositional sequence exhibited by the TLP.1 chromitite leader layers appears, therefore, to be less evolved, and may reflect a more limited interaction between the Townlands pegmatite and the TLP.1 chromitite leaders.

Stevens (1944) examined a wide range of chromites from the western hemisphere and indicated the existence of complete solid solution between chromite and Ti-magnetite (Fig.21). Deer et al. (1962) questioned the existence of a complete solid solution series, and Eales (1979) demonstrated that a miscibility gap exists between the two phases in slowly cooled rocks. This 'spinel gap' has been well documented (inter alia Hill & Roeder, 1974; Eales et al., 1980) and appears to be related to the fact that chromite is an early crystallization phase, while Ti-magnetite only becomes stable at much lower temperatures.

Consequently, spinels intermediate in composition between chromite and Ti-magnetite are rare in slowly cooled layered mafic complexes and deep-seated ultramafic rocks (Cameron & Glover, 1973; Eales, 1979).

The triangular plots of Fig.26 indicate a partial bridging of the spinel gap by the TLP.1 chromitite. Cameron & Glover (1973) concluded that the

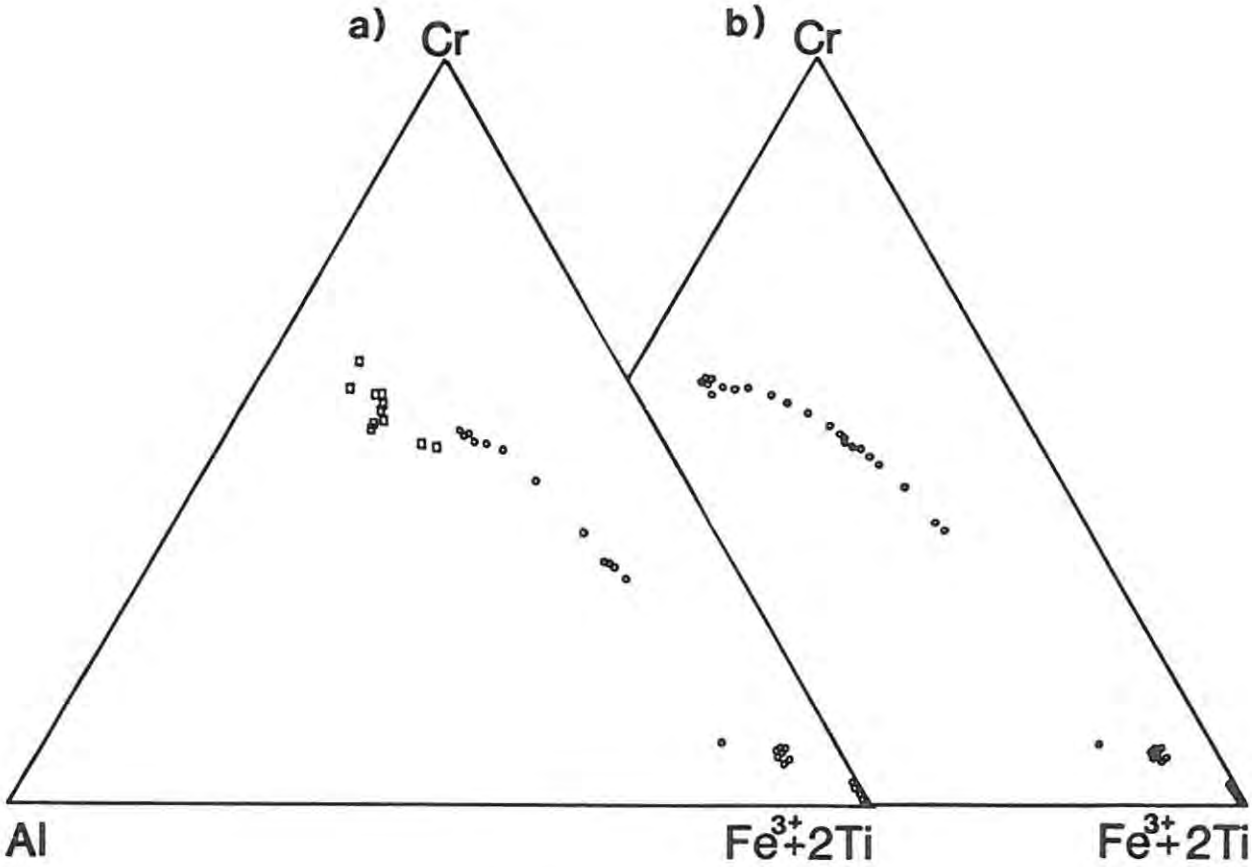

Figure 26. Triangular Cr-Al-(Fe^{3+} + 2Ti) diagrams of: a) spinel compositions from Tl/19 plus disseminated chromite, b) spinel compositions from sample Tl/33. Circles represent chromite grains from chromitite layers; squares represent disseminated chromite grains.

complete gradation in the composition of their chromitites was caused by the replacement and removal of Cr, Al and Mg coupled with the addition of Fe, Ti and V. The mechanism that they proposed, involves the migration of pegmatite fluids rich in Fe, Ti and V along grain boundaries and fractures, followed by solid state diffusion of cations along chemical gradients between the pegmatite and chromitite.

It appears that many chromitite horizons affected by ultramafic pegmatites are thickened to varying degrees by the addition of

Ti-magnetite (R.N. Scoon, pers. comm.). In fig.27 the MMF ratio (Mg/(Mg+Fe)) is plotted against the number of cations per 32 oxygens

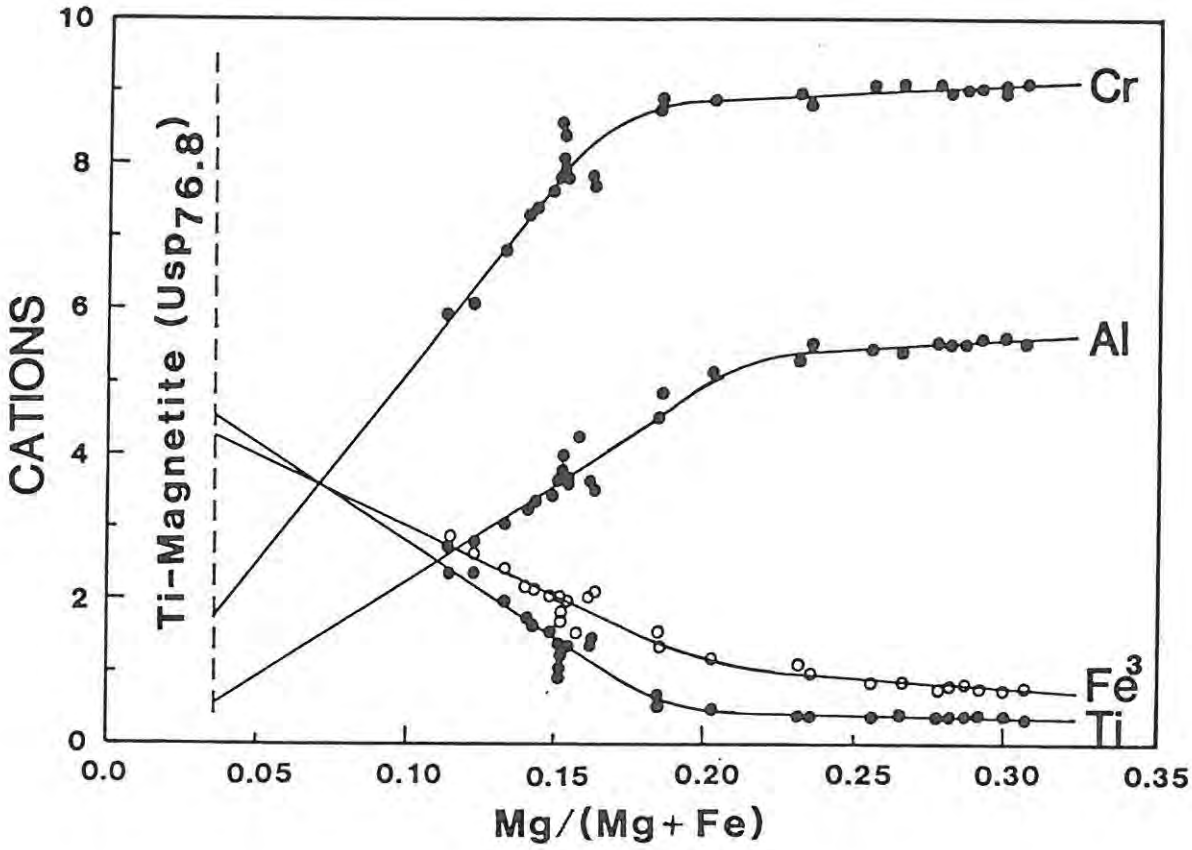

Figure 27. Plot of the MMF (Mg/(Mg+Fe)) ratio versus the number of cations per 32 oxygens for Fe^{3+}, Cr, Al, Ti, of the upper chromitite leader (T1/33). Note the possible existence of mixing lines between chromite and Ti-magnetite ($Usp_{76.8}$).

(Fe^{3+}, Cr, Al and Ti), for the upper chromitite leader (T1/33). In all cases, it is possible to construct extrapolated mixing lines between the Ti-poor aluminium chromite compositions and Ti-magnetite having a theoretical composition corresponding to $Usp_{76.8}$. This composition falls within the compositional range for common primary Fe-Ti spinels which, according to Haggerty (1976), varies between $Usp_{50}Mt_{50}$ and $Usp_{80}Mt_{20}$, and also compares favourably with bulk compositions of Ti-magnetite from near to top of the upper zone of the Bushveld Complex (I.M. Reynolds, pers. comm.). It is suggested, therefore, that the intermediate spinels might result from mixing between chromite and a magnetite-ulvöspinel solid solution rather than by direct reaction between chromite and pegmatite fluids. A possible mechanism that might be involved in this process is discussed in section 6.4.

6.3 Ilmenite

Ilmenite has trigonal symmetry and a chemical formula that may be expressed as $(Fe^{2+},Mg,Mn)Ti^{4+}O_3$, although Mg and Mn are very minor constituents (Deer et. al., 1962). It has a structure similar to that of hematite and consists, basically, of alternating layers of oxygen and iron ions. The oxygen ions were arranged in a distorted hexagonal packing arrangement, while successive cation layers contain equal numbers of cations in octahedral coordination (Deer et al., 1962). Complete solid solution exists between ilmenite and hematite at high temperatures, but exsolution may occur at lower temperatures. As a result, Lindsley (1976) proposed the compositional formula $Fe^{3+}_{(2-2x)}Fe^{2+}Ti_xO_3$, where x is the mole fraction of ilmenite.

Microprobe analyses were carried out on ilmenite grains from all the sample localities, the majority of which yielded fairly consistent results (appendix 2). Ilmenite present within the main body of the pegmatite occurs in two distinctly different textural forms. It most commonly occurs as large anhedral grains that attain 5mm in diameter. These crystals are usually grouped together in aggregates that exhibit granular textures and well-developed triple junctions between grains (Fig.29a). Isolated ilmenite grains generally exhibit irregular morphologies and occupy the interstices between silicate minerals. Ilmenite aggregates are also commonly associated with sulphide blebs. Many grains show the development of twin lamellae, probably orientated parallel to the (10$\bar{1}$1) crystallographic planes. In most cases, single lamellae are present (Fig. 29(a)) but in a few grains multiple twinning was observed (Fig.29b). According to Ramdohr (1980), the majority of twin lamellae in ilmenite are a result of deformation, but as there appears to be little deformation within the Townlands pipe, the twin lamellae may represent annealing twins. The second occurrence of ilmenite is in the form of patchy fine-scale latticeworks within Ti-magnetite (Figs.25(a)-(d)), as described in the previous section.

The ilmenite present in the TLP.1 chromitite leader layers is characterised by a different set of textures to that displayed by the ilmenite from the main body of the pegmatite. These textures are somewhat unusual and are very similar to those described by Cameron & Glover (1973). The ilmenite grains are most common towards the margins of the chromitite layers and are intimately associated with the

intermediate chromian Ti-magnetite spinels described in the previous section. Ilmenite decreases in abundance with increasing distance from the margins of the chromitite layers and is rare towards the centre of the thicker chromitite layers.

The most common mode of occurrence of the ilmenite is in the form of irregular grains and clusters of grains concentrated along the boundaries between polygonal spinel crystals. This situation applies to both the disseminated spinel grains (Fig.28(f)) and those forming the chromitite layers (Fig.29(c),(d)). Long lath-like bodies of ilmenite up to 2mm in length were observed in several of the chromitite layers. These lath-like bodies may traverse across several spinel grains and are most abundant close to the margins of the chromitite layers (Fig. 29(e)). The larger ilmenite grains and lath-like bodies are often rimmed by a narrow zone of dark grey spinel (Fig. 29(f)). Similar haloes of dark spinel were noted by Cameron & Desborough (1964), who reported that these zones are depleted in divalent cations and Ti^{4+} ions in the correct proportions to produce ilmenite. The ilmenite grains and bodies are also compositionally zoned, and exhibit an increase in Cr content from < 0.2wt percent Cr_2O_3 in their cores to ± 4.7wt percent Cr_2O_3 at their margins (e.g. Sample T1/19). This compositional zoning both within and adjacent to ilmenite grains probably reflects the diffusion gradients responsible for the formation of the ilmenite.

The ilmenite grains located along the spinel grain boundaries are indicative of external granules formed by 'oxidation-exsolution' from a magnetite-ulvöspinel solid solution at high subsolidus temperatures and high oxygen fugacities. In some cases, tapered ilmenite lamellae radiate inwards from spinel grain boundaries and appear to represent lamellae that have nucleated at the grain boundary and grown inwards into their chromian Ti-magnetite host parallel to (111) (Fig.29(d)). It is suggested, therefore, that the ilmenite associated with the chromitite leader layers formed by 'oxidation-exsolution' from the magnetite-ulvöspinel solid solution component of the intermediate spinels. The large lath-like bodies of ilmenite are more difficult to interpret in terms of these mechanisms, but one possibility is that they formed by nucleation along pre-existing fractures in the chromitite layers. These fractures would have been highly favourable sites for nucleation and rapid growth during high temperature 'oxidation-exsolution' of the ilmenite.

6.4 Discussion

Ti-magnetite and ilmenite from the main body of the Townlands pegmatite occur as coarse, well-annealed grains and there is no evidence to suggest that they were not formed at the same time as the rest of the pegmatite. The range of microstructures exhibited by the Ti-magnetite grains are analogous to those found in Ti-magnetite grains that have crystallized from a melt at high temperature and undergone slow cooling. The Spencer-Lindsley diagram yielded re-equilibrium temperatures of 580°C-800°C, but the temperature of formation of these phases would be expected to be far higher. The textural and compositional features of the Fe-Ti-oxides suggests, therefore, that these phases formed at high temperatures and may well have crystallized from a magmatic liquid.

The Ti-magnetite grains from 6 level haulage contain relatively high Cr contents and it is interesting to note that the adjacent 'spotted anorthosite' from the underground exposures contains minor amounts of chromite. Consequently, it is possible that some of this chromite may have been incorporated into a pegmatite melt, thereby providing 'seeds' for the precipitation of titanomagnetite. The high temperatures required in such a situation would then have caused the subsequent homogenization of the Cr-bearing Ti-magnetite grains. The proposal is at this stage, tentative, as it requires a pegmatite melt as a pre-requisite. It should be borne in mind, therefore, that these compositions could also be interpreted in terms of high temperature replacement processes.

In comparison to the UG2 chromitite layers of the adjacent layered suite of the Bushveld Complex, the TLP.1 chromitite layers are well annealed and appear to have acquired additional material in the form of Fe^{2+}, Fe^{3+} and Ti^{4+}. The introduction of this material has resulted in the formation of spinels intermediate in composition between chromite and Ti-magnetite. These intermediate spinels are rare in slowly cooled igneous rocks, but have been reported from metamorphosed ultramafic rocks (inter alia Purvis et al., 1972; Loferski & Lipin, 1983; Reynolds & Eales, in prep.). Reynolds & Eales (in prep.) noted the presence of unusual spinels consisting of unmixed intergrowths of chromite or chromian spinel (sensu stricto) and magnetite or chromian magnetite, from the Tugela Rand intrusion situated in the Natal mobile belt. The spinels are hosted by ultramafic igneous rocks that have been subjected to upper amphibolite facies metamorphism. They suggested a mechanism for the

formation of these spinels, whereby magnetite is initially released from olivine during serpentinization and deposited around original chromite grains. During prograde metamorphism (600-650°C), homogenization to intermediate spinels occurred, followed by exsolution on slow cooling. The intermediate products are characterised by depletion in Al, Cr and Mg and enrichment in Fe^{2+} and Fe^{3+} relative to the original magmatic chromite (Reynolds & Eales, in prep.).

A similar mechanism to that proposed by Reynolds & Eales (in prep.) is invoked for the formation of the intermediate spinels present in the TLP.1 chromitite layers. It is suggested that Fe^{2+}, Fe^{3+} and Ti^{4+} were introduced into the chromitite layers and precipitated around the chromite grains as titanomagnetite. This process occurred at a temperature high enough to permit the complete homogenization of the intermediate spinel grains. A subsequent slow cooling rate and high fO_2 allowed for extensive 'oxidation-exsolution' of ilmenite from the magnetite-ulvöspinel component of the homogenized intermediate spinels. The high Ti content of the intermediate spinels indicates that the enrichment of Fe^{2+}, Fe^{3+} and Ti^{4+} could not have been achieved by the release of Ti-poor magnetite from olivine during serpentinization. It is concluded, therefore, that the titanomagnetite introduced into the chromitite layers was derived from the pegmatite during its formation. The components required for the precipitation of titanomagnetite could have been introduced by migrating pegmatite fluids rich in Fe and Ti. However, if the pegmatite crystallized from a melt, this could explain the scarcity of Ti-magnetite in samples from the remaining portions of borehole TLP.1, compared to samples from borehole TLP.2 and 6 level haulage. In this case, the chromite could have provided 'seeds', or readily available nucleation sites, for the precipitation of titanomagnetite, thereby removing titanomagnetite components from the melt in the immediate vicinity of the chromitite layers. Whatever the process involved in the formation of the intermediate spinels, it is evident that the temperatures involved must have been high. The magnetite-ulvöspinel solvus is intersected at $\pm$600°C (Haggerty, 1976). It is suggested, therefore, that the temperatures involved during the precipitation of titanomagnetite may be in excess of 800°C, which is the temperature at which magnetite-ulvöspinel solid solutions crystallize from magmatic liquids (Reynolds, 1978).

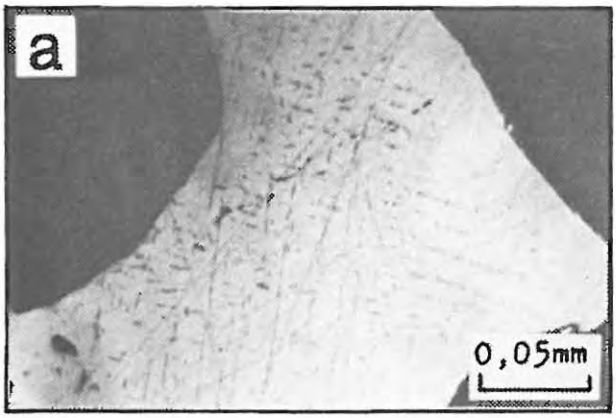
a
0,05mm

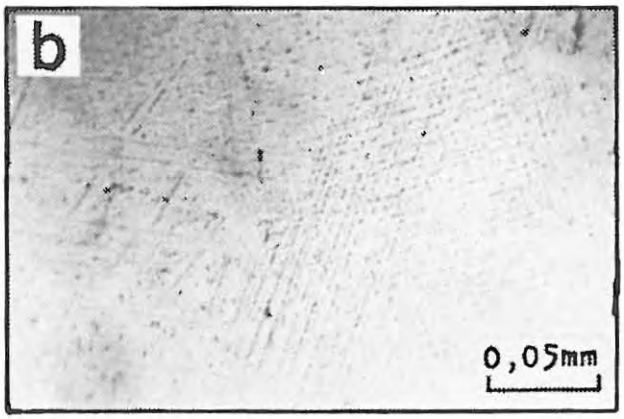
b
0,05mm

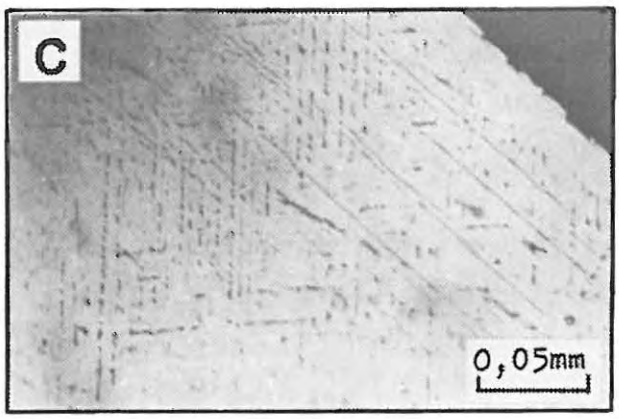
c
0,05mm

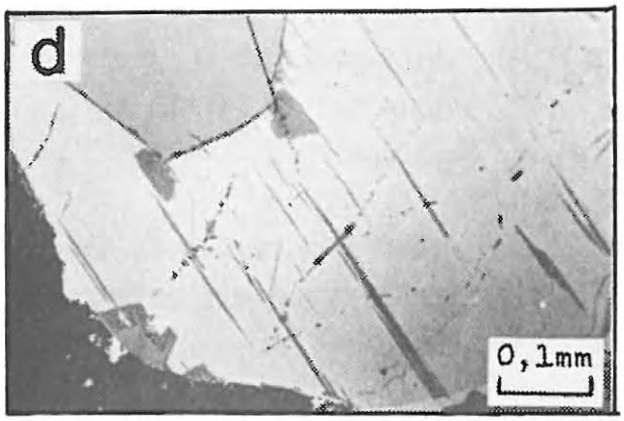
d
0,1mm

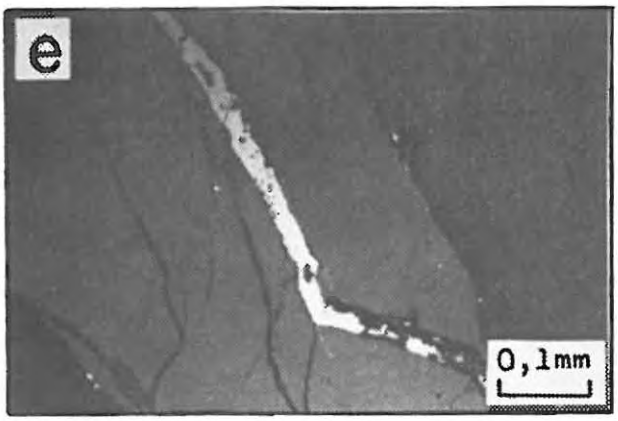
e
0,1mm

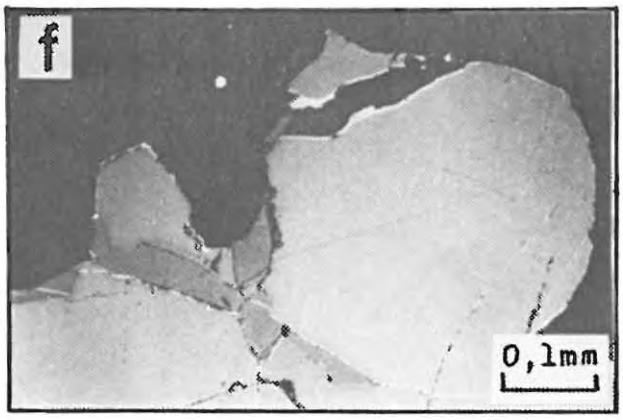
f
0,1mm

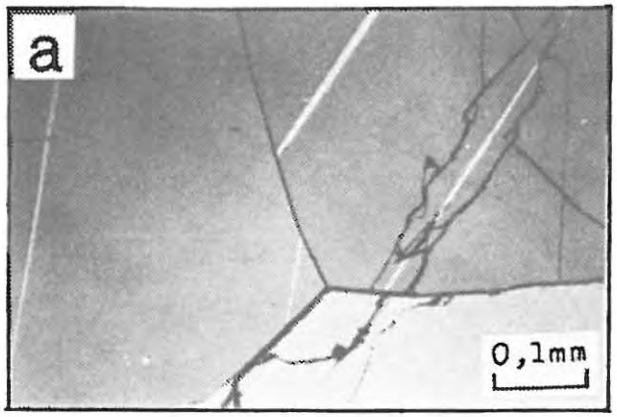
a
0,1mm

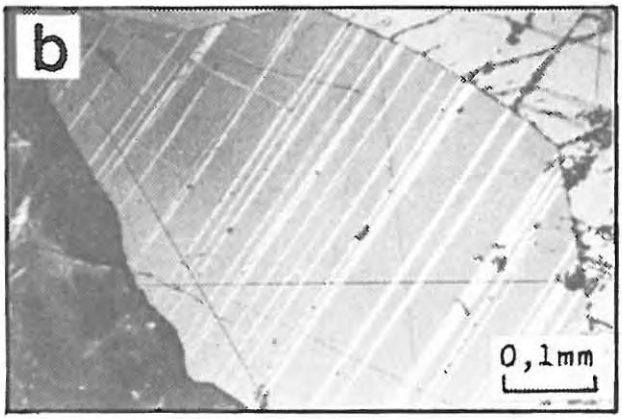
b
0,1mm


c
0,1mm

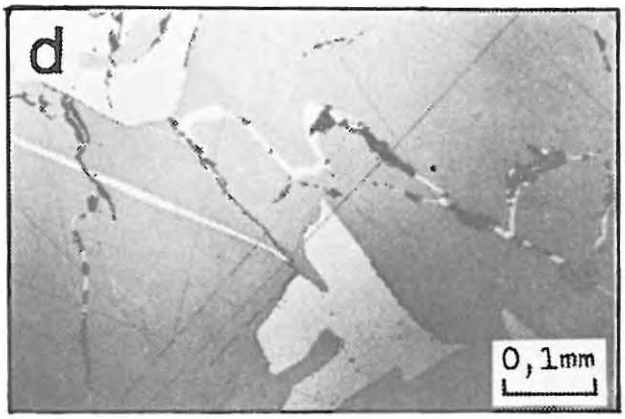
d
0,1mm

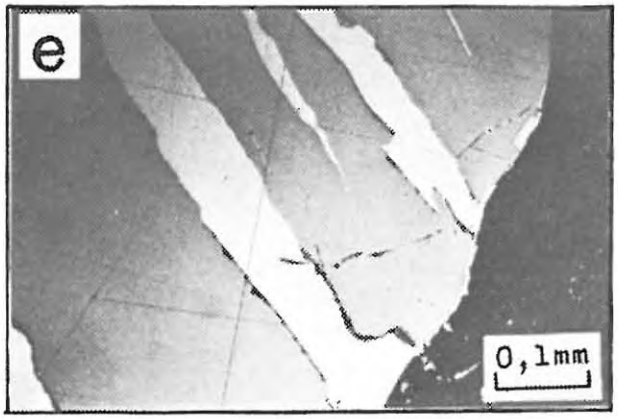
e
0,1mm


f
0,05mm

7. ORE MINERALOGY

7.1 Introduction

Sulphides and associated opaque mineral phases are minor constituents of the Townlands pegmatite, but the unusual assemblages and textural relationships observed in preliminary investigations, prompted a more detailed examination. The study is, however, by no means complete and scope still exists for further work. Initial investigations were carried out by the J.C.I. Minerals Processing Research Laboratory and a brief account of their findings was given by Viljoen et. al. (1983). Of particular interest was their recognition of a number of apparently hitherto undescribed phases, including Cl- and Zn-bearing Cu-Fe sulphides.

During the present study, a total of 56 polished sections were prepared for reflected light examination, the majority being taken from borehole TLP.1. In addition, three representative sections were prepared from borehole TLP.2, one each from TLP.3 and TLP.4, two from borehole TLP.5 and four from 6 level haulage samples. Priority was given to the identification of the major phases present and an interpretation of their mutual relationships. Grateful acknowledgement is made to the J.C.I. Research Laboratory for carrying out the chemical analyses reported in this chapter. The analyses were performed by means of energy dispersive electron microprobe techniques, on sections prepared by the author.

7.2 Phase Relations

It is widely believed that many of the sulphide assemblages associated with large mafic and ultramafic layered intrusions are produced by the segregation of immiscible sulphide droplets from a silicate magma (Naldrett, 1969). Subsequent crystallization of the immiscible sulphide liquid yields a characteristic primary assemblage, the principal constituents of which are pyrrhotite, pentlandite, chalcopyrite and frequently magnetite, cubanite and pyrite. The majority of sulphide assemblages in the Townlands pipe may be represented within the Fe-Ni-Cu-S quaternary system, which has been the subject of extensive experimental investigation. Kullerud et. al. (1969) summarised the high temperature ($>400°C$) phase relations of the Cu-Fe-S, Cu-Ni-S and Fe-Ni-S ternary systems, extrapolated into the Fe-Ni-Cu-S system. Craig & Kullerud (1969) considered the high temperature relationships in the

Fe-Ni-Cu-S system as a whole, but the conclusions reached in both studies are, more or less, coincident. Craig (1973) investigated the low temperature (<400°) phase fields of the Fe-Ni-S system, while Power & Fine (1976) have reviewed phase relations in the Fe-rich portion of the Fe-S system. Some of the more significant aspects of these studies are discussed below.

The Fe-Ni-Cu-S quaternary system is dominated, at very high temperatures (>1100°C) by a large field of liquid immiscibility in the S-rich portion of the system, and by a wide extent of homogeneous liquid in the central parts (Fig.30). It was noted that by 1100°C, a pyrrhotite-rich Fe-Ni-monosulphide solid solution forms from the homogeneous liquid. With decreasing temperature, Ni enters the monosulphide solid solution (Mss), which expands across the Fe-Ni-S face of the quaternary system (Fig.31).

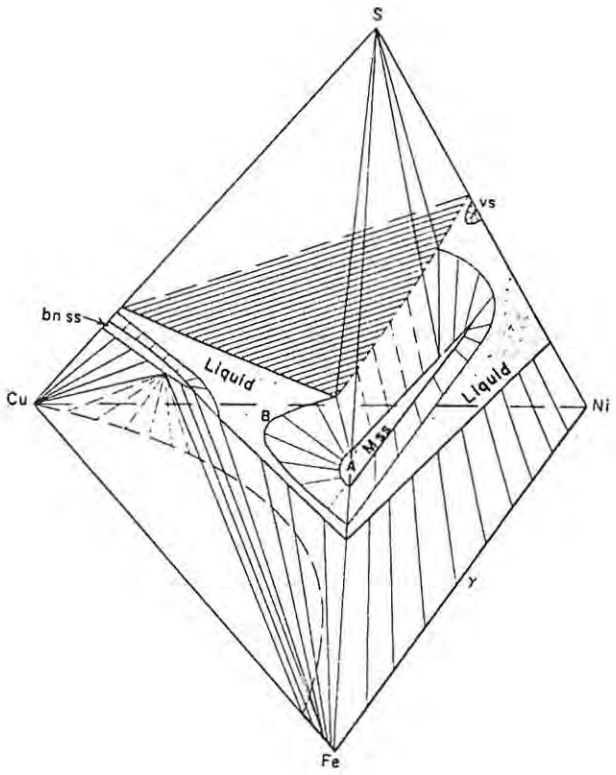

Figure 30. Schematic 1000°C isothermal diagram of the Cu-Fe-Ni-S system under hydrous conditions. The homogeneous sulphide liquid is indicated by the shaded area, while the field of liquid immiscibility is illustrated by the striped area (from Craig & Kullerud, 1969).

Naldrett (1969) investigated the Fe-S-O system and commented on the existence of tie-lines between pyrrhotite and magnetite at 900°C, which implies that magnetite is able to co-precipitate with the early-formed pyrrhotite-rich solid solution, depending on the oxygen fugacity.

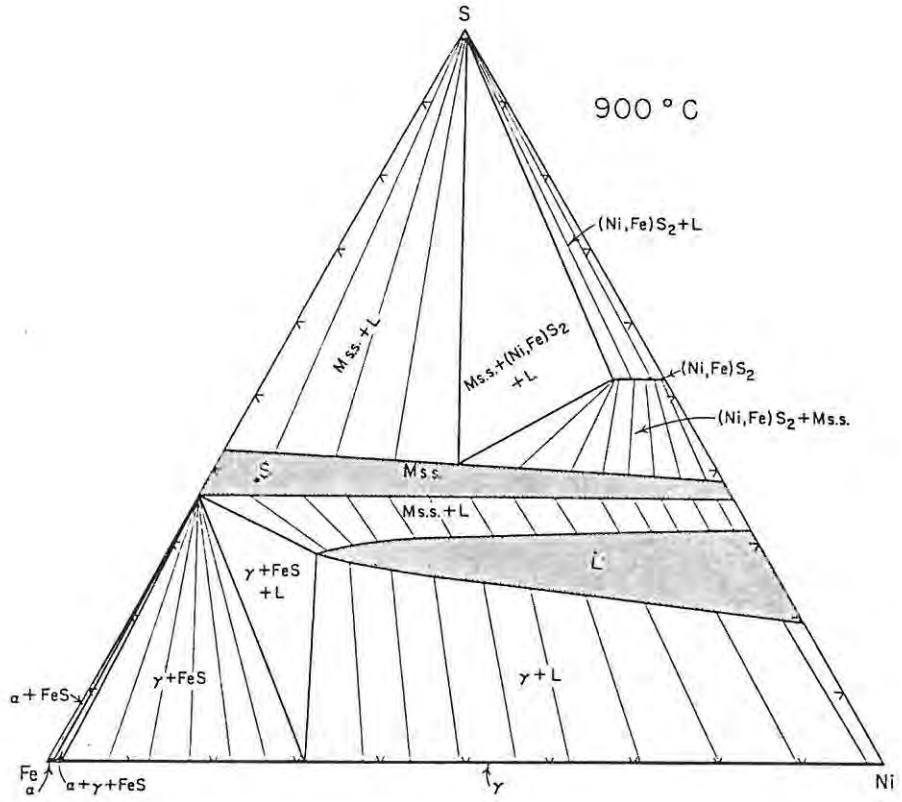

Figure 31. Phase relations in the Fe-Ni-S system at 900°C in the presence of vapour. Note the extent of the Mss across the face of the diagram (from Kullerud et. al., 1969).

Kullerud (1969) and Craig & Kullerud (1969) suggested that a mechanism exists within the temperature range 1150°C - 865°C, whereby a Cu-rich liquid may segregate from the sulphide liquid to form a chalcopyrite-rich intermediate solid solution. This solid solution precipitates out from the central 'homogeneous' liquid at $\pm$960°C and at about 590°C, it decomposes to form separate chalcopyrite and cubanite solid solutions (Fig.32).

As the temperature decreases further, sulphide phases continue to segregate from the sulphide melt. NiS_2 crystallises at 1007°C and liquid immiscibility in the Fe-Ni-S system disappears at 991°C. Below 900°C, the Mss field narrows and at 862°C a $(Ni,Fe)_{3+x}S_2$ phase crystallises, which subsequently reacts with the Mss, at $\bar{}$610°C, to produce pentlandite (Fig.33). The absence of most of the high temperature phases and the presence of low temperature sulphides in natural samples is indicative of extensive re-equilibration at low temperatures (Kullerud et. al., 1969).

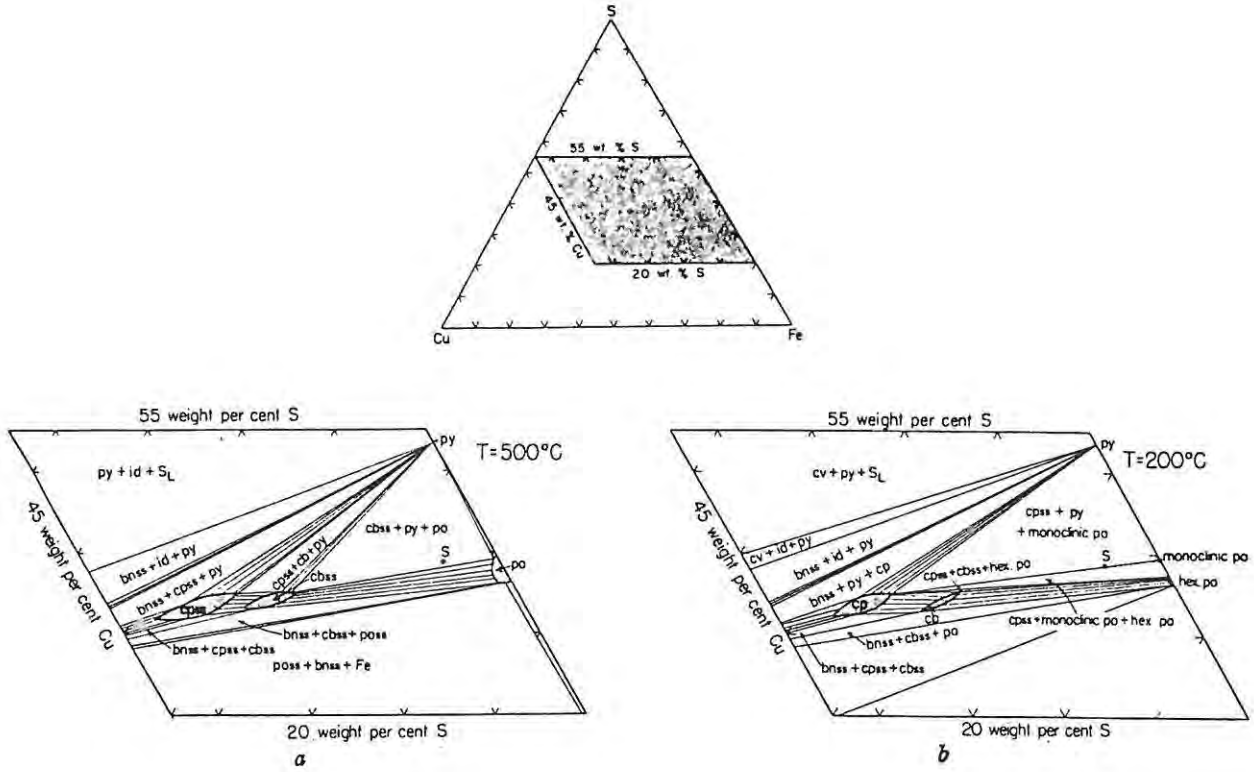

Figure 32a. Phase relations in part of the Cu-Fe-S system at 500°C, coexisting with vapour (from Kullerud et al., 1969).

b. Phase relations in part of the Cu-Fe-S system at 200°C, coexisting with vapour (from Kullerud et. al., 1969).

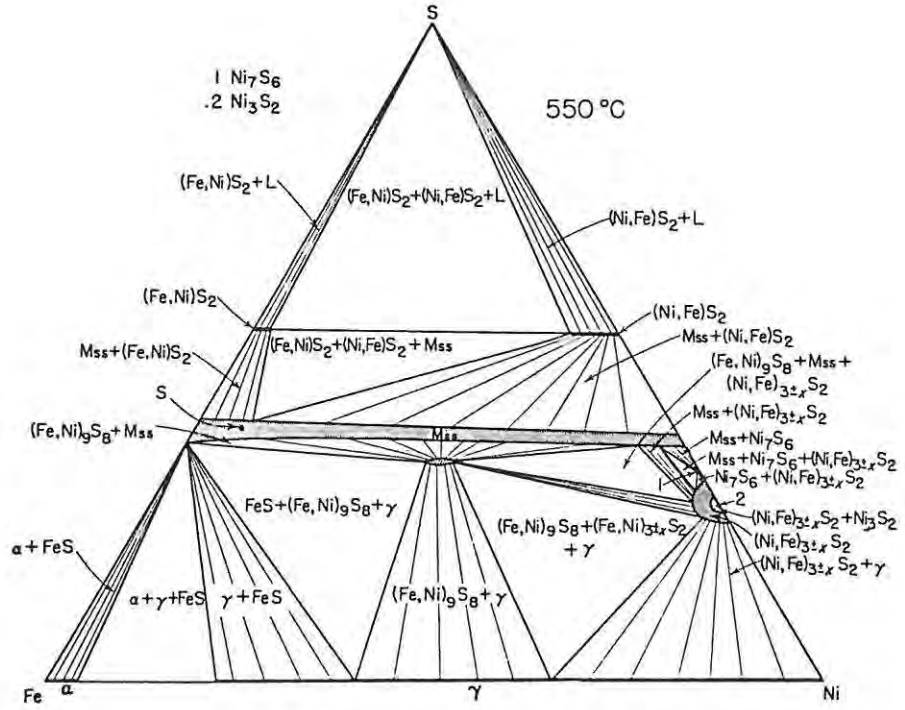

Figure 33. Phase relations in the Fe-Ni-S system at 550°C, coexisting with vapour (from Kullerud et. al., 1969).

The study of low temperature experimental phase relations is complicated by difficulties involved in attaining equilibrium, and the phase relationships are still not fully understood. Kullerud et. al. (1969) compiled a tentative phase diagram for the Fe-Ni-S system at ±130°C, based largely on investigations of natural systems (Fig.34). Craig (1973)

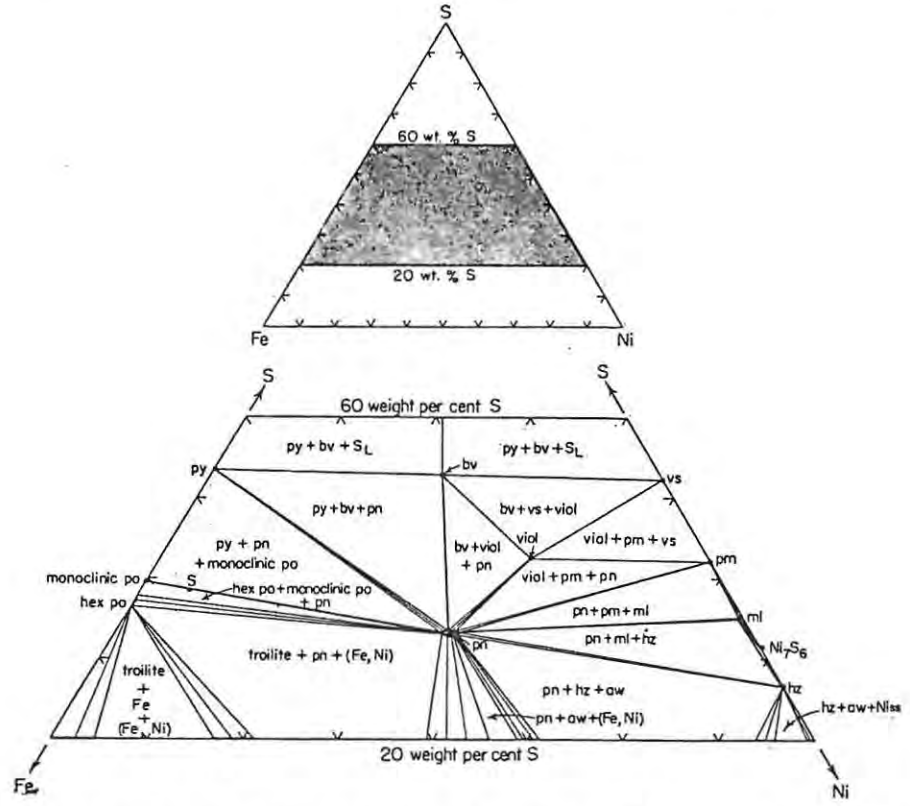

Figure 34. Tentative phase diagram for part of the Fe-Ni-S system at 130°C, coexisting with vapour (from Kullerud et. al., 1969).

presented an alternative set of low temperature phase diagrams, from annealing experiments (Fig.35). His investigations indicated that the Mss field decreases in size below 600°C, but only begins to break up at 282°C, when millerite (NiS) forms. At 263°C, separate Fe-rich and Ni-rich solid solutions form from the Mss and the Ni-rich phase exsolves to yield two further solid solutions at 225°C. The persistence of the Mss to such low temperatures prohibits the formation of pyrite-pentlandite assemblages at temperatures above 213°C. Therefore, apart from pyrrhotite, pentlandite, pyrite, chalcopyrite and cubanite, the remaining sulphides represented in Fig.34 are only stable at low temperatures and result from secondary alteration processes such as metamorphism, serpentinization and supergene alteration (Kullerud et. al., 1969).

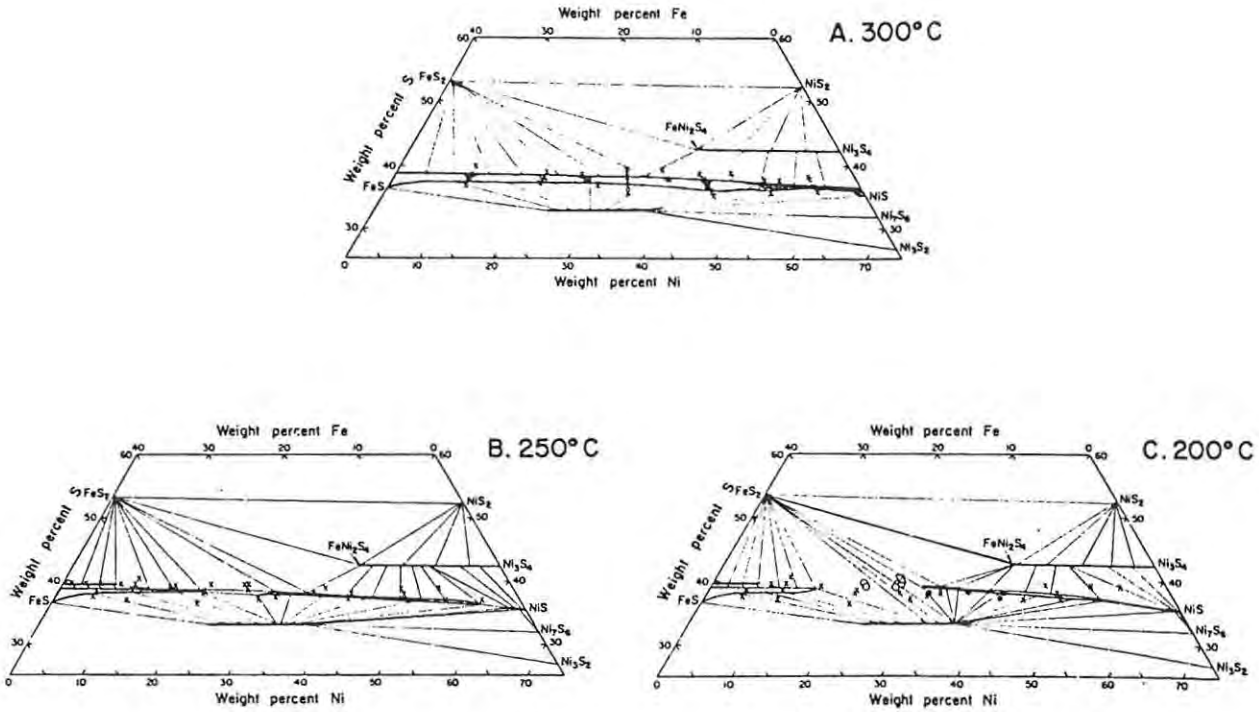

Figure 35. Phase relations in part of the Fe-Ni-S system at (A) 300°C, (B) 250°C, (C) 200°C (from Craig, 1973).

The stability fields of phases represented in the Fe-rich portion of the Fe-S system at low temperatures are discussed by Power & Fine (1976) and summarised in Fig.36. The nomenclature used in the diagram is based on the superstructure of the pyrrhotite group, which may be integral or non-integral values of the cell-edges of the hexagonal Ni-As type

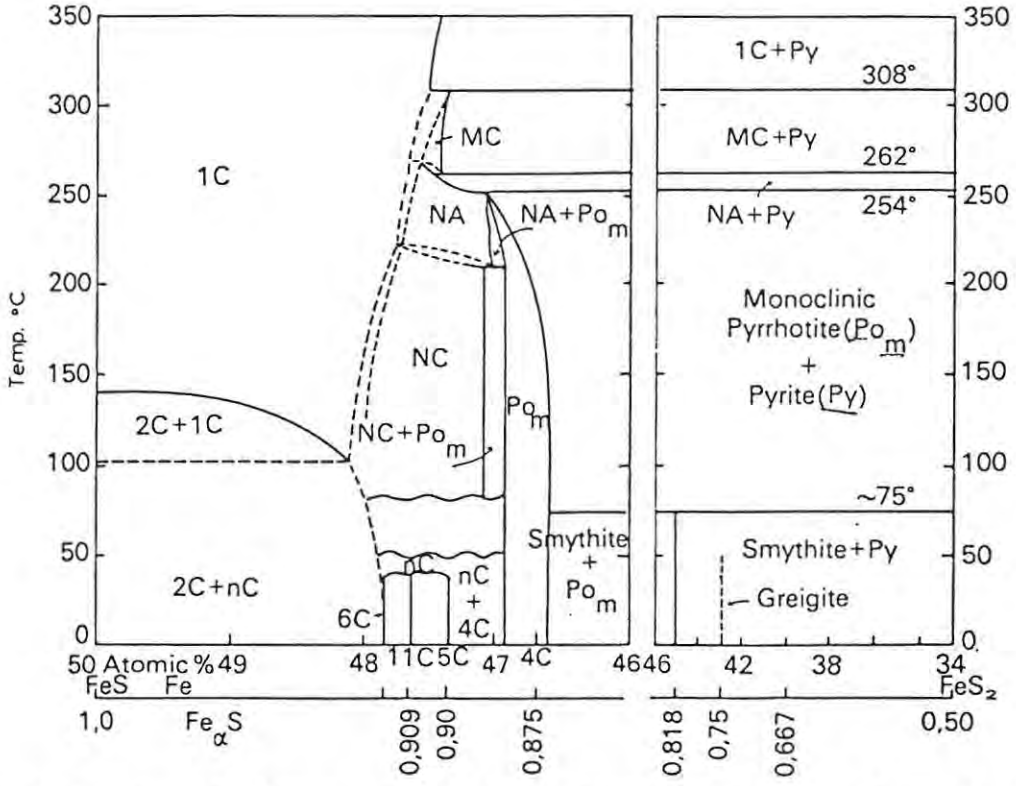

Figure 36. Phase relations in the Fe-S system from FeS to FeS_2, below 350°C (from Power & Fine, 1976).

framework. For instance, troilite has a 'C' axis equal to 2C, where C refers to the cell-edge dimensions of NiAs. The compositions Fe_9S_{10}, $Fe_{10}S_{11}$, and $Fe_{11}S_{12}$ are, therefore, termed 5C, 11C and 6C pyrrhotites, respectively (Power & Fine, 1976). Studies by Morimoto et. al. (1975) suggest that the stoichiometric pyrrhotites that are stable in nature, include FeS (2C), $Fe_{11}S_{12}$ (6C), Fe_9S_{10} (5C), Fe_7S_8 (4C), and possibly $Fe_{10}S_{11}$ (11C). Natural pyrrhotite compositions that range between FeS and $Fe_{10}S_{11}$, may represent mixtures of 2C + nC (Troilite + hexagonal pyrrhotite), while those between $Fe_{11}S_{12}$ and Fe_9S_{10}, consist only of mixtures of nC (hexagonal pyrrhotite). Compositions that range between $Fe_{10}S_{11}$ and Fe_7S_8 consist only of mixtures of nC + 4C (hexagonal + monoclinic pyrrhotite).

Cabri (1973) re-examined the low temperature phase relations of the Cu-Fe-S system subsequent to the discovery of the Cu-Fe sulphides mooihoekite ($Cu_9Fe_9S_{16}$) and haycockite ($Cu_4Fe_5S_8$). Mooihoekite and haycockite, together with talnakhite are all compositionally similar to chalcopyrite (Fig.37) and Cabri (1973) concluded that all three of these phases are only stable at low temperatures. Synthetic talnakhite is only stable below ±186°C and mooihoekite can only exist below ±167°C. Cabri (1973) was unable to synthesize haycockite, but suggested that it is also, probably, only stable below 200°C. All three phases are rare in nature and do not form part of common primary assemblages. This suggests that their stability may be dependent on rather special conditions prevailing during secondary processes.

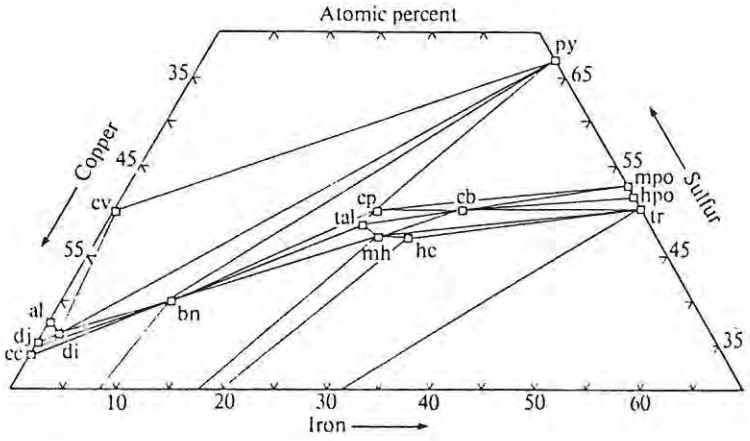

Figure 37. Possible phase relations in the central portion of the Cu-Fe-S system at 25°C (from Vaughan & Craig, 1978). Abbreviations: cc, chalcocite; dj, djurleite; di, digenite; al, anilite; cv, covellite; bn, bornite; tal, talnakhite; mh, mooihoekite; hc, haycockite; cp, chalcopyrite; cb, cubanite; py, pyrite; mpo, monoclinic pyrrhotite; hpo, hexagonal pyrrhotite; tr, troilite.

7.3 General Textural Relationships

The Townlands pegmatite is host to a wide range of sulphides and other associated opaque phases, including the rare Cu-Fe sulphides mooihoekite and haycockite. The largest and most diverse sulphide population was observed in borehole TLP.1, where the samples examined contain 1-2% of sulphides. The proportion of sulphides contained in sections from the remaining sample localities seldom exceeds 1%. The TLP.1 sections also host the largest sulphide aggregates which sometimes attain 3-4cm in diameter. This is in contrast to samples from other localities in which sulphide aggregates rarely exceed 1cm in diameter.

The nature of the ore mineral assemblages varies between sample localities and, in the case of borehole TLP.1, with position in the borehole itself. All of the sulphide assemblages are dominated by the presence of troilite, and contain variable amounts of other major phases, including chalcopyrite, mooihoekite, haycockite, pentlandite, cubanite, sphalerite and pyrite. The sulphide assemblages in samples from boreholes TLP.2, TLP.4 and 6 level haulage are relatively simple and consist of small amounts of troilite, chalcopyrite, cubanite and pentlandite. Borehole TLP.5 hosts a slightly different assemblage that includes, in order of abundance, troilite, cubanite, pentlandite, chalcopyrite and pyrite. The occurrence of mooihoekite, haycockite and sphalerite is almost exclusively confined to borehole TLP.1, although small amounts of these three phases are present in borehole TLP.3. The upper portions of borehole TLP.1 are characterised by the presence of native copper and complex sub-microscopic sulphide intergrowths that are associated with troilite. The intergrowths exhibit unusual textures and mineralogies, and are discussed in section 7.4.12. To avoid confusion with other sulphide intergrowths, they will be referred to as 'complex intergrowths'. The lower parts of borehole TLP.1 contain the highest proportions of mooihoekite, haycockite and sphalerite.

The sulphides of the Townlands pegmatite tend to occur either as relatively large aggregates or as small, disseminated grains that are interstitial to the surrounding silicate minerals. The situation is, however, more complex in the presence of the thicker serpentine veinlets. The disseminated grains usually exhibit rounded to sub-rounded shapes. In contrast, the larger aggregates generally show irregular morphologies with rounded to slightly embayed grain boundaries at places

where they are in contact with silicate minerals. Polygonal aggregates of ilmenite and lesser amounts of Ti-magnetite are commonly attached to, or associated with the sulphide bodies. Secondary magnetite, derived from the serpentinization of olivine, is invariably present in intimate association with the bulk of the sulphide aggregates.

As mentioned in chapter 4, a distinctive feature of the Townlands pegmatite is the presence of widespread anastomosing veinlet and fracture systems that are commonly filled with serpentine and lesser amounts of secondary magnetite. The unusual silicate mineral, ilvaite, is a common accessory phase that is hosted by serpentine, particularly in the vicinity of sulphide blebs. Borehole TLP.1 contains the largest concentration of serpentine veinlets and fractures, which appear to have affected most of the sulphide aggregates to some extent. The most obvious effects are the precipitation of abundant secondary magnetite in and around the sulphide bodies and the apparent 'alteration' of many sulphide minerals. Some sulphide bodies are cut by secondary magnetite veinlets of varying thickness (Fig.40(a)), but in most cases the magnetite is present in the form of stringers, inclusions consisting of polygonal aggregates, and lensoid lamellar-like bodies that are developed along cleavage planes. Magnetite may also form thin rims around sulphide bodies or occur as irregular massive aggregates attached to the sulphides. The apparent 'alteration' effects of the sulphides are discussed in the next section.

Samples from the remaining localities appear not to have been subjected to as great a degree of alteration as those from borehole TLP.1. It may not, therefore, be coincidental that many of the sulphide aggregates that are associated with serpentine veinlets contain abundant mooihoekite, haycockite, sphalerite, native copper and complex intergrowths. The sections that exhibit the lowest number of serpentine veinlets or fractures contain significantly simpler assemblages of troilite, chalcopyrite, cubanite and pentlandite, which may represent a primary sulphide assemblage. This suggests that the genesis of the complex sulphide aggregates that include mooihoekite and haycockite might be related to conditions that existed during the serpentinization process.

7.4 Ore Mineral Descriptions

7.4.1 Troilite

Troilite is a member of the pyrrhotite group, which spans the compositional range from stoichiometric FeS (troilite) to cation-deficient Fe_7S_8 (monoclinic pyrrhotite) (Fig.36). Pure troilite is hexagonal, with a NiAs-type structure (Craig & Scott, 1974). Small amounts of Mn, Co and, to a lesser extent, Ni may substitute for Fe in the troilite lattice. Troilite is the most abundant sulphide in the majority of pegmatite samples, and its identity was confirmed by means of X-ray powder photography, X-ray powder diffractometry and electron microprobe analysis (Table 3).

Although a common constituent of meteorites and lunar rocks, troilite is found only occasionally in terrestrial rocks (Craig & Scott, 1974; Vaughan & Craig, 1978). The bulk of the pyrrhotite present in natural geological samples usually consists of an intergrowth of two or more different types of pyrrhotite (Power & Fine, 1976). Troilite may co-exist with other hexagonal pyrrhotites, but mixtures of troilite and monoclinic pyrrhotite are not structurally permissible (Fig.36). The various members of the pyrrhotite family possess very similar optical properties and the presence of intergrowths may only be observed after the samples have tarnished or have been etched. The simplest method of identification involves the use of X-ray diffraction techniques (Ramdhor, 1980). Arnold (1956) developed a simple X-ray diffraction method for the determination of pyrrhotite compositions and this was subsequently refined by Arnold & Reichen (1962). The application of this technique is further discussed by Arnold (1962, 1966) and Graham (1969). The cell dimensions of pyrrhotite decrease systematically with a decrease in the Fe/S ratio and Arnold (1956) was able to produce an experimental curve relating the position of the pyrrhotite (102) reflection to its Fe/S ratio (Fig.38).

Natural tarnishing of troilite in old polished sections and etching with concentrated nitric acid (Ramdhor, 1980), failed to reveal the presence of pyrrhotite intergrowths in the Townlands pipe samples. The apparent lack of hexagonal pyrrhotite coexisting with troilite was confirmed by X-ray powder diffraction (CoK_α radiation), using the technique of Arnold & Reichen (1962). Troilite was removed from six different polished

sections by means of a sharp needle and the powder obtained was finely ground in an agate pestel and mortar under acetone to prevent oxidation. Smear mounts were then prepared and the samples were scanned between 50.0° and 53.0° 2θ, at a scan speed of 1/2° 2θ/min. In each case, a single peak at ±50.68° 2θ (d(102) = 2.091) was produced, which is characteristic of troilite (Fig.39). The presence of hexagonal pyrrhotite would have been reflected in the appearance of a second peak at 51.12° 2θ. Any hexagonal pyrrhotite present is, therefore, in quantities below the level of detection for the technique (i.e. $< \pm 5\%$).

Troilite is generally the most abundant component of larger sulphide aggregates within the pegmatite samples, although it may be locally subordinate to mooihoekite, haycockite or cubanite. It occurs as anhedral grains, commonly forming the core to large sulphide bodies which may be mantled by chalcopyrite + pentlandite ± cubanite, or mooihoekite/haycockite. Troilite that is present around the outer margins of sulphide aggregates occurs as smaller, sub-rounded, discrete grains or polygonal aggregates that are set in a chalcopyrite matrix. Troilite often forms the bulk of large sulphide blebs (1-4cm in diameter) in the samples from the upper parts of TLP.1, while mooihoekite and haycockite are important associates in the lower portion. Small, disseminated sulphide bodies containing troilite are rounded to sub-rounded in shape, but tend to be angular where associated with serpentine veinlets and fractures.

Toilite that is in contact with mooihoekite and haycockite, invariably shows the development of Cu-rich rims (Cabri & Hall, 1972) along mutual interfaces and along fractures and veinlets within the troilite (Fig.40(b)). The rims are pale yellow in plane polarised reflected light and sometimes exhibit a tarnished 'leading edge' against troilite (Fig.40(c)). Small embayed remnants of troilite are frequently present as inclusions within mooihoekite and haycockite grains, and the textural relationships appear to indicate that troilite is replaced to varying degrees by the two low temperature Cu-Fe sulphides. Similar alteration rims that are often zoned occur adjacent to native copper veinlets and stringers that cut troilite grains (Fig.42(a)). The complex intergrowths mentioned in the previous section are hosted by troilite blebs in the upper parts of borehole TLP.1. These intergrowths are developed along the margins of the troilite bodies and along fractures and veinlets within such grains. The complex intergrowths sometimes contain small

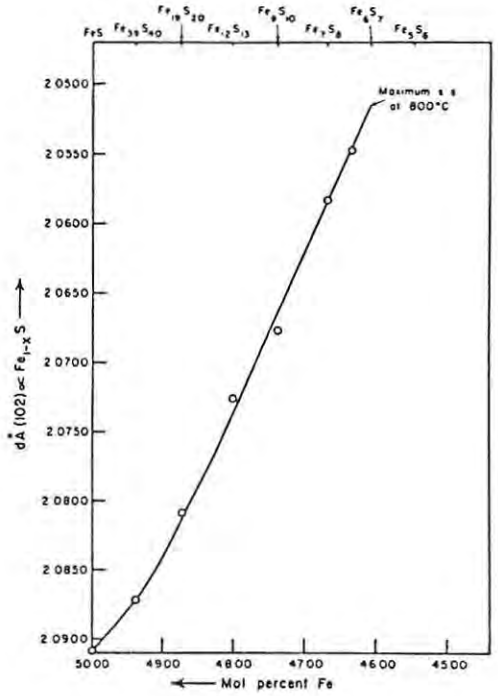

Figure 38. Curve illustrating the relationship between 'd' spacings of the (102) X-ray reflections and the iron content of synthetic pyrrhotites (from Arnold, 1956).

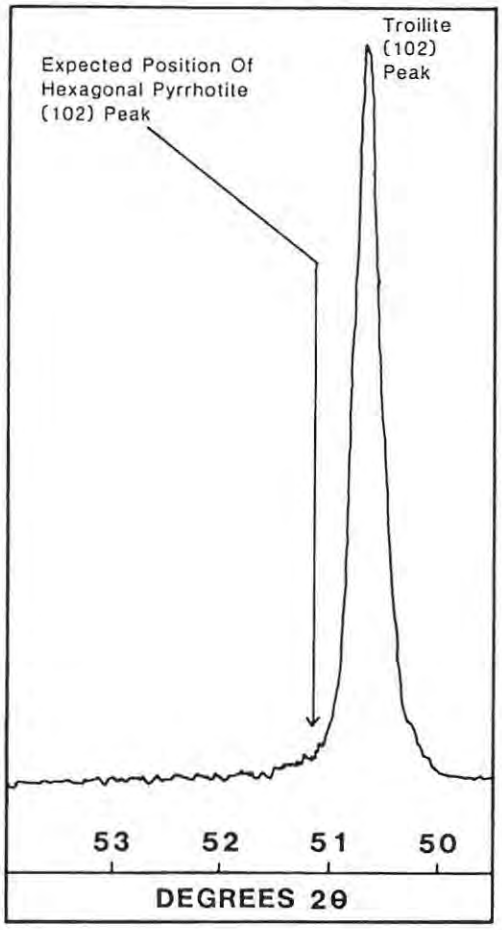

Figure 39. Characteristic d(102) X-ray reflection for troilite and the expected position of the hexagonal pyrrhotite peak. (Scan speed: 1/2° 2θ/min; Fe-filtered Co radiation).

SAMPLE NO.	Tl/209 (i)	Tl/209 (ii)	Tl/253 (iii)	Theoretical FeS
S	35.87	36.25	35.97	37.00
Fe	61.87	62.82	62.62	63.00
Co	-	-	-	-
Ni	-	-	-	-
Cu	0.50	-	0.22	-
TOTAL	98.25	99.07	98.81	100.00

Table 3. Representative microprobe analyses of troilite (J.C.I. Research Lab).

troilite inclusions and it appears that they may also have been formed by the replacement of troilite (Figs.41(d)-(f)).

Flame-like exsolution bodies of pentlandite are common within the troilite, and other intergrowths include magnetite, native copper and chalcopyrite. Secondary alteration of troilite, although not widespread, was noted in two samples from borehole TLP.5. The troilite grains in this case display weakly developed, but distinct 'birds eye' textures, produced by the alteration of troilite to a mixture of marcasite and pyrite (Fig.42(c)). The presence of 'birds eye' textures and the mineral violarite were mentioned in the J.C.I. laboratory report (1981). Violarite is a common supergene alteration product of pentlandite (Nickel et. al., 1977) and, as the TLP.5 samples are located immediately below the zone of silicate mineral weathering, it appears that the troilite alteration is a result of weathering processes.

7.4.2 Chalcopyrite

Chalcopyrite exhibits tetragonal crystal symmetry and may be represented by the chemical formula $CuFeS_2$. At high temperatures Fe, Zn, Ni, Co and Sn may be incorporated into the chalcopyrite structure, to be exsolved at low temperatures as cubanite, sphalerite and stannite (Ramdhor, 1980). Chalcopyrite is relatively abundant in the pegmatite sulphide-bearing sections, but is easily mistaken for haycockite and fresh mooihoekite, both of which possess very similar optical properties. Representative microprobe analyses of several chalcopyrite grains are presented in table 4.

SAMPLE NO.	T1/60	T1/88	T5/2 (i)	T5/2 (ii)	Theoretical $CuFeS_2$
S	34.93	34.27	34.80	34.63	35.00
Fe	30.85	31.26	31.75	32.25	30.00
Co	-	-	-	-	-
Ni	-	-	-	-	-
Cu	34.22	33.32	33.62	32.26	35.00
TOTAL	100.00	98.85	100.16	99.15	100.00

Table 4. Representative microprobe analyses of chalcopyrite (J.C.I. Research Lab).

Chalcopyrite in the pegmatite samples most commonly occurs as aggregates of polygonal grains that are located towards the margins of larger sulphide aggregates, but may also form coarse, discrete grains or intergrowths with troilite, cubanite and/or pentlandite. Intergrowths of chalcopyrite and cubanite typically take the form of parallel, alternating exsolution lamellae of variable width and length (Fig.41(a)). In some instances, narrow lamellae of secondary magnetite are developed between individual chalcopyrite and cubanite lamellae. The relationships between pentlandite and chalcopyrite are somewhat complex. Chalcopyrite, in a few areas is developed along cracks and well developed octahedral cleavage planes within pentlandite, suggesting partial replacement of the pentlandite by chalcopyrite (Fig.40(d)). The relevant chalcopyrite grains also contain irregularly shaped remnant pentlandite inclusions. Another, unusual texture that is occassionally observed, takes the form of thin, somewhat diffuse chalcopyrite lamellae, ($\pm$0.1mm in length) that are developed in a pentlandite matrix (Fig.40(e)).

Chalcopyrite may also occur as thin transgressive veinlets that cut silicate minerals, usually in the vicinity of sulphide aggregates, while small rounded disseminations are relatively abundant. Angular chalcopyrite grains sometimes occur as inclusions within secondary magnetite, and may indicate replacment of original chalcopyrite by magnetite. Inclusions within chalcopyrite grains include pentlandite, troilite, cubanite, magnetite and wispy stringers of bornite. Relationships between chalcopyrite and haycockite are difficult to discern, but are probably similar to those that are observed in sections containing tarnished mooihoekite. In the latter case, mooihoekite occurs along cracks, cleavage planes and grain boundaries within chalcopyrite

aggregates. Embayed remnants of chalcopyrite are also present in mooihoekite, which displays similar replacement textures towards chalcopyrite as is the case for troilite. Supergene alteration of the chalcopyrite is rare and grains in only one section from borehole TLP.4 show very minor alteration to covellite.

7.4.3 Mooihoekite and Haycockite

The recognition of the Cu-Fe sulphides mooihoekite and haycockite as discrete stoichiometric phases, by Cabri & Hall (1972), has resolved many of the discrepancies in 'chalcopyrite' composition reported in the earlier literature. The minerals were first identified in sections from the Mooihoek pipe (hortonolite dunite pegmatite) of the eastern Bushveld Complex. The only other occurrence, located by Cabri & Hall (1972), is in troctolites from the base of the Duluth Gabbro Complex, Minnesota, U.S.A. As a result of their apparent rareity and unusual nature, the two sulphides are discussed in some detail.

Mooihoekite ($Cu_9Fe_9S_{16}$) displays tetragonal crystal symmetry, while haycockite ($Cu_4Fe_5S_8$) is orthorhombic or pseudo-tetragonal. Mooihoekite and haycockite, in freshly polished sections, under reflected light, exhibit very similar optical properties to those of chalcopyrite and untarnished talnakhite. Talnakhite ($Cu_9Fe_8S_{16}$), which also resembles chalcopyrite in composition, was first described by Cabri (1967) in samples from Norils'k, western Siberia. Mooihoekite is weakly anisotropic, while haycockite is weakly to moderately anisotropic. Both mooihoekite and talnakhite tarnish very rapidly on exposure to the atmosphere, from yellow, through various hues of pinkish brown, to a dark purple, with talnakhite eventually becoming iridescent (Cabri & Hall, 1972). Intergrowths of mooihoekite plus talnakhite or chalcopyrite plus haycockite are, therefore, difficult to resolve by optical methods alone, and confirmation by X-ray diffraction or electron microprobe analysis is usually necessary. Mooihoekite, present in sections from the Townlands pegmatite, was identified by X-ray powder photography, while the presence of haycockite was confirmed by electron microprobe analysis. No talnakhite was detected either during the present study or during the initial investigation by the J.C.I. Research Laboratory. The X-ray diffraction data for mooihoekite generated in this study, together with the data of Cabri & Hall (1972), are listed in table 5. Microprobe analyses of the two sulphides in Townlands pegmatite samples are presented in table 6, together with the type-analyses of Cabri & Hall (1972).

MOOIHOEKITE					HAYCOCKITE			
	1	2		3		4	5	
I	d(meas.)	d(calc)	hkl	d(meas.)	I	d(meas.)	d(calc)	hkl
1/2	7.48	7.481	110	7.51				
					1/2	6.82	6.825	112
		5.290	200					
		4.789	101	4.77				
					2	4.42	4.428	204
		4.363	111					
2	3.76	3.769	201	3.76	1	3.74	3.748	206
1/2	3.34	3.346	310					
10	3.06	3.070	221	3.07	10	3.07	3.071	226
1	2.83	2.840	311					
1	2.68	2.685	002	2.66*	4	2.67	2.678	400
2	2.64	2.645	400		3	2.62	2.624	0.0.12
1/2	2.49	2.494	330		1/2	2.42	2.421	2.2.10
		2.366	420					
		2.315	411					
1/2	2.26	2.262	311		1	2.28	2.275	336
1	2.17	2.165	421					
1	2.09	2.094	312	2.09				
8	1.881	1.884	402	1.877*	6	1.889	1.893	440
5	1.870	1.870	440		8	1.876	1.874	4.0.12
		1.827	332					
4	1.612	1.615	223	1.612	6	1.612	1.612	626
6	1.593	1.597	621	1.598	4	1.586	1.588	2.2.18
2	1.528	1.535	442		1	1.535	1.536	4.4.12
1	1.341	1.343	004		2	1.333	1.339	800
4	1.321	1.323	800		1/2	1.325	1.327	656
					2	1.313	1.312	0.0.24
5	1.219	1.222	623		3	1.227	1.227	666
2	1.213	1.215	661		5	1.214	1.217	6.2.18
		1.197	404					
		1.183	840					
4	1.089	1.091	444	1.091	6	1.089	1.089	8.4.12
6	1.081	1.083	842	1.083	4	1.077	1.079	4.4.24
		1.032	225		3	1.031	1.030	10.2.6
2	1.022	1.023	663	1.021	2	1.022	1.024	6.6.18
3	1.018	1.019	10.2.1		2	1.011	1.012	2.2.30
4	0.942	0.942	804	0.941	3	0.946	0.947	880
2	0.935	0.935	880		6	0.937	0.937	8.0.24

1 : X-ray diffraction powder data for Mooihoekite from the Mooihoek pipe (Cabri & Hall, 1972).

2 : Theoretical X-ray diffraction powder data (Cabri & Hall, 1972).

3 : X-ray diffraction powder data for mooihoekite from the Townlands pipe.

4 : X-ray diffraction powder data for haycockite from the Mooihoek pipe (Cabri & Hall, 1972).

5 : Theoretical X-ray diffraction powder data (Cabri & Hall, 1972).

* Broad line, not resolved.

Table 5. X-ray diffraction powder data for mooihoekite and haycockite.

MOOIHOEKITE			
SAMPLE NO.	1	T1/209	T1/226	Theoretical $Cu_9Fe_9S_{16}$
S	31.93 - 33.29 (32.44)	32.40	32.26	32.00
Fe	31.38 - 32.40 (31.88)	32.08	32.01	32.00
Co	-	-	-	-
Ni	0.24 - 0.30 (0.26)	0.47	-	-
Cu	34.87 - 36.71 (35.91)	35.07	34.82	36.00
TOTAL	99.51 - 100.94 (100.49)	100.01	99.09	100.00

HAYCOCKITE			
SAMPLE NO.	1	T1/226	Theoretical $Cu_4Fe_5S_8$
S	31.94 - 32.86 (32.41)	32.59	32.50
Fe	34.64 - 35.46 (35.03)	35.72	35.00
Co	-	-	
Ni	0.36 - 0.58 (0.40)	-	
Cu	31.83 - 32.55 (32.16)	31.62	32.50
TOTAL	98.87 - 100.94 (100.14)	99.94	100.00

1 : Cabri & Hall (1972)
T1/209, T1/226 : pegmatite samples (J.C.I. Research Laboratory)

Table 6. Microprobe analyses of mooihoekite and haycockite

Mooihoekite and haycockite are relatively abundant in sections from borehole TLP.1 and minor amounts are present in samples from borehole TLP.3. No mooihoekite or haycockite was detected in samples from the remaining localities. The occurrence of the two minerals in sulphide aggregates is characterised by the presence of abundant Ti-poor magnetite inclusions, in the form of discrete anhedral grains, lenticular stringers and transgressive veinlets. Mooihoekite and haycockite are most commonly developed along the outer margins of sulphide aggregates, but 'radiate' inwards along fractures, magnetite veinlets and grain boundaries. Consequently, they exhibit very irregular morphologies and complex grain boundary relationships.

The textural relationships between mooihoekite or haycockite and the other major sulphides troilite, chalcopyrite, cubanite and pentlandite appear to illustrate various stages of replacement by mooihoekite and/or

haycockite. In all cases, mooihoekite and haycockite occur as wispy lamellae along grain boundaries, cracks, and cleavage planes within adjacent sulphide grains. Troilite develops Cu-rich rims in areas where it is in contact with either of the two phases (Fig.40(b)), while chalcopyrite, cubanite (Fig.41(b)) and pentlandite (Fig.41(c)) all show the development of similar embayed and irregular grain boundaries against mooihoekite and haycockite. The partial replacement of sulphide minerals by mooihoekite is most readily observed once the mooihoekite has been allowed to tarnish. Replacement by haycockite is not as readily discerned because of the close similarity of haycockite to chalcopyrite.

Mooihoekite tarnishes within a few hours of polishing and in several sections unusual textural patterns were revealed by the tarnishing effects. In these cases, some mooihoekite grains show the presence of spindle-shaped lamellae that display different tarnishing hues to that of the surrounding matrix (Fig.40(f)). The lamellae are usually oriented in three directions and may reflect the existence of twinning. The nature of the lamellae is suggestive of inversion twinning, caused by the inversion of a higher temperature polymorph to a lower temperature form (I.M. Reynolds, pers. comm.). Both mooihoekite and haycockite often exhibit a 'patchy' texture, which may be a result of their replacement origin, as the texture is invariably associated with small embayed remnants of troilite, chalcopyrite, cubanite and pentlandite. Fine feather-like inclusions of mackinawite are sometimes present, while anhedral sphalerite grains of varying size and shape are very common inclusions in the larger mooihoekite and haycockite aggregates (Fig.42(b)). The sections from the upper parts of borehole TLP.1 that contain mooihoekite and haycockite may also host transgressive veinlets that consist of native copper, magnetite and valeriite. The association of native copper with the Cu-Fe sulphides may be significant in terms of their petrogenesis and is discussed further in section 7.5.

7.4.4 Cubanite

Cubanite approximates the chemical formula $CuFe_2S_3$, but at high temperatures substantial amounts of Fe are soluble in its structure. According to Ramdhor (1980), the high temperature solid solution breaks down on cooling, to form chalcopyrite + cubanite, chalcopyrite + pyrrhotite or chalcopyrite + mackinawite. Yund & Kullerud (1966) reported that cubanite is cubic above 252° $\pm$ 3°C, tetragonal to below

213°C and orthorhombic at very low temperatures. Their studies also indicated that cubanite is stable to low temperatures and does not decompose to form pyrrhotite + chalcopyrite, as suggested by Ramdhor (1980). Cubanite from the Townlands pipe is generally present in subordinate amounts to troilite, chalcopyrite, mooihoekite and haycockite, except in the sections from borehole TLP.5, where it is the dominant sulphide constituent. Identification was confirmed by X-ray powder photography and electron microprobe analyses. Representative microprobe analyses are presented in table 7.

SAMPLE NO.	T1/88	T5/2 (i)	T5/2 (ii)	Theoretical $CuFe_2S_3$
S	35.13	35.95	35.50	35.50
Fe	41.13	42.06	40.68	41.50
Co	-	-	-	-
Ni	-	-	-	-
Cu	23.11	23.11	23.78	23.00
TOTAL	99.37	101.12	99.96	100.00

Table 7. Representative microprobe analyses of cubanite (J.C.I. Research Lab)

The cubanite present in the TLP.5 sections occurs, most frequently, as massive grains with irregular grain boundaries and morphologies. Very elongated, thin chalcopyrite exsolution lamellae, up to 0.2mm in length, and rounded troilite inclusions are relatively abundant in most grains. Cubanite from the remaining sample localities generally occurs as thin-tabular lamellar intergrowths with chalcopyrite (Fig.41(a)). In a few instances, magnetite is developed between the individual exsolution lamellae. Inclusions in cubanite include chalcopyrite, troilite and occasional pentlandite 'flames'. Cubanite appears to be replaced by mooihoekite and haycockite in a similar manner to that displayed by chalcopyrite and occurs as embayed grains containing mooihoekite and haycockite that are developed along fractures and cleavage cracks (Fig.41(b)).

7.4.5 Pentlandite

Pentlandite (cubic) was considered to have a structural formula represented by $(Fe,Ni)_9S_8$. Investigations by Knop et. al. (1965), however, revealed that pentlandite is actually a natural (Fe, Co, Ni, S) phase, in which the Fe:Ni:Co ratio displays considerable variation. They

distinguished between Co-poor and Co-rich pentlandites with Ni:Fe ratios of 1.00 - 1.15 and 0.70 - 1.29, respectively, and proposed the formula $(Fe,Co,Ni)_{9+x}S_8, x \geqslant 0$, for naturally occurring pentlandites. Rajamani & Prewitt (1973) examined pentlandites from various localities and suggested an alternative structural formula of $M_{9-x}S_8$ for Ni-rich pentlandites and $M_{9+x}S_8$ for Fe-rich pentlandites, where M = Fe, Ni, Co and $x \geqslant 0$.

Kouvo et. al. (1959) reported the presence of pentlandite from sulphide deposits in Finland in which Co contents range between 1.92 and 49.33 percent. The Co-rich pentlandite grains apparently display little change in optical properties, other than being slightly lighter in colour than Ni-rich pentlandite. Petruk et. al. (1969) reported a cobalt pentlandite of composition 54.1% Co, 10.4% Ni, 34.2% S, from the Langis mine, Ontario. The wide range in pentlandite compositions has since been investigated by Harris & Nickel (1972) and Misra & Fleet (1973). Misra & Fleet (1973) concluded that the Ni:Fe ratio of pentlandite appears to be related to the nature of the host assemblage. Harris and Nickel (1972) recognised several characteristic assemblages and distinguished between pentlandite + troilite and pentlandite + pyrrhotite associations. In the former assemblage, pentlandite exhibits the lowest Ni:Fe ratios and Co concentrations of 0.8 - 6.3at percent, while in the latter case, pentlandite contains < 3.0at percent Co and exhibits higher Ni:Fe ratios. Cobalt pentlandite crystals with very high Co contents occur in pentlandite + heazlewoodite (±awaruite) assemblages (Harris & Nickel, 1972). The pentlandite in the Townlands pegmatite is associated with troilite and exhibits Co levels of 2.41 - 7.20wt percent (table 8). Earlier analyses by the J.C.I. Research Laboratory, however, suggest that these values may be slightly low, due to analytical difficulties related to the overlap of Co K_α and Fe K_β peaks.

SAMPLE NO.	T1/60	T5/2 (i)	T5/2 (ii)	Theoretical $(Fe,Ni)_9S_8$
S	32.65	32.60	32.73	33.00
Fe	29.73	29.38	28.78	33.50
Co	7.20	2.41	2.68	-
Ni	28.93	33.66	34.70	33.50
Cu	-	-	-	-
TOTAL	98.51	98.06	98.89	100.00

Table 8. Representative microprobe analyses of pentlandite (J.C.I. Research Lab)

Pentlandite present in sulphide-bearing sections from the Townlands pegmatite exhibits two main modes of occurrence. It most commonly forms coarse, sub-rounded discrete grains that are usually situated near the margins of large sulphide bodies. The second mode of occurrence is as abundant flame-like inclusions in troilite (Fig.41(d)) and, to a much lesser extent, cubanite. Pentlandite displays evidence of partial replacement by chalcopyrite (Fig.40(d)) and by both mooihoekite and haycockite (Fig.41(c)). In both cases, the pentlandite grains display irregular or embayed grain boundaries at places where they are in contact with chalcopyrite, mooihoekite or haycockite. These phases are also commonly developed along fractures and cleavage planes in the pentlandite. In addition, small, irregular inclusions of pentlandite are often located within adjacent chalcopyrite or mooihoekite and haycockite grains. The relationship between chalcopyrite and pentlandite is complex and, in some cases chalcopyrite occurs as thin, diffuse lamellae ($\pm$0.1mm in length), apparently intergrown with pentlandite (Fig.40(e)). The reverse situation was also noted, in one section from borehole TLP.1, in which very diffuse lensoid lamellae of pentlandite are hosted by chalcopyrite. Mackinawite, is invariably present as fine feather-like inclusions in coarse pentlandite. There is some debate, however, as to whether mackinawite is formed by exsolution processes (Ramdhor, 1980), or by the alteration of pentlandite (Chamberlain & Delabio, 1965).

7.4.6 Mackinawite

The optical properties of mackinawite are very similar to those of valeriite and for many years only valeriite was reported in the geological literature (Ramdhor, 1980). Mackinawite was recognised as being a discrete sulphide phase by Kouvo et. al. (1963) in samples from sulphide deposits in Finland. It has tetragonal crystal symmetry and Kouvo et. al. (1963) proposed a compositional formula represented by FeS or $Fe_{1-x}S$. Fairly substantial amounts of Co and up to 8.26 percent Ni (Chamberlain & Delabio, 1965) are, however, soluble in the mackinawite structure. The structure of mackinawite is sulphur-deficient and Takeno & Clark (1967), therefore, proposed the formula $Fe_{1+x}S$, which is analagous to that proposed by Taylor & Finger (1971) (FeS_{1-x}).

The optical properties of mackinawite and valeriite observed in the Townlands pipe samples are in agreement with those reported by Kouvo et. al. (1963) and Chamberlain & Delabio (1965), and are summarised in

table 9. The presence of mackinawite in the pegmatite sections was confirmed by X-ray diffraction powder photography. The origin of mackinawite appears to be somewhat controversial. Chamberlain & Delabio

	Mackinawite	Valleriite
Color	pinkish gray close to pyrrhotite	dull bronze similar to graphite
Bireflectance	moderate to high pink to gray	extreme under high power creamy bronze to purple
Anisotropism	high, but decreasing with time after polishing. under completely crossed nicols: grayish white to dark gray under incompletely crossed nicols: bluish white to Sienna brown (diagnostic)	extreme white to bronze, remaining much the same only less intense under incompletely crossed nicols.
Reflectivity	not measured, but in same range as pyrrhotite	not measured, but very low, in same range as graphite
Vickers hardness (50 g load)	58	30
Polish	fair, always with scratches	very poor, showing semi-matte surface despite all efforts to polish

Table 9. Comparison of the optical and physical properties of mackinawite and valeriite (from Chamberlain & Delabio, 1965).

(1965) studied the occurrence of mackinawite and valeriite in dunite and pyroxenite of the Muskox intrusion, Canada and concluded that mackinawite forms by selective replacement of pentlandite. They based their argument on their observations that mackinawite never occurs as oriented intergrowths, but only as irregular grains whose shape is controlled by the prominent pentlandite cleavage planes. They also noted that mackinawite is invariably associated with serpentine, and concluded that the mineral forms at moderate to low temperatures during the serpentinization of olivine. Ramdhor (1980), however, suggested that mackinawite is rare as a replacing mineral and results from the unmixing of high temperature chalcopyrite and pentlandite solid solutions.

Mackinawite in sulphide aggregates from the Townlands pegmatite, most frequently occurs as fine, feather-like intergrowths in coarse pentlandite (Fig.41(e)). The intergrowths are usually strongly oriented in three different directions, probably corresponding to the pentlandite octahedral cleavage planes. Many of these coarse pentlandite grains are, however, largely unaffected by serpentine or magnetite veinlets and it is

possible that the mackinawite is a product of exsolution rather than replacement. Small wispy laths of mackinawite occassionally occur as inclusions in mooihoekite and haycockite, but in contrast to the aforementioned case, the mackinawite is usually developed adjacent to fractures or magnetite stringers and veinlets. It is possible, therefore, that the mackinawite inlcusions in mooihoekite and haycockite formed during the replacement of the primary sulphide assemblage by mooihoekite and haycockite. Mackinawite also takes the form of oriented platelets that exhibit pseudo-rectangular shapes and are sometimes associated with mooihoekite and/or haycockite, but more often, form part of the complex intergrowths. These platelets are described in more detail in section 7.4.12.

7.4.7 Valeriite

Valeriite is easily confused with mackinawite and differences between their respective optical and physical properties are summarised in table 9. According to Evans et. al. (1964), valeriite was first described in samples from Nya Kopparberg, Sweden, by Blomstrand in 1870. The chemical formula of the mineral is close to $CuFeS_2$, but its structure allows for the inclusion of intermediate layers, usually composed of $Mg(OH)_2$ and occassionally $Ni(OH)_2$ and $Fe(OH)_2$ (Ramdhor, 1980). Valeriite therefore possesses a complicated mixed-layer structure, which may be best represented by $1.5\,[(Fe,Cu)_{2-x}S_2]$ and $1.[(Mg_7Al_3)(OH)_2]$ (Ramdhor, 1980). As a result of the layered structure, valeriite is extremely soft and has a hardness less than that of graphite (VHN = 30).

Valeriite has been reported from numerous localities, but according to Ramdhor (1980), it is invariably associated with serpentine in areas containing Cu-bearing sulphides, and may replace cubanite, pyrrhotite, pentlandite, magnetite and serpentine. The identification of valeriite in sections from the Townlands pegmatite was confirmed by X-ray powder photograpy. The distribution of valeriite is restricted to a few sections from borehole TLP.1, where it occurs as irregular slivers, platelets and wispy grains (<0.1mm in length) that are sometimes arranged in radiating aggregates (Fig.41(f)).

The valeriite grains are usually intimately associated with transgressive serpentine veinlets that contain native copper and magnetite, but may

also occur in serpentine veinlets that cut silicate minerals adjacent to sulphide aggregates. Minor inclusions of valeriite occur with mooihoekite and haycockite and at the margins of one large haycockite-dominated sulphide bleb, valeriite grains associated with native copper are intimately intergrown with the haycockite (Fig.41(f)). In addition, small mooihoekite and haycockite grains occassionally occur as inclusions in valeriite - native copper aggregates. Consequently, it appears that valeriite may represent a late stage phase that formed by reactions which may have involved one or more of serptentine, native copper, mooihoekite, haycockite and magnetite.

7.4.8 Native Copper

Native copper is easily recognised in freshly polished sections, by its brilliant orange-brown colour which gradually darkens to reddish brown hues on prelonged exposure to the atmosphere. It is isotropic and exhibits an extremely high reflectivity. The occurrence of native copper in the Townlands pipe is restricted to samples from the upper 120m of borehole TLP.1 and no trace of the metal was detected below this depth or in sections from any of the other sample localities.

The native copper is most commonly located in veinlets adjacent to, and within, sulphide aggregates containing mooihoekite and/or haycockite. The metal may be the sole occupant of thin veinlets or occur as discontinuous stringers in the centre of veinlets comprising secondary magnetite, serpentine and occassional valeriite (Fig.41(f)). The copper stringers seldom exceed 1mm in width, but may be of extremely variable length. Thin veinlets and fine networks of native copper occupying original serpentine veinlets and fractures, are sometimes developed in the silicate matrix surrounding sulphide aggregates. The metal may form thin partial rims around the sulphide bodies and also occurs as irregular stringers and sub-rounded inclusions in mooihoekite, haycockite and troilite.

Native copper veinlets that traverse troilite grains also produce Cu-rich rims in the troilite that are similar to those developed between troilite and mooihoekite or haycockite. The rims are, however, zoned in this case (Fig.42(a)), and in some instances thin rims of mooihoekite are developed on either side of the copper veinlets. Native copper in the presence of abundant valeriite, forms intimate intergrowths with valeriite and

secondary magnetite. Textural relationships and the transgressive nature of the copper veinlets indicates that the native copper could not have formed part of the primary magmatic sulphide assemblage of the Townlands pegmatite and there are two possible explanations for its origin. It either formed during late-stage deuteric processes, or it has been produced by reaction between aqueous solutions and copper-bearing sulphides. The textural relationships and the presence of unaltered native copper veinlets in troilite, however, suggest that the former proposal may be more feasible.

7.4.9 Sphalerite

Sphalerite exhibits cubic crystal symmetry and may be represented by the chemical formula ZnS. It is, however, rarely pure and frequently contains small amounts of one or more of Cu, Fe, Mn, Sn, Cd and, to a minor extent, Ga, In, Tl and Hg (Ramdhor, 1980). The structure of sphalerite resembles that of chalcopyrite, stannite, fahlore and cubanite, and oriented inclusions of these phases are relatively common in sphalerite (Vaughan & Craig, 1978; Ramdhor, 1980).

The presence of sphalerite in pegmatite sections from boreholes TLP.1 and TLP.3 was confirmed by X-ray powder photography and electron microprobe analyses. Representative analyses of sphalerite are presented in table 10. Sphalerite occurs almost exclusively as inclusions in mooihoekite and haycockite (Fig.42(b)). The inclusions vary in size (<0.05mm - 0.2mm), but are usually sub-rounded in shape and situated close to the margins of sulphide aggregates. The sphalerite is dull blue-grey in colour, and shows the development of pale blue, possibly copper-rich,

SAMPLE NO.	Tl/88 (i)	Tl/88 (ii)	Theoretical ZnS
S	33.13	32.91	33.00
Fe	5.64	5.67	-
Cu	0.49	1.08	-
Zn	59.90	59.47	67.00
TOTAL	99.16	99.13	100.00

Table 10. Representative microprobe analyses of sphalerite (J.C.I. Research Lab)

rims at grain boundaries with mooihoekite and haycockite. These rims also occur along fractures within individual sphalerite grains. The

larger inclusions contain small exsolution bodies of chalcopyrite, which may be rounded to sub-rounded in shape, or occur as lens-like lamellae oriented parallel to the cubic cleavage planes of sphalerite. The association of sphalerite with mooihoekite and haycockite suggests that the mineral may be a secondary phase, formed during the replacement of the primary sulphide assemblage by mooihoekite and haycockite.

7.4.10 Pyrite

Pyrite (cubic) has the composition FeS_2, but, according to Ramdhor (1980), may contain minor proportions of Ni, Co, Cu, Zn, Ag and Au. It is pale yellow in colour, has a high reflectivity and is isotropic. The pyrite in the Townlands pegmatite is confined to samples from borehole TLP.5. Identification was aided by X-ray powder photography and microprobe analysis.

The pyrite in sections from borehole TLP.5 occurs in two distinct textural forms. In the first case, it is in the form of blocky granular aggregates that are usually developed along grain boundaries between troilite and cubanite. These aggregates may also be present adjacent to cracks and thin magnetite veinlets. The aggregates generally consist of one relatively large, euhedral pyrite crystal that is surrounded by numerous smaller grains. The absence of pyrite from the other samples together with the textural relationships between pyrite and the adjacent sulphides, suggest that the pyrite may have formed as a result of secondary processes.

The second mode of occurrence of pyrite in borehole TLP.5 is in association with marcasite and results from the alteration of troilite. Marcasite (FeS_2) is also pale yellow in colour and exhibits a high reflectivity, but unlike pyrite, it is strongly anisotropic. The alteration of troilite to a mixture of pyrite and marcasite has produced distinctive 'bird's eye' textures (Fig.42(c)). The TLP.5 samples are located a short distance below the silicate mineral weathering zone and it is probable that the alteration is due to supergene effects.

7.4.11 Minor Constituents

In addition to the more abundant ore minerals, the sulphide aggregates contain a host of accessory phases. The majority are present in only minute amounts and those that were identified are listed below. Bornite

(Cu_5FeS_4), whose identification was confirmed by microprobe analysis, occurs as small inclusions in chalcopyrite in several samples from borehole TLP.1. One small micrometre-sized grain of native silver was located, adjacent to a copper-bearing veinlet, in a section from TLP.1. The silver is characterised by a higher reflectivity than the copper and is hosted by haycockite. Several small graphite platelets were noted in serpentine veinlets adjacent to sulphide bodies, in samples from borehole TLP.1. Occasional digenite (Cu_9S_5) grains are present as inclusions in mooihoekite and haycockite. Minute bodies of covellite are present in chalcopyrite in a sample from borehole TLP.4. The samples from borehole TLP.5 that contain pyrite, also contain very small grains of an anisotropic grey-blue phase with deep red internal reflections. The mineral occurs as irregular grains along fractures in sulphide aggregates and as thin veinlets in the sulphides and adjacent silicate matrix. Electron microprobe analysis indicates that this phase is an iron oxide, probably hematite.

Additional ore minerals listed by Viljoen et. al. (1983) include altaite, galena, niccolite, chalcocite, molybdenite, native bismuth, froodite, clausthalite, violarite and two unknown Cl-bearing phases, which may be of genetic importance. These phases were all reported to be in the micrometre-size range and were not specifically searched for in this study, as emphasis was placed on the major phases and their textural relationships.

7.4.12 Complex fine-scale sulphide intergrowths

The complex intergrowths appear to consist of many of the phases mentioned in previous sections, but are discussed separately because of their very unusual textural and grain boundary relationships. These composite intergrown grains were only noted in large, troilite-dominated, sulphide blebs in samples from the upper parts of borehole TLP.1. They are invariably developed around the margins of troilite agregates, but are also present along fractures and veinlets within such aggregates. Their overall grain boundary relationships with troilite are similar to those between mooihoekite/haycockite and troilite. This suggests that the complex fine-scale sulphide intergrowths may also have formed at the expense of troilite.

The complex intergrowths exhibit an array of unusual textures, but two basic types can be distinguished. The first group (Group 1) of

intergrowths is characterised by the presence of oriented, pseudo-rectangular mackinawite platelets that separate areas consisting of sub-microscopic intergrowths of two or more phases (Fig.42(d)). The second group (Group 2) of textures is more complex and consists of a sub-parallel arrangement of wavy, lenticular haycockite and/or chalcopyrite lamellae that separate zones consisting of two or more intimately related phases. Microprobe analyses of the lenticular lamellae yielded compositions intermediate between those of haycockite and chalcopyrite suggesting that they may consist of submicroscopic mixtures of these two phases. This latter group of composite grains is found in association with aggregates of what appear to be discrete phases, but also consist of extremely fine-grained intergrowths of several phases. These intergrowths cannot generally be resolved under the microscope at high magnification (100x oil immersion objective) and were only discerned during electron microscope studies kindly undertaken by the J.C.I. Research Laboratory (Figs.42(e),(f)).

Microprobe analyses of the various complex intergrown phases were performed by J.C.I. Research Laboratory and are presented in table 11. The majority of the analyses show the presence of Fe, Ni, Cu and sometimes Co, in addition to S. These represent very unusual compositions and it was considered probable that they might represent bulk analyses of submicrometre-sized intergrown phases. Normative calculations, based on average compositions of troilite, pentlandite, chalcopyrite, mooihoekite and haycockite in the Townlands pegmatite were, therefore, performed on a 'trial and error' basis. These calculations indicated that most of the analyses could be adequately interpreted as consisting of two or more phases that are common constituents of the TLP.1 sulphide assemblages. This interpretation is supported by the resolution of sub-microscopic intergrowths by scanning electron microscopy (Figs.42(e),(f)). The bulk electron microprobe analyses of these phases are listed in table 11, together with their normative compositions.

Consequently, the first group of fine-scale intergrowths, which are separated by mackinawite platelets probably consist of intergrowths of troilite, mooihoekite, haycockite, mackinawite and pentlandite. The second group of fine-scale intergrowths which is characterised by the presence of wavy lamellae of chalcopyrite and/or haycockite are more difficult to resolve, but also appear to consist of mixtures of mooihoekite (tarnished), pentlandite, troilite and possibly mackinawite. Further investigations are, however, required to fully understand and categorise these very unusual sulphide intergrowths and textures.

GROUP 1. Textures

SAMPLE NO.	T1/253 (i)	T1/253 (ii)	T1/253 (iii)	T1/253 (iv)	T1/253 (v)
S	32.87	35.46	32.14	35.56	33.13
Fe	42.25	55.03	40.34	59.68	39.13
Co	0.19	0.39	0.23	0.35	3.25
Ni	19.19	5.98	22.81	2.10	22.27
Cu	4.44	1.27	2.50	0.85	2.41
TOTAL	98.94	98.13	98.02	98.54	100.20
Approx. Normative Composition					
Tr	+16	-	26	91	27
Pn	55	17	66	6	65
Hy	14	4	8	3	8
Mh	-	-	-	-	-
Cp	-	-	-	-	-
Mk[1]	+15	79	-	-	-

GROUP 2. Textures

SAMPLE NO.	T1/209 (i)	T1/209 (ii)	T1/209 (iii)	T1/209 (iv)	T1/209[2] (v)	T1/209 (vi)
S	32.00	33.21	32.23	33.08	33.20	33.17
Fe	35.49	36.79	33.04	37.63	32.12	40.62
Co	1.07	2.96	-	2.58	-	0.82
Ni	13.20	22.32	1.03	23.72	0.69	20.31
Cu	16.27	4.26	33.83	2.95	34.70	5.05
TOTAL	99.03	99.54	100.13	99.96	100.71	99.96
Approx. Normative Composition						
Tr	9	22	3	23	-	28
Pn	39	65	3	69	2	58
Hy	52	13	-	-	+49	-
Mh	-	-	94	8	-	14
Cp	-	-	-	-	+49	-
Mk[1]	-	-	-	-	-	-

1 : Presence of mackinawite confirmed by microscopic examination.
2 : T1/209(v): Wavy lenticular lamellae of haycockite and/or chalcopyrite.

Tr = troilite; Pn = pentlandite; Hy = haycockite; Mh = mooihoekite; Mk = mackinawite; Cp = chalcopyrite.

Table 11. Representative composite microprobe analyses of complex sulphide intergrowths (J.C.I. research lab).

7.5 Discussion

The Townlands ultramafic pegmatite contains a very unusual and diverse assemblage of ore minerals, particularly with respect to the samples from borehole TLP.1. The most common sulphide assemblage encountered in the

pegmatite sections includes troilite, chalcopyrite, cubanite and pentlandite. This assemblage, with the exception of troilite whose place is usually taken by intermediate pyrrhotite, is typical of the primary sulphide assemblages commonly observed in igneous rocks that have crystallized from a melt.

The presence of troilite (FeS) as the dominant sulphide phase in the Townlands pegmatite is significant, as it is a rare mineral in terrestrial rocks and where present, it normally occurs as intergrowths with hexagonal pyrrhotite (Arnold, 1967; Craig & Scott, 1974; Vaughan & Craig, 1978). In contrast, troilite is a common constituent of meteorites and lunar rocks where it co-exists with native iron or iron-nickel alloys (Vaughan & Craig, 1978). There is no evidence to suggest that the troilite in the Townlands pegmatite formed by replacement of pre-existing sulphides, and its relative abundance may be related to its crystallization from a sulphur-poor melt. An alternative suggestion is that it crystallized from an Fe-rich pegmatitic magma in which the iron activity was very high and, therefore, condusive to the formation of troilite rather than intermediate pyrrhotite.

The only other sulphide phases present in significant quantities are mooihoekite and haycockite, which are confined to sections from boreholes TLP.1 and TLP.3. These two minerals have low temperature stability fields and appear to have formed by replacement of the 'primary' assemblage constituents (troilite + chalcopyrite + cubanite + pentlandite) of the pegmatite at low temperatures ($< 200°C$). The samples from borehole TLP.1 also contain a number of other unusual phases, which are present in minor amounts and include sphalerite, valeriite, mackinawite, native copper, graphite, digenite and native silver. The textural relationships of mooihoekite, haycockite and many of the minor phases indicate that they formed at a later stage than the sulphides of the 'primary' assemblage.

The solid-state replacement of phases such as troilite (FeS) and pentlandite ($(Fe,Ni)_9S_8$) by mooihoekite ($Cu_9Fe_9S_{16}$) and/or haycockite ($Cu_4Fe_5S_8$) clearly requires the introduction of significant amounts of copper into the system. The alteration of cubanite ($CuFe_2S_3$) and chalcopyrite ($CuFeS_2$), to either mooihoekite ($Cu_9Fe_9S_{16}$) or haycockite ($Cu_4Fe_5S_8$), requires the addition of considerably less copper. The chemical reactions that may have been

involved in the formation of mooihoekite ($Cu_9Fe_9S_{16}$) and haycockite ($Cu_4Fe_5S_8$) can be summarised as follows:

a) Troilite

i) $16FeS + 9Cu^{2+} \rightleftharpoons Cu_9Fe_9S_{16} + 7Fe^{2+}$

ii) $8FeS + 4Cu^{2+} \rightleftharpoons Cu_4Fe_5S_8 + 3Fe^{2+}$

b) Pentlandite

i) $2(Fe,Ni)_9S_8 + 9Cu^{2+} \rightleftharpoons Cu_9Fe_9S_{16} + 9Fe^{2+} + 18Ni^{2+}$

ii) $(Fe,Ni)_9S_8 + 4Cu^{2+} \rightleftharpoons Cu_4Fe_5S_8 + 4Fe^{2+} + 9Ni^{2+}$

c) Cubanite

i) $6\ CuFe_2S_3 + 3Cu^{2+} \rightleftharpoons Cu_9Fe_9S_{16} + 2FeS + Fe^{2+}$

ii) $3\ CuFe_2S_3 + Cu^{2+} \rightleftharpoons Cu_4Fe_5S_8 + FeS$

d) Chalcopyrite

i) $8\ CuFeS_2 + Cu^{2+} + Fe^{2+} \rightleftharpoons Cu_9Fe_9S_{16}$

ii) $4\ CuFeS_2 + Fe^{2+} \rightleftharpoons Cu_4Fe_5S_8$

The Fe^{2+} produced by the replacement of troilite may account for portion of the magnetite that is always found associated with mooihoekite and haycockite. Pentlandite is not an abundant sulphide phase in the pegmatite assemblages and the Ni^{2+} produced by its replacement might be incorporated into the associated magnetite, to form nickel-bearing magnetite. The alteration of cubanite releases FeS, which may have precipitated as mackinawite. Mackinawite is also found intergrown with mooihoekite and haycockite, and may, therefore, represent replaced cubanite. The replacement of chalcopyrite requires only the addition of minor Cu^{2+} and Fe^{2+}. The Fe^{2+} required for the chalcopyrite reaction is readily derived from one of the foregoing reactions.

The relative abundances of mooihoekite, haycockite and native copper are small and they probably constitute considerably less than 1 percent by volume of the pegmatite. The quantity of copper required for their formation is, therefore, not very significant, but the question still remains as to its origin. Copper veinlets often occupy pre-existing serpentine veinlets, which suggests that the replacement reactions occurred subsequent to, or during the final stages of the serpentinization process. The serpentinization of olivine has resulted in the development of a pervasive system of fractures and veinlets, which

would have facilitated the transport of copper-bearing solutions. Consequently, the permeability necessary for the movement of copper-bearing fluids was clearly in existence and there are two broad possibilities as to the source of the copper. One possibility is local derivation from the decomposition of copper-bearing sulphides in the immediate vicinity of the mooihoekite and haycockite grains. There is, however, no evidence to support this suggestion and it appears that the copper may have been derived from some source outside the environment of the sulphide aggregates.

Copper may be released during supergene alteration and transported down by groundwater solutions until it encounters a reducing environment at depth and is precipitated. Supergene enrichment is invariably accompanied by the formation of a characteristic sulphide assemblage that may include covellite, chalcocite and cuprite. None of these phases was, however, encountered in the sections from borehole TLP.1. Mooihoekite, haycockite and copper veinlets are also not found in samples from the other boreholes, although these penetrate to below the zone of weathering. Native copper occurs to a depth of 120m in borehole TLP.1, which may be somewhat thick for a zone in which supergene enrichment has taken place. Furthermore, the alteration would be expected to concentrate immediately below the water table, but there is no evidence for a gradual decrease in the degree of alteration with increasing depth. It appears unlikely, therefore, that the copper was introduced from above by supergene enrichment processes.

Another possibility is that the copper may have been transported by fluids from below. The source of copper from below is difficult to ascertain and there are a number of possibilities:

i) The copper could be derived from the decomposition of copper-bearing sulphides at lower levels within the pipe.

ii) The copper may have been introduced by hydrothermal solutions, the source of which is highly speculative. Water may be introduced into the system through structural disturbances either from meteoric-hydrothermal systems or by water released during metamorphism in the footwall sediments. Such fluids might scavenge copper from the rocks through which they pass, which may then be

precipitated in the pegmatite. There is, however no evidence of the alteration effects of mooihoekite and haycockite in the other boreholes and in the country rock. The source of the copper may, therefore, be localised to certain parts of the pegmatite.

iii) The geochemical behaviour of copper is not well understood, but it is not readily accepted into the structures of most of the common silicate minerals. The behaviour of copper is discussed in more detail in chapter 8, but estimated levels of copper in the silicate phases of borehole TLP.1 are in the range 100-200ppm. It is possible, therefore, that the serpentinization of olivine may have released sufficient copper to account for the relatively small quantities of mooihoekite, haycockite and native copper.

The samples from borehole TLP.1 also contain other unusual phases besides mooihoekite and haycockite, but in very small amounts. These phases include sphalerite, graphite and native silver. Small amounts of Zn are contained in olivine and the Zn required to form sphalerite is easily accounted for by the serpentinization of olivine. Native silver and graphite are present in insignificant amounts and may well represent late stage residua of a pegmatite melt. Other minor phases, such as valeriite and ilvaite, appear to have formed by secondary alteration reactions involving serpentine.

The close association of mooihoekite, haycockite and, in particular, native copper with serpentine veinlets indicates that the alteration of the 'primary' assemblage may well have been effected by the migration of copper-bearing fluids along pre-existing fractures. The question arises, however, as to the manner in which the copper might be transported. According to Barnes (1979), the solubilities of the common metal ions in solution are extremely low and transport can only be effected by the formation of aqueous complexes. Ligands able to complex metal ions under hydrothermal conditions are, however, limited in number, the most important being Cl^-, HS or H_2S and OH^-. The most powerful complexing ligand with respect to Cu, Zn, Ag and Fe appears to be Cl^- (Barnes, 1979). Steuber et. al. (1968) studied ultramafic rocks from numerous localites and concluded that the concentration of chlorine is significantly increased by the serpentinization of olivine. Rucklidge (1972) noted chlorine levels with a maximum of 0.8 percent in serpentine veinlets in dunite. Similar observations were made by Rucklidge &

Patterson (1977), who concluded that chlorine is highly mobile and represents a very powerful distributing agent for metal ions. Rucklidge & Patterson (1977) proposed a serpentinization reaction whereby olivine is converted to serpentine and a hydroxychloride phase:

$4\ M_2SiO_4 + 5H_2O + HCl \rightleftharpoons 2\ M_3Si_2O_5(OH)_4 + M_2(OH)_3Cl$, where M = Mg or Fe.

Under suitable oxygen fugacity conditions any iron present in the hydroxychloride phase is precipitated as magnetite (Rucklidge & Patterson, 1977):

$3Fe_2(OH)_3Cl_{aq} + O_2 \rightleftharpoons 2Fe_3O_4 + 3H_2O + 3HCl_{aq}$

This mechanism appears to provide an adequate mechanism for the release and transportion of metal ions such as Fe^{2+}, Cu^{2+} and Zn^{2+}, and accounts for the abundance of secondary magnetite associated with the veinlet and fracture systems that transgress the pegmatite. Further evidence of the presence of chlorine in the Townlands pegmatite is provided by the unknown Cl-bearing sulphides reported by Viljoen et al. (1983). The origin of the fluids responsible for the serpentinization of the olivine is discussed in chapter 9.

The unusual and complex nature of the sulphide assemblage of the Townlands pegmatite indicates a complicated history of formation, and a hypothetical paragenetic sequence may have involved the following steps:

i) The first stage involves the separation of minute quantities of immiscible sulphide liquid from an iron-rich melt. This is followed by the formation of a monosulphide solid solution (Mss) and an intermediate solid solution (Iss) at high temperatures. A high iron content, high iron activity and a low sulphur content for the magma may have given rise to an Fe-rich/S-poor Mss, which may be a pre-requisite for the formation of troilite.

ii) With decreasing temperature, the Iss decomposes to form separate chalcopyrite and cubanite solid solutions.

iii) The monosulphide solid solution remains stable to very low temperatures, but eventually breaks down to form troilite and pentlandite.

iv) The assemblage, troilite + pentlandite + chalcopyrite + cubanite resembles that observed in many other igneous rocks and is stable at low temperatures in many of the sample localities.

v) Subsequent to the formation of the 'primary' assemblage, aqueous fluids, possibly exploiting pre-existing cooling cracks, migrated upwards through the pegmatite causing serpentinization of olivine grains. The serpentinization process is accompanied by the precipitation of copious amounts of secondary magnetite and the release of metal ions (Cu^{2+}, Zn^{2+}, etc) into solution.

vi) At some stage during the serpentinization of olivine, there is minor alteration of the copper sulphides to valeriite and precipitation of ilvaite by reaction with the serpentine and Fe-rich olivine.

vii) The metal ions, such as Cu^{2+} and Zn^{2+}, are transported in solution as chloride complexes. On encountering pre-existing sulphides, Cu and minor Zn are deposited under low temperature conditions that are suitable for the alteration of the 'primary' sulphide assemblage to mooihoekite and haycockite, and for the formation of occassional sphalerite grains.

viii) During the final stages of the replacement process, the Cu-bearing solutions that migrate upwards through the pegmatite may encounter changing chemical controls. These chemical controls may include changing Eh/pH conditions, low fO_2 and low fS_2, which result in the precipitation of native copper along pre-existing serpentine veinlets and fractures.

ix) The fO_2 and fS_2 have remained low throughout the subsequent history of the pegmatite, resulting in the preservation of native copper and the other more unusual phases of the Townlands pipe.

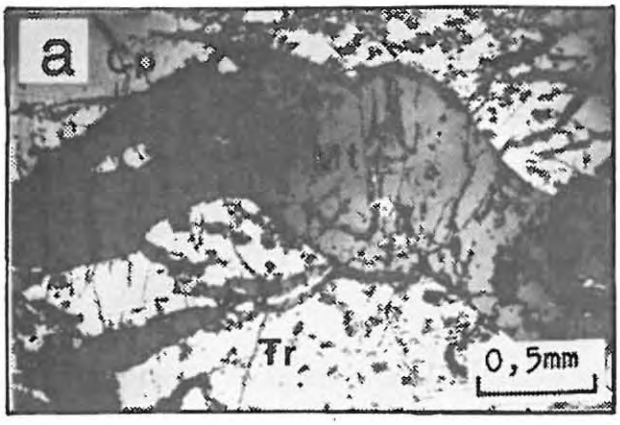
a
Cp
Mt
Tr
0,5mm

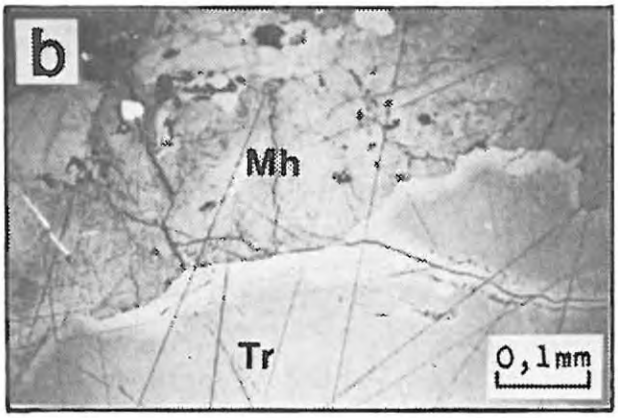
b
Mh
Tr
0,1mm

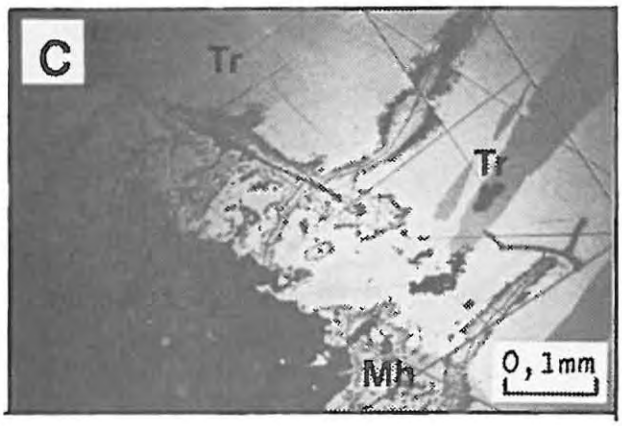
c
Tr
Tr
Mh
0,1mm

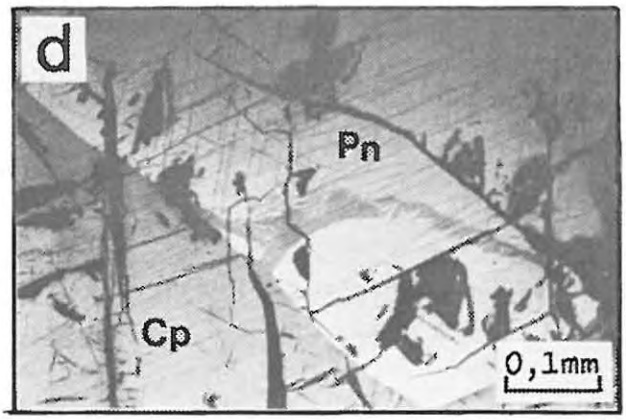
d
Pn
Cp
0,1mm

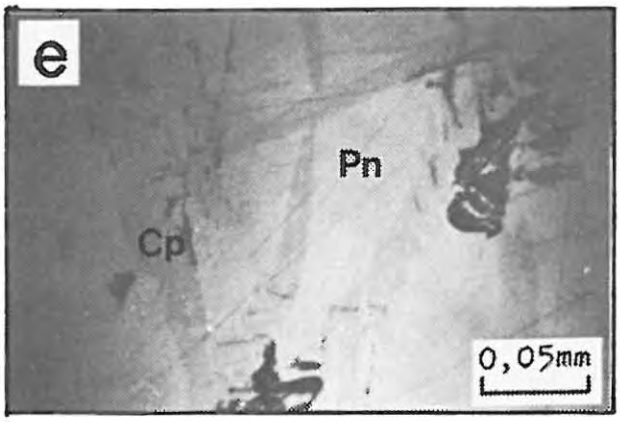
e
Pn
Cp
0,05mm

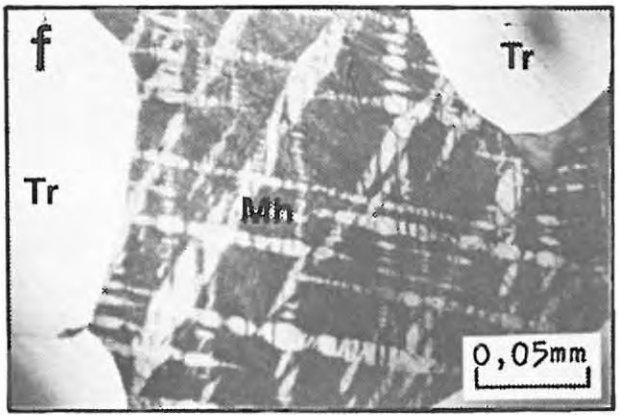
f
Tr
Tr
Mh
0,05mm

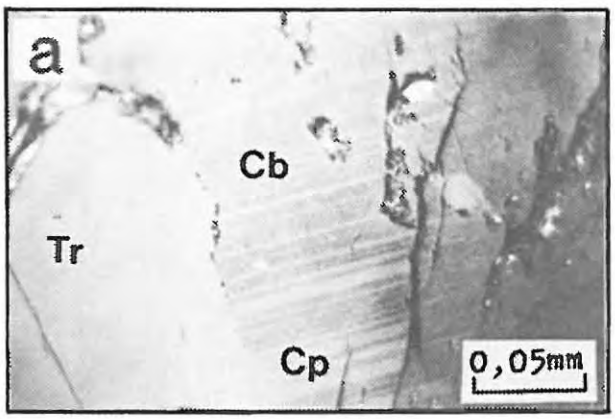
a
Cb
Tr
Cp
0,05mm

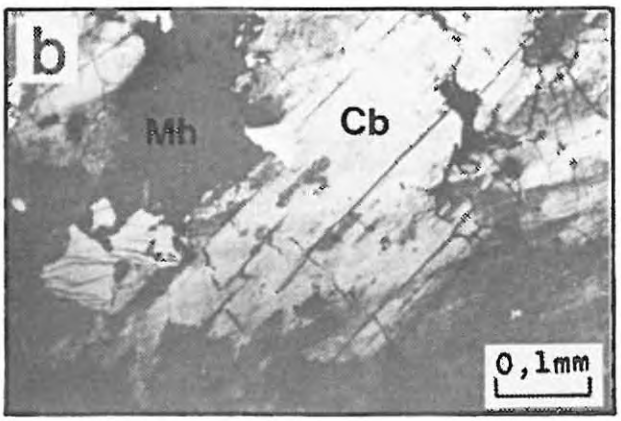
b
Mh
Cb
0,1mm

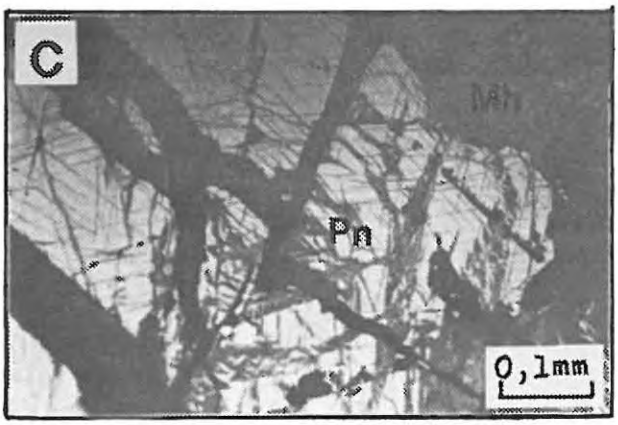
c
Mh
Pn
0,1mm

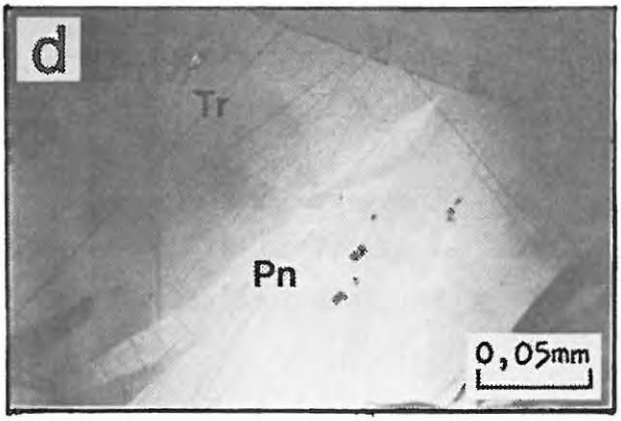
d
Tr
Pn
0,05mm

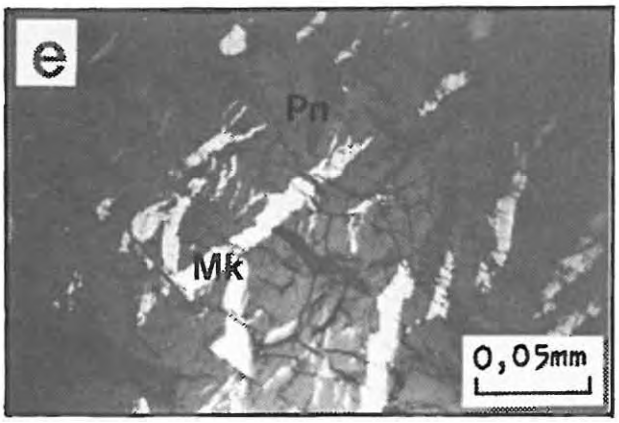
e
Pn
Mk
0,05mm

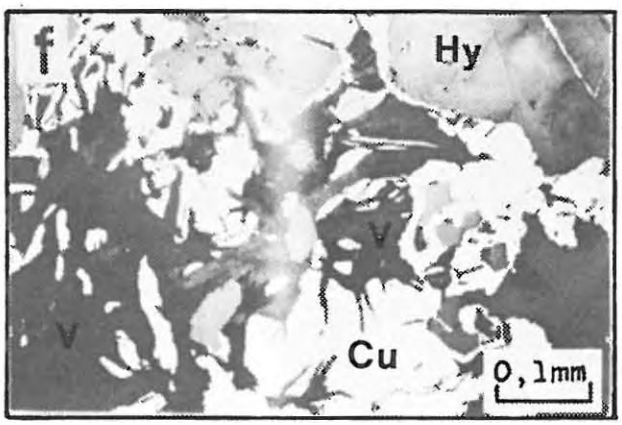
f
Hy
V
V
Cu
0,1mm

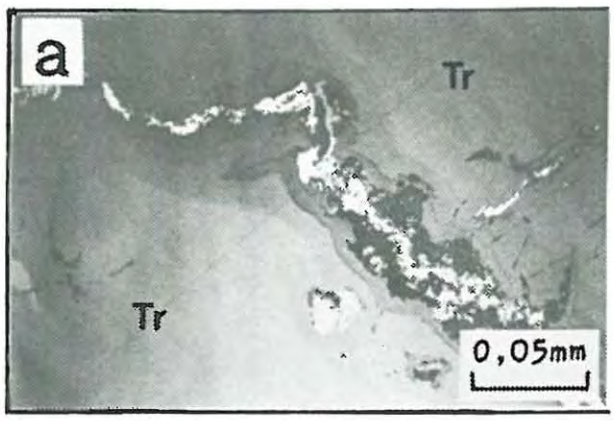
a
Tr
Tr
0,05mm

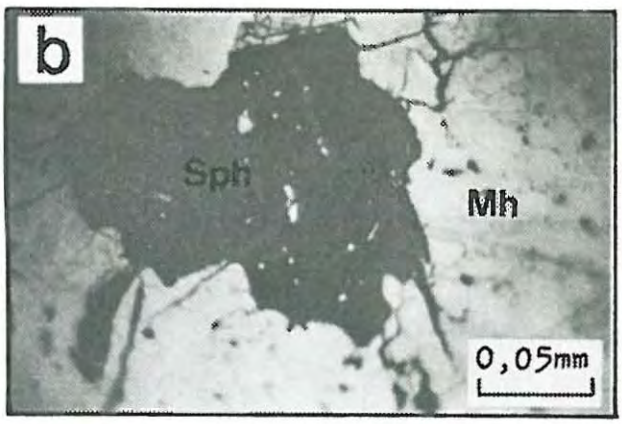
b
Sph
Mh
0,05mm

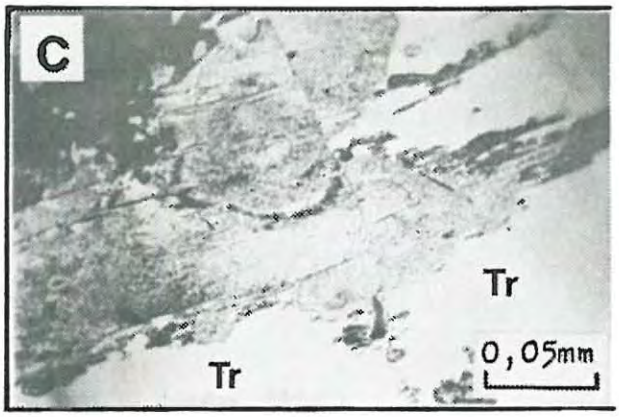
c
Tr
Tr
0,05mm

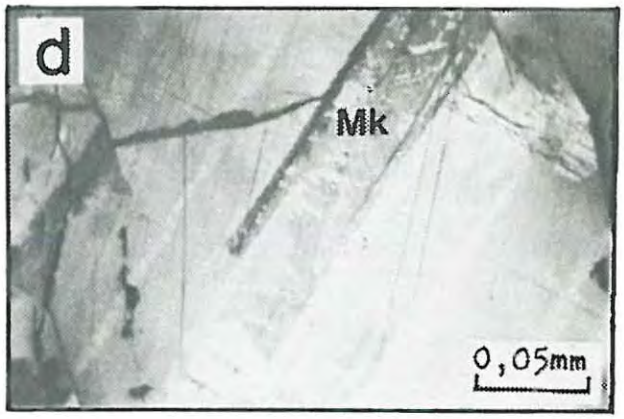
d
Mk
0,05mm

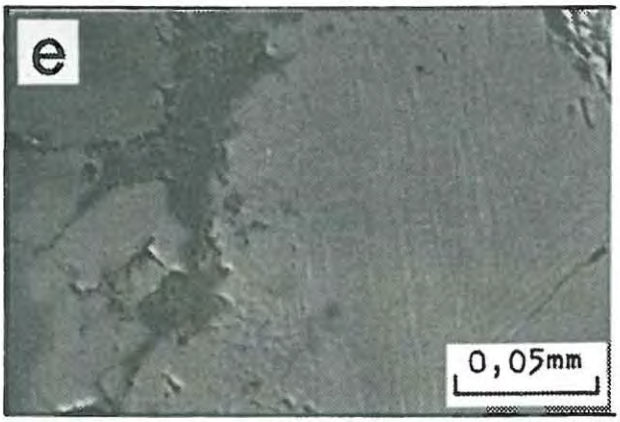
e
0,05mm

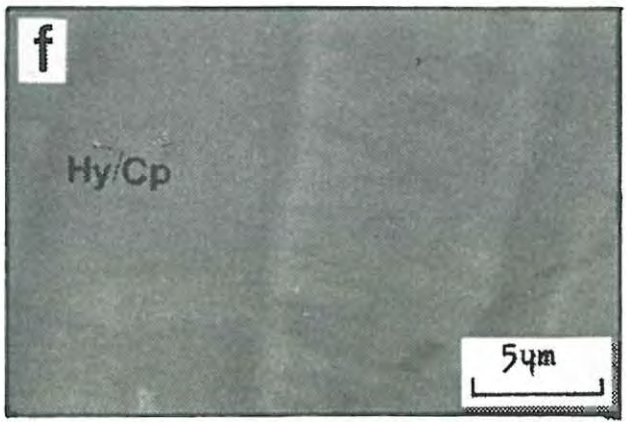
f
Hy/Cp
5µm

8. WHOLE ROCK GEOCHEMISTRY

8.1 Introduction

Whole rock geochemical data are presented for 51 ultramafic pegmatite samples from the three major sampling localities, TLP.1, TLP.2 and 6 level haulage, plus 11 'spotted' anorthosite samples from the layered Bushveld sequence in 6 level haulage. Analyses of both major and trace elements were performed using X-ray fluorescence spectrometry (XRF) techniques. Major elements were determined as weight percent oxides and include SiO_2, TiO_2, Al_2O_3. Fe_2O_3, MnO, MgO, CaO, Na_2O, K_2O and P_2O_5. The proportions of FeO : Fe_2O_3 were resolved, using the equation of Irvine & Barrager (1971), where

$$(wt\%)\ Fe_2O_3 = (wt\%)\ TiO_2 + 1.5$$

Trace element contents, in ppm (parts per million), were determined for Ba, Rb, Sr, Y, Zr, Nb, Zn, Cu, Ni, Co, Cr, V and Sc.

The major and trace element data shown in variation diagrams with SiO_2 as the abscissa all represent anhydrous values that have been normalised to 100 percent. The XRF analytical conditions, sample preparation methods, H_2O^- + L.O.I. inclusive analyses and the normalised analyses are all listed in appendix 3. The relevant sample locations are indicated in appendix 1.

8.2 Major element geochemistry

8.2.1 Major element variations

There is little available information on the whole rock geochemistry of layered igneous complexes, due largely to the presence of variable amounts of intercumulus material, which tends to blur any differentiation trends. Consequently, geochemical analyses of layered intrusions are of limited value, unless interpreted in terms of cumulus phase compositions and/or the chemistry of the associated magma (Wager and Brown, 1968). Although the Townlands pegmatite may not have crystallized from a magma, the overall chemistry of the rocks appear to be strongly dependent on mineral composition. The Townlands pegmatite consists of >90 percent of olivine and clinopyroxene, which also places a strong modal control on the behaviour of most of the major elements. In many instances, the linear trends exhibited by the variation diagrams represent mixing lines

between pure dunite and clinopyroxenite and simply reflect mineral chemistry. The variation diagrams presented in this chapter exclude the data points for samples TU33 and TU44, which contain anomolously high concentrations of apatite and Fe-Ti oxides.

The pegmatite samples generally contain insignificant amounts of plagioclase and therefore exhibit very low Al_2O_3 (Fig.44(a)), Na_2O (Fig.44(b)) and K_2O contents when compared to the 'spotted' anorthosites from 6 level haulage. The ultramafic rocks of 6 level haulage contain more Na and Al than those samples from borehole TLP.2 which, in turn, contain more than the TLP.1 rocks. This trend is due to the relative abundance of clinopyroxene which, unlike olivine, accepts small quantities of Na and Al into its structure. The K_2O contents of the pegmatite samples are below the detection limit.

Iron in the Fe^{3+} state is taken up by Ti-magnetite, secondary magnetite and, to a lesser extent, by clinopyroxene. The distribution of the Fe_2O_3 data points in Fig.44(c) reflects the relative abundances of these three phases in the various samples. The Townlands pipe rocks exhibit a much higher FeO content than those of the adjacent layered sequence (Fig.44(d)). Olivine possesses a significantly higher Fe^{2+} content than clinopyroxene with the result that the 6 level haulage samples reflect the lowest FeO levels. Although the TLP.2 pegmatite sections contain more clinopyroxene than those from borehole TLP.1, some of the TLP.2 samples show higher FeO levels, due to the more Fe-rich nature of their constituent minerals. This illustrates the marked effect of mineral chemistry on major element distribution over and above that of the strong modal control.

The mineral compositions of the layered cumulus rocks from the Bushveld Complex are presented in Fig.43, which shows an increase in their degree of fractionation with increasing height. It is apparent from this diagram that olivine disappears from the cumulus assemblage on reaching a composition of Fo_{85} and only reappears again in the upper zone where it exhibits a composition of Fo_{49}. The forsterite content continues to decrease towards the top of the sequence, where it approaches Fo_0. It is interesting to note that the majority of the Fe-rich pegmatite olivine grains exhibit forsterite contents of less than Fo_{50}. Clinopyroxene from the Bushveld Complex, coexisting with olivine of composition FO_{49}, exhibits a composition of $Wo_{38}En_{33}Fs_{29}$. In contrast, clinopyroxene

in equilibrium with olivine (Fo_{49}) from the Townlands pegmatite, exhibits a slightly more Mg-rich and Ca-rich composition of $Wo_{45}En_{37}Fs_{18}$. This discrepancy, as discussed in chapter 5 may reflect the absence of plagioclase from the ultramafic pegmatite phase assemblages.

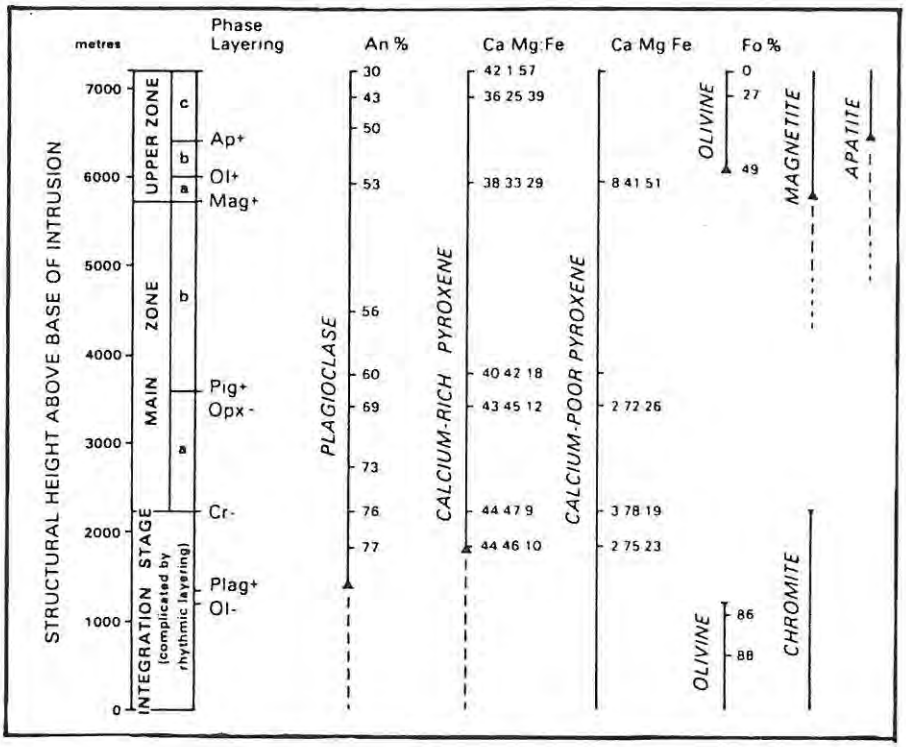

Figure 43. Minerals present in the layered cumulate rocks of the Bushveld Complex, and their compositions. Continuous vertical lines represent cumulus phases, broken vertical lines indicate that a mineral is present as an intercumulus phase only (from Wager & Brown, 1968).

The behaviour of MnO emulates that of FeO (Fig.44(e)), but also reveals the existence of two parallel trends that are related to differences in mineral chemistry between the TLP.2 plus 6 level haulage samples and the TLP.1 samples. In contrast, the MgO variation diagram indicates that the TLP.1 rocks exhibit the highest, and those of 6 level haulage the lowest, MgO levels (Fig. 44(f)). The CaO data clearly illustrate a strong modal control on the major element chemistry (Fig.44(g)). The olivine-rich TLP.1 rocks have the lowest CaO contents and those of 6 level haulage the highest, whereas the TLP.2 samples contain intermediate levels. The TLP.1 'marginal' zone samples contain highly variable amounts of clinopyroxene which is clearly indicated in Fig.44(g).

The TiO_2 and P_2O_5 contents of the pegmatite samples all show similar distribution patterns. Ti is contained in Ti-magnetite and ilmenite, with small amounts substituting in clinopyroxene, while P is almost exclusive to apatite. The distribution of TiO_2 (Fig.44(h)),

therefore, reflects the relative abundance of Fe-Ti oxides in which TLP.1 samples contain the lowest and those from 6 level haulage the greatest amounts. The ultramafic rocks from 6 level haulage contain up to 6 percent P_2O_5, while the TLP.2 samples exhibit negligible P_2O_5 levels (Fig.44(i)). Most of the TLP.1 analyses also show very low P_2O_5 contents, but a few samples in the vicinity of the TLP.1 'marginal' zone registered moderate P_2O_5 levels. It is interesting to note that both apatite and magnetite only appear as cumulus phases in the upper zone, but may exist as intercumulus phases from the upper parts of the main zone of the Bushveld Complex (Wager & Brown, 1968).

8.2.2 Discussion

The constituent phases of the Townlands pegmatite clearly exhibit textures and compositional variations that closely resemble those encountered in igneous rocks that have crystallized from a melt. Furthermore, the mineral compositions of the pegmatite are similar to those observed in the upper and upper main zones of the Bushveld Complex (Fig.43). Consequently it is possible that the pegmatite may have formed by crystallization from a relatively highly fractionated magmatic liquid. The major element geochemistry of the pegmatite samples is, therefore, compared to that of samples from the upper zone in table 12. The upper zone rocks, however, contain considerable amounts of plagioclase in comparison to the Townlands pipe, in which plagioclase is an accessory phase. For this reason, partial normative recalculations were performed on the upper zone analyses to 'remove' the plagioclase components (Table 12). The analyses of the pegmatite samples from borehole TLP.2 and 6 level haulage compare favourably with the recalculated analyses of the upper zone samples. The TLP.1 samples are, however, depleted in TiO_2, MnO, CaO and P_2O_5 and enriched in MgO compared to the upper zone samples. Consequently, it appears that the portion of the pegmatite represented by borehole TLP.2 and 6 level haulage samples may have crystallized from a relatively highly fractionated melt, similar in composition to that responsible for the formation of the upper zone rocks. The portion of the pegmatite represented by the samples from borehole TLP.1, in contrast, may have crystallized from a less evolved melt. The pegmatite is largely hosted by 'spotted' anorthosite, and some 'dilution' of the pegmatite melt, by reaction with one or more of the 'spotted' anorthosite components, may also have occurred during the formation of the pegmatite. These proposals are tentative at this stage and as a further test, the trace element distribution patterns are discussed in the next section in terms of a fractionating melt.

SAMPLE NO.	UZ1	UZ2	UZ3	TLP.1	TLP.2	6 L.H.
SiO_2	38.41	38.38	33.24	35.56	35.88	38.27
TiO_2	4.35	3.20	4.73	0.31	1.59	2.58
Al_2O_3	0.00	0.00	0.00	0.16	0.74	1.27
Fe_2O_3	7.12	6.87	7.66	1.85	3.12	4.12
FeO	36.59	30.57	36.30	38.00	39.33	29.56
MnO	0.77	0.55	0.61	0.47	0.55	0.44
MgO	3.67	7.86	7.93	21.88	13.14	11.44
CaO	6.98	10.72	8.64	1.72	5.51	11.22
Na_2O	0.00	0.00	0.00	0.02	0.07	0.07
K_2O	0.02	1.32	0.59	0.00	0.03	0.01
P_2O_5	2.09	0.53	0.29	0.03	0.04	1.02
TOTAL	100.00	100.00	100.00	100.00	100.00	100.00

UZ1, UZ2, UZ3 : Upper zone samples (I.M. Reynolds, unpubl. data).
TLP.1 : Average analysis for borehole TLP.1 samples.
TLP.2 : Average analysis for borehole TLP.2 samples.
6 L.H.: Average analysis for 6 level haulage samples.

Table 12. Major element analyses of rocks from the upper zone of the Bushveld Complex (I.M. Reynolds, unpubl. data) and average major element analyses of samples from the Townlands pegmatite.

8.3 Trace element geochemistry

8.3.1 Theoretical models

Trace elements are considered to be non-stoichiometric constituents of crystallising minerals that distribute themselves in some manner between the crystallising phases and the associated parent magma (Paster et. al., 1974). The partitioning of trace elements between precipitating phases and the melt have been considered in terms of theoretical models and some of the more important models have been summarised by Arth (1976). The models are based on the assumptions that the trace elements form dilute solid solutions in accordance with Henry's law, and that equilibrium or near-equilibrium conditions are prevalent (Arth, 1976). If Henry's law is obeyed, the degree to which an element is partitioned between the melt

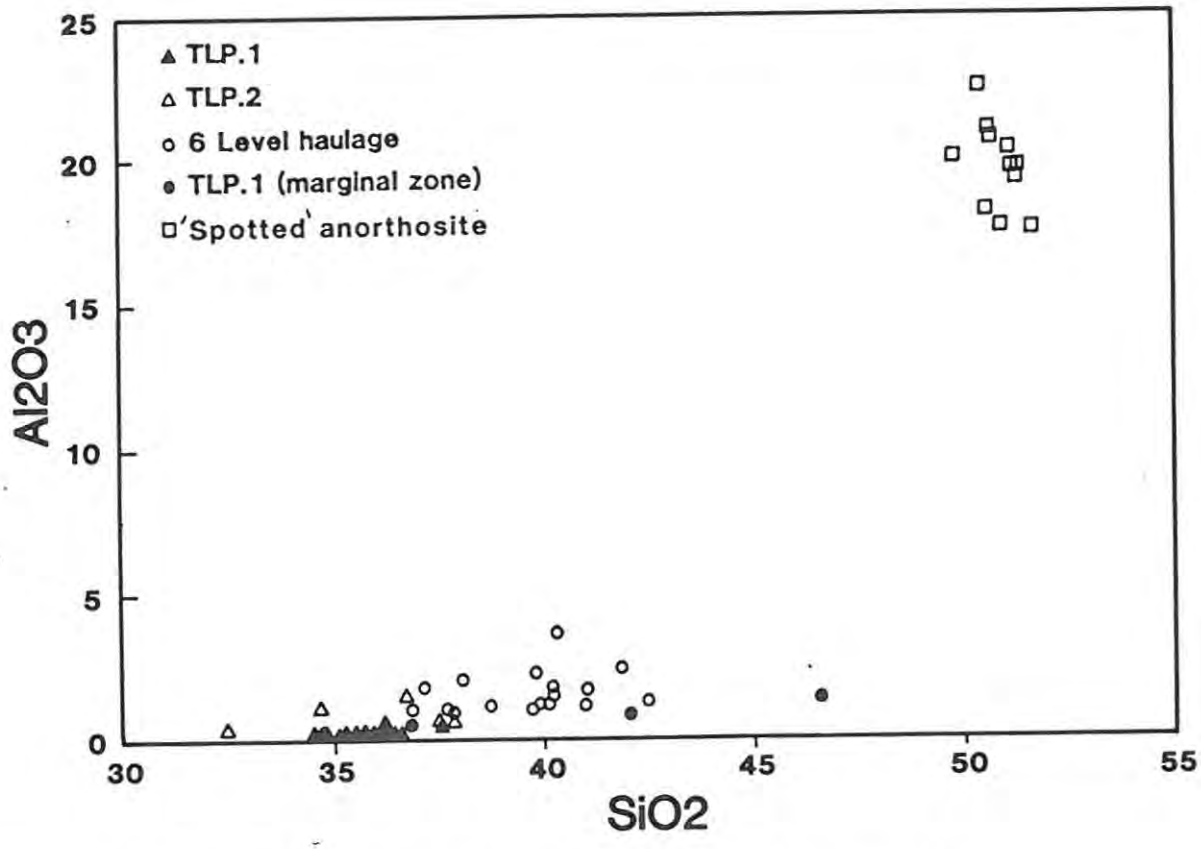

Figure 44(a). Plot of Al_2O_3 versus SiO_2 (weight % oxides).

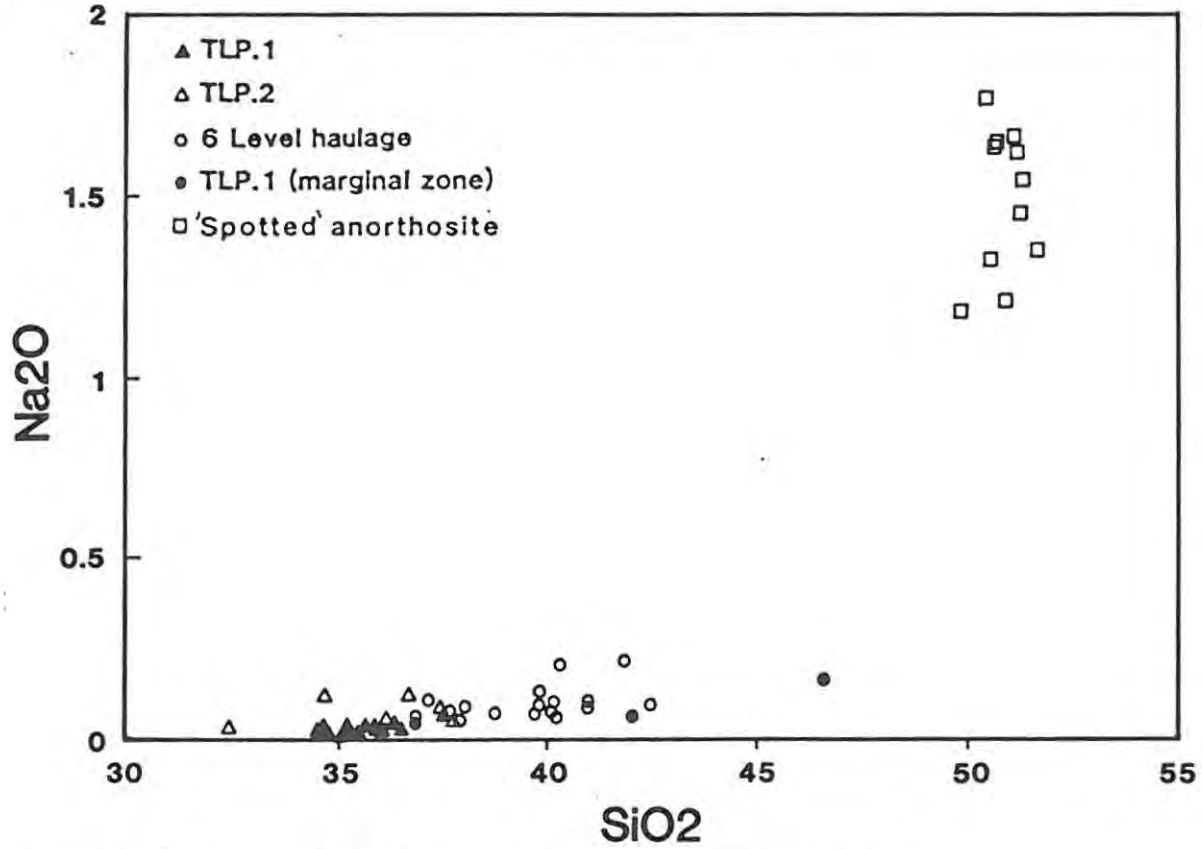

Figure 44(b). Plot of Na_2O versus SiO_2 (weight % oxides).

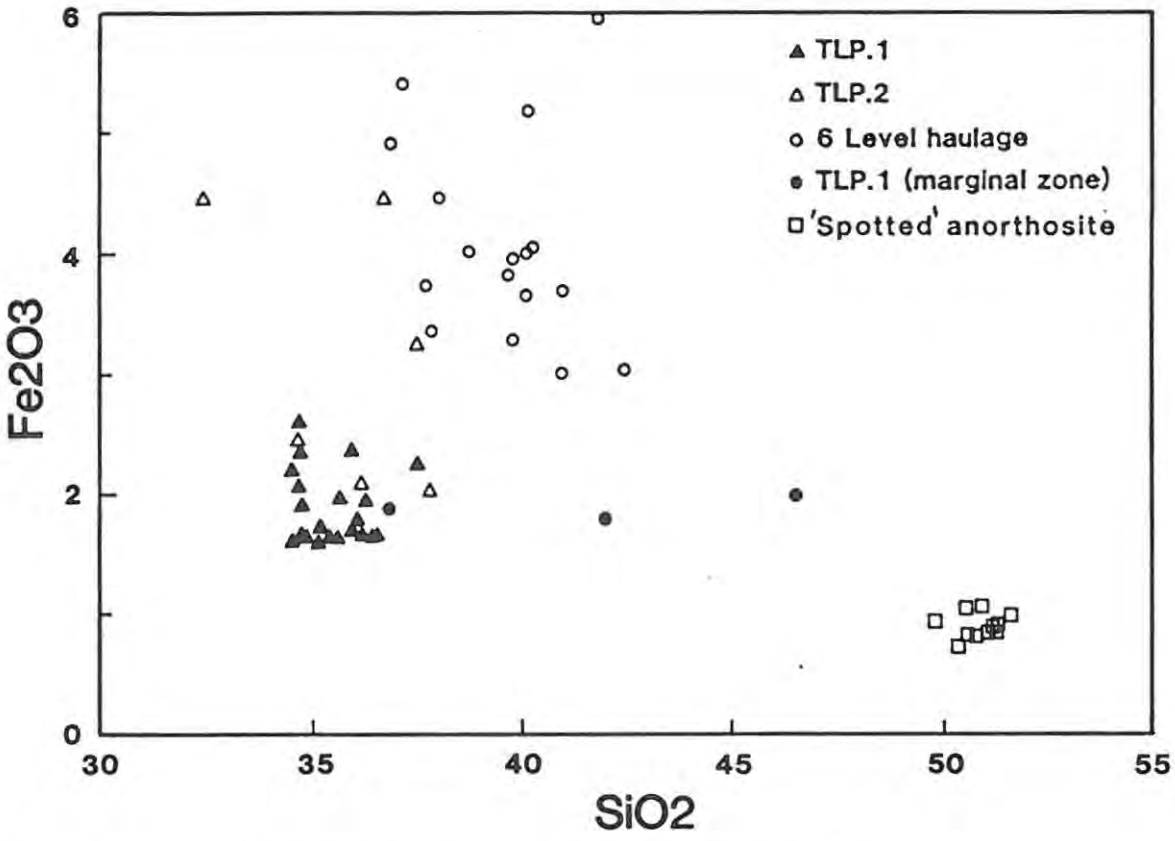

Figure 44(c). Plot of Fe_2O_3 versus SiO_2 (weight % oxides).

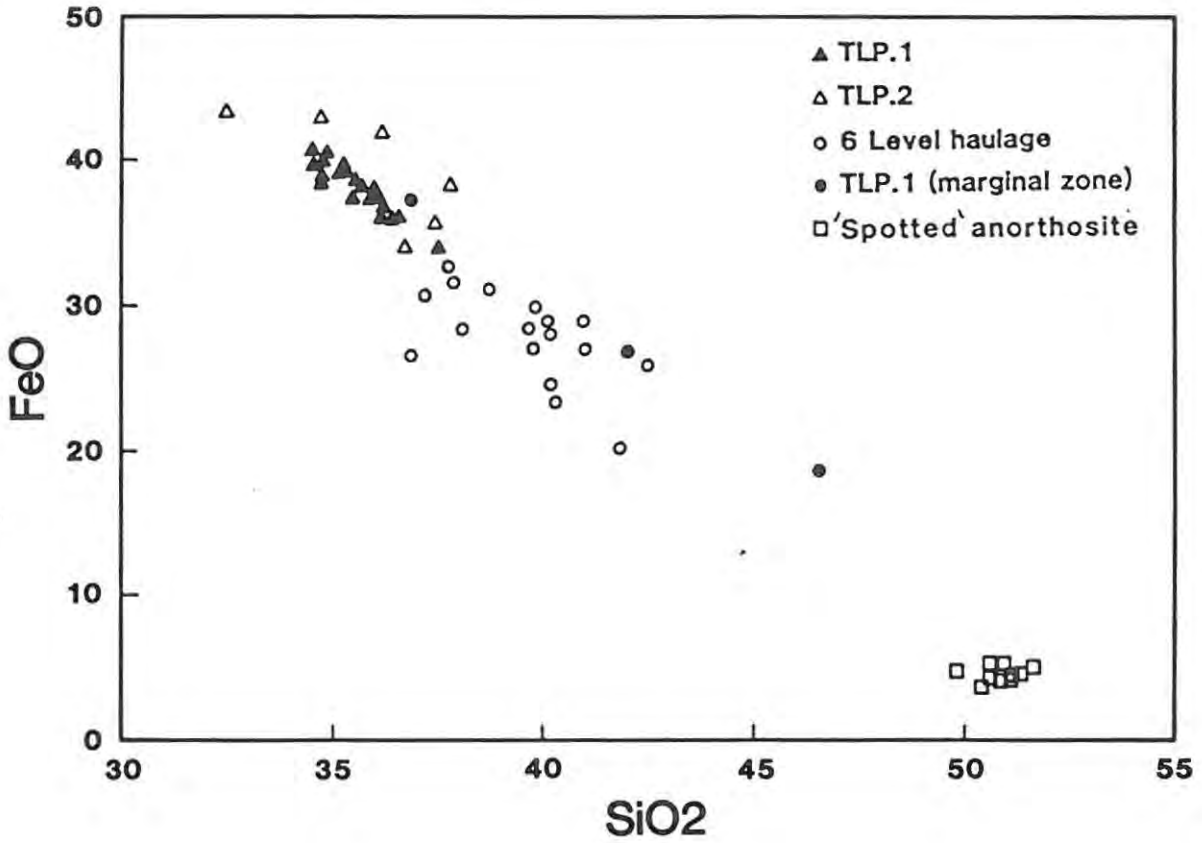

Figure 44(d). Plot of FeO versus SiO_2 (weight % oxides).

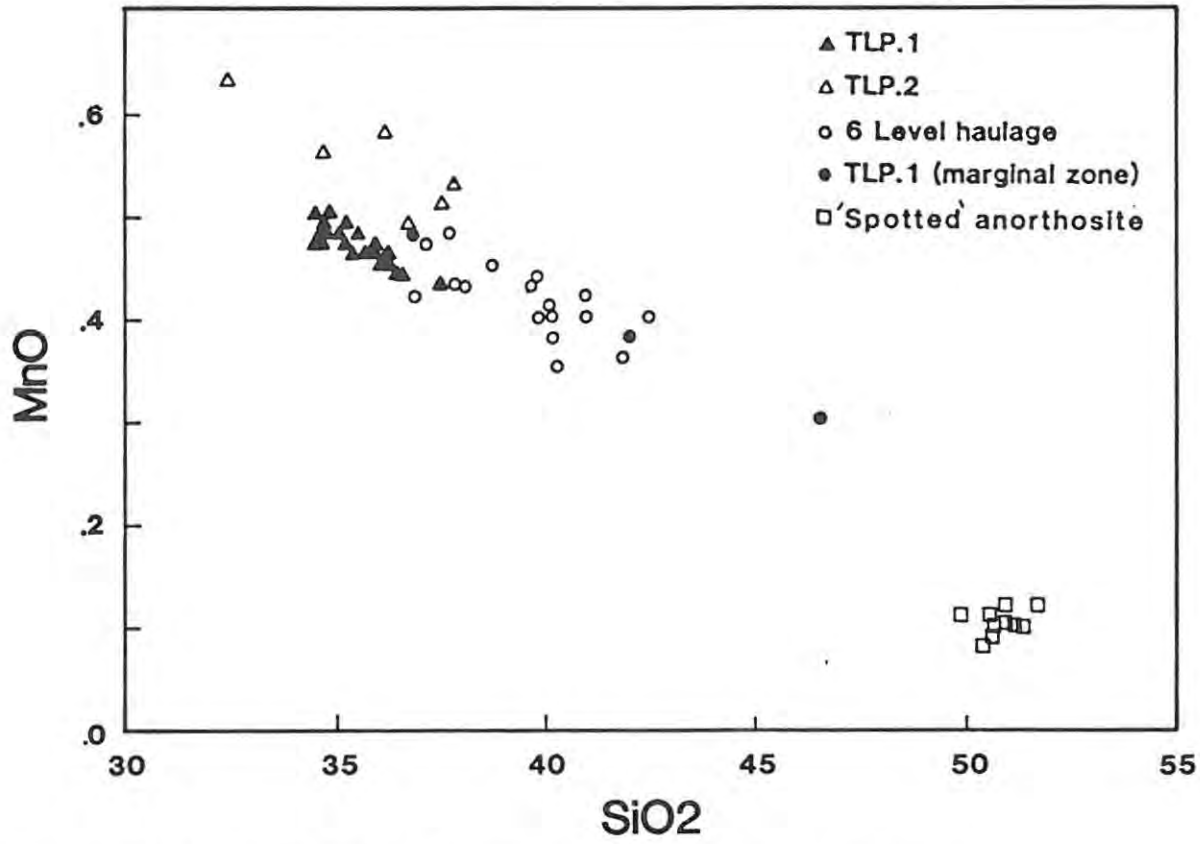

Figure 44(e). Plot of MnO versus SiO_2 (weight % oxides).

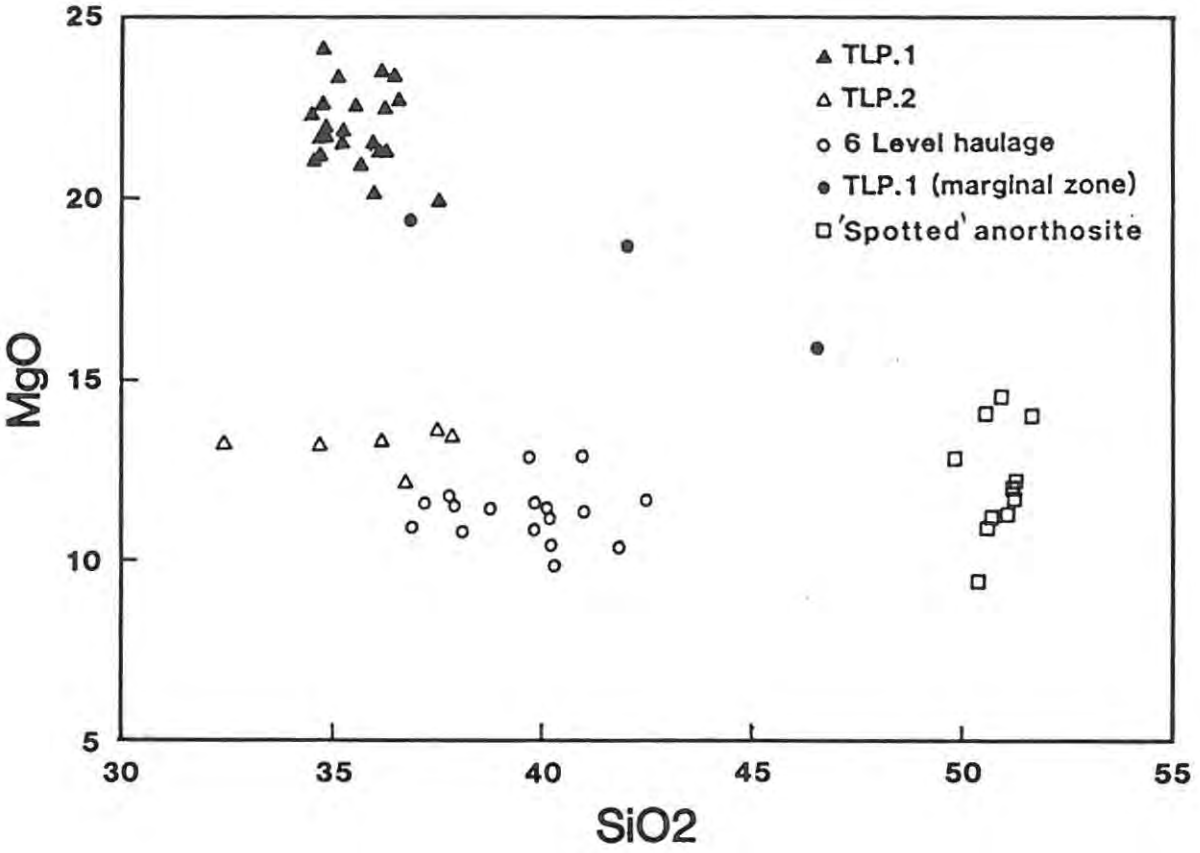

Figure 44(f). Plot of MgO versus SiO_2 (weight % oxides).

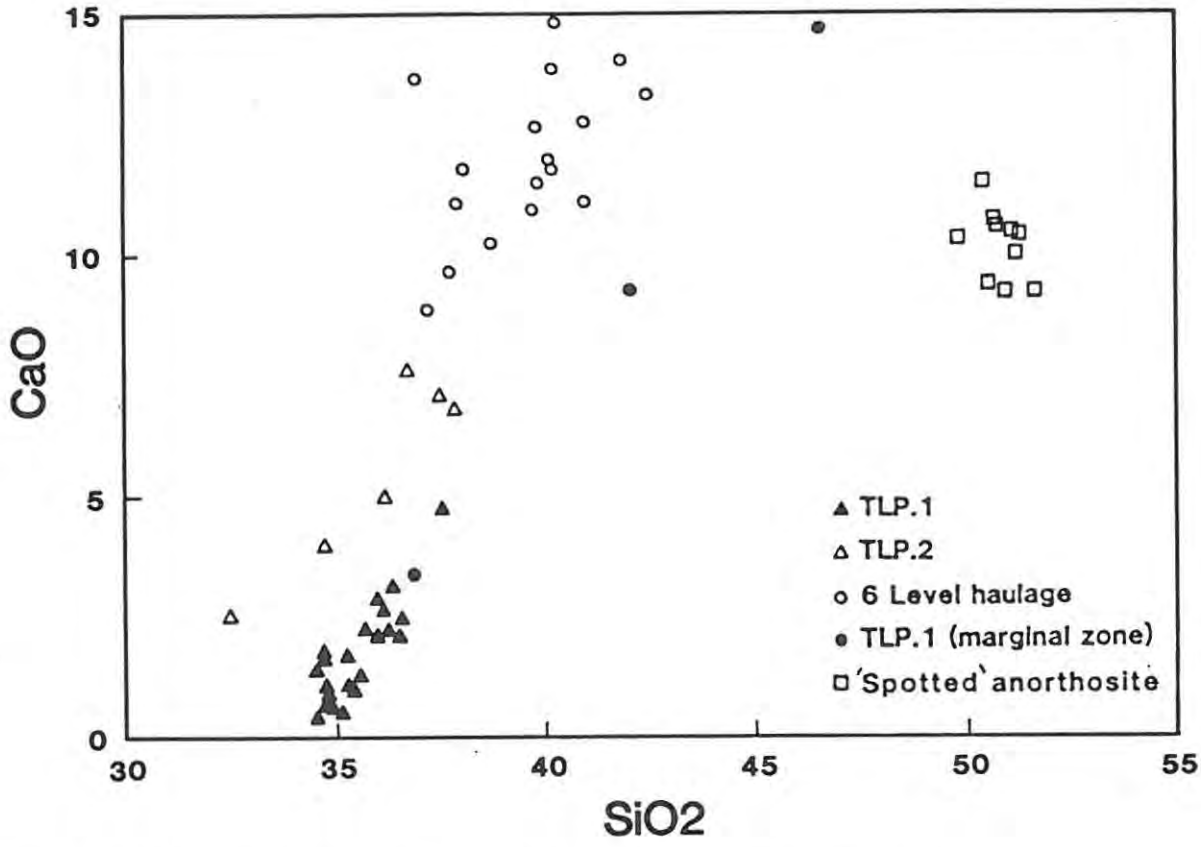

Figure 44(g). Plot of CaO versus SiO_2 (weight % oxides).

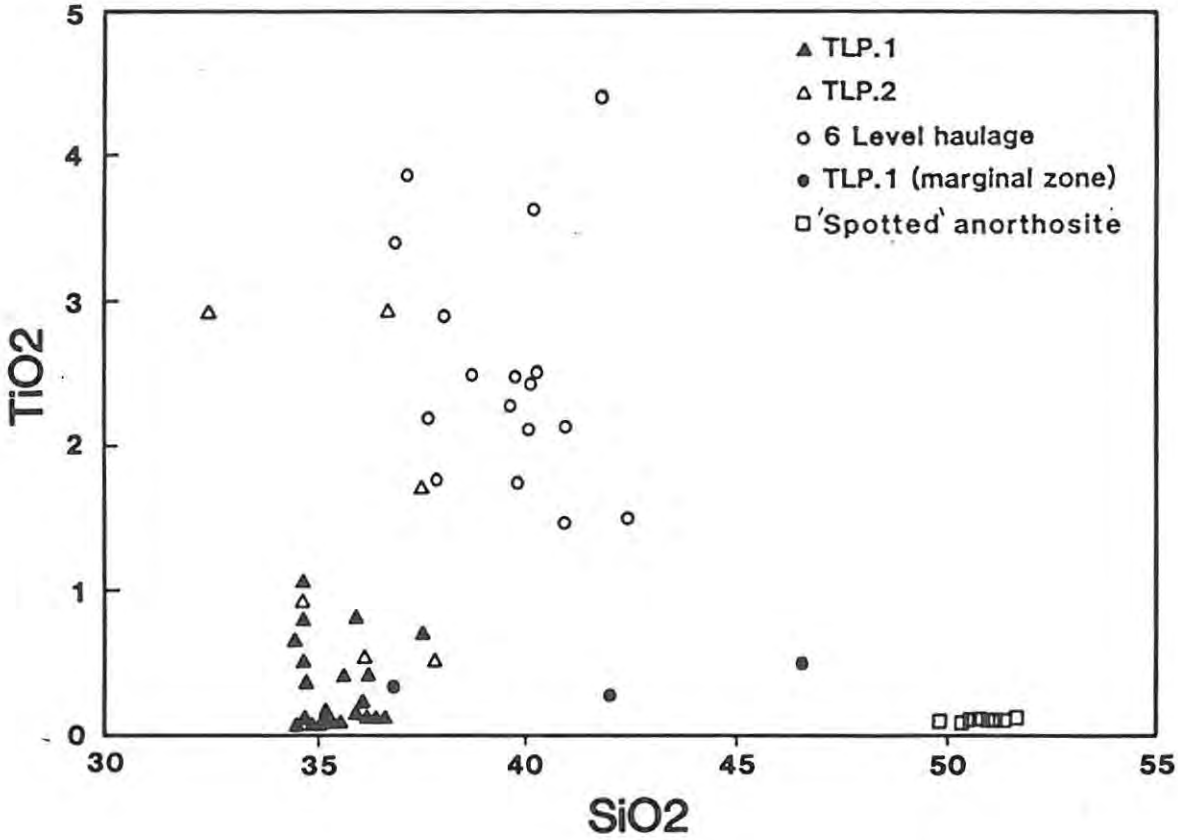

Figure 44(h). Plot of TiO_2 versus SiO_2 (weight % oxides).

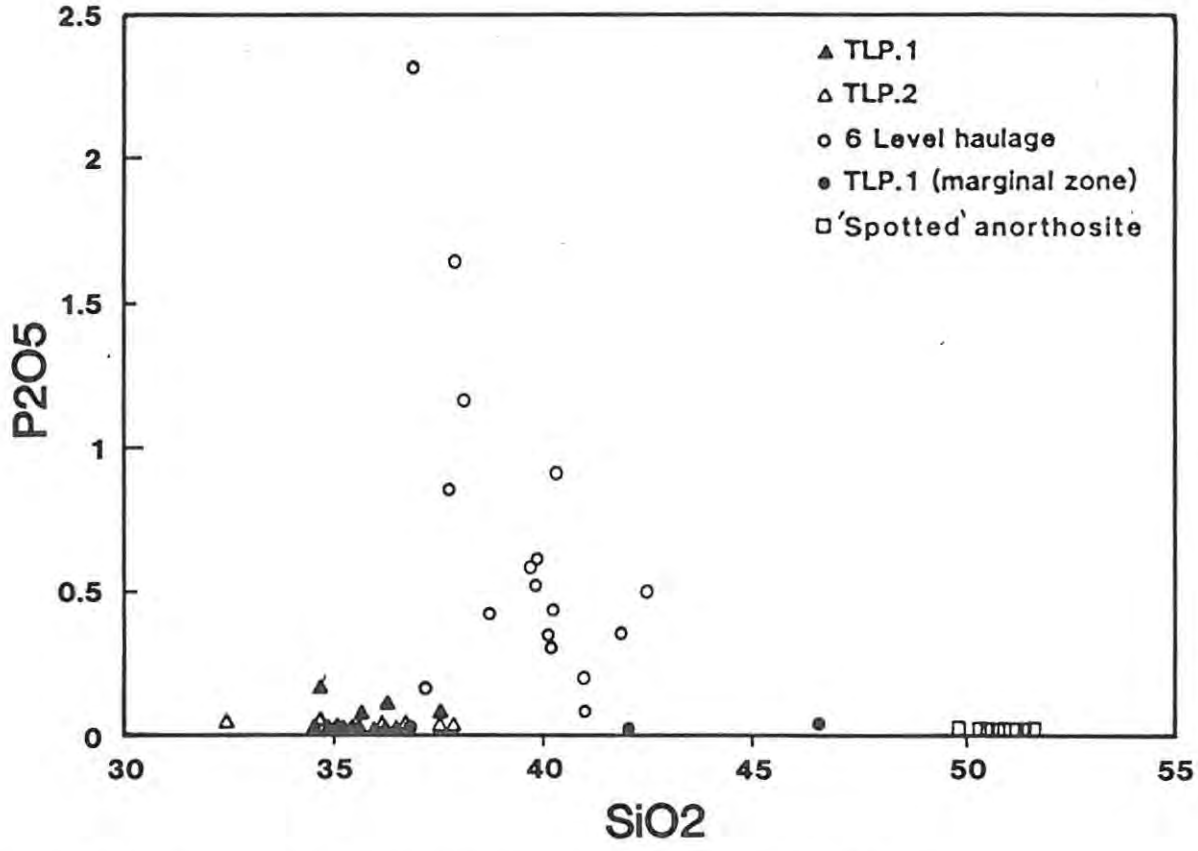

Figure 44(i). Plot of P_2O_5 versus SiO_2 (weight % oxides).

and a crystallising mineral can be expressed by means of a distribution coefficient (K), where

$$K = \frac{C_i \text{ (crystal)}}{C_i \text{ (liquid)}} \qquad (C_i = \text{concentration of trace element i})$$

The theoretical models relating to the partitioning of trace elements during fractional crystallisation are based on the attainment of equilibrium either between the surface of the crystallising phase (Greenland, 1970), or between the bulk of the phase and the melt (Arth, 1976). The equation applicable to the latter condition is analogous to the partial melting model of Shaw (1970) and may be expressed as follows:

$$\frac{C_l}{C_i} = \frac{1}{F' + \frac{D_s}{D_s}(1-F')},$$

where F' is the fraction of liquid remaining, C_i is the concentration of the element in the original melt, C_l is the concentration in the differentiated liquid and D_s is the bulk distribution coefficient, given by:

$$D_s = W^a K^{a/L} + W^B K^{B/L} + \ldots\ldots\ldots,$$

where K is the solid-liquid partition coefficient and W^a is the weight fraction of 'a' in the crystallising phases (Arth, 1976). According to Arth (1976), the surface-equilibrium model is more applicable to rapidly cooled magmas, while the total equilibrium model is best suited to slowly cooled intrusive bodies. The latter model is therefore deemed more appropriate for the Townlands pegmatite.

A modified version of Shaw's (1970) partial melting diagram is presented in Fig.45 to illustrate the fractional crystallisation behaviour of the trace elements. The diagram illustrates that elements having distribution coefficients of unity (D = 1) are distributed equally between the melt and crystallising minerals. Trace elements with high coefficients (D>1) are preferentially partitioned into the precipitating phases, and the element concentrations in the liquid decrease steadily with increased fractionation. These elements are termed <u>compatible</u> elements. <u>Incompatible</u> elements possess low partition coefficients (D<1) and display an affinity for the melt. With increasing differentiation, the incompatible elements will become enriched in the melt. Consequently, if the Townlands pipe does represent crystallisation from a highly fractionated liquid, it should contain high concentrations of incompatible elements and slightly lower compatible element levels, relative to the less evolved surrounding layered rocks.

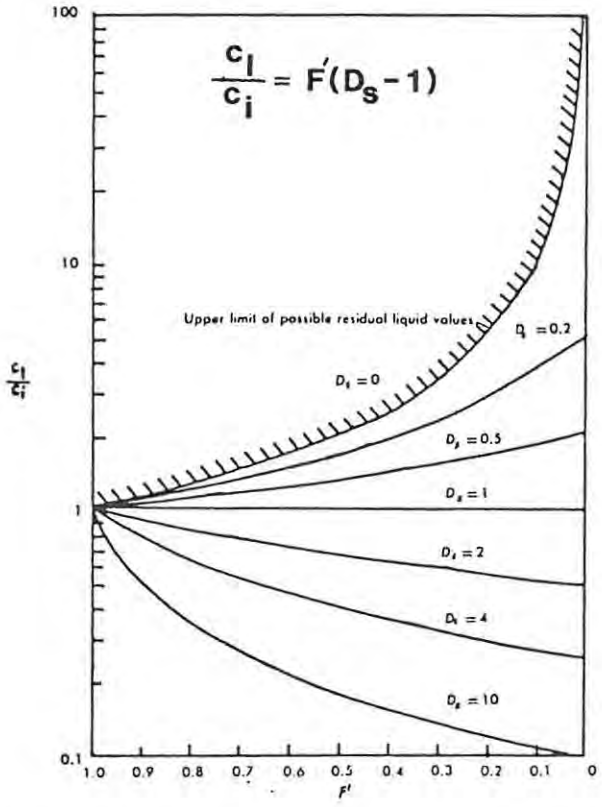

Figure 45. Illustration of the behaviour of a trace element during fractional crystallisation involving bulk equilibrium; F' is the fraction of liquid remaining, C_i is the element concentration in the original melt, C_l is the concentration in the differentiated melt and D_s is the bulk distribution coefficient (reproduced from Shaw, 1970).

8.3.2 Trace element variations

The distribution of certain trace elements with respect to olivine and clinopyroxene was mentioned in chapter 5. Partition coefficients appear to be dependent on a number of variable physical and chemical parameters, including bulk composition, temperature, pressure, fO_2 and the adherence to Henry's law (Irving, 1978). The behaviour of the coefficients is further complicated by the presence of intercumulus phases that may be trapped in slowly cooled intrusives (Paster et. al., 1974). As a result, quantitative evaluations of trace element distributions within the Townlands pegmatite are handicapped. Selected partition coefficients relevant to tholeiitic melts are presented in table 13 and are used in the absence of more specific data as a basis for a qualitative discussion of trace element distribution.

The incompatible trace elements ($D<1$), in terms of the major phases olivine and clinopyroxene, are taken to include Ti, P, Ba, Rb, Sr, and

ELEMENT	OLIVINE	CLINOPYROXENE	MAGNETITE	PLAGIOCLASE
Ti	0.02[1]	0.35[1]	7.5[1]	0.04[1]
P	0.02-0.04[2]	0.01-0.02[2]	-	-
Ba	0.05[3]	0.05[3]	-	0.68[3]
Sr	0.01-0.02[4]	0.2-0.3[5]	-	1.5-2.2[5]
Rb	0.01[4]	0.01-0.28[4]	-	0.03-0.19[4]
Zr	0.01[1]	0.1[1]	0.1[1]	0.01[1]
Y	0.01[1]	0.5[1]	0.2[1]	0.03[1]
Nb	0.01[1]	0.1[1]	0.4[1]	0.01[1]
Zn	1.8[3]	0.49[3]	2.6[3]	0.13[3]
Cu	0.02[3]	0.18[6]	0.42[3]	0.004[3]
Ni	124.13/MgO-0.897[7]	1.5-14[8]	19[9]	4.4[6]
Co	3.1[3]	0.5-2.0[8]	3.4[3]	0.03[3]
Cr	0.2-0.3[10]	5-40[11]	27-58[9]	0.02[6]
V	0.05[12]	3.4[13]	24-63[9]	0.01[6]
Sc	0.33[3]	3.3[3]	0.73[3]	0.008[3]

Sources of data:
1: Pearce & Norry (1979); 2: Anderson & Greenland (1969); 3: Paster et. al. (1974); 4: Philpotts & Schnetzler (1970); 5: Sun et al. (1974); 6: Bougault & Hekinian (1974); 7: Hart & Davis (1978); 8: Lindström & Weill (1978); 9: Ewart et. al. (1973); 10: Irving (1978); 11: Campbell & Borley (1974); 12: Duke (1976); 13: Ringwood (1970).

TABLE 13. Selected Trace element partition coefficients used in this study.

the second transition series elements Y, Zr and Nb. Although Ti and P are essentially major elements, they are included in the above grouping because of their incompatible behaviour, i.e. they become enriched in the melt with increasing differentiation.

The distribution coefficients of Ba, Rb and Sr for olivine and clinopyroxene are very low (table 13) and all three would be expected to enrich in highly fractionated rocks. The Ba content of the pegmatite

samples (5 - 29ppm) is lower than that of the associated 'spotted' anorthosites (54 - 107ppm) (Fig.46(a)). This apparently contradictory relationship may, however, be due to the fact that plagioclase possesses a much higher partition coefficient for Ba (D_{Ba}^{plag} = 0.68) than the pegmatite phases ($D_{Ba}^{ol/cpx}$<0.05). Rb is readily accepted into the mica structure, but in most of the analysed samples, Rb is below the lower limit of detection (0.8ppm). Only those samples from TLP.1 and 6 level haulage that contain small amounts of accessory biotite contained any Rb (maximum of 3.2ppm) (Fig.46(b)). Strontium is rejected by olivine and clinopyroxene, but readily substitutes in plagioclase (D_{Sr}^{plag} = 1.5 - 2.2). Consequently, it is not possible to compare the high Sr values of the layered rocks (239 - 351ppm) with those of the pegmatite. The highest Sr contents reported for pegmatite are restricted to samples from 6 level haulage (8 - 53ppm), followed by those from boreholes TLP.2 (4 - 21ppm) and TLP.1 (0 - 7ppm) (Fig.46(c)). This trend for the pegmatite rocks is similar to that displayed by both Ti and P (Figs.44(h) & (i)).

Zirconium, Y and Nb are all members of the second transition series and exhibit similar behavioural patterns that are characterised by low partition coefficients for olivine, clinopyroxene, magnetite and plagioclase. The Zr contents of the 6 level haulage rocks (5.2 - 22.7ppm) and some of the TLP.2 samples (4.3 - 12.3ppm) are higher than those of the 'spotted' anorthosites (2.4 - 7.1ppm), in contrast to the TLP.1 rocks that exhibit slightly lower levels (1 - 6.4ppm) (Fig.46(d)). Yttrium exhibits a somewhat more incompatible behaviour in that all the pegmatite samples show higher Y levels than those of the layered rocks (Fig.46(e)). The ultramafic rocks of 6 level haulage contain the highest levels of Y (6.6 - 25.9ppm), followed by TLP.2 (6.9 - 9.2ppm), TLP.1 (3.4 - 9.0ppm) and the'spotted' anorthosites (2.2 - 4.6ppm). The Nb values are very low and no Nb was detected in samples from borehole TLP.1 or the layered rocks. Only a few samples from TLP.2 (<1.9ppm) and 6 level haulage (maximum of 7.6ppm) were found to contain small amounts of Nb.

The compatible elements (D>1) that may substitute in olivine or clinopyroxene, include Ni, Zn, Co, Cr, V and Sc, all of which belong to the first transition series of metals. Although Cu forms part of this series, it possesses low partition coefficients for olivine, clinopyroxene and plagioclase, and should enrich in the melt, with increasing fractionation. The discussion of Cu is, however, retained in

this section, because of its close relationship with Ni. There appears to be some disagreement as to the D value of Cu for magnetite. Ewart et. al. (1973) obtained partition coefficients of 1.3 - 2.3, while Paster et. al. (1974) determined a much lower value of 0.42. As a result, the influence of magnetite, an important accessory phase, on the distribution of Cu cannot be predicted with any certainty. Ni, in contrast to Cu, exhibits high D values with respect to olivine and clinopyroxene and is readily depleted from the melt by the early precipitation of olivine and clinopyroxene. Therefore, if the pegmatite rocks are products of a highly fractionated liquid, they might be expected to contain relatively low Ni abundances. Unfortunately, both the Ni and Cu distributions are masked by the presence of variable amounts of Ni- and Cu- bearing sulphides (Figs.43(f),(g)). This masking is especially severe in the case of the TLP.1 samples which contain both native copper veinlets and the highest proportion of sulphides. In an effort to resolve the situation, Cu is plotted against Ni in Fig.46(h), which shows a positive correlation between Cu and Ni for most of the sample localities. This positive correlation is especially well developed with respect to the samples from borehole TLP.1. The D value for Cu substituting in olivine is low, while that for Ni is high. In addition, both Cu and Ni exhibit high D values with respect to sulphide phases and the positive correlation may, therefore, reflect the abundance of sulphides in certain samples. Consequently, those samples that exhibit the lowest Cu and Ni levels may be sulphide-poor or even sulphide-free. The lowest Cu levels contained in samples from borehole TLP.1 span the range between 100 and 200ppm. As the TLP.1 rocks are dominated by olivine, these Cu contents may represent the levels contained in the olivine grains. The lowest Cu levels of the remaining samples are also mostly in the range 100-200ppm. These Cu levels are higher than those of the 'spotted' anorthosite samples and it appears that both Cu and Ni are enriched in the pegmatite with respect to the layered rocks. In addition, the TLP.1 samples contain the highest Ni contents, followed by samples from borehole TLP.2 and 6 level haulage, in accordance with the relative abundance of olivine.

Zinc is slightly less compatible than Ni towards the pegmatite minerals, as it has high distribution coefficients for olivine (1.8) and magnetite (2.6), but a low coefficient for clinopyroxene (0.49). As a result, the distribution is modally controlled with respect to the relative abundances of olivine and clinopyroxene and this is reflected in Fig.46(i). The TLP.1 rocks exhibit the highest and those of 6 level

haulage the lowest Zn contents. Zinc has low partition coefficients for both plagioclase and orthopyroxene and predictably the pegmatite samples contain significantly more Zn than the 'spotted' anorthosites.

Cobalt appears to be the only trace element, with the exception of Ni, that is compatible towards olivine (D_{Co}^{ol} = 3.1), clinopyroxene (D_{Co}^{cpx} = 0,5 - 2.0) and magnetite (D_{Co}^{mt} = 3.4). Cobalt is rejected by plagioclase, which accounts for the low Co levels in of the 'spotted' anorthosites. Cobalt exhibits a similar behaviour to Ni towards the pegmatite samples and those of TLP.1 contain the largest, while the 6 level haulage rocks contain the smallest quantities of Co (Fig.46(j)).

Chrome is accepted into the structures of clinopyroxene (D_{Cr}^{cpx} = 5 - 40), and magnetite (D_{Cr}^{mt} = 27 - 58), but is rejected by olivine (D_{Cr}^{ol} = 0.2 - 0.3). The high Cr concentrations in the layered rocks are due largely to the presence of minor amounts of chromite (Fig.46(k)). TLP.1 and TLP.2 samples all contain low Cr values, while those of 6 level haulage have contents comparable with the 'spotted' anorthosites. The higher Cr contents of the 6 level haulage rocks results from the presence of Cr in Ti-magnetite and, to a much lesser extent, clinopyroxene. The behaviour of V parallels that of Cr, except for the fact that the pegmatite samples contain greater amounts of V than the layered rocks (Fig.46(l)). TLP.1 and TLP.2 sections have similar V levels, while those of 6 level haulage are far higher. This trend is due to the high partition coefficient of V with respect to clinopyroxene (D_{V}^{cpx} = 3.4) and magnetite (D_{V}^{mt} = 24 - 63).

Scandium can substitute for Ca in clinopyroxene (D_{Sc}^{cpx} = 3.3), but is not compatible with the structures of olivine and magnetite. The distribution of the Sc data points resembles that of CaO and reflects the strong modal effect of clinopyroxene. Consequently, the 6 level haulage samples have the highest and those of TLP.1, the lowest Sc contents (Fig.46(m)).

8.3.3 Discussion

The trace element distributions and abundances have revealed several significant factors concerning the crystallisation history of the Townlands pipe. The incompatible elements Ti, P, Y and, to a lesser extent, Zr and Nb, are enriched in the pegmatite, with respect to the

layered rocks. Sr is excluded, because of its strong affinity for plagioclase, while the Rb levels are very low and inconclusive. Ba appears to exhibit a contradictory behaviour, which may, however, be attributable to its preferential substitution in plagioclase of the 'spotted' anorthosites. Apart from Ba, the incompatible element trends appear to support the hypothesis that part of the pegmatite represented by samples from borehole TLP.2 and 6 level haulage may have crystallized from a relatively highly fractionated parent liquid. By the same argument, the portion of the pegmatite in the vicinity of borehole TLP.1, may have crystallized from a less evolved melt. However, the enrichment of some of the incompatible elements is not as great as might be expected and possible explanations are considered in the concluding chapter of this study.

The majority of the compatible elements do not display complete compatibility towards the pegmatite phases olivine, clinopyroxene and magnetite, resulting in a strong modal control on their respective distributions. The situation is further complicated by the presence of varying quantitites of sulphides, which contain abundant Cu and Ni, as well as minor amounts of Zn and Co.

In conclusion, a characteristic feature of most of the trace element variation diagrams is the grouping of the data points, according to sample location. For most of the compatible trace elements (and the major elements), their distribution is modally controlled. In the case of the incompatible elements there is increasing enrichment in the order TLP.1→TLP.2 →6 level haulage. Co and Ni, the only compatible elements with respect to both olivine and clinopyroxene, exhibit increasing enrichment in the order 6 level haulage→TLP.2→TLP.1. If the Townlands pipe consists of two adjoining pegmatite bodies, as suggested by the silicate mineralogical data, then the trace element distributions support the proposal that the northerly body (TLP.2 and 6 level haulage samples) is more highly fractionated than the southerly body (TLP.1, TLP.3, TLP.4, TLP.5 samples). In addition, the margin of the northerly body (6 level haulage) is enriched in incompatibles, compared to the core (TLP.2). According to Pearce and Norry (1979), Ti, Zr, Y and Nb have high field strengths (charge/radius ratio) and are not influenced by deuteric effects. Consequently, the discrepancies in trace element abundances may be related to the relative movement of intercumulus material between the margin and the core of the northerly body. This suggestion is also discussed in more detail in the concluding chapter.

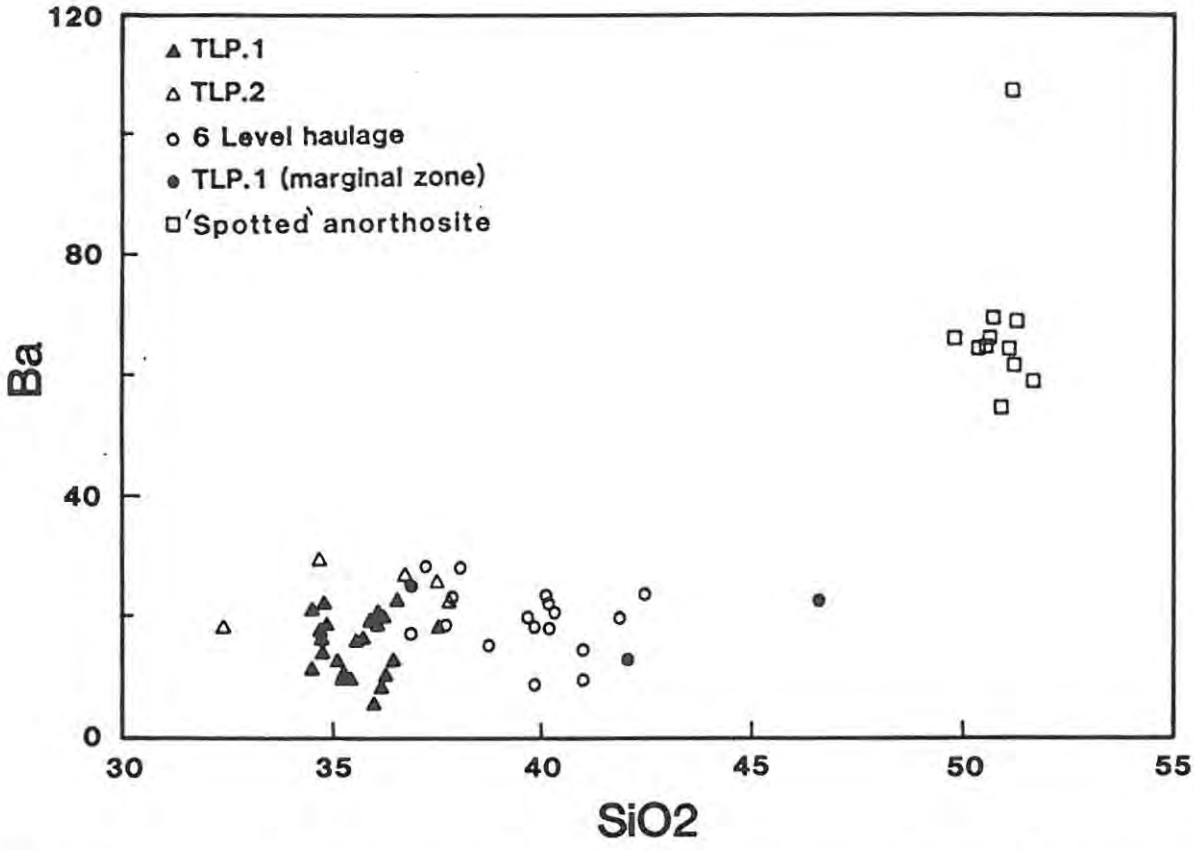

Figure 46(a). Plot of Ba (in parts per million) versus weight percent SiO_2.

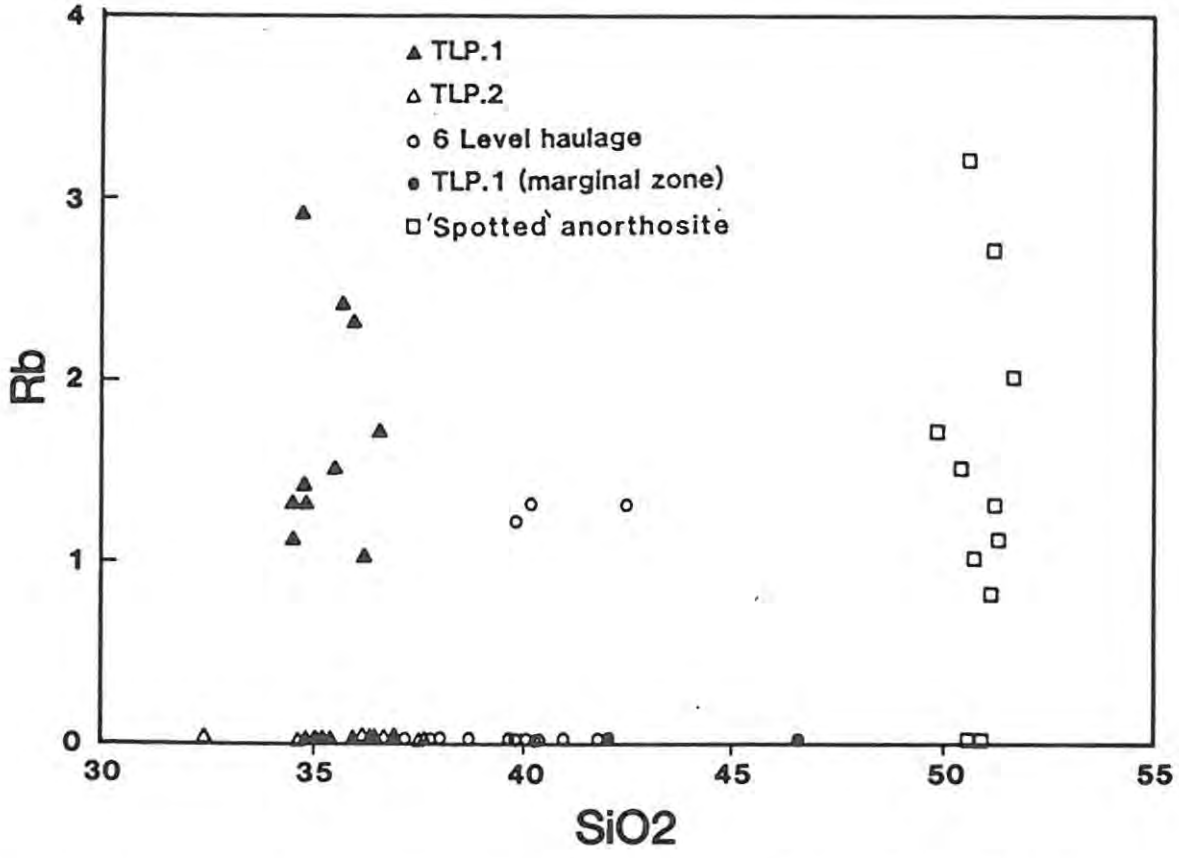

Figure 46(b). Plot of Rb (in parts per million) versus weight percent SiO_2.

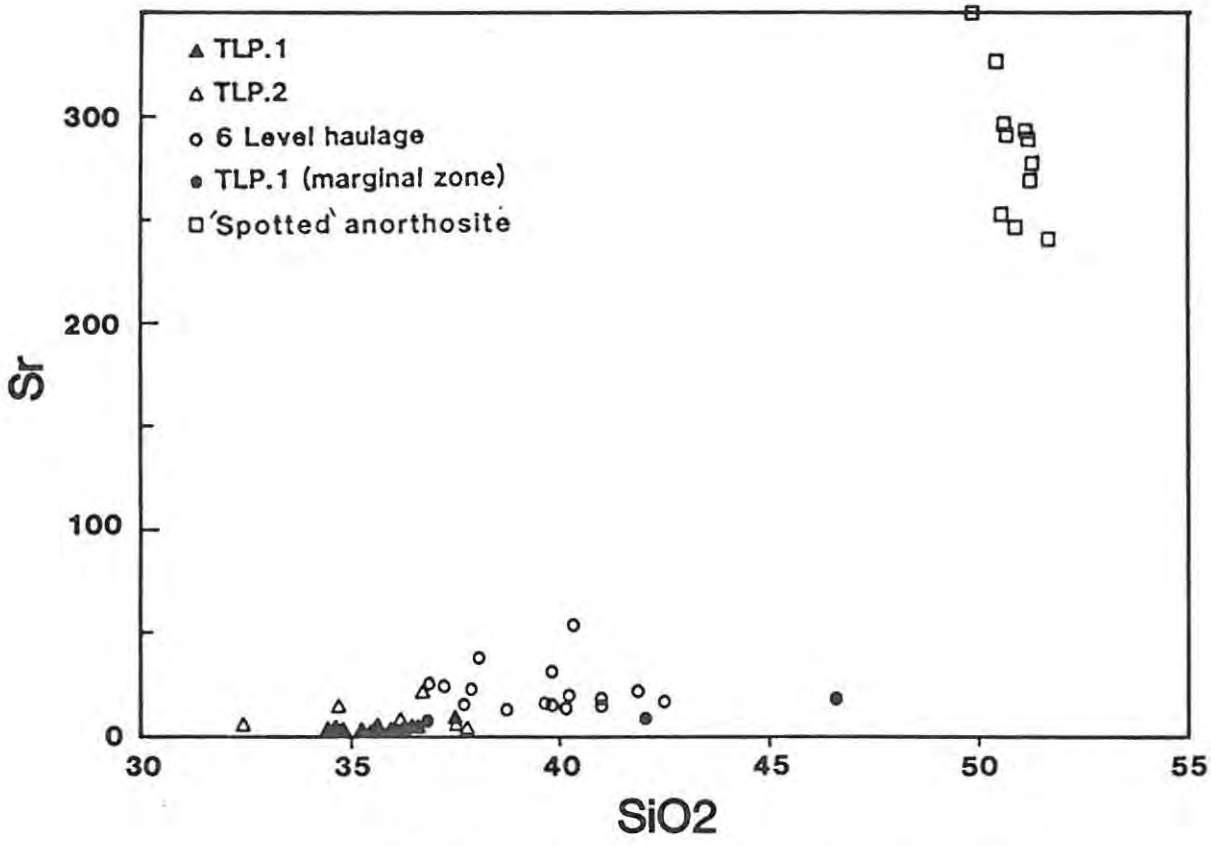

Figure 46(c). Plot of Sr (in parts per million) versus weight percent SiO_2.

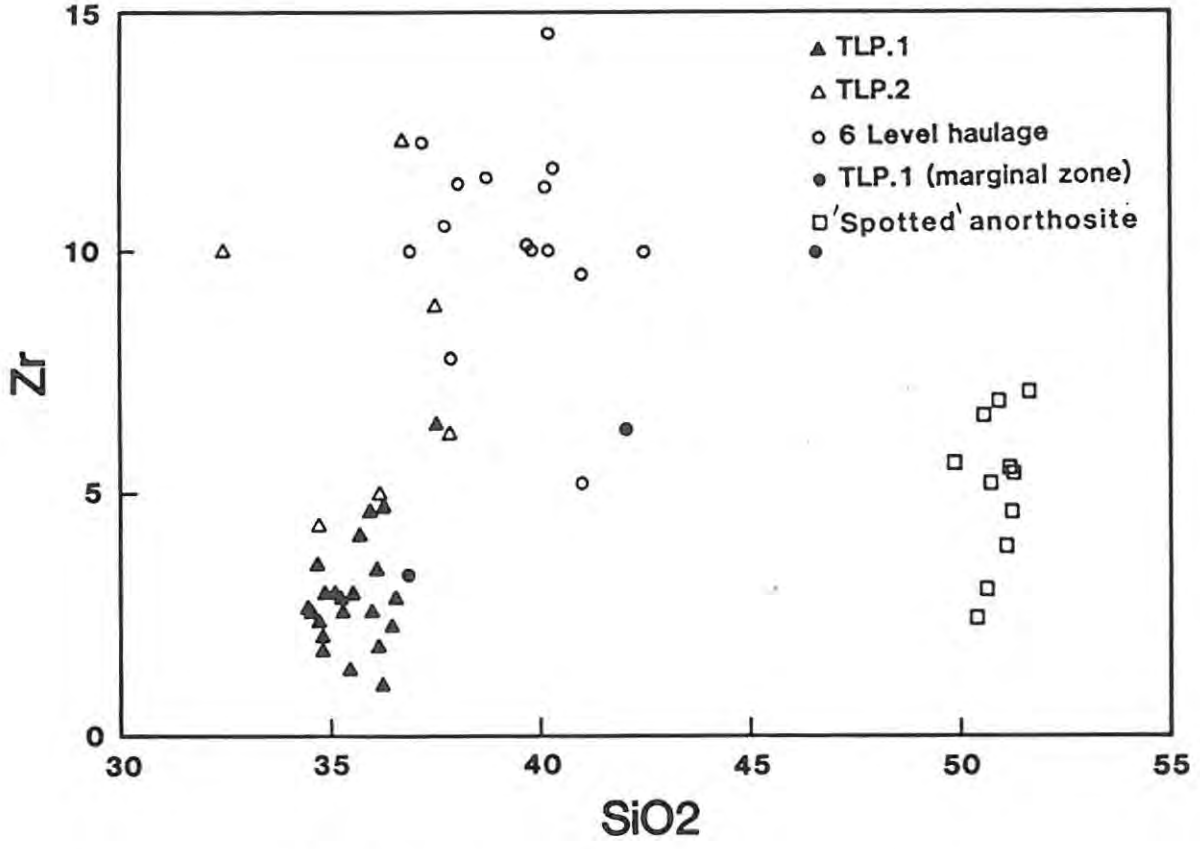

Figure 46(d). Plot of Zr (in parts per million) versus weight percent SiO_2.

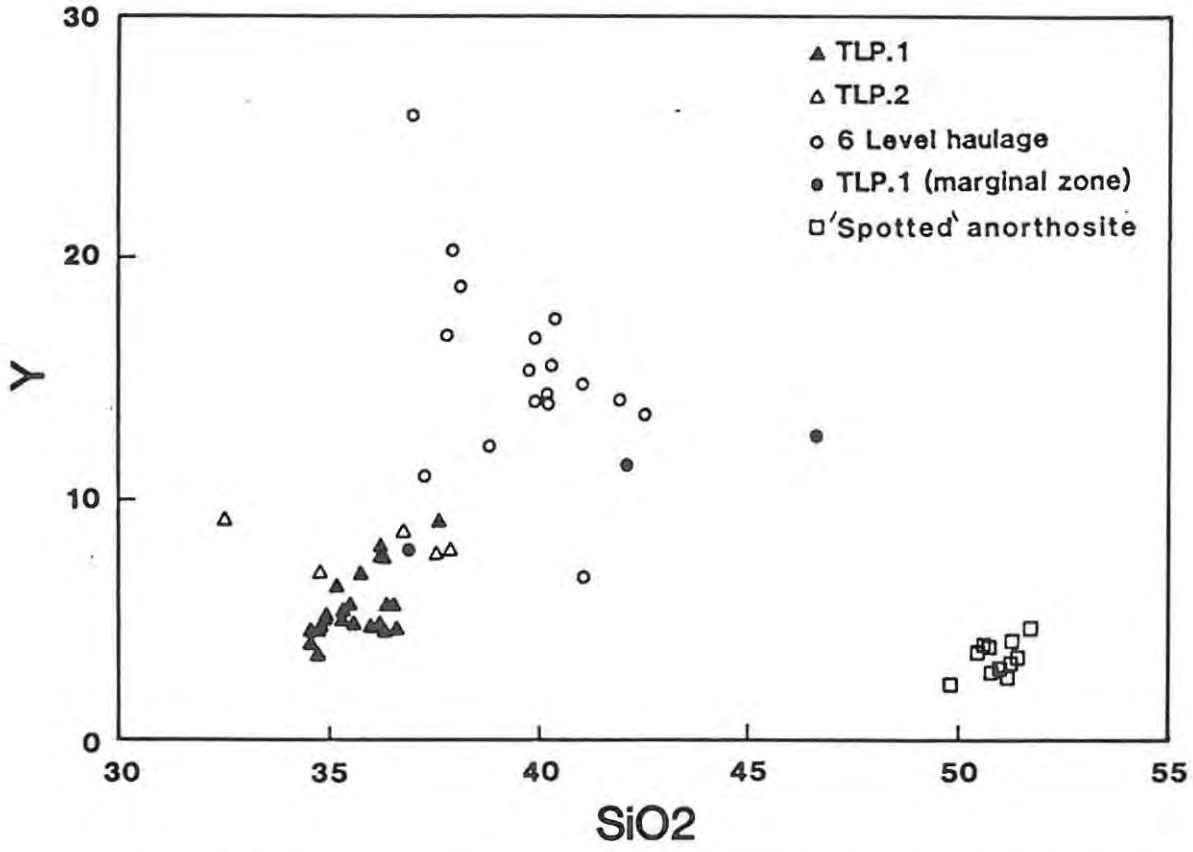

Figure 46(e). Plot of Y (in parts per million) versus weight percent SiO_2.

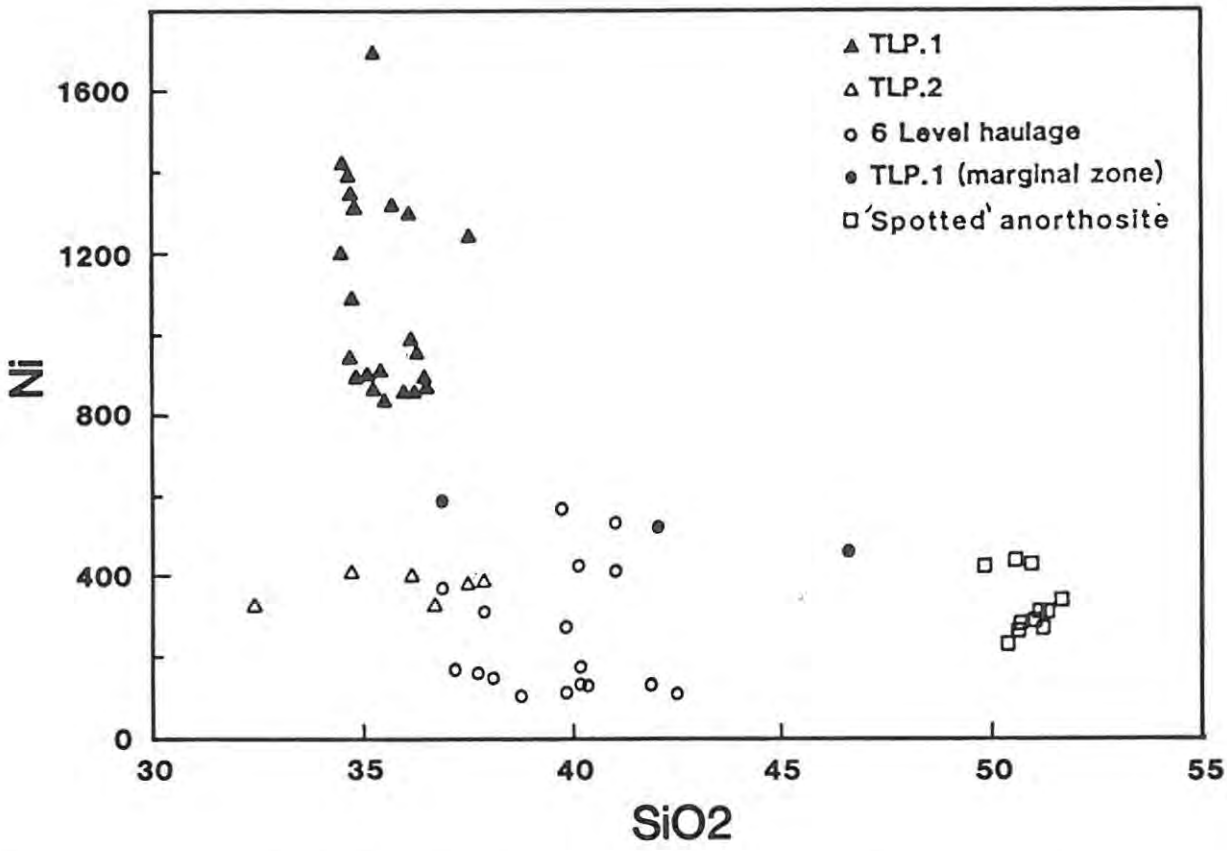

Figure 46(f). Plot of Ni (in parts per million) versus weight percent SiO_2.

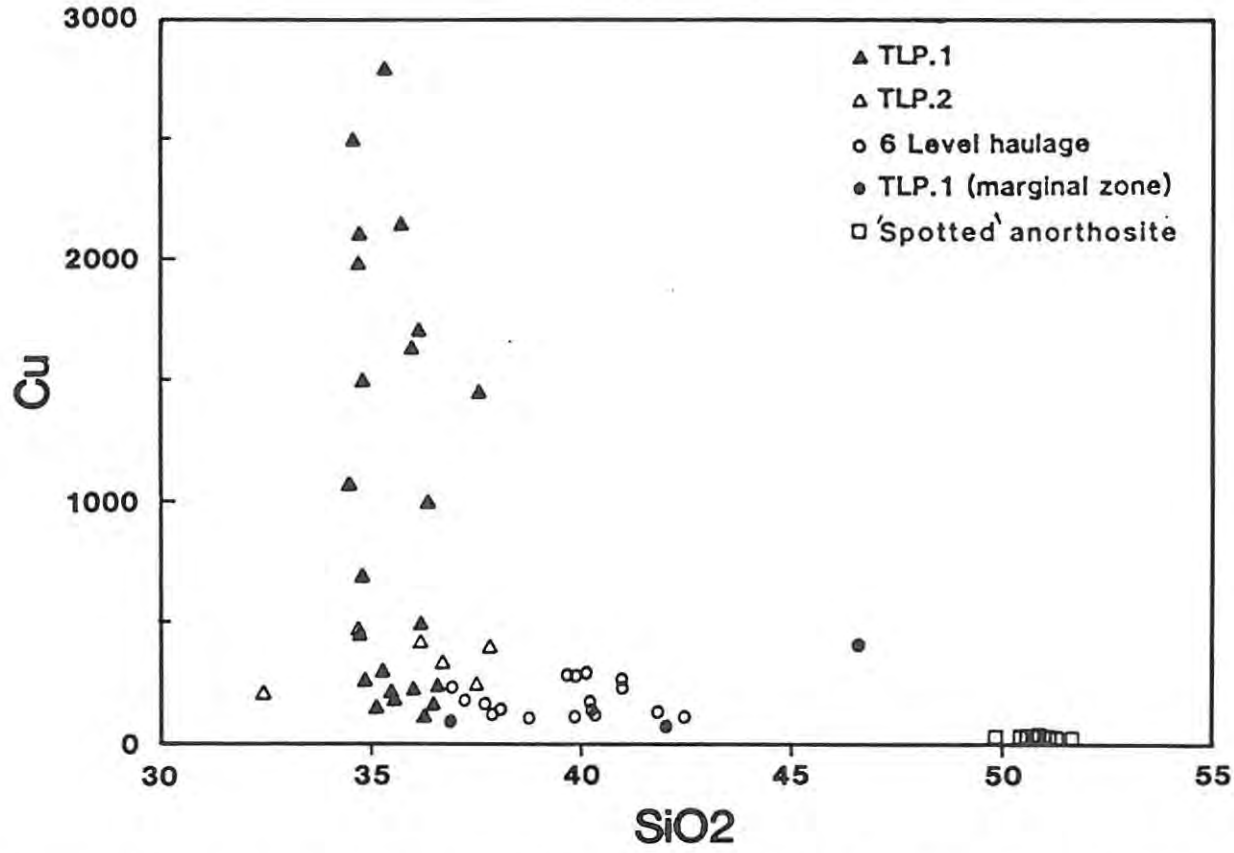

Figure 46(g). Plot of Cu (in parts per million) versus weight percent SiO_2.

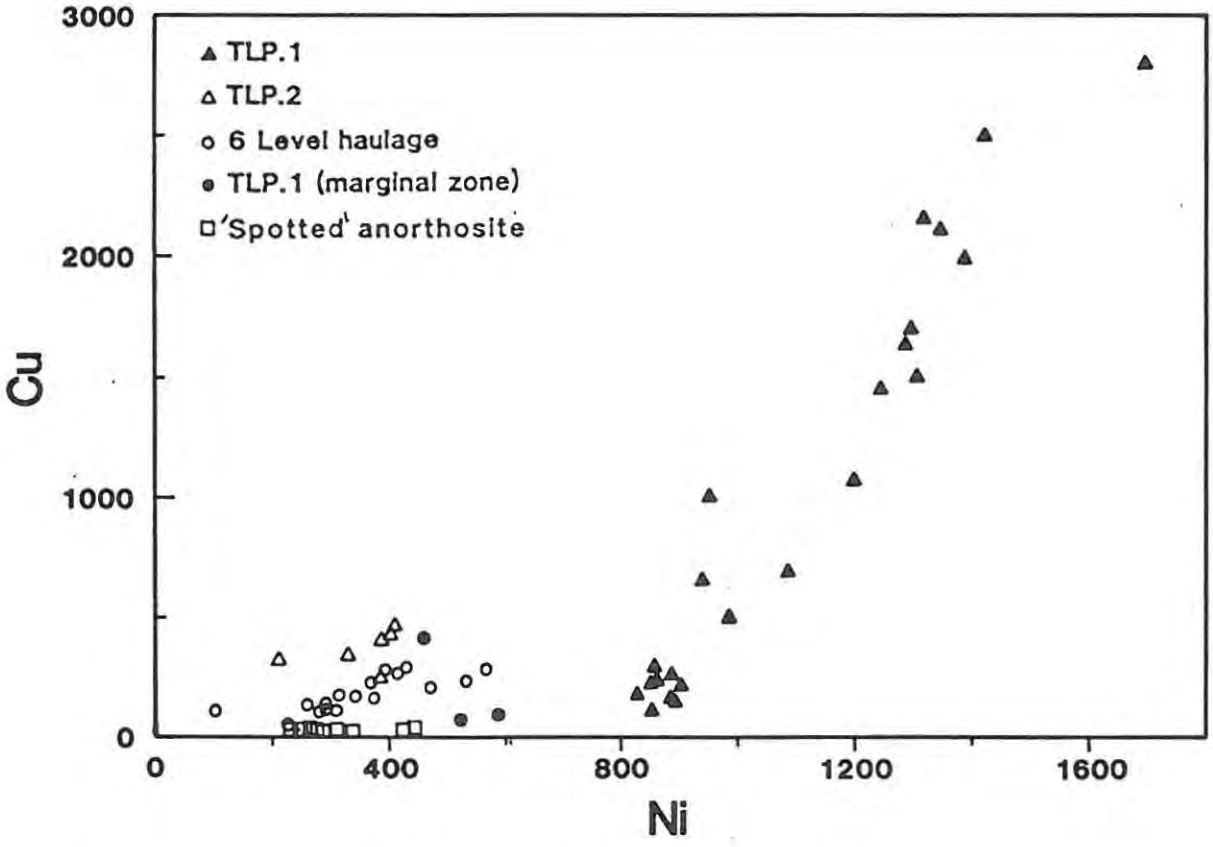

Figure 46(h). Plot of Cu versus Ni (in parts per million).

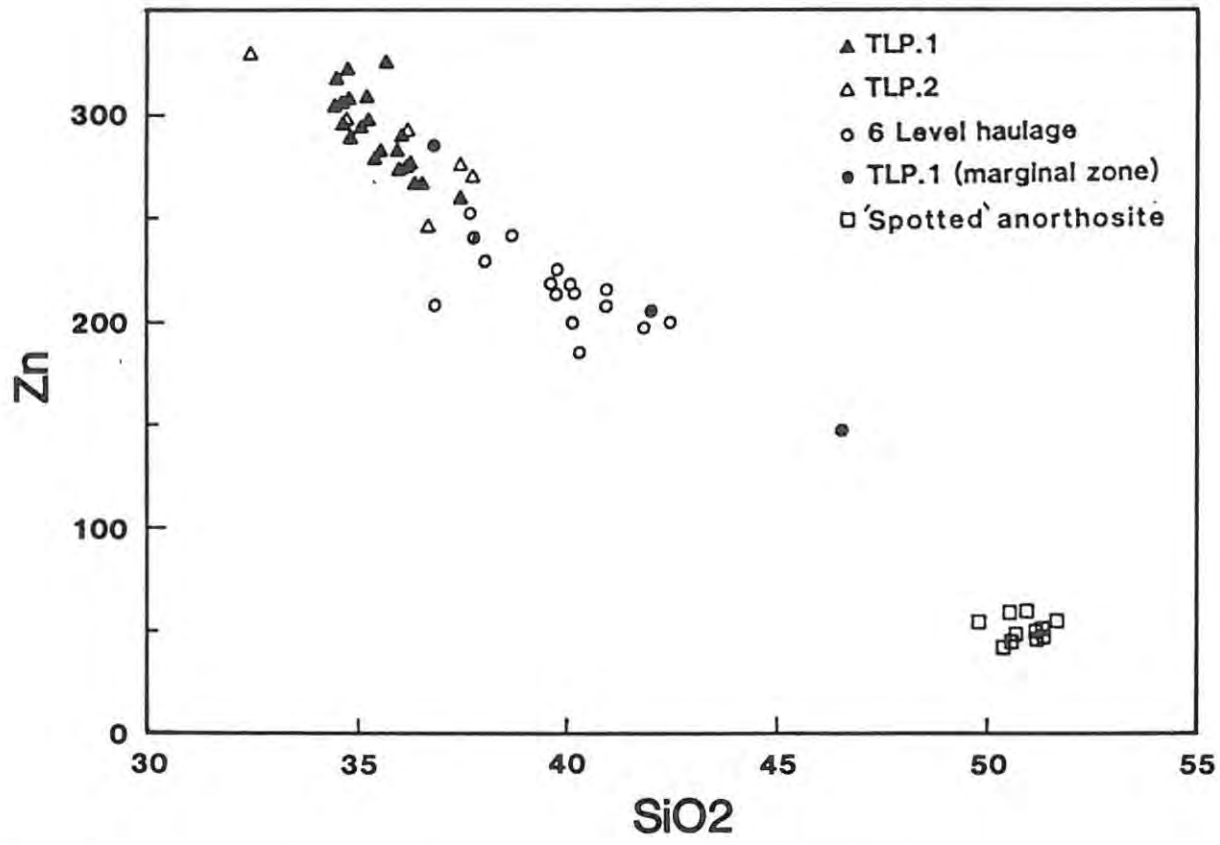

Figure 46(i). Plot of Zn (in parts per million) versus weight percent SiO_2.

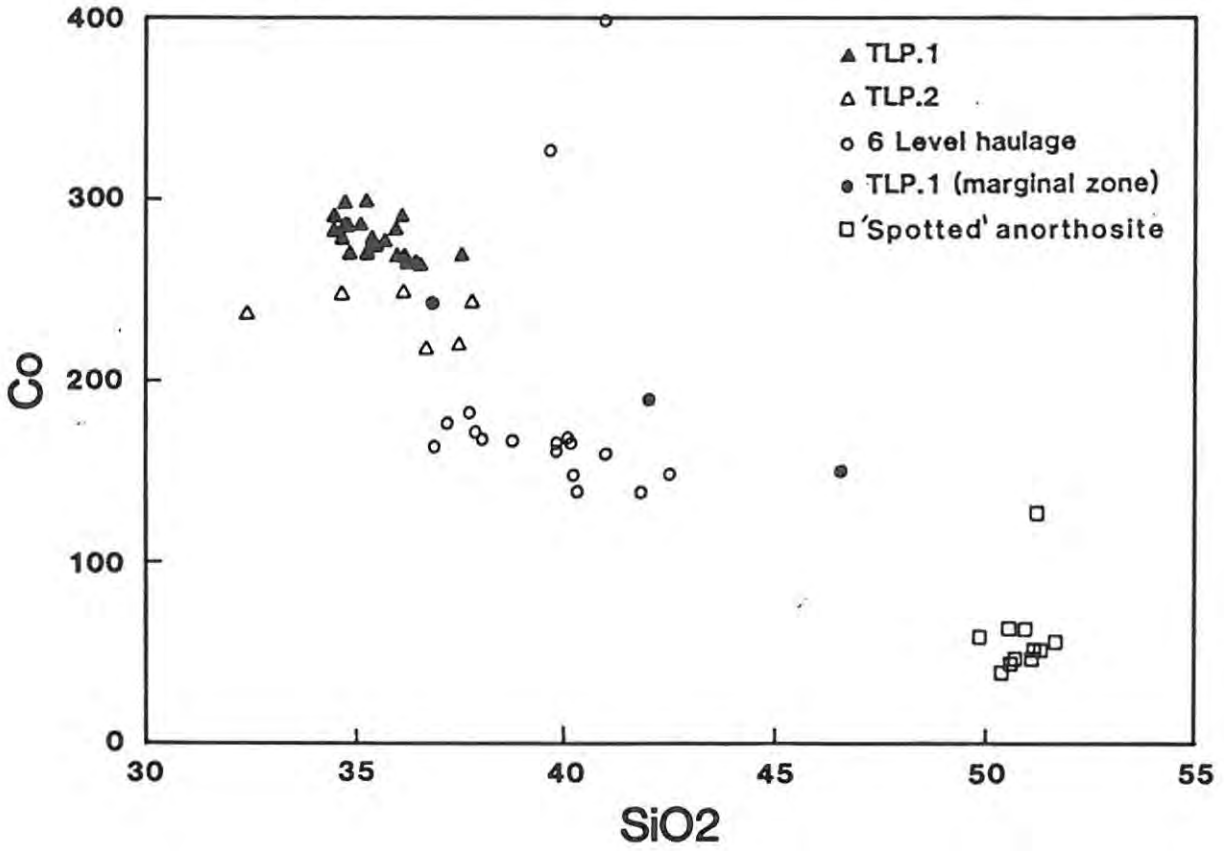

Figure 46(j). Plot of Co (in parts per million) versus weight percent SiO_2.

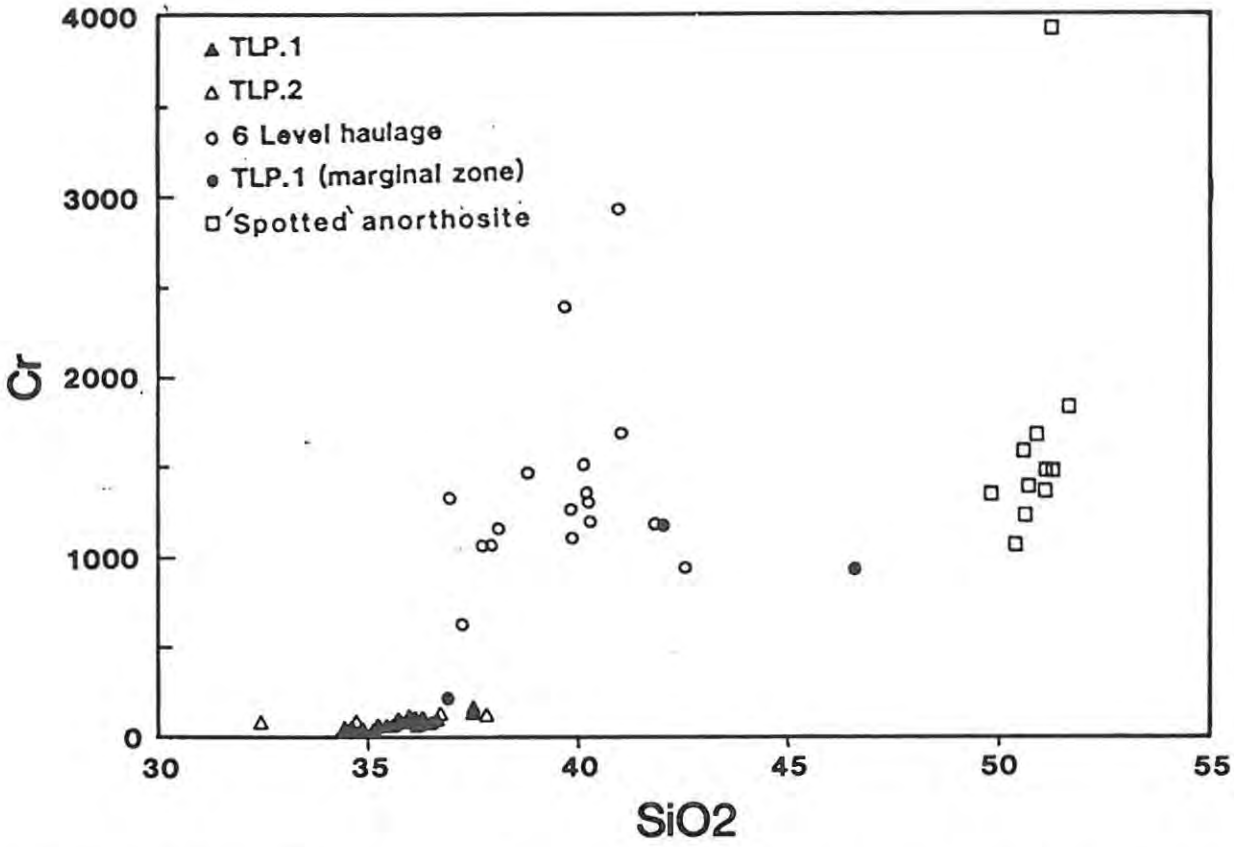

Figure 46(k). Plot of Cr (in parts per million) versus weight percent SiO_2.

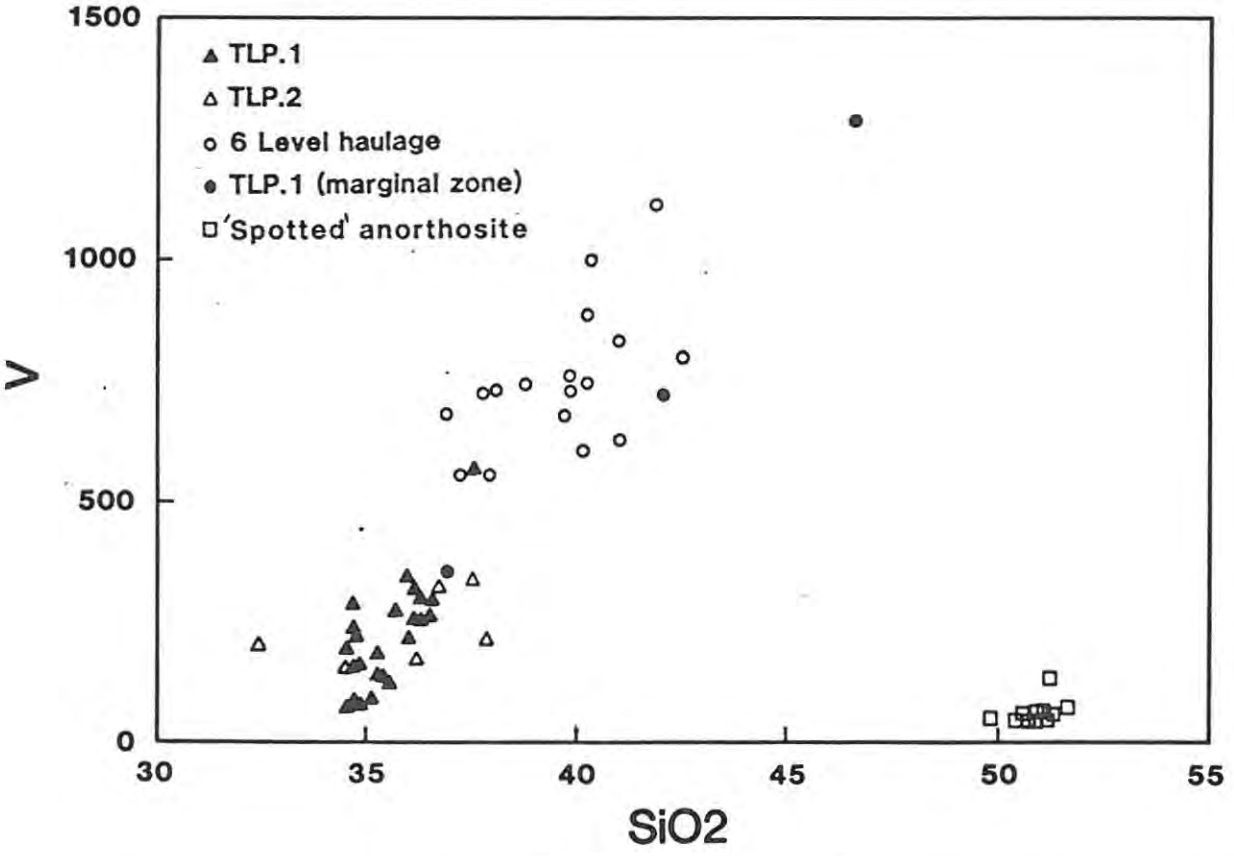

Figure 46(l). Plot of V (in parts per million) versus weight percent SiO_2.

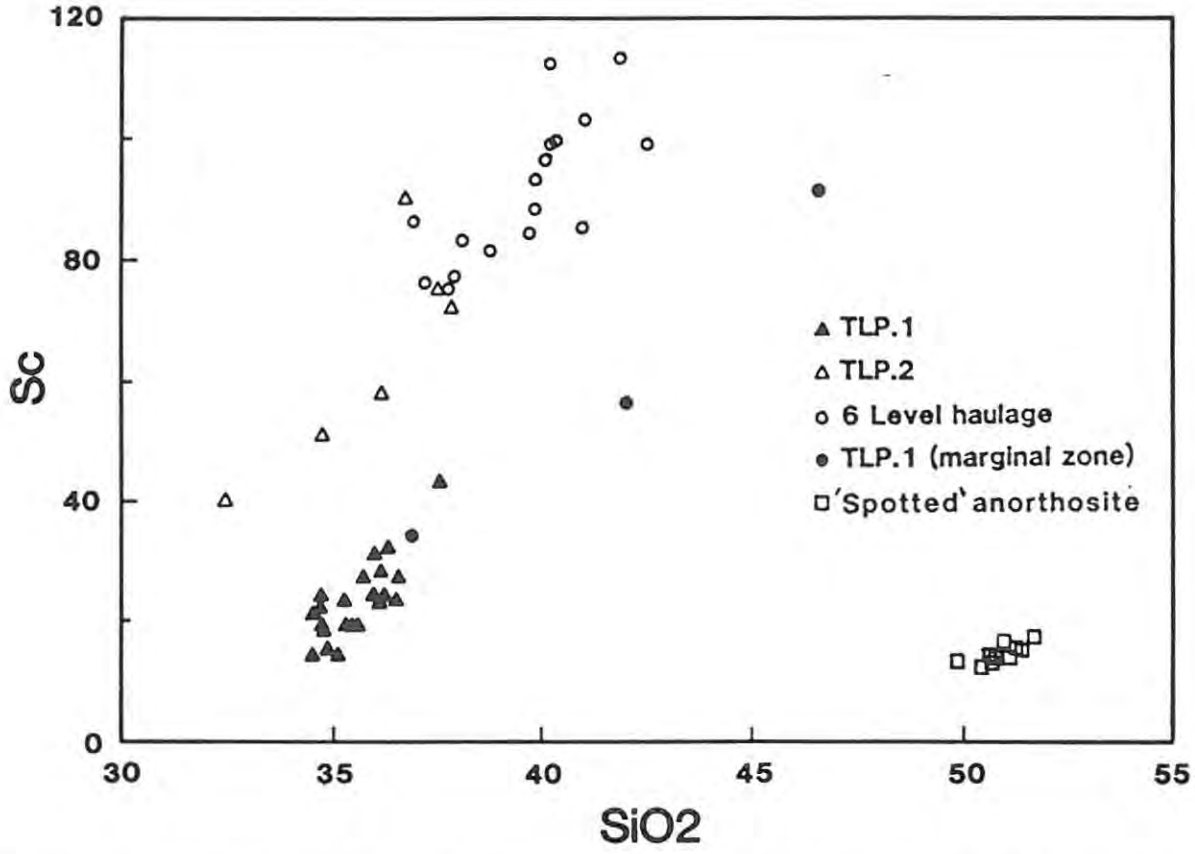

Figure 46(m) Plot of Sc (in parts per million) versus weight percent SiO_2.

9. SUMMARY AND CONCLUSIONS

1) The Townlands pipe is a relatively large plug-like body of Fe-rich ultramafic pegmatite. It transgresses the rocks of the upper critical zone of the Bushveld Complex at high angles to the layering and, according to results obtained from the J.C.I. gravity survey, is limited to a depth of ±500m below surface. The pegmatite body exhibits a distinctive negative magnetic anomaly and has caused some structural disturbance in the surrounding layered suite. The layered rocks are downwarped around the periphery of the pegmatite and are cut by northeasterly trending faults on its northern side.

2) Surface outcrop is extremely poor and sampling was limited to five vertical boreholes, three of which extend to a depth of only 30m, and one underground exposure along 6 level haulage. The deepest borehole, TLP.1 intersected the UG2 chromitite and associated layers at a vertical depth of 260m.

3) The pegmatite is composed largely of olivine and clinopyroxene and varies in composition between dunite and wehrlite. The central portion of the pipe is dominated by olivine, while the marginal zones plus the pegmatitic material in the vicinity of the UG2 layers (TLP.1 'marginal' zone) contain approximately equal amounts of clinopyroxene and olivine. Accessory phases include ilmenite, Ti-magnetite, apatite, amphiboles, chlorite-group minerals, biotite, ilvaite and an unusual assemblage of ore minerals. The pegmatite minerals, particularly those in the borehole TLP.1 samples, are cut by a pervasive system of veinlets and fractures that contain serpentine and secondary magnetite.

4) The olivine and clinopyroxene grains of the pegmatite exhibit compositional and textural characteristics that are analogous to those encountered in igneous rocks that have crystallized from an Fe-enriched differentiated melt of basaltic parentage. The borehole TLP.2 and 6 level haulage samples display similar mineral compositions with respect to both olivine (Fo_{30}-Fo_{33}) and clinopyroxene ($Wo_{45}En_{30}Fs_{25}$). The remaining samples are more variable in composition, but also occupy a similar compositional field with respect to olivine (Fo_{46}-Fo_{52}) and clinopyroxene ($Wo_{45}En_{37}Fs_{18}$). The TLP.1 'marginal' zone samples exhibit variable compositions, intermediate between those of the pegmatite and those of the layered rocks intersected by borehole TLP.1.

5) Mineralogical investigations indicate that the majority of the contact zones between the ultramafic pegmatite and the 'spotted' anorthosite exposed in 6 level haulage, are very sharp. Variations in mineral composition, with respect to olivine and clinopyroxene of the pegmatite, and orthopyroxene of the 'spotted' anorthosite, are restricted to a 2cm wide zone adjacent to the contact.

6) Ilmenite and, to a slightly lesser extent, Ti-magnetite are the most common accessory phases in the samples from borehole TLP.2 and 6 level haulage. The Ti-magnetite grains exhibit textures and microstructures indicative of those formed at high temperatures in slowly cooled igneous rocks. Application of the Spencer & Lindsley (1981) geothermometer, for co-existing Ti-magnetite/ilmenite mineral pairs, yields subsolidus re-equilibration temperatures that range between 580°C and 800°C at log fO_2 = -17 to -21. These provide minimum lower temperature limits for the formation of the oxide assemblage.

7) The chromitite leader layers intersected by borehole TLP.1 display marked textural and compositional differences in comparison with the UG2 layers of the adjacent layered suite. The margins of the leader layers are enriched in Fe^{2+}, Fe^{3+}, Ti^{4+} and Mn^{2+} and contain abundant ilmenite. It appears that additional material in the form of a magnetite-ulvöspinel solid solution may have precipitated around the pre-existing chromite grains. High prevailing temperatures caused homogenization of these zoned grains to yield spinels of intermediate composition, and slow cooling under high fO_2 conditions resulted in extensive 'oxidation-exsolution' of ilmenite.

8) The ore minerals of the Townlands pegmatite are present in accessory amounts, but display a very unusual range of phases and textural relationships. All the sample localities contain, what appears to be, a 'primary' sulphide assemblage that includes troilite, chalcopyrite, cubanite and pentlandite. The samples from borehole TLP.1 and, to a lesser extent borehole TLP.3, also contain a number of unusual phases such as mooihoekite, haycockite, native copper and valeriite. Other accessory phases observed in the ore mineral assemblage include sphalerite, mackinawite, pyrite, bornite, marcasite, digenite, graphite, native silver, hematite and covellite. Mooihoekite and haycockite appear to have formed by the replacement of the 'primary' sulphide assemblage at low temperatures ($<$ 200°C). This replacement process appears to have involved the introduction of additional copper by fluids that may have been responsible for the serpentinization of the pegmatite olivine.

9) Many of the major and trace element distribution patterns are modally controlled with respect to the relative abundances of olivine and clinopyroxene. The pegmatite is somewhat enriched in incompatible elements with respect to the adjacent 'spotted' anorthosite, but the enrichment is, possibly, not as great as might be expected for a pegmatite that crystallized from a highly fractionated melt. The incompatible element enrichment trend also varies according to sample locality and increases in the order TLP1 $\longrightarrow$ TLP.2 $\longrightarrow$ 6 level haulage.

There has been little concensus of opinion with regard to the genesis of Fe-rich ultramafic pegmatites and several possibilities have been advocated. Wagner (1929) suggested that the formation of these pegmatite bodies could be explained by magmatic replacement processes. Cameron & Desborough (1964) favoured an origin involving metasomatic replacement of the layered rocks by high pressure, high temperature fluids. Willemse (1969a) concluded that evidence also exists for an intrusive origin for some ultramafic pegmatites. Extending the ideas of Wagner (1929), Jones (1974) and Viljoen & Scoon (in press) proposed a model to account for the genesis of many of these pegmatite bodies. In terms of this model the layered rocks are replaced by migrating intercumulus liquids undergoing iron enrichment. Schiffries (1982) suggested that the Driekop pipe in the eastern Bushveld Complex formed by metasomatic replacement processes involving high temperature chloride solutions. Gross chemical differences exist between the Driekop and Townlands pipes and this mechanism does not appear to be applicable to the Townlands pipe. Raedeke & McCallum (1984) suggested that certain dunite pegmatites in the Stillwater Complex may have formed from the alteration of pre-existing orthopyroxene by a late-stage hydrous vapour, according to the following reaction:

$$2MgSiO_3(En) + 2H_2O(V) \rightleftharpoons Mg_2SiO_4(Ol) + Si(OH)_4(V)$$

The Townlands pegmatite is, however, hosted by plagioclase-rich rocks and this mechanism can, therefore, be discarded as a possible genetic model.

There are, therefore, three basic genetic models that might be applicable to the Townlands pipe and these include an origin by metasomatic replacement, magmatic replacement and forceful intrusion. Metasomatic replacement involves the alteration of pre-existing phases by high temperature solutions, but the mechanisms involved in magmatic replacement (inter alia Wagner, 1929; Jones, 1974; Viljoen & Scoon, in press) are not well understood or well documented. It is suggested,

however, that certain features that are characteristic of metasomatic replacement, such as the presence of mineralogical and geochemical alteration haloes, might also be applicable to magmatic replacement processes. The available evidence on the Townlands pegmatite is in favour of a magmatic intrusive origin and the main arguments against either metasomatic or magmatic replacement are summarised as follows:

i) The surrounding layered rocks are structurally disturbed adjacent to the pegmatite. This is manifested in a downwarping of the layers around the margins of the pipe. The relationship between the formation of the pegmatite and the associated faulting on the northern side of the body is not known. Schiffries (1983) interpreted the downwarping of the layers adjacent to the Driekop pipe as resulting from a volume change during the replacement of the layered rocks. The layers surrounding the Townlands pipe appear, however, to have been plastically deformed, and this can only be achieved at high temperature.

ii) The intersection of the UG2 chromitite layers in borehole TLP.1 has been cited by Viljoen et al. (1983) as evidence for a magmatic replacement origin for the pegmatite. This layered zone is, however, displaced some 20m above its expected position and may also be interpreted as representing part of a large xenolith that was transported upwards during emplacement of the pegmatite melt.

iii) The minerals of the pegmatite are coarse-grained, well-annealed and compositionally homogeneous, which is suggestive of a high temperature of formation.

iv) Both olivine and clinopyroxene of the pegmatite exhibit textural and compositional features that closely resemble those encountered in igneous rocks that have crystallized from a melt at elevated temperature. Furthermore, the pegmatite mineral compositions are similar to those of cumulus rocks from the upper zone of the Bushveld Complex.

v) The majority of the Ti-magnetite grains in the pegmatite exhibit microstructures typical of those formed at high temperature in slowly cooled igneous rocks. Application of the Spencer & Lindsley (1981) geothermometer yielded minimum re-equilibration temperatures

of 580°C - 800°C. The temperature of formation of the oxide assemblage may, therefore, be in excess of 800°C and it is doubtful whether such temperatures could be attained by metasomatic fluids.

vi) The chromitite leader layers of borehole TLP.1 are composed of well-annealed grains that exhibit exsolution textures indicative of formation at high temperatures.

vii) The 'primary' sulphide assemblage of the pegmatite is similar to that observed in igneous rocks that have crystallized from high temperature melts. This assemblage is unusual in that it includes troilite, but there is no evidence to suggest that the assemblage represents a relict feature of pre-existing rocks.

viii) The major element geochemical data for the pegmatite compares favourably with that of samples from the upper zone of the Bushveld Complex. The trace element data is also, in general, consistent with an origin of the pegmatite by crystallization from a fractionated magmatic liquid.

ix) The most convincing evidence in favour of an intrusive origin for the Townlands pipe is provided by the sharp contacts between the pegmatite and the adjacent 'spotted' anorthosites. There is no evidence for the presence of geochemical or mineralogical alteration haloes either within the body of the pegmatite or in the adjacent layered rocks. This situation is not consistent with metasomatic replacement processes and may also be contrary to an origin by magmatic replacement.

x) There are problems associated with metasomatic replacement processes with regard to the source and origin of the fluids and the origin of the fluid components necessary to achieve replacement of pre-existing layered rocks. In contrast, the source and origin of a parental pegmatite melt may be more easily explained in terms of the theories applied to the crystallization of the Bushveld and other layered complexes.

There appears, therefore, to be much evidence against an origin for the pegmatite either by metasomatic replacement or in terms of the chloride solution model of Schiffries (1983). In view of the lack of any

quantitative information on the processes that might be involved in magmatic replacement, a genetic model involving the forceful intrusion of a fractionated melt is considered to be the most feasible of the three models. The only portion of the pegmatite that might be interpreted as having a replacement origin is the TLP.1 'marginal' zone, adjacent to the layered sequence intersected by borehole TLP.1. Mineral compositions in this zone are variable and there appears to be a mixing relationship between the mineral compositions of the pegmatite and those of the layered rock. This zone may have formed as a result of any of the above-mentioned processes, as follows:

i) Metasomatic replacement of the layered rocks by high temperature volatile-rich pegmatite fluids derived from the adjacent pegmatite melt. This mechanism appears to offer the best explanation for the alteration of the UG2 chromitite layers.

ii) Magmatic replacement of the layers at high temperature, subsequent to the emplacement of the main body of the pegmatite melt.

iii) Assimilation of the layered rocks by the pegmatite melt. This mechanism may be applicable to the TLP.1 'marginal' zone, but it is doubtful whether this process could have achieved passive alteration of the chromitite layers.

Determination of the physical nature and the exact processes that might be involved in the accumulation of a pegmatite melt are beyond the scope of this investigation. It is surmised, however, that the liquid was probably relatively Fe-rich and dense, but with a low viscosity. The J.C.I. gravity survey indicated a limited depth of 500m for the pipe, which suggests that the pegmatite liquid was probably derived from within the confines of the layered sequence of the critical zone of the Bushveld Complex. In addition, the whole rock geochemical data and mineral compositions indicate that the pegmatite probably crystallized from a relatively highly fractionated melt. Consequently, it is suggested that the Townlands pipe formed by crystallization from an Fe-rich liquid derived from late-stage intercumulus material trapped during the crystallization of the layered sequence. The pegmatite is hosted by plagioclase-rich rocks and the intercumulus fluids associated with the crystallization of such rocks may have been purged of plagioclase components. This may explain the lack of plagioclase in the Townlands

pegmatite. A simplified model is proposed for the accumulation of large quantities of intercumulus fluids and involves the following stages:

i) Crystallization of plagioclase-rich cumulus rocks containing entrapped intercumulus liquid. Estimates by Wager et al. (1960) and Jackson (1961) indicate that between 20 and 50 volume percent of interprecipitate liquid may be present during the initial stages of crystallization.

ii) Continued post-cumulus growth of plagioclase results in the depletion of plagioclase components and the enrichment of the intercumulus liquids in Fe, incompatible elements and volatile components such as H_2O, CO_2, H_2 and O_2. It is surmised that this Fe-rich liquid will have a high density and low viscosity, and will tend to remain in situ until forced to migrate.

iii) Migration of the intercumulus fluids to a zone of structural weakness, in response to an increasing overburden pressure from overlying layers. This zone of structural weakness may take the form of incipient joint and fracture systems, shear zones or fault planes.

iv) Accumulation of the Fe-rich intercumulus material along the zone of structural weakness as a result of further increases in overburden pressure and/or tectonic activity. The forceful emplacement of this material will force aside pre-existing layered rocks and may result in the assimilation of some layered material by the Fe-rich melt. This may account for the structural disturbance of the layered suite in the vicinity of the Townlands pipe.

v) Crystallization of the pegmatite from the accumulated Fe-rich liquid in response to decreasing temperatures. The coarse grain-size of the pegmatite may be attributed to a relatively high volatile content in the melt, which would allow for rapid ionic mobilities. The presence of only minor amounts of oxide material in the pegmatite suggests, however, that the fO_2 of the liquid must have been low. Eggler & Burnham (1973) demonstrated that the fO_2 is controlled by the initial Fe_2O_3/FeO ratio of the magma and will increase, by no more than 1.3 log units, from the original buffer, with differentiation. They also noted that H_2O present

in a magma need not be oxidising if it is in equilibrium with silicate-oxide assemblages. The Fe-rich pegmatite melt may, therefore, have been enriched in volatile components such as H_2O and CO_2, while still maintaining a relatively low fO_2.

Any intercumulus liquid that has undergone iron enrichment might be expected to contain high concentrations of incompatible elements. The rocks of the Townlands pipe are, however, not as enriched in incompatible elements as might be expected. A possible explanation involves a continuation of the fractionation process after emplacement of the pegmatite melt. In terms of this process, late-stage volatiles and some of the incompatible elements may have been driven off during the final stages of crystallization. This material may ultimately have entered the overlying magma chamber.

The presence of two magnetic 'eyes' forming the main magnetic anomaly of the Townlands pipe, each with its own characteristic range of mineral compositions, suggests that the Townlands pipe may consist of two or more separate, but adjoining pegmatite bodies. The northerly part of the pegmatite, represented by samples from boreholes TLP.2 and 6 level haulage, appears to have crystallized from a more evolved melt than the southerly body, which is represented by samples from the remaining boreholes. Consequently, it is suggested that the northerly portion of the Townlands pipe may have been emplaced at a later stage to the southerly part and may, therefore, represent the accumulation of a more highly differentiated intercumulus liquid.

The pegmatite samples exhibit an unusual sulphide assemblage, which appears to contain a primary assemblage consisting of troilite, chalcopyrite, cubanite and pentlandite. The majority of the unusual sulphides, such as mooihoekite and haycockite are concentrated in samples from borehole TLP.1. Mooihoekite and haycockite appear to have formed by replacement of the primary assemblage. The reactions involved in these processes require the addition of copper, and minor amounts of zinc to form sphalerite. The association of the sulphide aggregates with the serpentine veinlet and fracture systems may not be coincidental. It is suggested, therefore, that the Cu and Zn may have been released during the serpentinization of the olivine and transported as chloride complexes in aqueous solutions. The origin of these aqueous solutions is uncertain, but it is interesting to note that the unusual assemblages are

restricted to the southerly portion of the Townlands pipe. Consequently, it is postulated that the generation of aqueous fluids may be related to the emplacement of the northerly part of the pegmatite, at a later stage to the southerly portion.

It must be noted that the conclusions reached in this study are, of necessity, somewhat tentative, due largely to a lack of sample density. It is suggested, therefore, that in any future exploration of the Townlands pipe, at least two inclined or horizontal boreholes, sited in the adjacent layered rocks, should be drilled through the pegmatite. It is obvious that further work on pegmatite bodies such as the Townlands pipe is necessary, as these bodies appear to be intimately related to the crystallization history of the Bushveld Complex.

APPENDIX 1

SAMPLE LOCALITIES

The location of the relevant samples from the five boreholes drilled into the Townlands pipe are tabulated in Table 1B. Sample localities along 6 level haulage are indicated in Fig. 1A. Borehole logs for TLP.1 and the remaining boreholes TLP.2, TLP.3, TLP.4 and TLP.5 are presented in Figs. 1B, and 1C, respectively. The symbols applicable to the borehole logs are listed in Table 1A.

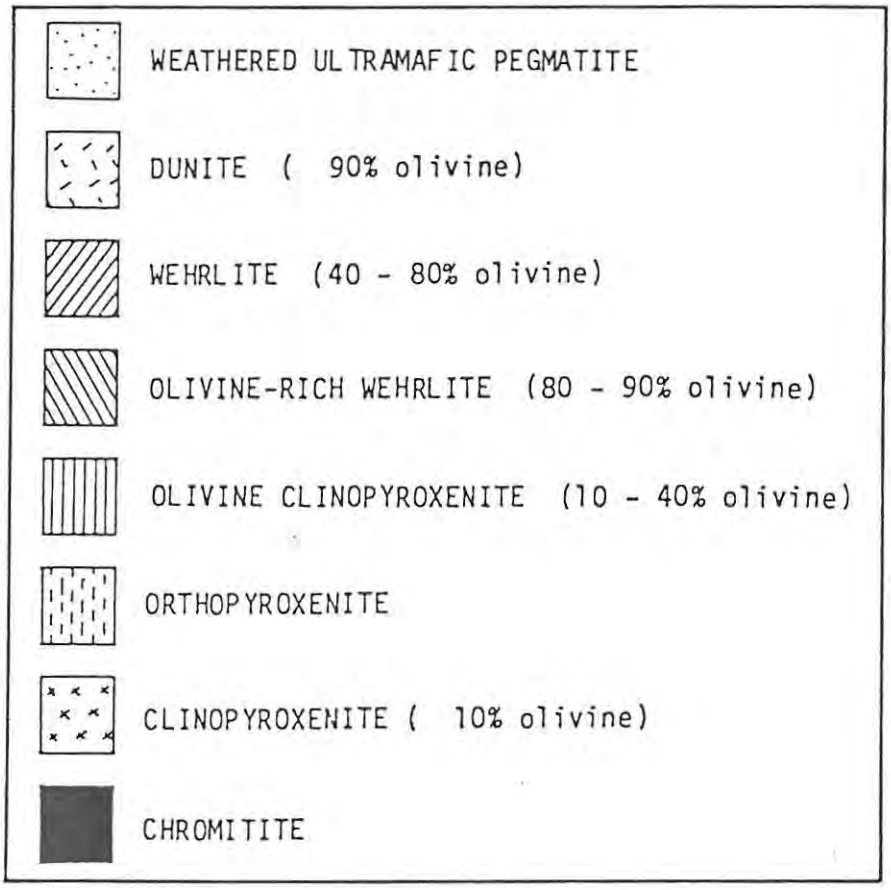

Table 1A. Borehole log symbols

BOREHOLE CORE SAMPLES

SAMPLE NO.	DEPTH BELOW SURFACE (m)	SAMPLE NO.	DEPTH BELOW SURFACE (m)
	TLP.1		
T1/1	269.41 - 269.57	T1/143	161.00 - 161.18
T1/7	264.84 - 264.98	T1/144	106.17 - 160.50
T1/8	263.71 - 263.84	T1/148	155.07 - 155.25
T1/9	261.94 - 262.08	T1/151	149.25 - 150.11
T1/12	261.69 - 261.75	T1/157	143.31 - 143.59
T1/16	261.40 - 261.52	T1/161	139.59 - 139.73
T1/19	261.00 - 261.22	T1/176	129.31 - 129.53
T1/20	260.90 - 261.00	T1/199	119.90 - 120.11
T1/27	260.22 - 260.28	T1/209	116.22 - 116.32
T1/29	260.03 - 260.14	T1/219	112.99 - 114.16
T1/31	259.72 - 259.88	T1/226	111.45 - 111.74
T1/32	259.48 - 259.72	T1/227	110.29 - 150.11
T1/33	259.38 - 259.48	T1/231	106.18 - 106.46
T1/37	258.86 - 259.09	T1/235	100.62 - 100.76
T1/43	256.52 - 256.85	T1/237	100.04 - 100.25
T1/48	252.80 - 261.00	T1/246	91.34 - 91.54
T1/51	250.12 - 250.49	T1/253	82.70 - 82.91
T1/58	244.79 - 244.99	T1/257	79.49 - 79.66
T1/60	241.96 - 242.23	T1/258	79.02 - 79.14
T1/65	238.68 - 238.82	T1/267	69.80 - 69.96
T1/73	230.76 - 230.05	T1/274	61.32 - 61.44
T1/84	219.50 - 219.81	T1/277	57.19 - 57.40
T1/88	216.45 - 216.83	T1/284	50.62 - 50.86
T1/93	209.73 - 209.89	T1/292	40.89 - 41.04
T1/103	200.92 - 201.10	T1/296	36.30 - 36.43
T1/112	190.45 - 190.76	T1/300	31.20 - 31.43
T1/124	179.44 - 179.61	T1/301	29.58 - 29.81
T1/134	169.22 - 169.45	T1/307	22.30 - 22.45
	TLP.2		
T2/1	80.00 - 80.27	T2/23	50.02 - 50.16
T2/2	80.80 - 81.00	T2/29	40.00 - 40.27
T2/7	71.77 - 71.92	T2/32	36.16 - 36.34
T2/8	70.27 - 70.45	T2/36	32.53 - 32.65
T2/10	66.77 - 66.98	T2/37	31.02 - 31.17
T2/17	59.60 - 59.80	T2/41	24.02 - 31.17
T1/18	58.22 - 58.33		
	TLP.3		
T3/2	36.28 - 36.38	T3/5	31.24 - 31.38
T3/3	35.43 - 35.53		
	TLP.4		
T4/1	31.02 - 31.24	T4/3	26.99 - 27.13
T4/2	28.58 - 28.75	T4/5	25.50 - 25.60
	TLP.5		
T5/1	30.94 - 31.14	T5/4	29.03 - 29.23
T5/2	30.56 - 30.81	T5/5	26.98 - 27.20
T5/3	30.00 - 30.13		

TABLE 1B. Borehole core sample localities.

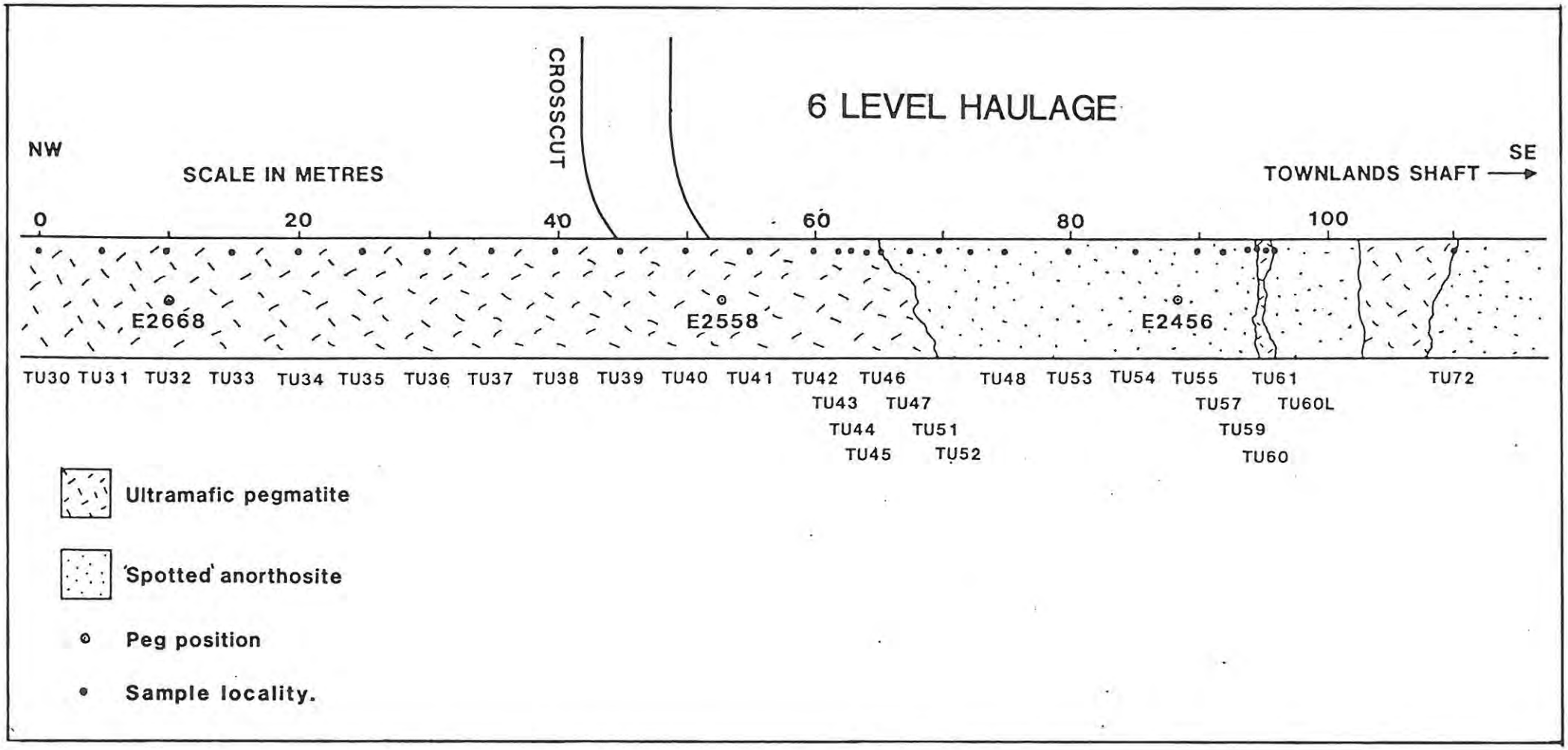

Figure 1A. 6 Level Haulage sample localities

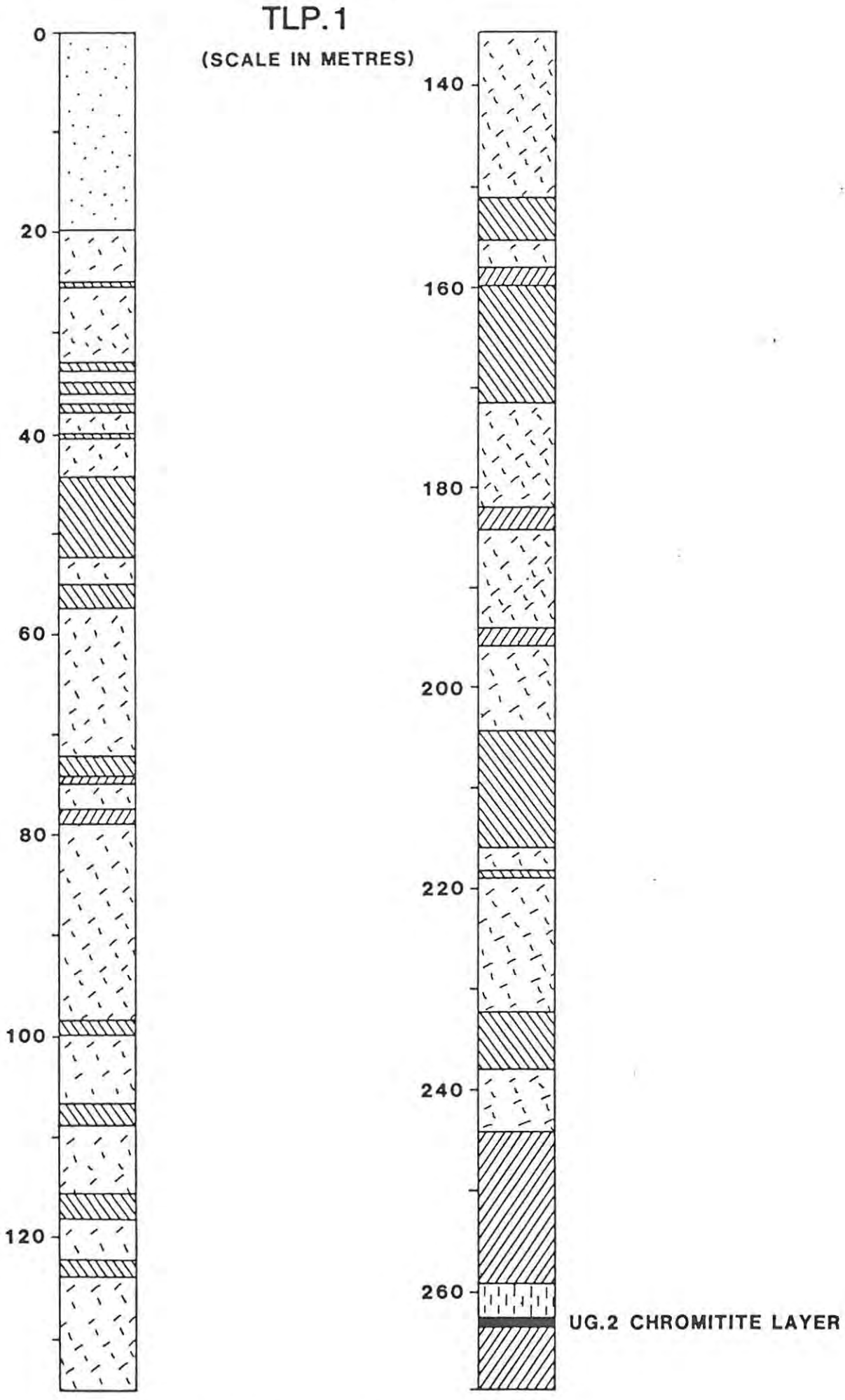

Figure 1B. TLP.1 borehole log.

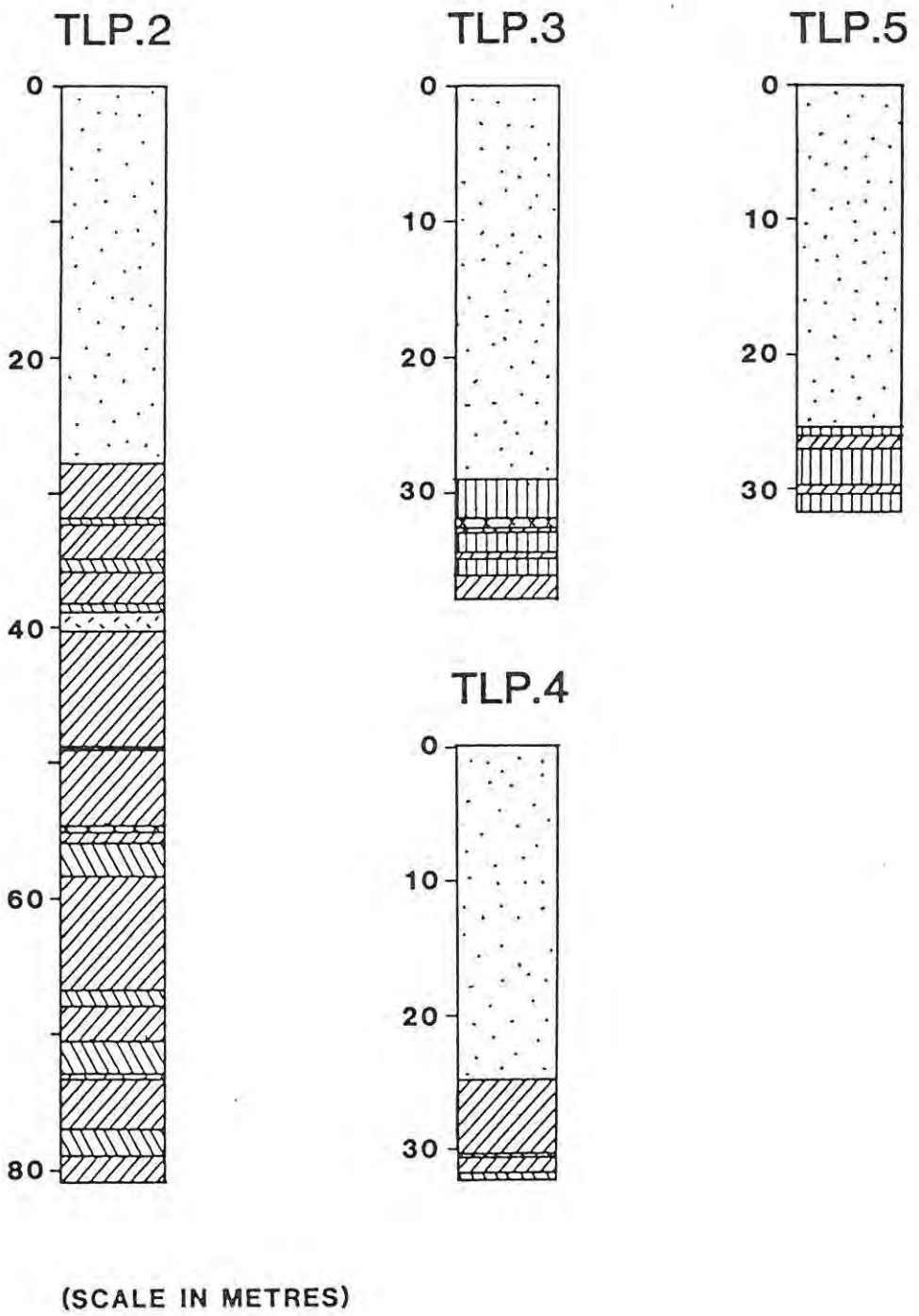

Figure 1C. Borehole Logs.

APPENDIX 2

ELECTRON MICROPROBE ANALYSIS

Polished thin sections were prepared, using graded diamond abrasives ranging between 15um and 0.25um in size, following standard procedures in use in the Geology Department at Rhodes University. Microprobe analyses were performed on the Rhodes University Cambridge Microscan V electron microprobe, operated at 20kV. A speciman current of 30nA was maintained by frequent reference to a Faraday Cage.

Data reduction was achieved using standard Geology Department computer programmes, which use the Bence-Albee correction factors (Bence & Albee, 1968). The programs also make corrections for dead-time. Operating conditions are tabulated in table 2A. Microprobe analyses of olivine, clinopyroxene, orthopyroxene, ilmenite, Ti-magnetite and chromite are listed in tables 2B-2G, respectively.

TABLE 2A. MICROPROBE ANALYTICAL CONDITIONS

Mineral	Element	Specimen Current	Accelerating potential	Counter	Standard	Crystal	Av Std. Counts
Olivine	Si(7)	30nA	20kV	flow	St.J.Is.01	R.A.P.	17 634
	Fe(7)	30nA	20kV	flow	St.J.Is.01	LiF(220)	6 885
	Mn(8)	30nA	20kV	flow	Rhodonite	LiF(220)	30 854
	Mg(7)	30nA	20kV	flow	St.J.Is.01	R.A.P.	15 683
	Ca(4)	30nA	20kV	flow	Px 5182	LiF(220)	12 615
	Ni(9)	30nA	20kV	flow	Ni-Mt	LiF(220)	1 035
Pyroxene	Si(3)	30nA	20kV	flow	Jadeite	R.A.P.	28 136
	Ti(3)	30nA	20kV	flow	ilmenite	LiF(220)	28 942
	Al(3)	30nA	20kV	flow	Jadeite	R.A.P.	15 283
	Fe(7)	30nA	20kV	flow	St.J.Is.01	LiF(220)	6 864
	Mn(8)	30nA	20kV	flow	Rhodonite	LiF(220)	30 643
	Mg(7)	30nA	20kV	flow	St.J.Is.01	R.A.P.	15 993
	Ca(5)	30nA	20kV	flow	Px Pxl	LiF(220)	14 840
	Na(3)	30nA	20kV	flow	Jadeite	R.A.P.	1 251
	Cr(10)	30nA	20kV	flow	Chromite	LiF(220)	35 103
	Ni(9)	30nA	20kV	flow	Ni-mt	LiF(220)	1 032
Ilvaite	Si(7)	30nA	20kV	flow	St.J.Is.01	R.A.P.	18 036
	Ti(3)	30nA	20kV	flow	ilmenite	LiF(220)	28 600
	Fe(4)	30nA	20kV	flow	Px 5182	LiF(220)	20 538
	Mn(8)	30nA	20kV	flow	Rhodonite	LiF(220)	30 169
	Mg(4)	30nA	20kV	flow	Px 5182	R.A.P.	3 670
	Ca(4)	30nA	20kV	flow	Px 5182	LiF(220)	12 297
Fe-Ti Oxides	Ti(3)	30nA	20kV	flow	ilmenite	LiF(220)	28 888
	Al(8)	30nA	20kV	flow	Spinel (UCT)	R.A.P.	38 865
	Fe(9)	30nA	20kV	flow	Ni-mt	LiF(220)	69 547
	Mn(8)	30nA	20kV	flow	Rhodonite	LiF(220)	30 625
	Mg(8)	30nA	20kV	flow	Spinel	R.A.P.	9 695
	Cr(10)	30nA	20kV	flow	Chromite	LiF(220)	35 076

TABLE 2B. ELECTRON MICROPROBE ANALYSES OF OLIVINE

	TLP.1								TLP.1 ('Marginal' Zone)					
	T1/58	T1/93	T1/157	T1/219	T1/231	T1/258	T1/277	T1/300	T1/1	T1/7	T1/19A	T1/19B	T1/27	T1/31
SiO_2	34.38	34.30	34.75	34.87	35.65	34.51	35.26	35.27	35.69	34.33	36.38	35.58	37.25	36.53
FeO	42.90	43.07	42.92	43.69	40.46	41.44	41.21	41.04	38.11	44.05	32.94	42.58	29.70	33.54
MnO	0.55	0.53	0.54	0.60	0.50	0.48	0.55	0.50	0.48	0.60	0.44	0.56	0.37	0.43
MgO	21.32	21.05	21.73	21.29	24.15	22.90	23.04	23.55	25.73	21.07	29.96	22.88	33.19	29.95
CaO	0.07	0.08	0.08	0.08	0.04	0.07	0.04	0.11	0.46	0.07	0.09	0.09	0.04	0.04
NiO	0.13	0.10	0.11	0.12	0.10	0.14	0.14	0.09	0.14	0.08	0.16	0.06	0.19	0.11
TOTAL	99.35	99.12	100.12	100.65	100.89	99.54	100.24	100.56	100.61	100.20	99.97	101.74	100.74	100.59
Number of ions on the basis of 4 oxygens														
Si	1.003	1.004	1.004	1.006	1.007	0.997	1.008	1.004	1.001	0.998	1.000	1.006	0.998	0.999
Fe	1.047	1.055	1.037	1.054	0.955	1.002	0.985	0.977	0.894	1.071	0.757	1.007	0.665	0.767
Mn	0.014	0.013	0.013	0.015	0.012	0.012	0.013	0.012	0.011	0.015	0.010	0.013	0.008	0.010
Mg	0.927	0.919	0.936	0.915	1.016	0.986	0.981	0.999	1.076	0.913	1.227	0.964	1.325	1.221
Ca	0.002	0.003	0.002	0.002	0.001	0.002	0.001	0.003	0.014	0.002	0.003	0.003	0.001	0.001
Ni	0.003	0.002	0.003	0.003	0.002	0.003	0.003	0.002	0.003	0.002	0.004	0.001	0.004	0.002
	2.996	2.995	2.995	2.995	2.993	3.002	2.991	2.997	2.999	3.001	3.001	2.994	3.001	3.000
Fo	46.97	46.55	47.43	46.48	51.54	49.62	49.91	50.56	54.61	46.01	61.84	48.92	66.57	61.40
Fa	53.03	53.45	52.57	53.52	48.46	50.38	50.09	49.44	45.39	53.99	38.16	51.08	33.43	38.60

TABLE 2B (continued). ELECTRON MICROPROBE ANALYSES OF OLIVINE

	TLP.1 ('Marginal' Zone)				TLP.2							TLP.3	
	T1/32A	T1/32B	T1/37	T1/43	T2/1	T2/7	T2/10	T2/18	T2/32	T2/36	T2/41	T3/2	T3/3
SiO_2	37.05	36.94	35.62	35.66	32.76	33.16	33.17	33.64	32.96	32.95	33.05	34.74	35.91
FeO	33.14	33.14	36.31	38.00	52.59	51.64	52.66	48.83	52.53	52.56	52.59	44.67	38.44
MnO	0.41	0.43	0.49	0.45	0.74	0.74	0.77	0.65	0.74	0.75	0.76	0.55	0.47
MgO	30.66	30.38	27.90	26.16	13.95	14.05	13.33	17.18	13.93	13.73	13.86	20.44	26.07
CaO	0.04	0.05	0.03	0.04	0.04	0.09	0.10	0.08	0.15	0.12	0.06	0.07	0.07
NiO	0.12	0.11	0.16	0.10	0.03	0.08	0.01	0.04	0.01	0.02	0.03	0.14	0.14
TOTAL	101.42	101.04	100.51	100.41	100.51	99.75	100.03	100.42	100.31	100.13	100.35	100.61	101.10
Number of ions on the basis of 4 oxygens													
Si	1.001	1.003	0.991	1.000	1.000	1.011	1.013	1.001	1.003	1.005	1.006	1.007	1.002
Fe	0.749	0.752	0.845	0.892	1.343	1.316	1.345	1.216	1.337	1.341	1.338	1.083	0.897
Mn	0.009	0.010	0.012	0.011	0.019	0.019	0.020	0.016	0.019	0.019	0.020	0.014	0.011
Mg	1.235	1.229	1.157	1.094	0.635	0.638	0.607	0.762	0.632	0.624	0.628	0.883	1.084
Ca	0.001	0.001	0.001	0.001	0.001	0.003	0.003	0.003	0.005	0.004	0.002	0.002	0.002
Ni	0.003	0.002	0.004	0.002	0.001	0.002	0.000	0.001	0.000	0.000	0.001	0.003	0.003
	2.998	2.997	3.010	3.000	2.999	2.989	2.988	2.999	2.996	2.993	2.995	2.992	2.999
Fo	62.24	62.03	57.79	55.09	32.10	32.65	31.09	38.54	32.09	31.76	31.96	44.92	54.72
Fa	37.76	37.97	42.21	44.91	67.90	67.35	68.91	61.46	67.91	68.24	68.04	55.08	45.28

TABLE 2B (continued). ELECTRON MICROPROBE ANALYSES OF OLIVINE

	TLP.3	TLP.4				TLP.5				6 Level Haulage			
	T3/5	T4/1	T4/2	T4/3	T4/5	T5/1	T5/3	T5/4	T5/5	TU20	TU21	TU30	TU34
SiO_2	36.09	34.74	34.72	36.72	33.54	35.05	34.94	34.83	33.37	35.36	34.71	32.83	32.79
FeO	37.60	42.33	40.94	32.68	49.38	41.51	41.33	43.14	52.36	41.68	44.40	52.41	52.21
MnO	0.47	0.55	0.48	0.40	0.72	0.49	0.52	0.52	0.73	0.54	0.65	0.78	0.73
MgO	25.91	21.92	23.21	30.60	15.88	23.14	22.76	21.88	14.30	23.60	21.45	14.03	13.84
CaO	0.07	0.10	0.12	0.06	0.08	0.10	0.28	0.08	0.05	0.04	0.05	0.08	0.08
NiO	0.16	0.10	0.07	0.16	0.06	0.06	0.10	0.10	0.08	0.08	0.02	0.02	0.01
TOTAL	100.29	99.74	99.54	100.62	99.66	100.34	99.93	100.54	100.89	101.29	101.34	100.15	99.66
Number of ions on the basis of 4 oxygens													
Si	1.011	1.005	1.000	1.000	1.010	1.002	1.004	1.003	1.007	1.001	0.997	1.001	1.004
Fe	0.881	1.025	0.986	0.744	1.244	0.993	0.993	1.039	1.321	0.987	1.067	1.337	1.338
Mn	0.011	0.013	0.012	0.009	0.018	0.012	0.013	0.013	0.019	0.013	0.016	0.020	0.019
Mg	1.081	0.946	0.996	1.242	0.713	0.986	0.975	0.939	0.643	0.996	0.919	0.638	0.632
Ca	0.002	0.003	0.004	0.002	0.003	0.003	0.009	0.002	0.002	0.001	0.002	0.003	0.003
Ni	0.004	0.002	0.002	0.004	0.002	0.001	0.002	0.002	0.002	0.002	0.002	0.000	0.000
	2.990	2.994	3.000	3.001	2.990	2.997	2.996	2.998	2.994	3.000	3.003	2.999	2.996
Fo	55.12	47.99	50.26	62.53	36.43	49.83	49.53	47.47	32.74	50.22	46.26	32.30	32.08
Fa	44.88	52.01	49.74	37.47	63.57	50.17	50.47	52.53	67.26	49.78	53.74	67.70	67.92

TABLE 2B (continued). ELECTRON MICROPROBE ANALYSES OF OLIVINE

	6 Level Haulage												
	TU36	TU38	TU41	TU44	TU46A	TU46B*	TU60/A	TU60/B	TU60/C	TU60/D	TU60L/A	TU60L/B	TU72
SiO_2	33.06	33.06	33.06	33.04	32.93	38.82	33.05	33.23	34.08	34.68	33.30	34.44	34.39
FeO	51.84	52.57	52.41	51.20	52.89	19.82	52.41	51.21	44.41	43.68	50.04	43.30	42.26
MnO	0.70	0.72	0.71	0.71	0.74	0.23	0.69	0.65	0.56	0.56	0.69	0.53	0.54
MgO	14.53	14.19	14.28	14.22	14.14	40.71	13.96	14.84	20.16	21.32	15.68	21.35	22.07
CaO	0.07	0.06	0.06	0.07	0.09	0.07	0.13	0.05	0.03	0.05	0.04	0.04	0.00
NiO	0.04	0.04	0.06	0.04	0.08	0.34	0.04	0.02	0.08	0.09	0.07	0.10	0.13
TOTAL	100.24	100.64	100.58	99.28	100.86	99.99	100.28	100.00	99.31	100.38	99.82	99.75	99.39
Number of ions on the basis of 4 oxygens													
Si	1.003	1.002	1.002	1.010	0.998	0.999	1.005	1.007	1.003	1.003	1.005	1.002	1.000
Fe	1.315	1.333	1.329	1.309	1.341	0.427	1.333	1.298	1.093	1.057	1.263	1.054	1.028
Mn	0.018	0.018	0.018	0.018	0.019	0.005	0.018	0.017	0.014	0.014	0.018	0.013	0.013
Mg	0.657	0.641	0.645	0.648	0.639	1.561	0.633	0.670	0.884	0.919	0.705	0.926	0.956
Ca	0.002	0.002	0.002	0.002	0.003	0.002	0.004	0.002	0.001	0.002	0.001	0.001	0.000
Ni	0.001	0.001	0.001	0.001	0.002	0.007	0.001	0.000	0.002	0.002	0.002	0.002	0.003
	2.996	2.997	2.997	2.988	3.002	3.001	2.994	2.994	2.997	2.997	2.994	2.998	3.000
Fo	33.31	32.48	32.68	33.11	32.27	78.54	32.19	34.05	44.72	46.52	35.83	46.77	48.20
Fa	66.69	67.52	67.32	66.89	67.73	21.46	67.81	65.95	55.28	53.48	64.17	53.23	51.80

* Cumulus olivine

TABLE 2C. ELECTRON MICROPROBE ANALYSES OF CLINOPYROXENE

	TLP.1									TLP.1 ('Marginal' Zone)				
	T1/88	T1/93	T1/143	T1/157	T1/219	T1/231	T1/258	T1/277	T1/296	T1/1	T1/16*	T1/19A*	T1/19B	T1/19C
SiO_2	52.24	52.11	52.43	51.96	51.99	52.40	52.68	51.63	51.71	51.43	52.61	52.42	53.03	51.27
TiO_2	0.49	0.54	0.52	0.53	0.61	0.44	0.35	0.48	0.57	0.38	0.44	0.27	0.49	0.55
Al_2O_3	1.26	1.54	1.80	1.29	1.30	1.47	1.37	1.31	1.13	1.61	1.96	2.11	2.08	1.61
FeO	11.31	11.39	11.31	11.18	12.35	10.09	9.56	11.28	11.17	9.67	6.02	6.63	8.09	12.52
MnO	0.26	0.24	0.23	0.24	0.27	0.25	0.22	0.24	0.22	0.26	0.19	0.21	0.18	0.26
MgO	12.77	12.86	13.49	12.69	11.54	13.84	13.95	12.65	12.66	13.39	15.68	16.15	15.02	11.93
CaO	22.16	21.05	21.98	21.19	22.40	22.14	21.56	21.65	21.70	22.35	22.44	21.12	21.75	21.36
Na_2O	0.12	0.14	0.14	0.23	0.16	0.28	0.03	0.20	0.11	0.05	0.23	0.12	0.30	0.12
Cr_2O_3	0.08	0.09	0.04	0.12	0.05	0.10	0.18	0.08	0.05	0.32	0.75	0.82	0.60	0.21
NiO	0.03	0.03	0.02	0.00	0.00	0.03	0.01	0.01	0.02	0.04	0.02	0.03	0.02	0.04
TOTAL	100.72	99.90	101.95	99.43	100.66	101.04	99.91	99.53	99.34	99.50	100.34	99.88	101.56	99.87
Number of ions on the basis of 6 oxygens (Z = 2)														
Si	1.957	1.963	1.938	1.967	1.960	1.947	1.968	1.957	1.962	1.940	1.936	1.935	1.939	1.947
Al	0.043	0.037	0.062	0.033	0.040	0.053	0.032	0.043	0.038	0.060	0.064	0.065	0.061	0.053
Ti	0.014	0.015	0.014	0.015	0.017	0.012	0.010	0.014	0.016	0.011	0.012	0.007	0.013	0.016
Al	0.013	0.027	0.016	0.025	0.018	0.011	0.028	0.016	0.013	0.012	0.021	0.003	0.029	0.019
Fe	0.354	0.359	0.350	0.354	0.389	0.314	0.299	0.358	0.355	0.305	0.185	0.205	0.247	0.398
Mn	0.008	0.008	0.007	0.008	0.009	0.008	0.007	0.008	0.007	0.008	0.006	0.007	0.006	0.008
Mg	0.713	0.722	0.743	0.716	0.648	0.766	0.777	0.715	0.716	0.753	0.860	0.889	0.818	0.675
Ca	0.890	0.849	0.870	0.859	0.905	0.881	0.863	0.879	0.882	0.904	0.885	0.836	0.852	0.869
Na	0.009	0.010	0.010	0.017	0.012	0.020	0.002	0.015	0.008	0.004	0.016	0.009	0.021	0.009
Cr	0.002	0.003	0.001	0.004	0.001	0.003	0.005	0.002	0.002	0.010	0.022	0.024	0.017	0.006
Ni	0.001	0.001	0.001	0.000	0.000	0.001	0.000	0.000	0.001	0.001	0.001	0.001	0.001	0.001
X + Y	2.004	1.994	2.012	1.998	1.999	2.016	1.991	2.007	2.000	2.008	2.007	2.004	2.005	2.002
En	36.43	37.40	37.85	37.11	33.38	39.07	40.07	36.62	36.66	38.38	44.56	46.07	42.67	34.77
Fs	18.11	18.59	17.81	18.35	20.04	15.99	15.41	18.32	18.15	15.56	9.60	10.61	12.90	20.48
Wo	45.46	44.01	44.34	44.55	46.58	44.94	44.52	45.06	45.18	46.06	45.85	43.32	44.43	44.76

* Cumulus Clinopyroxene

TABLE 2C (continued). ELECTRON MICROPROBE ANALYSES OF CLINOPYROXENE

	TLP.1 ('Marginal' Zone)								TLP.2				
	T1/27*	T1/29	T1/31	T1/32A	T1/32B	T1/32C	T1/32D	T1/43	T2/1	T2/18	T2/32	T2/36	T2/41
SiO_2	52.75	53.42	52.65	52.74	52.69	52.95	53.16	52.46	51.39	50.91	50.12	50.91	50.85
TiO_2	0.27	0.33	0.37	0.21	0.36	0.33	0.27	0.43	0.41	0.40	0.67	0.60	0.64
Al_2O_3	1.87	1.71	1.97	0.99	1.61	1.93	1.61	1.90	1.39	1.66	1.95	1.84	2.05
FeO	5.80	6.89	7.80	9.79	8.80	8.31	7.70	9.41	14.68	13.40	15.65	15.65	14.56
MnO	0.18	0.22	0.24	0.25	0.24	0.23	0.22	0.25	0.27	0.29	0.29	0.30	0.27
MgO	15.49	15.58	14.62	13.93	13.89	14.73	14.91	13.79	10.36	11.49	10.06	10.01	10.35
CaO	22.65	22.51	21.79	22.38	21.78	21.25	21.87	22.59	21.12	21.44	20.82	22.02	20.98
Na_2O	0.27	0.15	0.21	0.08	0.12	0.22	0.12	0.10	0.14	0.20	0.20	0.18	0.30
Cr_2O_3	0.74	0.62	0.65	0.20	0.38	0.55	0.61	0.49	0.03	0.09	0.04	0.04	0.04
NiO	0.02	0.01	0.01	0.02	0.02	0.02	0.02	0.01	0.00	0.02	0.00	0.03	0.02
TOTAL	100.03	101.43	100.30	100.58	99.89	100.52	100.48	101.42	99.79	99.90	99.80	101.58	100.06
Number of ions on the basis of 6 oxygens (Z = 2)													
Si	1.945	1.948	1.948	1.965	1.964	1.954	1.960	1.938	1.969	1.943	1.933	1.932	1.944
Al	0.055	0.052	0.052	0.035	0.036	0.046	0.040	0.062	0.031	0.057	0.067	0.068	0.056
Ti	0.007	0.009	0.010	0.006	0.010	0.009	0.007	0.012	0.012	0.011	0.019	0.017	0.018
Al	0.026	0.022	0.034	0.009	0.035	0.038	0.030	0.021	0.032	0.018	0.022	0.014	0.036
Fe	0.179	0.210	0.241	0.305	0.274	0.257	0.237	0.291	0.470	0.428	0.505	0.497	0.466
Mn	0.006	0.007	0.008	0.008	0.008	0.007	0.007	0.008	0.009	0.009	0.009	0.010	0.009
Mg	0.851	0.847	0.806	0.774	0.772	0.810	0.819	0.759	0.591	0.653	0.578	0.566	0.590
Ca	0.895	0.880	0.864	0.894	0.870	0.840	0.864	0.894	0.867	0.877	0.860	0.896	0.859
Na	0.019	0.011	0.015	0.006	0.009	0.016	0.009	0.007	0.004	0.015	0.015	0.013	0.022
Cr	0.022	0.018	0.019	0.006	0.011	0.016	0.018	0.014	0.001	0.003	0.001	0.001	0.001
Ni	0.001	0.000	0.000	0.001	0.001	0.001	0.001	0.000	0.000	0.001	0.000	0.001	0.001
X + Y	2.006	2.003	1.997	2.007	1.990	1.994	1.992	2.006	1.986	2.014	2.010	2.015	2.002
En	44.21	43.72	42.18	39.22	40.27	42.48	42.05	39.05	30.67	33.38	29.75	28.91	30.80
Fs	9.29	10.85	12.63	15.47	14.31	13.45	12.36	14.95	24.39	21.84	25.97	25.36	24.31
Wo	46.48	45.42	45.20	45.31	45.40	44.06	44.98	45.99	44.95	44.78	44.27	45.72	44.89

* Cumulus Clinopyroxene

TABLE 2C (continued). ELECTRON MICROPROBE ANALYSES OF CLINOPYROXENE

	TLP.3			TLP.4			TLP.5			6 Level Haulage			
	T3/2	T3/3	T3/5	T4/1	T4/2	T4/3	T5/1	T5/3	T5/4	TU20	TU21	TU30	TU34
SiO_2	51.89	51.45	51.16	51.28	51.48	53.33	52.43	51.50	52.80	52.07	51.85	50.68	50.92
TiO_2	0.57	0.58	0.43	0.39	0.53	0.31	0.41	0.58	0.65	0.50	0.33	0.58	0.63
Al_2O_3	1.61	1.96	1.53	1.55	1.29	1.77	1.35	1.54	1.46	1.84	1.63	1.92	1.75
FeO	12.45	9.74	9.81	10.51	11.42	8.66	10.68	11.43	12.02	11.60	11.41	14.88	14.92
MnO	0.25	0.24	0.24	0.24	0.21	0.23	0.25	0.29	0.25	0.29	0.28	0.30	0.28
MgO	12.19	13.89	13.53	12.90	12.96	14.93	13.65	13.02	12.97	13.40	13.34	10.17	10.45
CaO	21.53	20.87	21.95	21.11	20.97	21.74	20.91	21.79	20.93	20.43	20.92	22.58	20.86
Na_2O	0.11	0.12	0.12	0.15	0.16	0.06	0.16	0.15	0.19	0.20	0.18	0.17	0.16
Cr_2O_3	0.08	0.12	0.11	0.12	0.06	0.12	0.14	0.11	0.13	0.07	0.16	0.09	0.08
NiO	0.04	0.03	0.04	0.02	0.03	0.02	0.04	0.02	0.04	0.03	0.00	0.04	0.02
TOTAL	100.72	99.00	98.92	98.27	99.11	101.16	100.02	100.43	101.44	100.43	100.10	101.41	100.06
Number of ions on the basis of 6 oxygens (Z = 2)													
Si	1.951	1.942	1.942	1.959	1.957	1.958	1.965	1.938	1.961	1.950	1.950	1.925	1.949
Al	0.049	0.058	0.058	0.041	0.043	0.042	0.035	0.062	.0.039	0.050	0.050	0.075	0.051
Ti	0.016	0.016	0.012	0.011	0.015	0.009	0.012	0.016	0.018	0.014	0.009	0.017	0.018
Al	0.022	0.029	0.010	0.029	0.015	0.035	0.025	0.006	0.025	0.031	0.022	0.011	0.028
Fe	0.391	0.308	0.311	0.336	0.363	0.266	0.335	0.360	0.373	0.363	0.359	0.473	0.478
Mn	0.008	0.008	0.008	0.008	0.007	0.007	0.008	0.009	0.008	0.009	0.009	0.010	0.009
Mg	0.683	0.781	0.766	0.735	0.734	0.817	0.762	0.730	0.718	0.748	0.748	0.576	0.560
Ca	0.867	0.844	0.893	0.864	0.854	0.855	0.840	0.879	0.833	0.820	0.843	0.919	0.855
Na	0.008	0.009	0.009	0.011	0.012	0.004	0.012	0.011	0.014	0.015	0.013	0.013	0.012
Cr	0.002	0.004	0.003	0.004	0.002	0.003	0.004	0.003	0.004	0.002	0.005	0.003	0.002
Ni	0.001	0.001	0.001	0.001	0.001	0.001	0.001	0.001	0.001	0.001	0.000	0.001	0.001
X + Y	2.000	2.000	2.014	1.998	2.004	1.997	1.998	2.015	1.994	2.002	2.008	2.021	1.999
En	35.17	40.42	38.86	37.97	37.62	42.15	39.36	37.09	37.31	38.73	38.35	29.26	30.90
Fs	20.16	15.91	15.81	17.36	18.60	13.72	17.28	18.27	19.40	18.81	18.41	24.03	24.76
Wo	44.67	43.67	45.33	44.67	43.77	44.13	43.35	44.63	43.29	42.45	43.24	46.71	44.35

TABLE 2C (continued). ELECTRON MICROPROBE ANALYSES OF CLINOPYROXENE

	6 Level Haulage												
	TU36	TU38	TU41	TU44	TU46A	TU60/A	TU60/B	TU60/C	TU60/D	TU60L/A	TU60L/B	TU72/A	TU72/B
SiO_2	50.52	51.16	50.66	51.21	50.52	51.35	50.70	51.24	51.99	51.50	51.61	50.42	51.76
TiO_2	0.62	0.61	0.57	0.02	0.64	0.53	0.62	0.62	0.35	0.44	0.35	0.61	0.56
Al_2O_3	1.88	1.86	1.84	1.69	2.00	1.67	1.99	1.87	1.57	1.48	1.55	2.06	1.93
FeO	14.79	14.82	15.29	13.86	15.35	15.26	14.94	13.51	11.28	14.22	11.10	12.00	10.82
MnO	0.26	0.27	0.29	0.31	0.29	0.27	0.31	0.25	0.26	0.28	0.26	0.23	0.27
MgO	9.90	10.55	10.53	10.50	10.41	10.49	10.64	11.53	12.95	11.47	13.02	12.82	13.45
CaO	22.11	21.00	21.75	22.59	21.79	20.98	20.62	20.63	21.05	20.41	20.85	20.32	21.08
Na_2O	0.04	0.12	0.10	0.19	0.06	0.18	0.13	0.15	0.21	0.21	0.19	0.22	0.26
Cr_2O_3	0.07	0.10	0.09	0.10	0.12	0.07	0.09	0.08	0.41	0.08	0.34	0.20	0.25
NiO	0.01	0.03	0.03	0.03	0.02	0.02	0.00	0.03	0.01	0.02	0.04	0.03	0.01
TOTAL	100.20	100.52	101.15	100.50	101.20	100.81	100.04	99.91	100.08	100.11	99.31	99.01	100.39
Number of ions on the basis of 6 oxygens (Z = 2)													
Si	1.937	1.947	1.928	1.951	1.922	1.952	1.940	1.949	1.956	1.960	1.955	1.927	1.923
Al	0.063	0.053	0.072	0.049	0.078	0.048	0.060	0.051	0.044	0.040	0.045	0.073	0.077
Ti	0.018	0.017	0.016	0.001	0.018	0.015	0.018	0.018	0.010	0.018	0.010	0.018	0.016
Al	0.022	0.030	0.011	0.027	0.012	0.027	0.030	0.033	0.026	0.026	0.024	0.020	0.008
Fe	0.474	0.472	0.487	0.442	0.488	0.485	0.478	0.430	0.355	0.453	0.352	0.384	0.336
Mn	0.008	0.009	0.009	0.010	0.009	0.009	0.010	0.008	0.008	0.009	0.008	0.007	0.008
Mg	0.566	0.598	0.597	0.597	0.590	0.594	0.607	0.653	0.726	0.650	0.735	0.730	0.745
Ca	0.909	0.856	0.887	0.922	0.888	0.855	0.845	0.841	0.849	0.832	0.846	0.832	0.839
Na	0.003	0.009	0.007	0.014	0.004	0.013	0.010	0.011	0.015	0.015	0.014	0.016	0.019
Cr	0.002	0.003	0.003	0.003	0.004	0.002	0.003	0.002	0.012	0.002	0.010	0.006	0.007
Ni	0.000	0.001	0.001	0.001	0.001	0.001	0.000	0.001	0.000	0.001	0.001	0.001	0.001
X + Y	2.003	1.996	2.017	2.016	2.015	2.001	2.001	1.996	2.001	2.001	2.002	2.014	1.979
En	29.04	31.06	30.30	30.42	30.01	30.73	31.43	33.97	37.63	33.61	38.03	37.53	38.79
Fs	24.34	24.49	24.69	22.53	24.83	25.09	24.77	22.34	18.39	23.38	18.19	19.71	17.51
Wo	46.62	44.45	45.00	47.02	45.16	44.19	43.80	43.70	43.98	43.00	43.78	42.76	43.71

TABLE 2D. ELECTRON MICROPROBE ANALYSES OF ORTHOPYROXENE

TLP. 1 ('Marginal' Zone)

	T1/9	T1/12	T1/16	T1/19	T1/20	T1/27	T1/29A	T1/31	T1/32	T1/37
SiO_2	55.26	55.06	54.40	54.87	54.25	54.40	54.50	53.89	53.97	54.17
TiO_2	0.21	0.18	0.15	0.23	0.24	0.14	0.13	0.19	0.17	0.19
Al_2O_3	1.09	1.13	1.24	0.99	1.08	1.17	1.11	0.98	1.13	1.16
FeO	13.92	13.92	15.67	18.33	16.01	16.02	16.30	19.49	18.47	20.78
MnO	0.31	0.30	0.32	0.39	0.29	0.34	0.31	0.43	0.41	0.41
MgO	28.33	28.19	26.68	25.15	26.74	27.27	26.66	24.29	24.46	23.22
CaO	1.15	1.07	1.13	1.13	1.60	1.19	1.19	1.38	1.21	1.20
Cr_2O_3	0.33	0.38	0.40	0.28	0.30	0.37	0.45	0.26	0.32	0.33
NiO	0.07	0.08	0.05	0.05	0.07	0.08	0.08	0.07	0.06	0.06
TOTAL	100.67	100.31	100.04	101.42	100.58	100.97	100.73	100.98	100.19	101.52
Number of ions on the basis of 6 oxygens (Z = 2)										
Si	1.967	1.967	1.965	1.976	1.956	1.952	1.962	1.966	1.973	1.973
Al	0.033	0.033	0.035	0.024	0.044	0.048	0.038	0.034	0.027	0.027
Ti	0.006	0.005	0.004	0.006	0.007	0.004	0.004	0.005	0.005	0.005
Al	0.008	0.015	0.018	0.018	0.002	0.001	0.009	0.008	0.022	0.023
Fe	0.414	0.416	0.473	0.552	0.483	0.481	0.491	0.595	0.564	0.633
Mn	0.009	0.009	0.010	0.012	0.009	0.010	0.009	0.013	0.013	0.013
Mg	1.503	1.501	1.436	1.350	1.437	1.459	1.430	1.320	1.332	1.260
Ca	0.044	0.041	0.044	0.044	0.062	0.046	0.046	0.054	0.047	0.047
Cr	0.009	0.011	0.011	0.008	0.009	0.010	0.013	0.007	0.009	0.010
Ni	0.002	0.002	0.001	0.001	0.002	0.002	0.002	0.002	0.002	0.002
X + Y	2.000	1.999	1.999	1.991	2.010	2.014	2.004	2.004	1.994	1.992
En	76.63	76.66	73.53	69.38	72.51	73.47	72.71	67.06	68.52	64.96
Fs	21.13	21.24	24.23	28.38	24.36	24.22	24.94	30.20	29.03	32.62
Wo	2.24	2.09	2.24	2.24	3.11	2.30	2.33	2.74	2.43	2.41

TABLE 2D (continued). ELECTRON MICROPROBE ANALYSES OF ORTHOPYROXENE

	6 Level Haulage										
	TU22	TU46	TU51	TU60/A	TU60/B	TU60/C	TU60/D	TU60L/A	TU60L/B	TU72/A	TU72/B
SiO_2	55.05	54.61	54.62	52.50	53.13	54.49	53.51	51.32	54.03	52.58	54.88
TiO_2	0.20	0.11	0.14	0.19	0.22	0.14	0.23	0.17	0.15	0.16	0.13
Al_2O_3	1.54	1.53	1.67	1.06	1.19	1.29	1.15	1.09	1.43	1.37	1.34
FeO	12.50	11.96	12.16	24.10	20.53	17.02	16.81	21.95	12.61	23.14	13.64
MnO	0.28	0.26	0.27	0.47	0.36	0.30	0.28	0.43	0.27	0.45	0.27
MgO	29.51	29.25	28.75	20.59	23.17	26.20	25.88	21.87	29.19	21.13	28.35
CaO	1.03	1.43	1.40	1.31	1.15	1.00	0.86	1.20	0.93	1.15	0.83
Cr_2O_3	0.39	0.46	0.49	0.31	0.28	0.43	0.30	0.31	0.46	0.38	0.49
NiO	0.07	0.06	0.07	0.03	0.04	0.03	0.03	0.03	0.03	0.04	0.03
TOTAL	100.57	99.67	99.57	100.56	100.07	100.89	99.05	98.37	99.10	99.25	99.96
Number of ions on the basis of 6 oxygens (Z = 2)											
Si	1.950	1.950	1.953	1.966	1.964	1.962	1.963	1.951	1.945	1.962	1.963
Al	0.050	0.050	0.047	0.034	0.036	0.038	0.037	0.049	0.055	0.038	0.037
Ti	0.005	0.003	0.004	0.005	0.006	0.004	0.006	0.005	0.004	0.004	0.003
Al	0.014	0.014	0.023	0.013	0.016	0.017	0.013	0.000	0.006	0.022	0.020
Fe	0.370	0.357	0.364	0.755	0.635	0.513	0.516	0.698	0.380	0.722	0.408
Mn	0.008	0.008	0.008	0.015	0.011	0.009	0.009	0.014	0.008	0.014	0.008
Mg	1.558	1.557	1.532	1.149	1.277	1.406	1.415	1.239	1.566	1.175	1.512
Ca	0.039	0.055	0.054	0.053	0.046	0.039	0.034	0.049	0.036	0.046	0.032
Cr	0.011	0.013	0.014	0.009	0.008	0.012	0.009	0.009	0.013	0.011	0.014
Ni	0.002	0.002	0.002	0.001	0.001	0.001	0.001	0.001	0.001	0.001	0.001
X + Y	2.007	2.008	2.001	2.001	2.000	2.001	2.002	2.015	2.014	1.997	1.998
En	79.19	79.08	78.59	58.73	65.24	71.84	72.03	62.40	79.03	60.47	77.46
Fs	18.82	18.14	18.65	38.58	32.44	26.19	26.25	35.14	19.16	37.16	20.91
Wo	1.99	2.78	2.75	2.69	2.33	1.97	1.72	2.46	1.81	2.37	1.63

TABLE 2E. ELECTRON MICROPROBE ANALYSES OF ILMENITE

	TLP. 1 ('Marginal' Zone)			TLP.1		TLP.2				
	T1/19A	T1/19B	T1/48	T1/148	T1/235	T2/10A	T2/10B	T2/10C	T2/32A	T2/32B
TiO_2	52.73	45.07	50.88	50.60	51.09	49.88	50.59	49.00	50.99	50.64
Cr_2O_3	0.21	4.63	0.07	0.02	0.12	0.05	0.04	0.03	0.01	0.01
Al_2O_3	0.21	1.70	0.24	0.20	0.22	0.26	0.22	0.26	0.23	0.22
Fe_2O_3	2.49	11.49	3.63	3.68	3.45	3.97	3.65	5.55	4.43	4.04
FeO	42.48	35.93	42.76	42.61	43.36	42.73	43.32	41.82	44.20	43.99
MgO	2.49	2.18	1.38	1.02	1.07	0.71	0.76	0.67	0.41	0.35
MnO	0.49	0.71	0.53	1.06	0.67	0.85	0.81	1.04	0.91	0.91
TOTAL	101.10	101.70	99.48	99.19	99.98	98.45	99.39	98.37	101.18	100.17
FeO + Fe_2O_3	44.97	47.42	46.39	46.29	46.81	46.70	46.97	47.37	48.63	48.03
Number of ions on the basis of 3 oxygens.										
Ti	0.972	0.826	0.961	0.962	0.964	0.958	0.962	0.941	0.955	0.958
Cr	0.004	0.089	0.001	0.000	0.002	0.001	0.001	0.001	0.000	0.000
Al	0.006	0.049	0.007	0.006	0.006	0.008	0.007	0.008	0.007	0.007
Fe^{3+}	0.046	0.210	0.069	0.070	0.065	0.076	0.069	0.107	0.083	0.077
Fe^{2+}	0.871	0.732	0.899	0.901	0.909	0.912	0.916	0.894	0.921	0.926
Mg	0.091	0.079	0.052	0.038	0.040	0.027	0.028	0.026	0.015	0.013
Mn	0.010	0.015	0.011	0.023	0.014	0.018	0.017	0.023	0.019	0.019

TABLE 2E (continued). ELECTRON MICROPROBE ANALYSES OF ILMENITE

	TLP. 2	TLP.3	TLP.4	TLP.5	6 Level Haulage					
	T2/36A	T3/2	T4/5	T5/5	TU30/A	TU30/B	TU36/A	TU36/B	TU44/A	TU44/B
TiO_2	50.52	50.85	50.49	50.88	51.11	50.94	50.31	50.16	49.69	50.39
Cr_2O_3	0.08	0.18	0.03	0.05	0.14	0.18	0.18	0.12	0.11	0.13
Al_2O_3	0.23	0.20	0.20	0.22	0.23	0.26	0.27	0.21	0.28	0.27
Fe_2O_3	4.08	3.72	3.62	3.68	2.81	3.03	3.79	3.86	5.09	3.91
FeO	43.22	42.40	42.45	43.83	43.94	43.84	43.15	42.82	42.45	43.04
MgO	0.86	1.59	1.36	0.69	0.71	0.68	0.28	0.36	0.92	0.95
MnO	0.67	0.49	0.52	0.69	0.75	0.75	1.57	1.62	0.59	0.57
TOTAL	99.66	99.42	98.67	100.04	99.68	99.67	99.55	99.16	99.13	99.26
FeO + Fe_2O_3	47.30	46.12	46.07	47.51	46.75	46.87	46.94	46.68	47.54	46.95
Number of ions on the basis of 3 oxygens.										
Ti	0.957	0.960	0.962	0.961	0.968	0.965	0.958	0.959	0.946	0.957
Cr	0.002	0.004	0.001	0.001	0.003	0.004	0.004	0.002	0.002	0.003
Al	0.007	0.006	0.006	0.007	0.007	0.008	0.008	0.006	0.008	0.008
Fe^{3+}	0.077	0.070	0.069	0.070	0.053	0.057	0.072	0.074	0.097	0.074
Fe^{2+}	0.911	0.891	0.900	0.920	0.926	0.924	0.914	0.910	0.899	0.910
Mg	0.032	0.059	0.051	0.026	0.027	0.026	0.010	0.014	0.035	0.036
Mn	0.014	0.010	0.011	0.015	0.016	0.016	0.034	0.035	0.013	0.012

TABLE 2F. ELECTRON MICROPROBE ANALYSES OF Ti- MAGNETITE

	TLP.2			6 Level Haulage												
	T2/10A	T2/10B	T2/10C	T2/32A	T2/32B	T2/32C	TU30/A	TU30/B	TU30/C	TU30/D	TU36/A	TU36/B	TU44/A	TU44/B	TU44/C	TU44/D
TiO_2	10.14	5.09	2.51	3.07	4.41	5.51	12.16	11.36	11.87	10.82	11.67	15.85	8.38	8.73	13.61	9.25
Cr_2O_3	0.01	0.03	0.00	0.04	0.02	0.01	4.56	4.39	4.87	4.51	5.82	6.67	4.03	5.06	4.13	5.24
Al_2O_3	0.96	0.47	0.28	0.60	1.07	1.55	3.33	3.26	3.37	3.30	5.93	3.23	3.10	3.16	2.86	2.82
Fe_2O_3	48.55	59.18	64.45	62.75	60.13	57.64	37.13	37.63	36.84	39.61	32.93	27.52	44.69	43.34	34.30	42.87
FeO	40.05	35.55	33.31	33.80	35.19	36.16	42.11	40.65	41.57	40.85	40.97	45.08	38.40	38.90	42.80	39.49
MgO	0.28	0.24	0.20	0.15	0.23	0.32	0.30	0.34	0.33	0.24	0.53	0.28	0.27	0.31	0.37	0.29
MnO	0.21	0.15	0.04	0.13	0.15	0.21	0.42	0.47	0.44	0.45	0.81	0.73	0.38	0.36	0.41	0.38
TOTAL	100.19	100.71	100.80	100.54	101.19	101.40	100.01	98.10	99.29	99.78	98.66	99.36	99.25	99.86	98.49	100.34
FeO + Fe_2O_3	88.60	94.73	97.76	96.55	95.32	93.80	79.24	78.28	78.41	80.46	73.90	72.60	83.09	82.24	77.10	82.36
Number of ions on the basis of 4 oxygens.																
Ti	0.288	0.145	0.072	0.088	0.125	0.155	0.340	0.324	0.334	0.304	0.326	0.445	0.238	0.246	0.387	0.259
Cr	0.000	0.001	0.000	0.001	0.001	0.000	0.134	0.132	0.144	0.133	0.171	0.197	0.120	0.150	0.123	0.154
Al	0.043	0.021	0.013	0.027	0.047	0.068	0.147	0.146	0.149	0.145	0.259	0.142	0.138	0.139	0.127	0.127
Fe^{3+}	1.380	1.688	1.844	1.796	1.702	1.622	1.039	1.074	1.038	1.113	0.919	0.772	1.267	1.220	0.976	1.203
Fe^{2+}	1.266	1.126	1.059	1.075	1.107	1.130	1.310	1.290	1.303	1.278	1.271	1.405	1.210	1.217	1.353	1.231
Mg	0.016	0.014	0.011	0.009	0.013	0.018	0.017	0.019	0.018	0.013	0.029	0.016	0.015	0.017	0.021	0.016
Mn	0.007	0.005	0.001	0.004	0.005	0.007	0.013	0.015	0.014	0.014	0.025	0.023	0.012	0.011	0.013	0.012

TABLE 2G. ELECTRON MICROPROBE ANALYSES OF CHROMITE

	TLP.1 ('Marginal Zone')											
	T19/A	T19/B	T19/C	T19/D	T19/E	T19/F	T19/G	T19/H	T19/I	T19/J	T19/K	T19/L
TiO_2	12.31	12.94	11.58	12.92	11.62	9.01	7.26	6.76	6.30	5.94	5.79	5.59
Cr_2O_3	21.44	23.27	22.88	23.43	26.63	31.27	34.32	35.06	35.37	36.60	36.69	37.16
Al_2O_3	6.27	6.81	6.59	6.52	7.23	8.47	9.32	10.21	10.81	11.05	11.01	11.23
Fe_2O_3	17.48	13.54	17.54	14.71	13.29	11.76	10.92	10.22	9.91	9.71	10.20	9.65
FeO	39.53	41.03	40.07	41.27	39.98	37.49	35.71	35.46	34.80	34.62	34.42	34.27
MgO	2.52	2.02	2.04	2.09	2.28	2.36	2.52	2.52	2.67	2.78	2.87	2.84
MnO	0.52	0.52	0.46	0.52	0.51	0.53	0.55	0.55	0.55	0.55	0.56	0.53
TOTAL	100.08	100.13	101.16	101.47	101.55	100.89	100.60	100.78	100.41	101.26	101.55	101.28
$FeO + Fe_2O_3$	57.01	54.57	57.61	55.98	53.27	49.25	46.63	45.68	44.71	44.33	44.62	41.92
Number of ions on the basis of 32 oxygens												
Ti	2.645	2.777	2.467	2.741	2.450	1.898	1.526	1.412	1.315	1.228	1.194	1.154
Fe^{2+}	2.645	2.777	2.467	2.741	2.450	1.898	1.526	1.412	1.315	1.228	1.194	1.154
Cr	4.842	5.249	5.125	5.226	5.904	6.928	7.582	7.700	7.762	7.955	7.951	8.065
Al	2.111	2.290	2.200	2.168	2.389	2.795	3.069	3.341	3.537	3.580	3.556	3.632
Fe^{3+}	3.758	2.907	3.740	3.125	2.806	2.481	2.297	2.136	2.072	2.010	2.106	1.995
Fe^{2+}	6.801	7.015	7.028	6.997	6.926	6.887	6.819	6.826	6.765	6.732	6.696	6.715
Mg	1.073	0.859	0.862	0.879	0.953	0.987	1.051	1.044	1.106	1.139	1.173	1.162
Mn	0.126	0.126	0.110	0.124	0.121	0.126	0.131	0.130	0.129	0.128	0.130	0.123

TABLE 2G (continued). ELECTRON MICROPROBE ANALYSES OF CHROMITE

	TLP.1 ('Marginal Zone')											
	T27/A	T27/B	T29/A	T29/B	T32/A	T32/B	T32/C	T32/D	T33/1	T33/2	T33/3	T33/4
TiO_2	2.32	3.51	1.84	3.60	3.05	5.74	5.04	3.53	10.72	10.93	9.26	8.27
Cr_2O_3	42.80	38.01	45.24	40.83	41.05	35.09	35.82	38.75	26.16	26.94	30.73	33.31
Al_2O_3	16.62	16.59	14.99	15.36	14.70	12.83	13.87	15.41	8.04	8.29	9.15	9.85
Fe_2O_3	4.68	6.11	4.92	5.63	5.99	8.51	7.99	6.68	13.34	12.23	11.33	10.23
FeO	27.17	31.96	26.77	29.36	31.13	34.89	34.13	32.52	37.87	37.90	36.59	35.80
MgO	5.88	3.43	5.68	5.15	3.47	2.37	2.61	3.01	2.76	2.99	3.15	3.30
MnO	0.56	0.63	0.56	0.58	0.61	0.65	0.57	0.63	0.51	0.50	0.51	0.47
TOTAL	100.03	100.25	100.01	100.51	100.01	100.09	100.04	100.53	99.40	99.78	100.73	101.23
$FeO + Fe_2O_3$	31.85	38.07	31.69	34.99	37.12	43.40	42.12	39.20	51.21	50.13	47.92	46.03
Number of ions on the basis of 32 oxygens.												
Ti	0.462	0.710	0.370	0.722	0.623	1.193	1.041	0.718	2.290	2.319	1.936	1.713
Fe^{2+}	0.462	0.710	0.370	0.722	0.623	1.193	1.041	0.718	2.290	2.319	1.936	1.713
Cr	8.958	8.084	9.553	8.603	8.820	7.666	7.777	8.289	5.876	6.009	6.756	7.255
Al	5.185	5.259	4.718	4.824	4.708	4.178	4.489	4.913	2.692	2.756	2.998	3.198
Fe^{3+}	0.933	1.238	0.989	1.129	1.225	1.770	1.652	1.362	2.852	2.597	2.373	2.121
Fe^{2+}	5.554	6.480	5.612	5.823	6.455	6.872	6.799	6.642	6.708	6.623	6.575	6.535
Mg	2.320	1.375	2.261	2.046	1.406	0.976	1.068	1.214	1.169	1.258	1.306	1.355
Mn	0.126	0.144	0.127	0.131	0.140	0.152	0.133	0.144	0.123	0.119	0.120	0.110

TABLE 2G (continued). ELECTRON MICROPROBE ANALYSES OF CHROMITE

	TLP.1 ('Marginal Zone')											
	T33/5	T33/6	T33/7	T33/8	T33/9	T33/10	T33/11	T33/12	T33/13	T33/14	T33/15	T33/16
TiO_2	7.77	7.31	6.96	6.46	6.34	6.37	6.48	5.81	4.90	4.11	3.21	2.42
Cr_2O_3	34.00	34.75	35.36	35.65	35.83	36.32	36.07	37.19	38.73	39.79	40.53	41.37
Al_2O_3	10.33	10.38	10.71	10.93	11.13	11.14	11.12	11.63	12.31	13.20	13.96	15.15
Fe_2O_3	10.13	9.65	10.01	9.68	9.71	9.25	9.43	8.60	8.01	7.31	7.33	6.38
FeO	35.43	34.61	34.09	33.51	33.91	33.96	34.02	33.54	32.92	32.20	30.60	30.07
MgO	3.33	3.42	3.73	3.65	3.42	3.45	3.48	3.38	3.32	3.39	3.87	3.84
MnO	0.51	0.51	0.53	0.50	0.53	0.52	0.55	0.52	0.55	0.54	0.56	0.53
TOTAL	101.50	100.63	101.40	100.38	100.88	101.01	101.16	100.68	100.75	100.54	100.06	99.75
$FeO + Fe_2O_3$	45.56	44.26	44.10	43.19	43.62	32.21	43.45	42.14	40.93	39.51	37.93	36.45
Number of ions on the basis of 32 oxygens.												
Ti	1.602	1.517	1.430	1.339	1.309	1.313	1.333	1.199	1.007	0.843	0.656	0.494
Fe^{2+}	1.602	1.517	1.430	1.339	1.309	1.313	1.333	1.199	1.007	0.843	0.656	0.494
Cr	7.369	7.585	7.636	7.765	7.776	8.868	7.805	8.065	8.372	8.574	8.712	8.869
Al	3.337	3.376	3.447	3.549	3.600	3.597	3.586	3.760	3.965	4.240	4.475	4.843
Fe^{3+}	2.090	2.005	2.058	2.008	2.007	1.909	1.944	1.777	1.649	1.500	1.500	1.302
Fe^{2+}	6.521	6.474	6.358	6.384	6.477	6.470	6.453	6.497	6.520	6.498	6.303	6.324
Mg	1.361	1.407	1.519	1.499	1.399	1.409	1.419	1.382	1.353	1.377	1.568	1.552
Mn	0.118	0.119	0.123	0.117	0.123	0.121	0.127	0.121	0.127	0.125	0.129	0.122

TABLE 2G (continued). ELECTRON MICROPROBE ANALYSES OF CHROMITE

	TLP.1 ('Marginal Zone')											
	T33/17	T33/18	T33/19	T33/20	T33/21	T33/22	T33/23	T33/24	T33/25	T33/26	T33/27	T33/28
TiO_2	2.20	1.85	1.81	1.88	1.83	1.90	1.80	1.75	1.82	1.78	1.77	1.79
Cr_2O_3	41.68	42.57	41.86	43.10	43.54	43.06	43.30	43.47	43.17	43.28	44.37	43.40
Al_2O_3	16.16	16.79	17.70	17.30	17.25	17.62	17.70	17.67	17.95	17.99	18.02	18.23
Fe_2O_3	5.68	5.36	4.81	4.03	4.11	3.92	4.07	3.59	3.64	3.61	3.83	3.61
FeO	29.57	28.58	28.40	27.64	27.49	26.91	26.75	26.91	26.55	26.25	26.38	26.38
MgO	4.19	4.81	4.89	5.30	5.55	5.89	6.00	5.78	6.11	6.29	6.54	6.31
MnO	0.55	0.53	0.56	0.54	0.49	0.54	0.56	0.54	0.52	0.49	0.53	0.57
TOTAL	100.02	100.49	100.03	99.72	100.26	99.84	100.17	99.70	99.75	99.69	101.44	100.29
$FeO + Fe_2O_3$	35.25	33.94	33.21	31.67	31.60	30.83	30.82	30.50	30.19	29.68	30.21	29.99
Number of ions on the basis of 32 oxygens.												
Ti	0.444	0.369	0.361	0.362	0.363	0.377	0.356	0.348	0.360	0.352	0.344	0.352
Fe^{2+}	0.444	0.369	0.361	0.362	0.363	0.377	0.356	0.348	0.360	0.352	0.344	0.352
Cr	8.849	8.935	8.780	9.053	9.088	8.985	8.999	9.085	8.987	9.003	9.072	8.969
Al	5.115	5.254	5.536	5.418	5.368	5.482	5.484	5.506	5.572	5.579	5.494	5.617
Fe^{3+}	1.147	1.072	0.961	0.807	0.817	0.780	0.805	0.714	0.721	0.715	0.745	0.710
Fe^{2+}	6.198	5.979	5.941	5.780	5.707	5.562	5.525	5.602	5.486	5.424	5.363	5.416
Mg	1.678	1.903	1.934	2.096	2.184	2.317	2.350	2.277	2.398	2.466	2.522	2.458
Mn	0.125	0.119	0.126	0.122	0.110	0.120	0.125	0.120	0.116	0.109	0.116	0.126

APPENDIX 3

X-RAY FLUORESCENCE SPECTROMETRY

The samples selected for X-ray fluorescence analysis were initially reduced in size by means of a manual core-splitter and coarsely crushed in a motorised jawcrusher. Further crushing was achieved using a Herzog swingmill. The samples were then finely ground to less than ±300# in an automatic agate pestel and mortar.

Pressed powder briquettes were prepared from ±4g of powder, while fusion discs were made after the method of Norrish & Hutton (1969). H_2O^- was determined by heating separate samples, contained in silica crucibles, at 110°C for a minimum of 4 hours. Loss of ignition (L.O.I.) was determined by heating for a minimum of 6 hours at 950°C. Further heating of several samples at 1200°C for 6 hours yielded insignificant variation in the L.O.I. calculations for 950°C.

The X-ray fluorescene analyses were performed on the Phillips 1410 X-ray spectrometer of the Geology Department, Rhodes University. Major element analyses, with the exception of sodium, were carried out on duplicate fusion discs. Sodium and the trace elements were determined on pressed powder pellets. All iron was determined as Fe_2O_3 and the proportion of FeO was estimated from the Irvine & Barager (1971) equation.

The raw data were processed using standard Geology Department computer programs, which allow for position, dead-time and background corrections, instrumental drift and spectral line interferences. Mass absorption coefficients for trace element data corrections were derived from the major element data using Heinrich's (1966) values. Working curves were determined from the following International and In-house rock standards:

Major elements	:	AGV-1, GSP-1, NIM-N, BCR-1, JG-1, PCC-1, DTS -1.
Na	:	BCR-1, G-2, GSP-1, AGV-1, NIM-N, PCC-1.
Ba	:	BCR-1, CAR-08, KRF-12, S-12.
Rb, Sr, Nb, Zr, Y	:	BCR-1, BHVO-1, G-2, RGM-1, SDC-1.
Co, Cr, V	:	BCR-1, BHVO-1, PCC-1, QLO-1, SDC-1.
Zn, Cu, Ni	:	S-9, S-12, S-15.
Sc	:	AGV-1, BCR-1, GSP-1, NIM-N.

Analytical conditions for the major and trace elements are indicated in table 3A, while the lower limits of detection and average absolute errors are listed in table 3B. Normalised major and trace elements and H_2O^- plus L.O.I. inclusive major element analyses are tabulated in tables 3C and 3D, respectively.

Element	Emission Line	Tube	kV	mA	Crystal	Time (secs)	Counter	Collimator	Specimen
Si	K_α	Cr	55	40	PET	40	flow	coarse	fusion disc
Ti	K_α	Cr	55	40	LIF200	10	flow	fine	fusion disc
Al	K_α	Cr	55	40	PET	40	flow	coarse	fusion disc
Fe	K_α	Cr	55	40	LIF200	20	flow	fine	fusion disc
Mn	K_α	Cr	55	40	LIF200	20	flow	coarse	fusion disc
Mg	K_α	Cr	55	40	TlAP	100	flow	fine	fusion disc
Ca	K_α	Cr	55	40	LIF200	10	flow	fine	fusion disc
Na	K_α	Cr	55	40	TlAP	100	flow	fine	powder pellet
K	K_α	Cr	55	40	LIF200	10	flow	fine	fusion disc
P	K_α	Cr	55	40	Ge	20	flow	coarse	fusion disc
Ba	K_α	Cr	55	40	LIF220	200	flow	fine	powder pellet
Rb	K_α	W	55	40	LIF220	200	scint	fine	powder pellet
Sr	K_α	W	55	40	LIF220	200	scint	fine	powder pellet
Y	K_α	W	55	40	LIF220	200	scint	fine	powder pellet
Zr	K_α	W	55	40	LIF220	200	scint	fine	powder pellet
Nb	K_α	W	55	40	LIF220	200	scint	fine	powder pellet
Zn	K_α	Mo	55	40	LIF220	200	flow/scint	fine	powder pellet
Cu	K_α	Mo	55	40	LIF220	200	flow/scint	fine	powder pellet
Ni	K_α	Mo	55	40	LIF220	200	flow/scint	fine	powder pellet
Co	K_α	W	55	40	LIF220	200	flow	fine	powder pellet
Cr	K_α	W	55	40	LIF220	200	flow	fine	powder pellet
V	K_α	W	55	40	LIF220	200	flow	fine	powder pellet
Sc	K_α	Cr	55	40	LIF200	200	flow	fine	powder pellet

TABLE 3A. X-ray fluorescence spectrometry analytical conditions.

ELEMENT	LLD (ppm)	ABSOLUTE ERROR (ppm)
Nb	0.86	0.25
Zr	0.61	0.18
Y	0.71	0.21
Sr	0.68	0.22
Rb	0.77	0.22
Sc	1.23	0.37
Zn	2.14	1.43
Cu	2.17	1.64
Ni	3.09	2.63
Ba	14.25	4.89
Co	4.11	1.12
Cr	4.00	1.87
V	5.17	1.55

TABLE 3B. Lower limits of detection (LLD) and average absolute errors for trace element analyses.

TABLE C. MAJOR AND TRACE ELEMENT XRF ANALYSES

H_2O- + L.O.I. EXCLUSIVE ANALYSES, NORMALIZED TO 100%

	TLP.1									
SAMPLE NO.	T1/1	T1/8	T1/51	T1/65	T1/73	T1/84	T1/93	T1/103	T1/112	T1/124
SiO_2	42.06	36.86	46.60	34.78	34.74	34.72	34.56	35.27	34.83	34.89
TiO_2	0.26	0.33	0.48	0.78	1.04	0.50	0.64	0.16	0.34	0.06
Al_2O_3	0.79	0.45	1.35	0.15	0.16	0.16	0.15	0.14	0.09	0.03
Fe_2O_3	1.78	1.87	1.99	2.33	2.59	2.05	2.19	1.72	1.89	1.62
FeO	26.79	37.26	18.59	38.69	38.22	38.60	39.60	39.09	39.83	40.44
MnO	0.38	0.48	0.30	0.49	0.47	0.48	0.50	0.47	0.48	0.50
MgO	18.63	19.33	15.81	21.72	21.15	21.58	20.98	21.45	21.63	21.89
CaO	9.23	3.36	14.67	1.04	1.59	1.74	1.35	1.65	0.85	0.56
Na_2O	0.06	0.04	0.16	0.01	0.02	0.03	0.02	0.03	0.02	0.00
K_2O	0.00	0.01	0.02	0.00	0.01	0.00	0.00	0.00	0.00	0.00
P_2O_5	0.16	0.16	0.03	0.01	0.02	0.16	0.02	0.03	0.04	0.01
TOTAL	100.00	100.00	100.00	100.00	100.00	100.00	100.00	100.00	100.00	100.00
Ba	12	25	22	16	16	17	21	9	22	18
Rb	-	-	-	2.9	-	-	1.1	-	1.4	1.3
Sr	8	7	18	-	1	3	2	3	3	-
Y	11.3	7.8	12.5	4.6	4.5	3.4	4.4	4.9	5.0	4.9
Zr	6.3	3.3	10.0	2.3	3.5	2.3	2.5	2.8	2.0	2.9
Nb	-	-	-	-	-	-	-	-	-	-
Zn	203	283	145	295	305	303	315	306	320	286
Cu	71	89	408	650	2098	1977	2493	2789	1488	258
Ni	520	587	458	937	1342	1386	1418	1694	1307	886
Co	188	242	149	277	284	283	281	297	285	268
Cr	1167	220	918	62	66	57	58	57	37	31
V	716	350	1283	218	282	236	189	183	159	74
Sc	56	34	91	19	24	22	21	23	18	15

TABLE C (continued). MAJOR AND TRACE ELEMENT XRF ANALYSES

H_2O- + L.O.I. EXCLUSIVE ANALYSES, NORMALIZED TO 100%

	TLP.1										
SAMPLE NO.	T1/134	T1/144	T1/151	T1/161	T1/176	T1/199	T1/227	T1/237	T1/246	T1/257	T1/267
SiO_2	35.72	35.29	35.99	37.57	36.15	35.57	36.33	36.17	36.26	36.00	34.54
TiO_2	0.40	0.09	0.79	0.69	0.22	0.09	0.40	0.12	0.11	0.14	0.05
Al_2O_3	0.22	0.09	0.25	0.48	0.25	0.09	0.28	0.18	0.23	0.15	0.03
Fe_2O_3	1.95	1.64	2.35	2.23	1.77	1.62	1.93	1.64	1.64	1.68	1.59
FeO	38.09	39.54	37.24	33.88	37.29	38.51	36.17	35.88	36.67	37.99	40.70
MnO	0.46	0.49	0.46	0.43	0.45	0.48	0.46	0.45	0.45	0.47	0.47
MgO	20.86	21.80	20.06	19.85	21.21	22.47	21.22	23.44	22.43	21.48	22.23
CaO	2.20	1.04	2.82	4.71	2.59	1.17	3.07	2.09	2.17	2.06	0.37
Na_2O	0.03	0.01	0.03	0.07	0.04	0.00	0.04	0.02	0.03	0.02	0.01
K_2O	0.01	0.00	0.01	0.02	0.01	0.00	0.01	0.00	0.00	0.01	0.00
P_2O_5	0.07	0.01	0.02	0.08	0.03	0.01	0.11	0.01	0.01	0.01	0.01
TOTAL	100.00	100.00	100.00	100.00	100.00	100.00	100.00	100.00	100.00	100.00	100.00
Ba	16	10	19	18	18	15	10	20	19	5	11
Rb	2.4	-	2.3	-	-	1.5	-	-	1.0	-	1.3
Sr	4	-	2	8	2	-	4	-	9	1	3
Y	6.8	5.3	4.5	9.0	7.9	4.7	5.5	4.8	4.4	4.6	3.9
Zr	4.1	2.5	4.6	6.4	3.4	2.9	4.7	1.8	1.0	2.5	2.6
Nb	-	-	-	-	-	-	-	-	-	-	-
Zn	323	295	280	257	287	280	274	271	272	280	302
Cu	2144	290	1628	1444	1698	172	996	488	108	217	1066
Ni	1314	856	1286	1239	1294	829	950	985	852	851	1198
Co	275	268	282	268	289	273	263	267	263	267	289
Cr	81	45	92	137	83	58	100	73	85	65	28
V	269	140	340	565	315	120	294	252	249	213	68
Sc	27	19	31	43	28	19	32	23	24	24	14

TABLE C (continued). MAJOR AND TRACE ELEMENT XRF ANALYSES

H_2O- + L.O.I. EXCLUSIVE ANALYSES, NORMALIZED TO 100%

	TLP.1					TLP.2					
SAMPLE NO.	T1/274	T1/284	T1/292	T1/301	T1/307	T2/2	T2/8	T2/17	T2/23	T2/29	T2/37
SiO_2	36.50	36.60	35.15	34.80	35.48	32.46	37.50	37.84	36.18	34.71	36.72
TiO_2	0.10	0.12	0.05	0.10	0.07	2.92	1.71	0.50	0.54	0.91	2.93
Al_2O_3	0.16	0.19	0.03	0.02	0.09	0.31	0.55	0.59	0.40	1.09	1.49
Fe_2O_3	1.63	1.65	1.58	1.64	1.61	4.45	3.24	2.03	2.07	2.45	4.45
FeO	35.78	35.89	38.94	39.76	37.25	43.42	35.69	38.19	41.85	42.94	33.96
MnO	0.44	0.44	0.48	0.49	0.46	0.63	0.51	0.53	0.58	0.56	0.49
MgO	23.30	22.65	23.30	22.53	24.12	13.23	13.57	13.43	13.30	13.18	12.13
CaO	2.05	2.42	0.45	0.62	0.90	2.51	7.11	6.80	5.00	3.89	7.64
Na_2O	0.02	0.02	0.00	0.00	0.00	0.03	0.07	0.05	0.05	0.12	0.12
K_2O	0.00	0.00	0.00	0.00	0.00	0.00	0.01	0.01	0.01	0.02	0.02
P_2O_5	0.01	0.01	0.02	0.04	0.02	0.05	0.04	0.03	0.03	0.05	0.04
TOTAL	100.00	100.00	100.00	100.00	100.00	100.00	100.00	100.00	100.00	100.00	100.00
Ba	12	22	12	14	9	18	26	22	8	29	27
Rb	-	1.7	-	-	-	-	-	-	-	-	-
Sr	4	3	-	-	-	5	6	4	7	14	21
Y	5.5	4.5	6.3	4.7	5.5	9.2	7.7	7.9	7.6	6.9	8.7
Zr	2.2	2.8	2.9	1.7	1.3	10.0	8.9	6.2	5.0	4.3	12.3
Nb	-	-	-	-	-	1.9	-	-	-	-	-
Zn	264	264	291	305	276	328	273	268	290	294	244
Cu	154	230	141	686	208	209	248	397	423	463	339
Ni	888	860	896	1083	904	328	385	389	404	409	329
Co	264	262	284	296	276	237	220	242	248	247	216
Cr	70	83	31	26	52	72	139	115	76	66	122
V	258	289	87	82	135	200	337	213	170	157	323
Sc	23	27	14	18	19	40	75	72	58	51	90

TABLE C (continued). MAJOR AND TRACE ELEMENT XRF ANALYSES

H_2O^- + L.O.I. EXCLUSIVE ANALYSES, NORMALIZED TO 100%

	6 Level Haulage									
SAMPLE NO.	TU30	TU31	TU32	TU33	TU34	TU35	TU36	TU37	TU38	TU39
SiO_2	39.84	40.22	29.01	38.09	40.24	37.75	37.21	42.50	39.85	38.78
TiO_2	2.46	2.42	4.07	2.89	3.62	2.17	3.86	1.48	1.72	2.49
Al_2O_3	2.27	1.75	0.78	2.01	1.43'	0.95	1.73	1.23	1.15	1.11
Fe_2O_3	3.94	3.99	5.63	4.44	5.16	3.72	5.40	3.03	3.26	4.01
FeO	27.03	27.95	30.75	28.35	24.48	32.62	30.70	25.85	29.86	31.03
MnO	0.40	0.40	0.45	0.43	0.38	0.48	0.47	0.40	0.44	0.45
MgO	10.80	11.11	9.73	10.76	10.36	11.76	11.52	11.62	11.56	11.41
CaO	12.60	11.74	13.41	11.75	13.83	9.61	8.82	13.29	11.45	10.22
Na_2O	0.13	0.10	0.03	0.09	0.06	0.07	0.10	0.09	0.09	0.07
K_2O	0.01	0.01	0.01	0.01	0.00	0.01	0.02	0.01	0.01	0.01
P_2O_5	0.52	0.30	6.14	1.16	0.43	0.85	0.16	0.49	0.60	0.42
TOTAL	100.00	100.00	100.00	100.00	100.00	100.00	100.00	100.00	100.00	100.00
Ba	18	17	23	28	22	18	28	23	8	15
Rb	-	1.3	-	-	-	-	-	1.3	1.2	-
Sr	30	15	51	36	18	14	24	16	14	12
Y	16.6	13.9	51.2	18.7	15.5	16.8	10.9	13.4	14.0	12.1
Zr	10.0	10.0	11.8	11.4	14.5	10.5	12.2	10.0	10.1	11.5
Nb	-	0.5	-	-	-	-	1.6	-	-	-
Zn	211	212	245	228	198	250	239	198	223	239
Cu	274	174	138	144	129	162	168	105	111	103
Ni	393	318	301	293	260	372	342	105	297	283
Co	165	165	170	166	146	182	176	148	162	166
Cr	1250	1340	1087	1152	1298	1050	612	930	1095	1448
V	753	1744	672	727	884	721	553	798	727	738
Sc	93	99	52	83	112	75	76	99	88	81

TABLE C (continued). MAJOR AND TRACE ELEMENT XRF ANALYSES

H_2O^- + L.O.I. EXCLUSIVE ANALYSES, NORMALIZED TO 100%

	6 Level Haulage									
SAMPLE NO.	TU40	TU41	TU42	TU43	TU44	TU45	TU46A	TU46B*	TU47*	TU48*
SiO_2	37.90	40.15	36.91	39.71	30.53	41.00	41.02	50.94	49.85	50.58
TiO_2	1.76	2.10	3.40	2.27	3.54	1.45	2.13	0.10	0.09	0.10
Al_2O_3	0.88	1.16	1.01	1.01	0.24	1.13	1.68	17.58	20.01	18.15
Fe_2O_3	3.34	3.64	4.90	3.81	5.08	2.99	3.66	1.04	0.92	1.03
FeO	31.44	28.78	26.48	28.41	43.04	28.87	26.94	5.21	4.61	5.13
MnO	0.43	0.41	0.42	0.43	0.60	0.42	0.40	0.12	0.11	0.11
MgO	11.50	11.38	10.87	12.81	13.11	12.83	11.27	14.47	12.78	14.05
CaO	11.05	11.95	13.64	10.90	2.73	11.04	12.71	9.20	10.31	9.37
Na_2O	0.05	0.07	0.05	0.07	0.01	0.09	0.10	1.21	1.18	1.32
K_2O	0.01	0.00	0.00	0.00	0.00	0.00	0.00	0.12	0.13	0.13
P_2O_5	1.64	0.34	2.31	0.58	1.13	0.19	0.08	0.02	0.02	0.02
TOTAL	100.00	100.00	100.00	100.00	100.00	100.00	100.00	100.00	100.00	100.00
Ba	23	23	17	19	18	14	9	54	66	65
Rb	-	-	-	-	-	-	-	-	1.7	3.2
Sr	22	14	25	16	8	15	17	245	351	251
Y	20.2	14.2	25.9	15.2	15.6	14.7	6.6	2.9	2.2	3.9
Zr	7.8	11.3	10.0	10.1	6.7	9.5	5.2	6.9	5.6	6.6
Nb	-	-	7.6	-	-	-	-	-	-	-
Zn	238	216	206	216	327	214	206	57	52	57
Cu	116	287	223	277	205	234	261	32	29	31
Ni	309	427	368	567	468	531	413	427	425	437
Co	171	167	163	325	214	397	158	62	58	62
Cr	1057	1499	1315	2374	280	2908	1674	1664	1346	1574
V	554	603	681	678	173	828	625	60	47	57
Sc	77	96	86	84	27	85	103	16	13	14

* 'Spotted' Anorthosite

TABLE C (continued). MAJOR AND TRACE ELEMENT XRF ANALYSES

H_2O^- + L.O.I. EXCLUSIVE ANALYSES, NORMALIZED TO 100%

	6 Level Haulage									
SAMPLE NO.	TU51*	TU52*	TU53*	TU54*	TU55*	TU57*	TU59*	TU60B*	TU60A	TU61
SiO_2	50.72	51.69	51.31	51.21	51.25	51.12	50.43	50.66	40.33	41.88
TiO_2	0.09	0.11	0.10	0.10	0.10	0.09	0.08	0.09	2.51	4.39
Al_2O_3	20.71	17.51	19.27	19.68	19.63	20.25	22.45	21.01	3.65	2.39
Fe_2O_3	0.81	0.98	0.89	0.87	0.87	0.84	0.71	0.80	4.03	5.95
FeO	4.03	4.92	4.45	4.35	4.35	4.19	3.53	4.02	23.39	20.11
MnO	0.10	0.12	0.10	0.10	0.10	0.10	0.08	0.09	0.35	0.36
MgO	11.16	13.97	12.16	11.97	11.75	11.21	9.36	10.89	9.84	10.33
CaO	10.57	9.20	10.04	9.98	10.37	10.43	11.48	10.71	14.78	13.99
Na_2O	1.64	1.35	1.54	1.62	1.45	1.66	1.76	1.63	0.20	0.21
K_2O	0.16	0.13	0.12	0.12	0.11	0.11	0.11	0.08	0.01	0.04
P_2O_5	0.02	0.02	0.02	0.01	0.01	0.01	0.02	0.01	0.91	0.35
TOTAL	100.00	100.00	100.00	100.00	100.00	100.46	100.00	100.00	100.00	100.00
Ba	69	59	69	107	61	64	64	66	20	19
Rb	1.0	2.0	1.1	2.7	1.3	0.8	1.5	-	-	-
Sr	290	239	276	287	268	291	325	295	53	22
Y	2.8	4.6	3.4	3.2	4.1	2.5	3.6	3.8	17.4	14.0
Zr	5.2	7.1	5.4	5.5	4.6	3.9	2.4	3.0	11.7	22.7
Nb	-	-	-	-	-	-	-	-	-	2.5
Zn	46	53	49	48	46	45	40	44	183	194
Cu	24	23	23	27	20	23	27	36	124	127
Ni	280	339	307	309	273	287	231	263	218	228
Co	45	55	50	50	125	46	38	43	138	138
Cr	1385	1820	1474	1466	3917	1358	1059	1223	1189	1176
V	50	69	55	55	130	51	43	48	993	1109
Sc	14	17.3	15	15	15	14	12	13	99	113

* 'Spotted' Anorthosite

TABLE D. H_2O-+ L.O.I INCLUSIVE MAJOR ELEMENT ANALYSES

	TLP.1									
SAMPLE NO.	T1/1	T1/8	T1/51	T1/65	T1/73	T1/84	T1/93	T1/103	T1/112	T1/124
SiO_2	41.42	35.92	46.19	33.63	33.62	33.59	33.53	33.81	33.68	33.66
TiO_2	0.26	0.32	0.48	0.75	1.01	0.48	0.62	0.15	0.33	0.06
Al_2O_3	0.78	0.43	1.33	0.15	0.16	0.15	0.14	0.14	0.08	0.03
Fe_2O_3	1.76	1.82	1.98	2.25	2.51	1.98	2.12	1.65	1.83	1.56
FeO	26.38	36.31	18.42	37.41	37.00	37.34	38.41	37.47	38.53	39.02
MnO	0.38	0.47	0.30	0.47	0.46	0.47	0.48	0.45	0.47	0.48
MgO	18.35	18.84	15.67	21.00	20.47	20.88	20.36	20.56	20.92	21.12
CaO	9.09	3.28	14.54	1.00	1.54	1.68	1.31	1.58	0.82	0.54
Na_2O	0.06	0.04	0.16	0.01	0.02	0.03	0.02	0.03	0.02	0.00
K_2O	0.00	0.01	0.02	0.00	0.01	0.00	0.00	0.00	0.00	0.00
P_2O_5	0.02	0.02	0.03	0.01	0.02	0.15	0.02	0.03	0.04	0.01
LOI	0.67	0.86	0.74	0.99	0.84	0.98	0.94	1.41	1.03	1.06
H_2O-	0.08	0.09	0.06	0.13	0.08	0.08	0.07	0.08	0.08	0.10
TOTAL	99.22	98.40	99.91	97.79	97.72	97.81	98.02	97.34	97.83	97.65

TABLE D (continued). H_2O- + L.O.I INCLUSIVE MAJOR ELEMENT ANALYSES

	TLP.1										
SAMPLE NO.	T1/134	T1/144	T1/151	T1/161	T1/176	T1/199	T1/227	T1/237	T1/246	T1/257	T1/267
SiO_2	34.38	34.32	34.68	36.45	34.92	34.66	35.49	35.52	35.55	34.98	33.60
TiO_2	0.38	0.09	0.76	0.67	0.21	0.08	0.39	0.11	0.10	0.13	0.05
Al_2O_3	0.21	0.09	0.24	0.47	0.25	0.09	0.27	0.18	0.22	0.14	0.03
Fe_2O_3	1.88	1.59	2.26	2.17	1.71	1.58	1.89	1.61	1.60	1.63	1.55
FeO	36.67	38.45	35.88	32.87	36.02	37.53	35.33	35.23	35.95	36.91	39.59
MnO	0.44	0.48	0.44	0.41	0.44	0.46	0.45	0.44	0.44	0.46	0.46
MgO	20.08	21.21	19.33	19.26	20.49	21.90	20.73	23.01	21.99	20.87	21.62
CaO	2.12	1.01	2.72	4.57	2.50	1.14	3.00	2.05	2.12	2.00	0.36
Na_2O	0.03	0.01	0.03	0.07	0.04	0.00	0.04	0.02	0.03	0.02	0.01
K_2O	0.01	0.00	0.01	0.02	0.01	0.00	0.01	0.00	0.00	0.01	0.00
P_2O_5	0.07	0.01	0.01	0.08	0.03	0.01	0.10	0.01	0.01	0.01	0.01
LOI	1.42	0.85	1.45	1.27	1.05	1.04	0.94	0.44	0.50	1.09	0.49
H_2O-	0.14	0.11	0.10	0.05	0.04	0.09	0.07	0.04	0.05	0.12	0.05
TOTAL	97.83	98.21	97.91	98.34	97.68	98.56	98.70	98.66	98.58	98.37	97.82

TABLE D (continued). H_2O-+ L.O.I INCLUSIVE MAJOR ELEMENT ANALYSES

	TLP.1					TLP.2					
SAMPLE NO.	T1/274	T1/284	T1/292	T1/301	T1/307	T2/2	T2/8	T2/17	T2/23	T2/29	T2/37
SiO_2	35.80	35.87	34.44	33.85	34.61	31.77	36.74	37.15	35.39	33.76	36.14
TiO_2	0.10	0.12	0.05	0.09	0.07	2.86	1.67	0.50	0.52	0.88	2.88
Al_2O_3	0.15	0.18	0.03	0.02	0.08	0.30	0.54	0.58	0.39	1.06	1.47
Fe_2O_3	1.60	1.62	1.55	1.59	1.57	4.36	3.17	2.00	2.02	2.38	4.38
FeO	35.10	35.17	38.16	38.67	36.34	42.49	34.97	37.50	40.94	41.76	33.43
MnO	0.43	0.43	0.47	0.48	0.45	0.61	0.57	0.52	0.57	0.55	0.48
MgO	22.86	22.20	22.83	21.91	23.54	12.95	13.30	13.19	13.01	12.82	11.94
CaO	2.02	2.38	0.44	0.60	0.88	2.45	6.97	6.68	4.89	3.87	7.52
Na_2O	0.02	0.02	0.00	0.00	0.00	0.03	0.06	0.05	0.05	0.11	0.12
K_2O	0.00	0.00	0.00	0.00	0.00	0.00	0.01	0.01	0.01	0.02	0.02
P_2O_5	0.01	0.01	0.02	0.04	0.02	0.05	0.03	0.03	0.03	0.04	0.04
LOI	0.37	0.76	0.30	0.90	1.11	0.06	0.74	0.75	0.69	1.36	0.72
H_2O-	0.09	0.10	0.07	0.09	0.15	0.06	0.09	0.05	0.05	0.08	0.07
TOTAL	98.57	98.84	98.37	98.24	98.82	97.99	98.80	98.98	99.56	98.69	99.21

TABLE D (continued). H_2O-+ L.O.I INCLUSIVE MAJOR ELEMENT ANALYSES

6 Level Haulage

SAMPLE NO.	TU30	TU31	TU32	TU33	TU34	TU35	TU36	TU37	TU38	TU39
SiO_2	39.14	38.28	27.99	36.89	39.18	36.59	36.21	41.43	38.85	38.14
TiO_2	2.42	2.30	3.93	2.80	3.53	2.11	3.76	1.45	1.68	2.45
Al_2O_3	2.23	1.67	0.75	1.95	1.39	0.92	1.68	1.20	1.12	1.10
Fe_2O_3	3.87	3.80	5.43	4.30	5.03	3.61	5.26	2.95	3.18	3.95
FeO	26.56	26.60	29.67	27.46	23.84	31.62	29.88	25.20	29.11	30.51
MnO	0.39	0.38	0.43	0.42	0.37	0.47	0.46	0.39	0.43	0.44
MgO	10.61	10.57	9.39	10.42	10.08	11.40	11.21	11.33	11.27	11.22
CaO	12.38	11.18	12.93	11.38	13.47	9.32	8.58	12.96	1.16	10.06
Na_2O	0.13	0.10	0.03	0.09	0.06	0.07	0.10	0.09	0.09	0.07
K_2O	0.01	0.01	0.01	0.01	0.00	0.01	0.02	0.01	0.01	0.01
P_2O_5	0.51	0.28	5.92	1.12	0.42	0.82	0.16	0.48	0.59	0.41
LOI	0.87	2.85	0.75	1.40	0.84	0.96	0.75	0.72	0.65	0.74
H_2O-	0.07	0.26	0.13	0.14	0.05	0.06	0.06	0.05	0.07	0.07
TOTAL	99.19	98.29	97.36	98.38	98.26	97.93	98.12	98.25	98.19	99.16

TABLE D (continued). H_2O-+ L.O.I INCLUSIVE MAJOR ELEMENT ANALYSES

	6 Level Haulage									
SAMPLE NO.	TU40	TU41	TU42	TU43	TU44	TU45	TU46A	TU46B*	TU47*	TU48*
SiO_2	36.10	39.10	35.67	38.64	29.67	39.90	40.04	49.97	48.76	50.01
TiO_2	1.68	2.05	3.28	2.21	3.44	1.41	2.08	0.10	0.08	0.10
Al_2O_3	0.84	1.13	0.98	0.98	0.23	1.10	1.64	17.24	19.57	17.95
Fe_2O_3	3.18	3.55	4.74	3.71	4.94	2.91	3.58	1.02	0.90	1.02
FeO	29.96	28.03	25.59	27.65	41.84	28.10	26.30	5.11	4.51	5.07
MnO	0.41	0.40	0.41	0.42	0.58	0.41	0.39	0.11	0.11	0.11
MgO	10.96	11.09	10.51	12.47	12.74	12.49	11.00	14.19	12.50	13.89
CaO	10.53	11.64	13.18	10.60	2.65	10.74	12.41	9.02	10.09	9.27
Na_2O	0.05	0.07	0.05	0.07	0.01	0.08	0.09	1.19	1.15	1.31
K_2O	0.01	0.00	0.00	0.00	0.00	0.00	0.00	0.12	0.13	0.13
P_2O_5	1.56	0.33	2.23	0.56	1.10	0.19	0.08	0.02	0.20	0.15
LOI	3.08	1.25	0.75	1.25	0.50	0.78	0.87	1.33	2.13	1.33
H_2O-	0.26	0.06	0.07	0.08	0.06	0.06	0.06	0.11	0.18	0.09
TOTAL	98.61	98.69	97.44	98.62	97.76	98.17	98.54	99.53	100.13	100.29

* 'Spotted' Anorthosite

TABLE D (continued). H_2O-+ L.O.I INCLUSIVE MAJOR ELEMENT ANALYSES

	6 Level Haulage									
SAMPLE NO.	TU51*	TU52*	TU53*	TU54*	TU55*	TU57*	TU59*	TU60B*	TU60A	TU61
SiO_2	50.16	50.75	51.15	51.20	50.64	51.00	49.91	50.26	39.55	40.27
TiO_2	0.09	0.11	0.10	0.10	0.10	0.09	0.08	0.08	2.46	4.22
Al_2O_3	20.48	17.20	19.21	19.68	19.40	20.20	22.22	20.84	3.58	2.30
Fe_2O_3	0.80	0.97	0.89	0.87	0.86	0.84	0.70	0.80	3.96	5.72
FeO	3.99	4.83	4.44	4.35	4.30	4.18	3.50	3.99	22.94	19.34
MnO	0.10	0.11	0.10	0.10	0.10	0.10	0.08	0.09	0.34	0.35
MgO	11.04	13.72	12.12	11.97	11.61	11.19	9.26	10.81	9.65	9.94
CaO	10.45	9.03	10.01	9.98	10.24	10.41	11.37	10.63	14.49	13.45
Na_2O	1.63	1.33	1.54	1.62	1.44	1.66	1.74	1.62	0.19	0.20
K_2O	0.16	0.12	0.12	0.12	0.11	0.11	0.11	0.08	0.01	0.04
P_2O_5	0.02	0.02	0.02	0.01	0.01	0.01	0.02	0.01	0.89	0.33
LOI	0.92	1.24	0.62	0.88	1.45	0.60	0.68	0.58	0.93	2.95
H_2O-	0.09	0.07	0.07	0.14	0.12	0.09	0.07	0.07	0.07	0.15
TOTAL	99.90	99.49	100.37	101.01	100.38	100.46	99.73	99.85	99.07	99.25

* 'Spotted' Anorthosite

APPENDIX 4

X-RAY DIFFRACTION POWDER PHOTOGRAPHY TECHNIQUES

Small quantities of selected sample material were removed from polished sections by means of a steel needle and crushed to a fine powder between glass slides. Rubber solution was added and the sample rolled between two glass plates to form tiny balls. The sample was then attached to a short strand of hair, mounted in a brass holder. The holder was transferred to a 57.3mm diameter Philips camera and X-ray powder photographs were obtained using Fe filtered Co radiation. Calculation of d-spacings were based on the following wavelengths for Co radiation (Fang & Bloss, 1966):

K_{α_1} = 1.78892
K_{α_2} = 1.79278
K_{α} = 1.79021

APPENDIX 5

X-RAY POWDER DIFFRACTION TECHNIQUES

Troilite samples selected for X-ray powder diffraction were scratched out by a steel needle and finely ground in an agate pestel and mortar under acetone. Smear mounts were then prepared and the samples were scanned between 50° and 53° 2θ at 1/2°2θ/min., using an Fe filter and Co radiation. Instrumental conditions were selected to obtain maximum resolution of the diffraction peaks.

ACKNOWLEDGEMENTS

I would like to express my sincere appreciation to the following people and organizations for their invaluable assistance during the preparation of this thesis.

1. The Council for Scientific and Industrial Research (CSP program) for financial support.

2. My supervisor, Dr I.M. Reynolds, and other staff-members of the geology department, who provided advice and willing assistance throughout.

3. Ronnie Hieber, Dave Kennedy and other members of the geological staff of Rustenburg Platinum Mines for their time and effort during the field work for the study.

4. The technical staff at Rhodes University, particularly Rob Skae, for their friendly and able assistance.

5. My fellow students, R.N. Scoon, I.E. Williams-Jones and A.A. Mitchell for their enthusiasm and ready advice.

6. Dr E. Kinloch of J.C.I. Research Laboratory for providing the sulphide microprobe data presented.

7. Kathy, for proof-reading the final draft of the thesis.

8. Angela Stuurman for undertaking the unenviable task of typing the manuscript.

REFERENCES

ANDERSON, A.T. and GREENLAND, L.P. (1969). Phosphorus fractionation diagram as a quantitative indicator of crystallization differentiation of basaltic liquids. Geochim. cosmochim. Acta, 33, 493-505.

ARNOLD, R.G. (1956). The pyrrhotite - pyrite relationship. Carnegie Inst. Wash. Year Book, 55, 177-178.

ARNOLD, R.G. (1962). Equilibrium relations between pyrrhotite and pyrite from 325°C to 743°C. Econ. Geol., 57, 72-90.

ARNOLD, R.G. (1967). Range in composition and structure of 82 natural terrestrial pyrrhotites. Can. Miner., 9, 31-50.

ARNOLD, R.G. and REICHEN, L.E. (1962). Measurement of the metal content of naturally occurring, metal-deficient, hexagonal pyrrhotite by an X-ray spacing method. Am. Miner., 47, 105-111.

ARTH, J.G. (1976). Behaviour of trace elements during magmatic processes. A summary of theoretical models and their applications. J. Research U.S. Geol. Surv., 4, 41-47.

ATKINS, F.B. (1969). Pyroxenes of the Bushveld Intrusion, South Africa. J. Petrology, 10, 222-249.

BARNES, H.L. (Ed.) (1979). Geochemistry of hydrothermal ore deposits, 2nd Edn. Wiley-Interscience, 798pp.

BATEMAN, A.M. (1951). The formation of late magmatic oxide ores. Econ. Geol., 46, 404-426.

BENCE, A.E. and ALBEE, A.L. (1968). Empirical correction factors for the electron microanalysis of silicates and oxides. J. Geol., 76, 382-403.

BERAN, A. (1980). A reflected light investigation of ilvaite. Mineralog. Petrogr. Mitt., 27, 225-230.

BERMAN, H. (1937). Constitution and classification of the natural silicates. Am. Miner., 22, 342-408.

BOUGAULT, H. and HEKINIAN, R. (1974). Rift valley in the Atlantic ocean near 36°50'N: Petrology and geochemistry of basaltic rocks. Earth Planet. Sc. Lett., 24, 249-261.

BOWLES, J.F.W. (1977). A method of tracing the temperature and oxygen fugacity histories of complex magnetite-ilmenite grains. Mineralog. Mag., 41, 103-109.

BROWN, G.M. (1957). Pyroxenes from the early and middle stages of fractionation of the Skaergaard intrusion, East Greenland. Mineralog. Mag., 31, 511-543.

BUDDINGTON, A.F. and LINDSLEY, D.H. (1964). Iron-titanium oxide minerals and synthetic equivalents. J. Petrol., 5, 310-357.

BURNS, R.G. (1970). Mineralogical applications of crystal field theory. Cambridge. Cambridge Univ. Press, 224p.

BURNS, R.G. and FYFE, W.S. (1966). Distribution of elements in geological processes. Chem. Geol., 1, 49-56.

BURT, D.M. (1971). Multisystems analysis of the relative stabilities of babingtonite and ilvaite. Carnegie Inst. Wash. Year book, 70, 189-195.

CABRI, L.J. (1967). A new copper-iron sulfide. Econ. Geol., 62, 910-925.

CABRI, L.J. (1973). New data on phase relations in the Cu-Fe-S system. Econ. Geol., 68, 443-454.

CABRI, L.J. and HALL, S.R. (1972). Mooihoekite and haycockite, two new copper-iron sulphides, and their relationship to chalcopyrite and talnakhite. Am. Miner., 57, 689-708.

CABRI, L.J., ROSENZWEIG, A. and PINCH, W.W. (1977a). Platinum - group minerals from Onverwacht. I. Pt-Fe-Cu-Ni alloys. Can. Miner., 15, 380-384.

CABRI, L.J., LAFLAMME, G.J.H. and STEWART, J.M. (1977b). Platinum - group minerals from Onverwacht. II. Platarsite, a new sulfarsenide of platinum. Can. Miner., 15, 385-388.

CABRI, L.J., STEWART, J.M., LAFLAMME, J.H.G. and SZYMáNSKI, J.T. (1977c). Platinum - group minerals from Onverwacht. III. Genkinite, $(Pt, Pd)_4 Sb_3$, a new mineral. Can. Miner., 15, 389-392.

CAMERON, E.N. and DESBOROUGH, G.A. (1964). Origin of certain magnetite-bearing pegmatites in the eastern part of the Bushveld Complex, South Africa. Econ. Geol., 59, 197-225.

CAMERON, E.N. and GLOVER, E.D. (1973). Unusual titanian-chromian spinels from the Eastern Bushveld Complex. Am. Miner., 58, 172-188.

CAMPBELL, I.H. (1977). A study of macro-rhythmic layering and cumulative processes in the Jimberlana intrusion, Western Australia. Part I: The upper layered series. J. Petrol., 18, 183-215.

CAMPBELL, I.H. and BORLEY, G.D. (1974). The geochemistry of pyroxenes from the lower layered series of the Jimberlana intrusion, Western Australia. Contr. Miner. Petrol., 47, 281-297.

CHAMBERLAIN, J.A. and DELABIO, R.N. (1965). Mackinawite and valeriite in the Muskox intrusion. Am. Miner., 50, 682-695.

COERTZE, F.J. (1960). Anorthosite emplaced in a shear zone in gabbro of the Bushveld Igneous Complex. Trans. geol. Soc. S.Afr., 63, 75-81.

COERTZE, F.J. (1966). The genesis and geological environment of the Bushveld magnetite in the area southwest of the Leolo mountains. Geol. Surv. S.Afr., Bull., 47, 57pp.

COERTZE, F.J. (1970). The geology of the western part of the Bushveld Igneous Complex. Geol. Soc. S.Afr. Special Publ. 1, 5-20.

COERTZE, F.J. (1974). The geology of the basic portion of the Western Bushveld Igneous Complex. Geol. Surv. S.Afr., Mem., 66, 148pp.

COERTZE, F.J. and SCHUMANN, F.W. (1962). The basic portion and associated minerals of the Bushveld Igneous Complex north of Pilanesburg. Geol. Surv. S.Afr., Bull., 38, 48pp.

CRAIG, J.R. (1973). Pyrite-pentlandite assemblages and other low temperature relations in the Fe-Ni-S system. Am. J. Sci., 273-A, 496-510.

CRAIG, J.R. and KULLERUD, G. (1969). Phase relations in the Cu-Fe-Ni-S system and their application to magmatic ore deposits. Econ. Geol. Monogr., 4, 344-358.

CRAIG, J.R. and SCOTT, S.D. (1974). Sulphide phase equilibria. In: Ribbe, P.H., Ed., Sulfide Mineralogy. Min. Soc. Amer., CSI-110.

DE BRUYN, P.L. (1944). A new occurrence of nickeliferous ore in the Bushveld Complex. Ann. Univ. Stellenbosch, 22, 63-96.

DEER, W.A., HOWIE, R.A. and ZUSSMAN, J. (1962). Rock-forming Minerals : Non-silicates, 1st Edn. Longmans, 371pp.

DEER, W.A., HOWIE, R.A. and ZUSSMAN, J. (1978). Rock-forming Minerals : Single-chain silicates, 2nd Edn. Longman, 668pp.

DEER, W.A., HOWIE, R.A. and ZUSSMAN, J. (1982). Rock-forming Minerals : Orthosilicates, 2nd Edn. Longman, 915pp.

DE KLERK, W.J. (1982). The geology, geochemistry and silicate mineralogy of the upper critical zone of the north-western Bushveld Complex at Rustenburg Platinum Mines, Union Section. Unpubl. M.Sc. thesis, 210pp.

DESBOROUGH, G.A. and AMOS, D.H. (1961). Ilvaite : A late magmatic occurrence in gabbro of Missouri. Am. Miner., 46, 1509-1511.

DUKE, J.M. (1976). Distribution of the period 4 transition elements among olivine, calcic clinopyroxene and mafic silicate liquid : Experimental results. J. Petrol., 17, 499-521.

EALES, H.V. (1979). Anomalous Karroo spinels along the chromite- titano-magnetite join. S.Afr. J. Sci., 75, 24-29.

EALES, H.V. and BOOTH, P.W.K. (1974). The Birds river gabbro complex, Dordrecht district. Trans. geol. Soc. S.Afr., 77, 1-15.

EALES, H.V., REYNOLDS, I.M. and GOUWS, D.A. (1980). The spinel-group minerals of the central Karoo tholeiitic province. Trans. geol. Soc. S.Afr. 83, 243-253.

EGGLER, D.H. and BURNHAM, C.W. (1973). Crystallization and fractionation trends in the system andesite - H_2O - CO_2 - O_2 at pressures to 10Kb. Bull. geol. Soc. Am., 84, 2517-2532.

EVANS, H.T., MILTON, C., CHAO, E.C.T., ADLER, I., MEAD, C., INGRAM, B. and BERNER, R.A. (1964). Valeriite and the new iron sulphide, Mackinawite. Prof. Pap. U.S. geol. Surv., 475-D, D64-D69.

EWART, A., BRYAN, W.B. and GILL, J.B. (1973). Mineralogy and geochemistry of the younger volcanic islands of Tonga, S.W. Pacific. J. Petrology, 14, 429-465.

FANG, J.H. and BLOSS, F.D. (1966). X-ray diffraction tables. Southern Illinois University Press.

FERGUSON, J., and McCARTHY, T.S. (1970). Origin of an ultramafic pegmatoid in the eastern part of the Bushveld Complex. Geol. Soc. S.Afr., Special Publ. 1, 74-79.

FLEET, M.E., MACRAE, N.D. and HERZBERG, G.T. (1977). Partition of nickel between olivine and sulphide : A test for immiscible sulphide liquids. Contr. Miner. Petrol., 65, 191-197.

GAIN, S.B. (1980). The geology and PGE distribution in the upper chromitite layers at Maandagshoek 254KT, eastern Bushveld Complex. Univ. Pretoria, Inst. Geol. Res. on the Bushveld Complex, Research Dept., 22, 24pp.

GRAHAM, A.R. (1969). Quantitative determination of hexagonal and monoclinic pyrrhotites by X-ray diffraction. Can. Miner., 10, 4-24.

GREENLAND, L.P. (1970). An equation for trace element distribution during magmatic crystallization. Am. Miner., 55, 455-465.

GUNN, B.M. (1971). Trace element partition during olivine fractionation of hawaiian basalts. Chem. Geol., 8, 1-13.

HAGGERTY, S.E. (1976). Oxidation of opaque mineral oxides in basalts, Hgl-98. In: Rumble, D., Ed., Oxide Minerals. Min. Soc. Amer.

HARRIS, D.C. and NICKEL E.H. (1972). Pentlandite compositions and associations in some mineral deposits. Can. Miner., 11, 861-878.

HART, S.R. and DAVIS, K.E. (1978). Nickel partitioning between olivine and silicate melt. Earth Planet. Sci. Lett., 40, 203-219.

HECKROODT, R.O. (1959). The geology around the dunite pipe on Driekop, eastern Transvaal. Trans. geol. Soc. S.Afr., 62, 59-73.

HEINRICH, K.F.J. (1966). X-ray absorption uncertainty. In: McKinley, T.D., Heinrich, K.F.J. and Wittry, D.B., Eds. The Electron Microprobe. Wiley, New York, 1035pp.

HESS, H.H. (1949). Chemical composition and optical properties of common clinopyroxenes. Am. Miner., 34, 621-666.

HILL, R., and ROEDER, P. (1974). The crystallization of spinel from basaltic liquid as a function of oxygen fugacity. J. Geol., 82, 709-729.

IRVINE, T.N. (1982). The terminology of layered intrusions. J. Petrology, 23, 127-162.

IRVINE, T.N. and BARRAGER, W.R.A. (1971). A guide to the chemical classification of the common volcanic rocks. Can. J. Earth Sci., 8, 523-548.

IRVINE, T.N. and KUSHIRO, I. (1976). Partitioning of Ni and Mg between olivine and silicate melts. Carnegie Inst. Wash. Year book, 75, 668-675.

IRVING, A.J. (1978). A review of experimental studies of crystal/liquid trace element partitioning. Geochim. cosmochim. Acta, 42, 743-770.

JACKSON, E.D. (1961). Primary textures and mineral associations in the ultramafic zone of the Stillwater Complex. Prof. Pap. U.S. geol. Surv., 358.

JAHNS, R.H. (1955). The study of pegmatites. Econ. Geol., 50th Anniv. vol., 1025-1130.

JOHANNESBURG INVESTMENT COMPANY (1981). Confidential Research Lab. report.

JONES, J.P. (1974). Pegmatitic bodies in mafic rocks of the Bushveld Complex, Bafokeng Leasehold Area, Western Transvaal. Unpubl. M.Sc. Thesis, Univ. Witwatersrand.

KNOP, O., IBRAHIM, M.A. and SUTARNO, (1965). Chalcogenides of the transition elements. IV. Pentlandite, a natural phase. Can. Miner., 8, 291-316.

KOUVO, O., HUHMA, M. and VUORELAINEN, Y. (1959). A natural cobalt analogue of pentlandite. Am. Miner., 44, 897-900.

KOUVO, O., VUORELAINEN, Y. and LONG, J.V.P. (1963). A tetragonal iron sulphide. Am. Miner., 48, 511-524.

KULLERUD, G., YUND, R.A. and MOH, G. (1969). Phase relations in the Cu-Fe-S; Cu-Ni-S; and Fe-Ni-S systems. Econ. Geol. Monogr. 4, 323-343.

LEEMAN, W.P. and LINDSTROM, D.J. (1978). Partitioning of Ni^{2+} between basaltic and synthetic melts and olivines - an experimental study. Geochim. cosmochim, Acta, 42, 801-816.

LEONARD, B.F., HILDEBRAND, F.A. and VLISIDIS, A.C. (1962). Members of the ludwigite-vonsenite series and their distinction from ilvaite. In: Engel, A.E.J., James, H.L. and Leonard, B.F., Eds. Petrologic studies. Geol. Soc. Amer., Buddington Volume, 523-568.

LIEBENBERG, L. (1970). The sulphides in the layered sequence of the Bushveld Igneous Complex. Geol. Soc. S.Afr., Spec. Publ., 1, 108-207.

LINDSLEY, D.H. (1976). Experimental studies of oxide minerals. In: Rumble, D., Ed. Oxide Minerals. Min. Soc. Amer, L61-88.

LINDSTRÖM, D.J. and WEILL, D.F. (1978). Partitioning of transition metals between diopside and coexisting silicate liquids. I. Nickel, cobalt and manganese. Geochim. cosmochim. Acta, 42, 817-831.

LOFERSKI, P.J. and LIPIN, B.R. (1983). Exsolution in metamorphosed chromite from the Red Lodge district, Montana. Am. Miner., 68, 777-789.

LOMBAARD, B.V. (1956). Chromite and dunite of the Bushveld Complex. Trans. geol. Soc. S.Afr., 59, 59-76.

MISRA, K.C. and FLEET, M.E. (1973). Chemical compositions of synthetic and natural pentlandite assemblages. Econ. Geol., 68, 518-539.

MORIMOTO, N., GYOBU, A., TSUKUMA, K. and KOTO, K. (1975). Superstructure and nonstoichiometry of intermediate pyrrhotite. Am. Miner., 60, 240-248.

MOSSOM, R. (1977). Johannesburg Consolidated Investment Co. Ltd.. Project report. Driekop 253KT, Forest Hill 117KT and HACKNEY 116KT. (Confidential report).

MYSEN, B.O. (1978). Experimental determination of nickel partition coefficients between liquid, pargasite, and garnet peridotite minerals and concentration limits of behaviour according to Henry's law at high pressure and temperature. Am. J. Sci., 278, 217-243.

NALDRETT, A.J. (1969). A portion of the system Fe-S-O between 900 and 1080°C and its application to sulphide ore magmas. J. Petrology, 10, 171-201.

NASLUND, H.R., HUGHES, J.M. and BIRNIE, R.W. (1983). Ilvaite, an alteration product replacing olivine in the Skaergaard intrusion. Am. Miner., 68, 1004-1008.

NICKEL, E.H., ALLCHURCH, P.D., MASON, M.G. and WILMSHURST, J.R. (1977). Supergene alteration at the Perseverance nickel deposit, Agnew, Western Australia. Econ. Geol., 72, 184-203.

NORRISH, K. and HUTTON, J.T. (1969). An accurate X-ray spectrographic method for the analysis of a wide range of geologic samples. Geochim. cosmochim. Acta, 33, 431-453.

PASTER, T.P., SCHAUWECKER, D.S. and HASKIN, L.A. (1974). The behaviour of some trace elements during solidification of the Skaergaard layered series. Geochim. cosmochim. Acta, 38, 1549-1577.

PEARCE, J.A. and NORRY, M.J. (1979). Petrogenetic implications of Ti, Zr, Y and Nb variations in volcanic rocks. Contr. Miner. Petrol., 69, 33-47.

PETRUK, W., HARRIS, D.C. and STEWART, J.M. (1969). Langisite, a new mineral, and the rare minerals cobalt pentlandite, siegenite, parkerite and bravoite from the Langis Mine, Cobalt-Gowganda area, Ontario. Can. Miner., 9, 597-616.

PEYERL, W. (1982). The influence of the Driekop Dunite pipe on the platinum-group mineralogy of the UG-2 chromitite in its vicinity. Econ. Geol., 77, 1432-1438.

PHILPOTTS, J.A. and SCHNETZLER, C.C. (1970). Phenocryst-matrix partition coefficients for K, Rb, Sr and Ba, with applications to anorthosite and basalt genesis. Geochim. cosmochim. Acta, 34, 307-322.

PLIMER, I.R. and ASHLEY, P.M. (1978). Manganoan ilvaite from Broken Hill, N.S.W. and Ban Ban, Queensland, Australia. Mineralog. Mag., 42, 85-88.

POWER, L.F. and FINE, H.A. (1976). The Iron-Sulphur System. Part 1. The structures and physical properties of the compounds of the low-temperature phase fields. Minerals Sci. Engng., 8, 106-126.

PURVIS, A.C., NESBITT, R.W. and HALLBERG, J.A. (1972). The geology of part of the Carr Boyd Rocks Complex. Econ. Geol., 67. 1093-1113.

PUTNIS, A. (1979). Electron petrography of high-temperature oxidation in olivine from the Rhum layered Intrusion. Mineralog. Mag., 43, 293-296.

RAEDEKE, L.D. and McCALLUM, I.S. (1984). Investigations in the Stillwater Complex: Part II. Petrology and petrogenesis of the ultramafic series. J. Petrology, 25, 395-420.

RAJAMANI, V. and PREWITT, C.T. (1973). Crystal chemistry of natural pentlandites. Can. Miner., 12, 178-187.

RAMDOHR, P. (1980). The Ore Minerals and their Intergrowths. 4th ed. 2 vols. Pergamon Press, 1207pp.

REYNOLDS, I.M. (1978). A mineralogical investigation of co-existing iron-titanium oxides from various igneous rocks with special reference to some South African titaniferous iron ores. Unpubl. PhD. thesis, 632pp.

REYNOLDS, I.M. (in press). Contrasted mineralogy and textural relationships in the uppermost Ti-magnetite layers of the Bushveld Complex in the Bierkraal area north of Rustenburg. Econ. Geol.

REYNOLDS, I.M. and EALES, H.V. (in prep.). Unmixed spinels of the Tugela Rand intrusion, Natal mobile belt, South Africa.

REYNOLDS, I.M. and SCOON, R.N. (1983). The iron-titanium oxide mineralogy of some ultramafic pegmatites from the critical and main zones of the Bushveld Complex. Symposium on the Bushveld Complex. Pretoria. (abstr.), 78-79.

RINGWOOD, A.E. (1970). Petrogenesis of Apollo 11 basalts and implications for lunar origin. J. Geophys. Res., 75, 6453-6479.

RUCKLIDGE, J.C. (1972). Chlorine in partially serpentinized dunite. Econ. Geol., 67, 38-40.

RUCKLIDGE, J.C., and PATTERSON, G.C. (1977). The role of chlorine in serpentinization. Contr. Miner. Petrol., 65, 39-44.

SCHIFFRIES, C.M. (1982). The petrogenesis of a platiniferous dunite pipe in the Bushveld Complex : Infiltration metasomatism by a chloride solution. Econ. Geol., 77, 1439-1453.

SCHWEITZER, E.L., PAPIKE, J.J. and BENCE, A.E. (1979). Statistical analysis of clinopyroxenes from deep-sea basalts. Am. Miner., 64, 501-513.

SCHWELLNUS, C.M. (1935). The nickel-copper occurrences in the Bushveld Igneous Complex, west of the Pilansberg. Geol. Surv. S.Afr. Bull., 5, 36pp.

SCHWELLNUS, J.S.I. et al. (1962). The geology of the Olifants River area, Transvaal. Explan. Sheet geol. Surv. Dep. Min. S.Afr., Nos. 2429B and 2430A.

SCOON, R.N. (1983) New structural and geochemical evidence supporting an intrusive origin for the Driekop ultramafic pipe. Symposium on the Bushveld Complex.Pretoria. (abstr.), 80-82.

SHAW, D.M. (1970). Trace element fractionation during anatexis. Geochim. cosmochim. Acta, 34, 237-243.

SIMKIN, T. and SMITH, J.V. (1970). Minor element distribution in olivine. J. Geol., 78, 304-325.

SÖHNGE, P.G. (1963). Genetic problems of pipe deposits in South Africa. Geol. Soc. S.Afr. Proc., V.66, 19-72.

SPENCER, K.J. and LINDSLEY, D.H. (1981). A solution model for co-existing iron-titanium oxides. Am. Miner., 66, 1189-1201.

STEUBER, A.M., HUANG, W.H. and JONES, W.D. (1968). Chlorine and fluorine abundances in ultramafic rocks. Geochim. cosmochim. Acta, 32, 353-358.

STEVENS, R.E. (1944). Composition of some chromites of the Western Hemisphere. Amer. Miner., 29, 1-34.

STORMER, J.C. (1983). The effects of recalculation on estimates of temperature and oxygen fugacity from analyses of multicomponent iron-titanium oxides. Am. Miner., 68, 586-594.

STUMPFL, E.F. and RUCKLIDGE, J.C. (1982). The platiniferous dunite pipes of the Eastern Bushveld. Econ. Geol., 77, 1419-1431.

SUN, C-O., WILLIAMS, R.J. and SUN, S-S. (1974). Distribution coefficients of Eu and Sr for plagioclase - liquid and clinopyroxene - liquid equilibria in oceanic ridge basalt : an experimental study. Geochim. cosmochim. Acta, 38, 1415-1433.

TAKAHASHI, E. (1978). Partitioning of Ni^{2+}, Co^{2+}, Fe^{2+}, Mn^{2+} and Mg^{2+} between olivine and silicate melts : compositional dependence of partition coefficients. Geochim. cosmochim. Acta, 42, 1829-1844.

TAKENO, S. and CLARK, H. (1967). Observations on tetragonal $(Fe, Ni, Co)_{1+x}S$, mackinawite. Quoted by Craig, J.R. and Scott, S.D. (1974). In: Ribbe, P.H., Ed. Sulphide Mineralogy. Min. Soc. Amer., CS25.

TANKARD, A.J., JACKSON, M.P.A., ERIKSSON, K.A., HOBDAY, D.K., HUNTER, D.R. and MINTER, W.E.L. (1982). Crustal evolution of Southern Africa. 3,8 Billion years of earth history. Springer-Verlag New York Inc, 523pp.

TARKIAN, M. and STUMPFL, E.F. (1975). Platinum Mineralogy of the Driekop Mine, South Africa. Mineralium Deposita, 10, 71-85.

TAYLOR, L.A. and FINGER, L.W. (1971). Structural refinement and composition of mackinawite. Carnegie Inst. Wash. Year book, 69, 318-322.

VERMAAK, C.F. (1976). The nickel pipes of Vlakfontein and vicinity, Western Transvaal. Econ. Geol., 71, 261-286.

VILJOEN, M.J., HIEBER, R. and PEYERL, W. (1983). The geology of the Townlands dunite/pegmatite pipe - Rustenburg Section. RPM. Symposium on the Bushveld Complex. Pretoria. (abstr.), 94-97.

VILJOEN, M.J. and SCOON, R.N. (in press). The distribution and main geological features of discordant bodies of iron-rich ultramafic pegmatite in the Bushveld Complex. Econ. Geol..

VON BACKSTRöM, J.W. (1960). Die geologie van Rustenburg en die omliggende gebied. Explan. Sheet (Rustenburg), Geol. Surv. S.Afr., 93pp.

VON GRUENEWALDT, G. (1973). The main and upper zones of the Bushveld Complex in the Roossenekal area, eastern Transvaal. Trans. geol. Soc. S.Afr., 76, 207-227.

VON GRUENEWALDT, G. (1979). A review of some recent concepts of the Bushveld Complex with particular reference to sulphide mineralization. Can. Miner., 17, 233-256.

WAGER, L.R. and BROWN, G.M. (1968). Layered igneous rocks. Oliver and Boyd, 588pp.

WAGER, L.R., BROWN, G.M. and WADSWORTH, W.J. (1960). Types of igneous cumulates. J. Petrology, 1, 73-85.

WAGER, L.R. and MITCHELL, R.L. (1951). The distribution of trace elements during strong fractionation of basic magma - a further study of the Skaergaard intrusion, East Greenland. Geochim. cosmochim. Acta, 1, 129-208.

WAGNER, P.A. (1925). Notes on the platinum deposits of the Bushveld Igneous Complex. Trans. geol. Soc. S.Afr., 28, 83-133.

WAGNER, P.A. (1929). The platinum deposits and mines of South Africa. Edinburgh : Oliver and Boyd, 326pp.

WASSERSTEIN, B. (1936). Some notes on the critical zone of the Bushveld gabbro at the Swartkop Chrome Mine in the Rustenburg district. Trans. geol. Soc. S.Afr., 39, 215-222.

WILLEMSE, J. (1969a). The geology of the Bushveld Igneous Complex, the largest repository of magmatic ore deposits in the world. Econ. Geol., Mon. 4, 1-22.

WILLEMSE, J. (1969b). The vanadiferous magnetic iron ore of the Bushveld Igneous Complex. Econ. Geol. Mon., 4, 187-208.

YUND, R.A. and KULLERUD, G. (1966). Thermal stability of assemblages in the Cu-Fe-S system. J. Petrology, 7, 454-488.